Investigations on the growth and characterisation of some technologically important single crystals for possible nonlinear optical applications

Thesis

submitted to Cochin University of Science and Technology

in partial fulfillment of the award of the degree of

Doctor of Philosophy

Submitted by

ARUN. K.J

DIVISION FOR RESEARCH IN ADVANCED MATERIALS,
PHYSICS DEPARTMENT

COCHIN UNIVERSITY OF SCIENCE AND TECHNOLOGY,
KOCHI-22, INDIA

December 2009

Certificate

*Certified that the work presented in this thesis entitled "**Investigations on the growth and characterisation of some technologically important single crystals for possible nonlinear optical applications**" is based on the authentic record of research work done by Mr. Arun.K.J under my guidance in the Department of Physics, Cochin University of Science and Technology, Cochin - 682 022 and has not been included in any other thesis submitted previously for the award of any degree.*

Date: 30/12/2009.

Place: Cochin-22

S Jayalekshmi

Dr. S. Jayalekshmi

Dr. S. JAYALEKSHMI
READER
Department of Physics
Cochin University of Science and Technology
Cochin-682 022

Declaration

Certified that the work presented in this thesis entitled ***"Investigations on the growth and characterisation of some technologically important single crystals for possible nonlinear optical applications"*** is based on the original research work done by me under the guidance and supervision of Dr.S.Jayalekshmi, Reader, Department of Physics, Cochin University of Science and Technology, Cochin - 682 022 and has not been included in any other thesis submitted previously for the award of any degree.

Date: 30-12-2009

Place: Cochin-22

Arun.K.J

Acknowledgement

I wish to express my heartfelt thanks to my guide, Dr. S. Jayalekshmi, Reader, Department of Physics, CUSAT, for her inspiration, invaluable guidance, suggestions and profuse assistance during my research work. Without her sincere help and competent advice, I am sure; my work would not have been completed.

I am indebted to Prof. M.R. Anantharaman, Head, Department of Physics, and former Heads of Department of Physics, CUSAT, for providing necessary facilities during my research work.

I thank all the faculty members and the administrative, library and laboratory staff of the Physics Department for their help.

I acknowledge my deep sense of gratitude to Dr.M.A.Ittyachen, former Director, School of Pure and Applied Physics, M.G.University, Kottayam (Professor Emeritus of Physics Department ,CUSAT during the past two years), for the fruitful discussions on the etching of crystals and for the help in growing KAP crystals in gel medium. I also thank Dr.Cyriac, Lecturer, SPAP; Mahatma Gandhi University for the help extended for carrying out microhardness studies.

I thank Dr. Reji Philip and Dr.M.Anija of Raman Research Institute, Bangalore for rendering the facilities to take the Z scan measurements on crystal samples.

I wish to express my sincere thanks to Professor K.T.Mathew and Dr.Jaimon Yohannan, Dept: of Electronics, CUSAT for allowing to conduct the dielectric studies by microwave cavity perturbation method.

Dr.R.Jayasree, Scientist, SCTIMST, Thiruvananthapuram was very helpful in recording the Photoluminescence spectrum of crystals and I extend my thanks to her.

I am thankful to Prof. V.P.N Nampoori, International School of Photonics, CUSAT for his encouragement and the help rendered to carry out the SHG, laser

damage threshold and Z scan experiments of the crystalline samples. I express my deep sense of gratitude to Dr.Santhi, Adhoc Lecturer; International School of Photonics, in fitting and analysing the Z scan data and to S.Mathew, research scholar for his particular help in assessing the SHG efficiency.

I thank Amritesh. M, Rajive Tomy and Dhannia.T, research scholars of the Division for Research in Advanced Materials (DREAM) laboratory, for their consistent help right from the year I joined CUSAT. I thank them for their concern, encouragement, and valuable suggestions. I express my deep heartfelt gratitude to Late: K.Raveendranath, former HOD of Physics, Aquinas College and a model research scholar of the DREAM laboratory, for his support and personal advice related to all academic and non academic matters. I especially thank Sreeja.R, research scholar of OED laboratory, for the help in conducting the Z scan measurements and for many technical discussions.

I wish to express my sincere thanks to my dear juniors, of the DREAM laboratory, Sreekanth Verma, Anil Kumar, Francis Xavier, Jeeju teacher, Sreevalsa teacher, Sajimol teacher, who helped me a lot during the entire phase of my work. They were ever ready with a helping hand whenever I faced academic and non - academic problems.

The services rendered by esteemed institutions like STIC, Cochin, RSIC, IIT, Chennai, IIT Mumbai, SCTIMST, Thiruvananthapuram are gratefully acknowledged.

I am greatly indebted to my loving wife Treesa Girly, children Carol and Cyril and Appachan and Ammachi for their prayers and support.

Above all I bow my head before God Almighty for His unending grace.

Arun K.J

Contents

Chapter 3

Chapter 4

GROWTH AND CHARACTERISATION OF GLYCINIUM OXALATE SINGLE CRYSTALS FOR NONLINEAR OPTICAL APPLICATIONS.....90-124

Chapter 5

GROWTH AND CHARECTERISATION OF NONLINEAR OPTICAL SINGLE CRYSTALS OF L-ALANINIUM OXALATE.....125-163

Chapter 6

INVESTIGATIONS ON THE GROWTH AND CHARACTERISATION OF POTASSIUM HYDROGEN PHTHALATE SINGLE CRYSTALS FOR NONLINEAR OPTICAL APPLICATIONS.....164-203

Chapter 7

****ꕥ****

Preface

In the modern world, the development of science & technology in many areas has been achieved through the growth of single crystals. Large sized single crystals are essential for device fabrication and efforts are taken to grow large single crystals in short duration with less cost.

The search for efficient and new materials in which to carry out investigations on non linear optical processes has been very active since the discovery of second harmonic generation (SHG) in quartz crystal by Franken and his co-workers in 1961.

Nonlinear optical (NLO) materials are expected to play a major role in photonics including optical information processing, sensor protector applications, data storage...etc. Some organic compounds exhibit large NLO response, in many cases, orders of magnitude larger than widely known inorganic materials. They also offer the flexibility of molecular design and the promise of virtually an unlimited number of crystalline structures. In this stimulating context, organic nonlinear materials have been recognized as forefront candidates for fundamental and applied investigations involving, in a joint effort, chemists, material scientists and optical engineers.

The database for nonlinear optical properties of materials, particularly organic, is in many cases inadequate for determining trends to guide synthesis efforts. Materials found in non-centrosymmetric, or acentric crystal classes, i.e. crystal classes lacking a center of inversion, can exhibit a variety of technologically important physical properties. Only a few molecules with large hyperpolarizability (γ) values crystallize in noncentrosymmetric structures, and a limited number of them are useful as NLO materials. There are crystals with large γ values and non centrosymmetry, but many of them do not have mechanical strength, thermal and air stability and perfection necessary for device fabrication.

Hence in the present work, more focus is given to the studies on the non linear optical properties of organic single crystals.

The thesis entitled ***"Investigations on the growth and characterisation of some technologically important single crystals for possible nonlinear optical applications"*** consists of seven chapters.

Chapter 1 is an introduction to crystal growth and nonlinear optical phenomena. The importance of crystal growth in material science and the various techniques of crystal growth are discussed. Various types of defects and imperfections that get incorporated into the crystal lattice during growth are considered. Salient features of the .nonlinear optical phenomena relevant to the present work are also addressed.

Chapter 2 deals with the fundamental theories of crystal growth and nonlinear optics that are central to the thesis.

Chapter 3 provides a brief description of the experimental techniques employed in the characterisation of grown crystals. These techniques include structural characterisation by powder X-ray diffraction and elemental analysis by EDAX and CHN analysis. The presence of noncentrosymmetry and the various functional groups are confirmed by FTIR and FT Raman vibrational spectral analysis. The optical transparency window, optical band gap and the linear optical constants are elucidated using UV/Vis/NIR absorption spectroscopy. Thermal characterisation of the grown crystals is done by using TGA/DTA and differential scanning calorimetry (DSC). Temperature dependence of the specific heat Cp is analysed using ratio method. Applications of optical microscopy and SEM to analyse the crystal surface are also discussed. Chemical etching technique to reveal the growth mechanism and dislocations present in the crystal is described in detail. Determination of the dielectric properties by microwave cavity perturbation technique in the S band is explained. Second harmonic generation in the grown crystals is studied by Kurtz and Perry technique. Techniques to investigate the photoluminescence and the laser damage threshold of the grown crystals are also explained in this chapter. Determination of the third order NLO properties of the crystals by Z scan technique is also briefly discussed.

Chapter 5 deals with the growth of single crystals of Glycinium oxalate (GLO) by solution evaporation technique and the various methods employed to characterise the crystal for possible nonlinear optical applications.

Chapter 6 gives a detailed account of the studies conducted on the growth and characterisation of single crystals of the charge transfer complex Laevo alaninum oxalate (LAO) grown from the precursors L alanine and oxalic acid by top seeded solution growth technique at ambient temperature.

The details of the growth of potassium hydrogen phthalate also known as potassium acid phthalate (KAP) single crystals by floating seed technique and also by sodium meta silicate gel growth method are included in **chapter 6**. This chapter also gives an account of the various charecterisation techniques employed to evaluate the prospects of this material for NLO applications.

Chapter 7 gives a summary of the important outcomes of the present investigations. It also gives a comparative assessment on the prospects of the three single crystals investigated in the present work, glycinium oxalate, l- alaninium oxalate and potassium hydrogen phthalate, for possible non linear optical applications. The scope for future investigations on these materials is also highlighted in this chapter.

Chapter 1

INTRODUCTION

Chapter 1

INTRODUCTION

This chapter gives a general introduction to the subject matter contained in the thesis. It deals with the general aspects related to the growth and structural properties of single crystals, and the general ideas related to the nonlinear optical properties of single crystals.

1.1 A BRIEF HISTORY OF CRYSTAL GROWTH

"Who dominates materials dominates technology." The ability to dominate materials requires an in-depth knowledge of the science and technology of crystal growth since crystals; especially single crystals have increasingly become a vital necessity in modern technology. Crystal growth is a universal phenomenon in the field of materials. It has a long history of evolution from "a substance potting art" to a science in its own right which was accelerated by the invention of the transistor in 1948, and the subsequent need for high purity semiconductor single crystals. As a result crystal growth has developed into a core discipline in materials science.

The evolution of our knowledge of crystal growth requires not only scientific understanding, but the driving force of applied technology which so often provides a significant influence in highlighting our lack of scientific knowledge and the need for a more refined science and indeed the development of new concepts.

Crystals are the unacknowledged pillars of modern technology. Crystal growth can be regarded as an ancient subject, owing to the fact that the crystallization of salt and sugar was known to the ancient Indian and Chinese civilizations. The subject of crystal growth was treated as part of crystallography and never had an independent identity until the last century. The fundamentals of crystal

growth were entirely bestowed upon the morphological studies of the naturally occurring crystals. Thus began the scientific approach for this subject during the 17^{th} century by Kepler, followed by quite a few others like Nicolous Steno, Descartes, Bartholinus, etc. This type of morphological study slowly led to the understanding of the atomistic process of crystal growth. Recent bursting research on nanostructured materials depends on the crystal growth theory and technology. In the early 20th century, crystal growth evolved as a separate branch of science and several theories from Kossel, Donnay-Harker, Volmer and Burton, Cabrera and Frank (BCF), etc., were proposed. Although the science of crystal growth originated through the explanations of Nicolous Steno in 1669, the actual impetus to this field began after the BCF theory was formulated and also when there was a great demand for crystals during World War II.

1.2 TECHNIQUES OF CRYSTALS GROWTH

The discovery of new properties and applications may be said to be directly related to the availability of a large range of single crystals. The demand for large and perfect single crystals for devices, initiated a search for understanding the basic parameters involved in the process of crystal growth. This resulted in considerably improving the technology of providing highly perfect crystals. This section deals with the techniques of crystal growth currently employed.

1.2.1 Growth from melt

Growth from melt is by far the fastest of the growth methods, as its rate does not depend on mass transport process. In principle, the crystals of all materials can be obtained from melt, provided they melt congruently, they do not decompose before melting and they do not undergo a phase transformation between the melting point and room temperature [14-16].

(a) Czochralski Method

In this method the melt is contained in a crucible. A seed fixed to a holder is brought into contact with the melt and after equilibrium is reached, the seed is pulled along with rotation during growth. Rotation of seed and crucible are employed to

optimise compositional and thermal homogenization of the melt and to control the geometric configuration of the crystal. Growth is generally carried out in controlled atmosphere or in vacuum. This method is widely used in silicon industry. Numerous other materials including oxides such as sapphire and ruby can be grown by this method [11- 13].

The major advantages of this method are (1) growth from a free surface accommodates the volume expansion associated with solidification of many materials such as semiconductors (2) complications that may arise due to wetting of the container by the melt is eliminated (3)large single crystals can be obtained at high speeds(4) high crystalline perfection can also be achieved(5) the method is convenient for doping(6) during growth the desired ambient atmosphere can be used, controlled and changed. However, the method does not lend itself readily to the growth of materials whose vapour pressure or that of one of their constituents is high at the melting point. The requirement for a crucible in Czochralski growth introduces the possibility of contamination of melt.

(b) Normal Freezing and Zone Melting

In the normal freezing method, the charge is contained in a closed container which can be mounted horizontally or vertically. A boat can also be used as a container. If a seed is not used, the entire charge is melted, solidification is initiated and the solid – melt interface is advanced horizontally by moving the container through a furnace with appropriate thermal gradients or by moving the furnace past the container. The interface can also be advanced by controlled power reduction. For obtaining specific orientation, a seed is commonly used at one end of the container. Single crystals with a preferred orientation are usually grown using a container with a tapered end. Vertical normal freezing, by advancing the growth interface upwards yields better crystals in some cases. Normal freezing methods are extensively used for growing single crystals of materials with volatile constituents [17].

In zone melting a molten zone is established at one end of the charge and is advanced by moving either the container or the furnace. By this method a

homogenous distribution of impurities can be achieved. Zone melting is best known as a purification method [19].

Directional solidification methods are simple and versatile. The vapour pressure of volatile constituents can be easily controlled in directional solidification methods [12, 15]. Growth can be carried out in evacuated and sealed containers. Shape and size of the crystal can also be controlled. Furthermore, growth can be carried out under stabilized thermal gradients which minimise convective interference in growth. The confining in these methods presents some limitations. When volume expansion is associated with solidification, pressure can be exerted to the growing crystal leading to high densities of lattice defects.

(c)Float – zoning

Float – zoning is essentially zone melting in a vertical configuration without a container. The zone is sustained by surface tension forces. Thus this method is suitable for materials with high surface tension and low density [17, 20]. The earliest of the crucible less technique is the Verneuil technique, where, a molten zone is formed on the top of the seed crystal with an oxygen hydrogen flame and to this zone, powder of the material is fed and growth proceeds by lowering the seed.

The unique advantage of float-zoning is the elimination of the melt container which reduces contamination. The instrumentation for float zoning is relatively simple for small diameter crystals. This method cannot be used for the growth of materials with high vapour pressure or of materials with volatile constituents.

1.2.2 Growth from Solution

In this process, a saturated solution of the material in an appropriate solvent is used, from which crystals grow after the solution is supersaturated by lowering the solution temperature. Solution growth is generally simple and inexpensive. Materials which melt incongruently decompose before melting or undergo a phase transformation between the melting point and room temperature, are grown from solutions. The methods of solution growth are usually classified according to the type

of the solvent used. They are mainly aqueous – solution, molten – salt (flux), metallic solution and hydrothermal growth.

1.2.2.1 Aqueous solution growth

The method rests on obtaining supersaturation without inducing spontaneous nucleation so that growth can proceed on the seed. Supersaturation can be achieved either by evaporation of the solvent or by decrease of the solution temperature. The method is often simple and inexpensive. It can lead to good quality crystals and lends itself to continuous operation. The growth can be visually inspected. The method is slow and has thus limitations for industrial production.

Low temperature aqueous solution growth can be subdivided in to the following methods.

- *Slow cooling method*
- *Slow evaporation method*
- *Temperature gradient method*

a) Crystallization by slow cooling method

This is the best method among others to grow bulk single crystals from solution. In this method, supersaturation is produced by a change in temperature throughout the crystallizer. The crystallization process is carried out in such a way that the point on the temperature dependence of the concentration moves into the metastable region along the saturation curve in the direction of lower solubility. The supersaturation requires systematic cooling and it is achieved by using a thermo stated crystallizer. The temperature at which such crystallization begins is usually within the range 45-75^{0}C and the lower limit of cooling is the room temperature.

b) Crystallization by solvent evaporation

In this method, an excess of a given solute is established by utilizing the difference between the rates of evaporation of the solvent and the solute. In contrast to the cooling method, in which the total mass of the system remains constant, in

solvent evaporation method, the solution loses particles, which are weakly bound to other components and the volume of the solution decreases. The vapour pressure of the solvent above the solution is higher than the vapour pressure of the solute and the solvent evaporates more rapidly and the solution becomes supersaturated. This is the oldest method of crystal growth and technically, it is very simple. Typical growth conditions involve temperature stabilization to about $\pm 0.005^0$C and rates of evaporation of a few mm^3/hr.

(c) Temperature gradient method

This method involves the transport of the material from a hot region containing the source material to be grown to a cooler region where the solution is supersaturated and the crystal grows.

Temperature –difference methods are based on the formation of two regions with different temperatures in the crystallizer. In one of them, the substance which is always in the form of the solid phase is dissolved, and in the other crystal growth takes place. In the simplest version a tall vessel is used, with its lower part containing the nutrient and its upper part the suspended seed. The temperature in the lower part is kept higher than in the upper part. This results in convection of the solution, which ensures continuous upward movement of the substance into the growth zone. This arrangement is used in the hydrothermal growing of crystals. In growth from low temperature aqueous solutions, two vessels connected by tubes are usually employed. The substance is dissolved in the vessel with the higher temperature and the crystal is grown in the other. The exchange between the vessels is achieved both by natural convection of the solution and by stirring with a mechanical agitator. At the beginning of the experiment, an equal temperature is set up in both vessels and maintained until the solution is completely saturated. Then the solution in the growth vessel is heated by a few degrees, and a seed is introduced. The vessel is held at this temperature for a short period and then cooled until the required temperature difference is established between the two volumes.

The main advantages of the method are:

- Crystal grows at fixed temperature

- This method is insensitive to changes in temperature, provided both the source and the growing crystal undergo the same change.
- Economy of solvent and solute.

1.2.2.2 Flux Growth

In this method molten salts are used as solvents. For oxides and solid solutions of oxides, which have very high melting points and/or decompose prior to melting these are the only satisfactory solvents. Molten salts of such composition should be contained in platinum or iridium crucibles. Growth from molten salts is obtained by decreasing the temperature of a saturated solution to acquire supersaturation. Seeds are commonly used and these can be withdrawn before the solution is solidified.

Flux growth is carried out at much lower temperatures than corresponding growth from melt. A distinct advantage of the method is that this is the only method for obtaining certain oxide solid solutions. However flux growth is very slow and requires precise temperature control. The purity of the crystals grown by this method is often marginal. Flux growth is an expensive technique.

1.2.2.3 Metallic Solution Growth.

Single crystals of metallic phases and inorganic compounds are readily obtained by solidification of saturated metallic solutions. Diamonds are being commercially prepared from transition-metal solutions under high pressure. Growth from metallic solution is now widely used for preparation of high quality epitaxial layers and solid solutions of III-V compounds.

In the case of semiconductors the crystalline perfection attained by liquid phase epitaxy (LPE) is better than that by melt growth. The thickness of LPE layers can be controlled to within several hundred angstrom units. The limitations of this method are that the growth is slow and is limited to small crystals or relatively thin layers. The purity of the crystal is limited by the purity of the solvent.

1.2.2.4 Hydrothermal growth

The technique is basically the same as the aqueous solution growth at elevated temperatures and pressures. The method is primarily used for the growth of large high quality quartz crystal used for piezoelectric applications. Crystals of any metal, their oxides and other components, which may be soluble in water only at high temperature and high pressure can be grown using this method

In the growth of quartz, α-quartz nutrient is used in an autoclave containing aqueous solution of a base (NaOH). Growth is carried out at about 4000^0C and pressure of 2000bars. In the hydrothermal method, the major disadvantage stems from the requirement of autoclave at elevated temperatures and pressures. Besides, considerable period of time is required for growing large crystals.

1.2.3 Growth from vapour

Bulk crystals as well as thin layers are prepared from vapour phase. Since gases can in general be obtained at very high purity and high purity conditions can be maintained during gaseous processes, vapour phase growth can lead to high purity crystals. The method is extensively used for the growth of high quality thin layers of materials such as Si, II—VI and III—V compound semiconductors; layers of metals and other inorganic compounds can be prepared from the vapour phase. Growth from the vapour phase can be obtained without involving chemical reactions [23-25]. When chemical reactions are involved they can be irreversible or reversible. Successful growth from vapour phase requires knowledge of the thermodynamic equilibrium among the reacting vapour constituents which may involve species other than the initial species. The kinetics of vapour growth is critically dependent on the concentration or the diffusion of the desired reacting species. The transport and/or equilibrium of the species are often controlled by the use of carrier gases.

In the irreversible reactions the reactants are brought into contact with the seed material at the appropriate temperature and pressure of the reaction. Where the products are not recycled an open tube arrangement is usually employed. This method is widely used in the preparation of Si layers. The thickness and doping level

of the layers is readily controlled and very high purity materials are obtained by this process. But the process is slow.

In the reversible reaction, the solid material can be brought into the vapour phase and then reformed under controlled conditions by reversing the direction of the reaction. Epitaxial layers of III-V compounds and solid solutions of these compounds are prepared by employing appropriate reversible reactions [26].

This is a method with which single crystals and epitaxial layers of high chemical purity and crystalline perfection can be obtained. The thickness and the doping of the layers can be closely controlled and the process can be recycled. But since the growth is slow, the method is not practical for bulk single crystals [27].

1.2.4 Gel growth

Gel growth is an alternative technique to solution growth with controlled diffusion and the growth process is free from convection. The growth of single crystals in gel is a self –purifying process, free from thermal strains whish are common in crystals grown from the melt.

Solutions of two suitable compounds which give rise to the required insoluble crystalline substance by mere chemical reaction between are allowed to diffuse into the gel medium. This method can also be found useful for growing crystals from the solutions of substances having very high solubility.

Based on the nature of physical changes and chemical reactions involved in the growth process, gel method can be classified into four categories [33-37].

- Chemical reaction method.
- Chemical reduction method
- Solubility reduction method
- Complex dilution method.

1.2.4.1 Chemical reaction method

Two different methods are employed in the chemical reaction gel growth experiments. They are

Single diffusion method and Double diffusion method

(a) Single diffusion Method

In this method, one of the components either AX or BY which is highly soluble in water and chemically inactive with the gel is impregnated in the acidified gel medium (known as inner reactant). After the gelation, the other component solution (known as outer reactant) is taken over the set gel. This solution on diffusion through gel medium reacts with the inner reactant and yields the crystal. At the same time, during the chemical reactions, some other compounds are being formed such as XY which is highly soluble in water and dissolve in water present in the hydro gel medium.

(b) Double diffusion method

Double diffusion principle is used when both the reactants are found chemically reactive with the hydro gel or found insoluble in water. Because of the diffusion, the two components can meet each other at the common region of the medium, normally the bent portion of the U tube. Then they react chemically without vigorous chemical effects allowing the formation of crystals in gel.

The major factors that control the nucleation and growth of crystals are the concentration of the feed solution, the pH of the gel, aging of the gel and the gel density. The optimum values of the various parameters for a particular material are found out by trial and error.

Since the crystals in gel medium are usually grown at room temperature it will have lower concentration of non-equilibrium defects than those grown at elevated temperatures. The crystals can be observed at all stages of growth. The solute concentration at the growth boundary is self regulating in accordance with the needs of the growth process since the crystals are grown by diffusion. The gel

medium provides unconstrained support for the growing crystal. The disadvantages of this method are the slow growth rate, which is essentially diffusion limited, the inability to control the nucleation, and the relatively small sizes of the crystals obtained.

1.2.4.2 Chemical reduction method.

Metals are grown by this method. The metallic complex is taken along with the SMS solution and is reduced by means of diffusion by a proper reducing agent into the gel. Slow reduction results in the formation of metallic crystals. For the growth of copper crystals, copper sulphate is incorporated into the gel. The reducing agent of hydroxylamine or hypo phosphoric acid poured over the set gel. Crystal of copper, nickel, cobalt, gold...etc has been grown by this method [38].

1.2.4.3 Solubility reduction method

This method is employed for the growth of water soluble substances. The substance to be grown is dissolved in water and incorporated with the gel forming solution. After the gelation, a solution which reduces the solubility of the material is added over the set gel to initiate crystallisation. Potassium dihydrogen phosphate crystals have been grown by this method by adding ethyl alcohol over the gel containing a saturated solution of KDP [39].

1.2.4.4. Complex dilution method

A chemical complex of the material to be grown is prepared with a complexing agent and then allowed to diffuse into a gel, free of active reagents. Decomplexion is achieved by steadily increasing the dilution and this leads to the higher supersaturation necessary for the crystal growth. Armington used this method for growing cuprous chloride crystals. Cuprous chloride is complexed with hydrochloric acid and then allowed to diffuse into a gel with HCl and free of other active reagents. Decomplexing sets in with increasing dilution leading to high supersaturation of cuprous chloride.

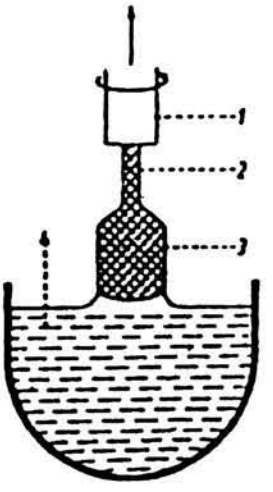

Fig 1.1 Czochralski – type system (1) Seed holder, (2) Seed, (3) Growing crystal, (4) Melt

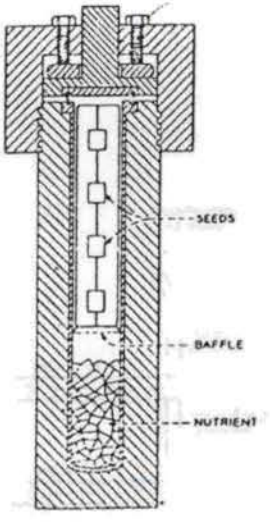

Fig 1.2. Hydrothermal growth arrangement

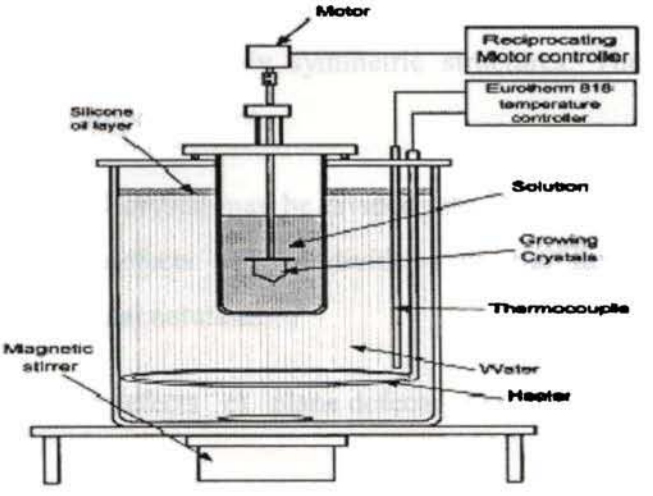

Fig 1.3 Crystallisation by solvent evapouration

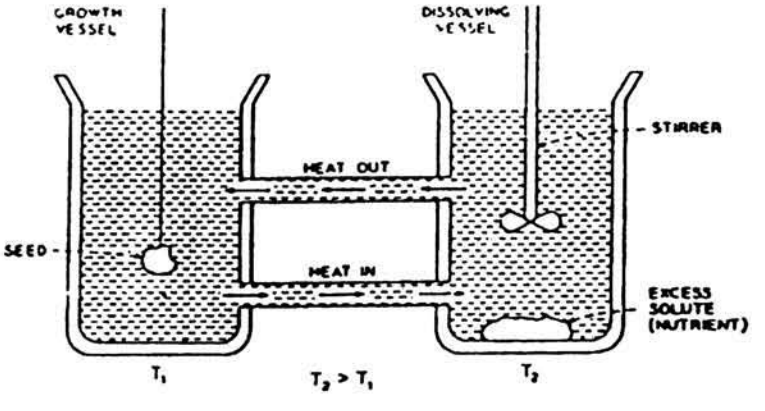

Fig.1.4 crystallisation by temperature gradient method

1.3 DEFECTS IN CRYSTALS

Most of the solid materials exist in crystalline form. Crystals are distinguished by their periodic highly symmetric structures. The word 'defect' indicates a disturbance or imperfections.

The defects in a real crystal may be divided into chemical defects and lattice defects [40- 44]. These defects can be divided into the following categories according to their dimensional nature as

a) Point defects b) Line defects c) plane defects d) volume defects.

1.3.1Point Defects

If the deviation from a periodic arrangement is localized to certain points within crystal lattice, it is called point defect. The point defects (fig. 1.8 & 1.9) in the crystal produce strains nearby but do not affect the long range order of the crystal.

1. Schottky Defects

Regular lattice sites are vacant. Lattice particles have migrated to the surface and have left their sites unoccupied. These defects are also called Schottky defects.

2. Interstitials

Lattice particles have moved from their regular sites, leaving vacancies behind, to interstitial positions in the lattice. The combination of an interstitial and a vacancy is called Frenkel defect.

1.3.2 Line Defects

Line defects are lattice imperfections along closed lines or open lines which end at the crystal surface. The crystal structure is disturbed around these lines in a volume whose radial extension is of the order of about one atomic separation. These one dimensional lattice defects are called dislocations. The geometry of dislocation is generally complex: however, it can be regarded as a combination of two special

types, the edge dislocation and the screw dislocation [45, 46]. They will be described in the following.

i) Edge Dislocation

A lattice plane which ends inside the crystal will strongly distort the lattice along its boundaries. The edge of the lattice "half" plane is dislocation line. Near it the environment of the lattice particle is different from that in the undisturbed crystal and the lattice forces are therefore changed.

i) Screw Dislocations

The lattice planes perpendicular to certain directions are degenerated into forming a single connected screw surface. The screw axis is the dislocation line; near it the lattice is strongly distorted.

Edge dislocation and screw dislocation are depicted in fig (1.5) and fig (1.6) respectively.

A dislocation line cannot end in the interior of a crystal. It must close on itself or end at another defect; outer surface, grain boundary or node formed with other dislocations. The displacement which defines the dislocation has the same value along its whole length.

1.3.3 Planar Defects

Two dimensional lattice defects (planar defects) are surfaces inside the crystal at which the periodic structure is disturbed. We distinguish essentially two types which may occur also in combination.

i) Grain Boundaries

The orientation of the crystal on one side of the surface is different from that on the other. A grain boundary may be considered to be a series of dislocations. A simple case is shown in figure 1.7, where the difference in orientation is small and where the grain boundary can be represented as a series of edges dislocations.

ii) Stacking Faults

Two lattice planes are mutually shifted by a vector which is not a lattice vector. Stacking faults are particularly marked in crystals with close packing. Such crystals are considered as constructed of plane layers of equally large spheres arranged as densely as possible. The spheres of one layer lie in the depressions of the lower layer. There are two possibilities of placing the layers upon each other.

The spheres of the third layers have the same positions as those of the first layer. The positions being characterized by the letters A, B, C the layer sequence can be described by ABABA..... This is the hexagonal close packing of spheres; the hexagonal axis is normal to the densest layers.

The spheres of only the fourth layer have the same positions as those of the first layer. The sequence of layers is thus ABCABCABC.....

1.3.4 Volume Defects

Volume defects can be produced due to foreign particle inclusion, large voids or pores or means of non – crystalline regions having a dimension of at least a few tenths of angstrom. These have important effects on the properties of crystalline solids [48].

1.4 DETECTION OF DEFECTS IN CRYSTALS

The increasing demand of crystals of better perfection for in the fabrication of electronic devices and in the understanding of the mechanism of plastic deformation has led to an interest in the development of a variety of methods for the detection of defects in crystals.

a) Growth Spiral

Frank (1949) observed that growth at very low super saturation can occur if the growing crystal contains screw dislocation. The crystal around a dislocation is not a stack of atomic planes. But it is a single atomic plane in the form of a helicoids

or spiral staircase. As growth increases, the step advances infinitely around the dislocation and crystal grows without nucleation of new layer. The part near the dislocation moves with greater angular velocity than parts farther away; and a spiral hills formed. If the Burgers vector of the dislocation is equal to single lattice spacing, the growth step will also be one lattice spacing in height. Thus the existence of steps on the crystal surface enables the detection of the point of screw dislocation. The surfaces of crystals grown at higher super saturation are fairly smooth without spirals.

b) Etch Pits

Etching is used for the detection and characterization of crystal defects. It is the removal of growth spirals reverse to its formation [49]. Etch pits corresponds to a point where a dislocation terminates on the surface. Electrolytic polishing of the crystal surface is necessary in order to avoid general etching due to the presence of steps. Dislocation lines which are in planes parallel and near to the surface can be revealed by etching. There are different types of etching techniques. A carefully controlled chemical attack or sometimes, a simple evaporation of an electrolytic alloy polished crystalline surface often brings forth preferential etching points. These points are associated with the intersection of dislocations with the etched surface. These etch pits reappear at very nearly the same places if we make successive polishing and etching.

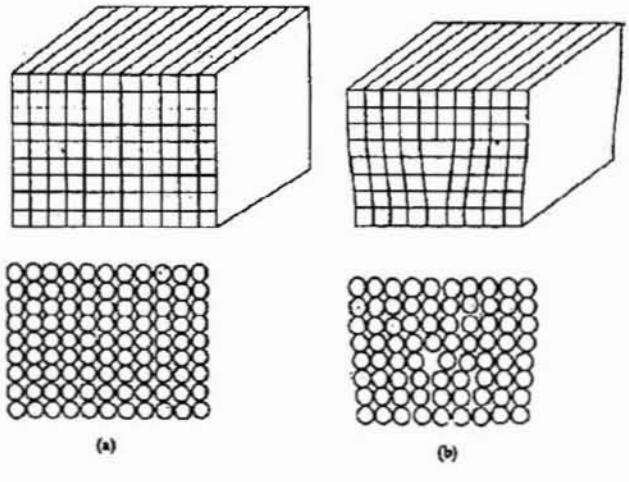

Fig 1.5 (a) perfect crystal and (b) crystal with edge dislocation.

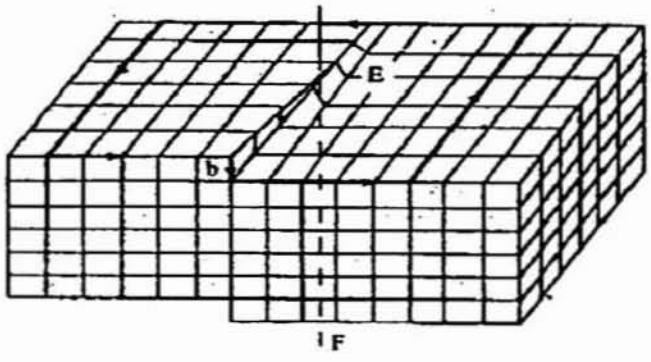

Fig 1.6 screw dislocation

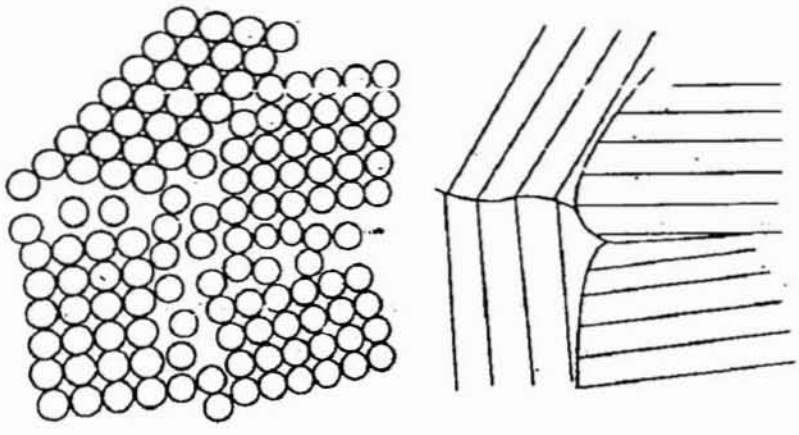

Fig 1.7 the distorted and unrelated atomic arrangements in a grain boundary

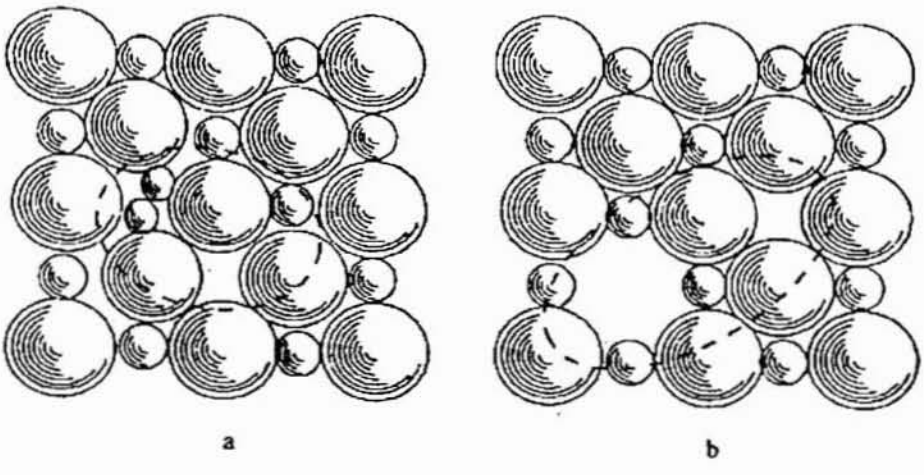

Fig 1.8 (a) Frenkel defect (b) Schottky defect

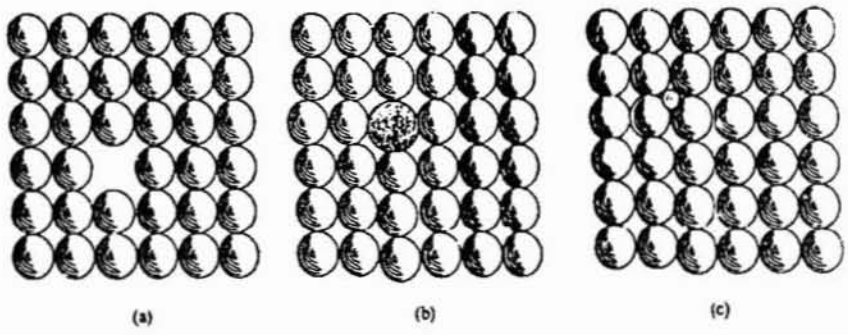

Fig 1.9 (a) vacancy (b) substitutional impurity (c) interstitial impurity

1.5 NONLINEAR OPTICS

Observation of the second harmonic generation (SHG) by P.A. Franken in 1961 marked the birth of nonlinear optics as a new discipline in the area of laser-matter interaction. Franken observed that light of 347.1 nm could be generated when a quartz crystal was irradiated with light of 694.2 nm, obtained from a ruby laser. He attributed this novel result to the coherent mixing of two optical fields at 694.1 nm in the crystal to produce 347.1 nm [52]. Non linear optics is essentially concerned with the study of phenomena that result from field induced modifications in the optical propertied of the materials [50]. This branch of science explores the coherent coupling of two or more electromagnetic fields in a non-linear medium. During these coupling processes, new frequencies can be generated that are the sum or the differences of the coupling frequencies. Though the discovery of SHG marked the birth of nonlinear optics as a new branch of experimental investigation, SHG is not the first nonlinear optical (NLO) effect to be observed. Optical pumping is a nonlinear optical phenomenon, which was known prior to the invention of laser [51]. Figure 1.10 clearly depicts the second harmonic generation in a nonlinear crystal in which a 1064nm laser radiation is converted into a 532 nm laser wave.

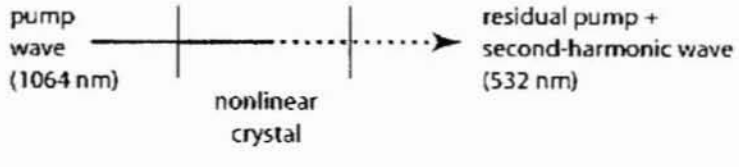

Fig 1.10 second harmonic generation in a nonlinear crystal

1.6 NONLINEAR OPTICAL MATERIALS

Nonlinear optical materials will be the key elements for future photonic technologies based on the fact that photons are capable of processing information with the speed of light.

Studies on the materials for nonlinear optical applications can be divided into three areas

- Discovery of new nonlinear materials.
- Growth and perfection of promising NLO crystals of desired shape and size for device applications.
- Improving the property modification of NLO crystals.

In the beginning studies were mainly concentrated on inorganic materials such as quartz, potassium dihydrogen phosphate (KDP), lithium niobate and semi conductors such as cadmium sulphide, selenium and tellurium. At the end of 1960's the Kurtz and Perry method was introduced which allowed for the first time a rapid qualitative screening of second order NLO effect in materials. The stage was set for rapid introduction of new materials, both organic and inorganic.

NLO materials are used on optical switching, frequency conversion and electro optic (EO) applications, especially in EO modulators. All of these applications rely on the manifestation of the molecular hyperpolarisability of the material.

Inorganic materials are much more matured in their applications to second order NLO than organics. Most commercial materials are inorganic especially for high power applications. However, organic materials are perceived as being structurally more diverse and therefore are believed to have more long term promise than inorganic. Organic solids have enormous range interesting properties that are almost continuously tunable. In the last three decades there has been increasing awareness of these systems as their interesting properties have been uncovered for example superconductivity, spin less conductivity in doped conjugated polymers and large nonlinear optical responses.

For optical applications, a NLO material should have the following characteristics [53- 55].

- Wide transparency domain
- Large nonlinear figure of merit for frequency conversion
- High laser damage threshold
- Availability in large single crystal forms
- Wide phase matching angle
- Ability to process into crystal and thin film form
- Ease of fabrication
- Nontoxicity and good environmental stability
- High mechanical strength and thermal stability
- Fast optical response time

For exhibiting SHG in materials, there are two factors, which determine the existence or absence of efficient SHG. Firstly, and fundamentally, the material should crystallize in a non centrosymmetric crystal structure. Secondly for maximum SHG efficiency, crystal should possess phase matching properties (i.e., the propagation speeds of the fundamental and harmonic waves should be identical in the crystal.)

1.7 ORGANIC NLO MATERIALS

The enhancement in the nonlinearity in comparison to inorganic materials arises due to the existence of π conjugation between electron donor and acceptor groups, chirality and hydrogen bonding in organic molecules. The acceptor-donor groups are generally attached to organic conjugated systems to generate NLO materials with large hyperpolarisability and to tailor their transparency. The large molecular hyperpolarisabilities are generally obtained from the charge transfer mechanism of the molecular structure. Therefore a wide variety of organic materials having electron donor and acceptor groups have been synthesized particularly for second order nonlinear optics and can also be used in electro optics and third order NLO applications.

The advantages of organic NLO material are [56- 60]

- They are generally cheap to synthesize
- They can be purified by conventional techniques
- High second order NLO efficiency
- Moderately greater resistance to damage to a laser beam
- They are birefringent
- Possible to chemically engineer molecular properties
- Low dielectric constant provided the crystals are pure.

Generally, a chiral organic molecule possessing large ground state dipole moment tends to crystallize into centro symmetric space group restricting their use for second order nonlinear optics. Various chemical as well as physical strategies have been implemented to introduce noncentrosymmetric crystal structures capable of displaying NLO activity. The various strategies employed for ensuring dipolar alignment favourable to generate NLO activity include

- Chirality
- Hydrogen bonding
- Guest host systems
- Electrical poling
- Co –crystallisation
- Organometallic structures.....

1.8 OBJECTIVES OF THE PRESENT WORK

Amino acids, Glycine and L- Alanine and their complexes are bio compatible materials and are studied widely owing to their potential applications in the field of medicine. They are formed as transparent crystals and are identified as systems with delocalised electrons. Delocalisation can be increased by reacting with carboxylic acids, thereby modifying the NLO behaviour. When glycine or L alanine is treated with oxalic acid the charge transfer complex formed due to the protonation of the amino group of the amino acid and the mono ionised oxalate ion in the crystal structure creates a donor- acceptor group resulting in intramolecular charge transfer

which results in increased hyperpolarizability. Both glycinium oxalate (GLO) and L-alaninium oxalate (LAO) are formed as noncentrosymmetric crystals.

Potassium hydrogen phthalate is a non centrosymmetric molecular ionic crystal. Potassium hydrogen phthalate crystals (KAP) are widely used in the field of X-ray spectroscopy as monochromator and also as analyser. It has interesting optical, piezoelectric and elastic properties. Recently, KAP crystals have been used as substrates for the deposition of thin films of organic nonlinear materials.

Studies on the growth and structural characterisation of all the three materials mentioned above have already been carried out and reported, but the NLO behaviour of these materials has not been dealt with in detail. In the present work, we concentrate on the NLO behaviour of these materials and try to establish a connection between the structure and the physical properties of these crystals and their NLO behaviour. Growth of large sized and optically perfect L-alaninium oxalate single crystals by solution growth technique and that of potassium hydrogen phthalate crystals using gel growth method are reported for the first time.

1.9 REFERENCES

[1] Mullin. J.B, Crystal Growth and Characterisation, North Holland Pub. Co, Amsterdam, 1973.

[2] Were. A.W, Crystal Growth: Principles and Progress of Crystal growth, Plenum Press, New York, 1987.

[3] S.Toschev, "Homogeneous Nucleation", north Holland, Amsterdam, 1973.

[4] B.K.Chakraverthy, Heterogenious nucleation and condensation on substrates in crystal growth: An Introduction, North Holland Publishers, Amsterdam, 1973.

[5] Gibbs. J.W, collected works, Longmans Green and Co, NY, 1962.

[6] W.Kossel, Nachr. Ges. Wiss. Gottingen, Math-Physik., Kl., 135(1927).

[7] W.K.Burton et al., Phil, Trans. Roy. Soc. London A 243, 299(1951).

[8] M.Volmer and W.Shultz, Z. Phys. Chem. A 156, 1(1931).

[9] A.Smekal, Handb. Phys 24,795(1933).

[10] F.C.Frank, "Growth and perfection of crystals" Wiley, N.Y., 1958

[11] Buckley.H.E, Crystal growth, Jhon Wiley, NY, 1951.

[12] Lauside, The growth of Single Crystals, Prentice Hall, NJ, 1970.

[13] Pamplin. B.R, Crystal Growth, Pergammon Press, Oxford, 1975.

[14] Brice.J.C, Crystal Growth Process, Jhon Wiley, New York, 1986.

[15] Elwell D, Crystal Growth from High Temperature solutions, Academic Press, NY, 1975.

[16] Barrat.C.S, Structure of Materials, Mc Graw Hills, New York, 1966.

[17] Kentaro Ino, Yukio Inatsu, Mat.Res.Bull 36,207(2001).

[18] Keer.H.V, Principles of The Solid State, Wiley Eastern Ltd, 1993.

[19] BridgmemanP.W, Proc.A..Acad.Arts.Sci, 60,305(1925)

[20] Shah. P.c, Ind.J.Phys, 67 A, 467, (1993).

[21] Kim.J.S, Lee.H.S, J.Cryst.Growth, 223, 376 (2001).

[22] Furyu.H,Murase.K, Mori. Y, J.Cryst.Growth198, 560 (1999).

[23] Archibald P, Parent. E, Solid State Technology, 19, 32(1990).

[24] K.Sunil, M.A.Ittyachen, Bull.Mater.Sci. 20, 231 (1997).

[25] Kaldis. E, J.Cryst. Growth, 17, 3(1972).

[26] Kulkarni. A.K, Bull.Mater.sci, 17, 1379 (1994).

[27] Scafer.H, Chemical Transport Reactions, Academic Press, New York, 1964.

[28] Setoguhi. M.J, J.Cryst.Growth, 99,879 (1990).

[29] Yokoyama.M, Ota.T, J.Cryst.Growth, 99, 875 (1990).

[30] Yokoyama. M, Yama.I, Takahashi.J, J.Cryst.Growth, 99, 875 (1990).

[31] Brice.J.C, The Growth of Crystals from Liquids, North Holland, Amsterdam, 1973.

[32] Hans.Z, Guo.N, Tang.K Zhao.H, J.Cryst.Growth219, 315(2000).

[33] Henisch. H.K, Crystal Growth in Gels, The Pennsylvania State university Press, 1970.

[34] Henisch. H.K, Crystals in Gels and Leisegang Rings, Cambridge University Press, 1988.

[35] Selvasekarapandian. S, Vivekananadan.K, Kolandaivel.P, Cryst.Res.Technol, 34, 873(1999).

[36] Roopkumar. R, Raman.G, Gnanam. F.D, Cryst.Res.Technol27,92(1992)

[37] Horouchi.N, Letaucheux. F, Robert. M.C, Zyss. J, J. Cryst. Growth 147, 361(1995).

[38] Kalkura.S.N, Devanarayanan.S, J.Cryst.Growth83, 446(1987).

[39] Armington. A. F, O'Connor.J.J, Mater. Res.Bull. 3,923(1968).

[40] Polanyi, M,Z.Physik, 89, 660(1934).

[41] Orowan,E,Z.Physik , 89, 634(1934).

[42] Taylor,G.I,Proc.Roy.Soc.A145, 362(1934).

[43] Burgers, J.M, Proc.Acad.Sci.Amsterdam 42, 293(1939)

[44] Mott, N.F.Nabarro,The strength of solids, Physical soc.London, (1948).

[45] Frank.F.C,Ibid.P.46, (1948).

[46] Horn, F.H,Phil.May.43, 1210(1952).

[47] Vogel.F.L, Phys.Rev.,90, 489,(1953).

[48] Cottrell.A.R, Dislocation and plastic flow in crystals, Oxford University Press, 1980.

[49] Van Bueren.H.G, Imperfections in Crystals, North Holland, 1960.

[50] P. N. Butcher, D. Cotter, The elements of nonlinear optics, Cambridge University Press, Cambridge,1990 .

[51] T. H. Maimnan, Nature 187,493(1960).

[52] P. A. Franken, A. F. Hill, C. W. Peters, Phys.Rev.Lett.7, 118(1961)

[53] N. Bloembergan, Nonlinear Optics, World Scientific, Singapore (1996).

[54] E.G. Sauter, Nonlinear optics. John Wiley& Sons Inc, Newyork (1996).

[55] Y. R. Shen, Principles of nonlinear optics, John Wiley and Sons, Newyork.

[56] L. Wood, F. J. Sharp, Nonlinear Optics& Electro-Optics hand book, McGraw Hill Inc. New York, (1994),

[57] Encyclopedia of lasers and optical technology, Elsevier, London.

[58] V.V. Rampal, .Photonics Elements and devices, Wheeler publishers, Allahabad.

[59] R. A. Fisher (Ed.), Optical Phase Conjugation, Academic press, 1983.

[60] Nalwa.H.S, Miyata.S, Nonlinear optics of Organic Molecules and Polymers, CRC Press, USA, 1997.

****ஜ۞ஜ****

Chapter 2

RELEVENT THEORETICAL ASPECTS

Chapter 2

RELEVENT THEORETICAL ASPECTS

This chapter deals with the fundamental theories of the various experimental techniques used in the present work for the growth of the single crystals and their nonlinear optical characterization. This includes a detailed description of the solution growth and gel growth techniques and the theoretical aspects of the nonlinear phenomena observed in the single crystals.

2.1 INTRODUCTION

The production of perfect single crystals for modern industry demands a thorough knowledge of the science and art of crystal growing. The growth of perfect single crystals has been developed over the years by the complimentary interaction of crystal growth theory and practice. Basic methods have been modified to produce perfect and useful single crystals and to enhance their applicability to specific materials and classes of materials. The overall crystal growth process is rather complex, as it is influenced by numerous interdependent parameters.

2.2 KINETICS OF CRYSTAL GROWTH

If a crystal is in dynamic equilibrium with its parent phase then the free energy will be at its minimum preventing the occurrence of any crystal growth. Therefore to enhance the chance of crystal growth, this equilibrium is disturbed by means of change in temperature, pressure, chemical potential, electrochemical potential or strain. Then the system releases energy to the surrounding to compensate the decrease in entropy due to ordering of atoms in the crystal with the subsequent

evolution of heat of crystallization. Though crystal growth is a non-equilibrium process, it must be kept near equilibrium and as near to a steady state process as possible, because the heat evolved must be removed to the surroundings. Hence for a successful crystal growth experiment, control over the crystal growth environment and consideration of growth kinetics both at macroscopic and at atomic levels are of vital importance.

Growth of crystal can be considered to comprise of three basic steps

1. Achievement of super saturation or super cooling
2. Formation of the crystal nuclei of microscopic size
3. Successive growth of crystal to yield distinct faces.

Nucleation is the precursor of the crystal growth. The condition of super saturation alone is not a sufficient criterion for a system to begin crystallization. Before crystals can start growing there must exist in the solution a number of minute solid bodies known as centres of crystallization, seeds, embryos or nuclei.

In a supersaturated or super cooled system when a few atoms or molecules join together a change in free energy takes place in the process of formation of cluster in a new phase. The cluster consisting of such atoms or molecules is called nuclei. The kinetics of phase change take place in four different steps.

- The development of the supersaturated state, which may arise due to chemical or photochemical reaction or the consequence of a change in temperature, pressure, tension or other chemical or physical condition
- The generation of minute nuclei.
- The growth of nuclei to form particles of microscopic dimensions or domains of the new phase and
- The relaxation process such as agglomeration by which the texture of the new phases changes.

Nucleation may occur spontaneously or it may be induced artificially. Based on this, nucleation is classified into two types.

- Homogenous Nucleation
- Heterogeneous Nucleation

The spontaneous formation of the crystalline nuclei in the interior of the parent phase is called Homogenous Nucleation. If the nuclei form heterogeneously around ions, impurity molecules or on dust particles, on surfaces or at structural singularities such as dislocation or other imperfections, it is called Heterogeneous Nucleation .The nucleation process was understood after realizing the under cooled and supersaturated phases, which refer to the unstable conditions.

All theories of homogeneous nucleation involve the concept of critical nucleus. It is envisaged that as a result of a statistical accident a number of atoms or molecules can come close together and form a rudimental crystal.

2.3 THEORIES OF CRYSTAL GROWTH.

The theories of crystal growth can be divided into two sections, one dealing with growth of ideal crystals and the other dealing with growth of real crystals.

2.3.1Growth of ideal crystals

Gibbs [1] made the first attempt to explain crystal growth on a thermodynamical basis. He considered crystal growth process as phase transformations, which are driven by chemical potential between the crystallizing and nutrient phases. In the case of such a transformation from vapour to solid forming crystals the minimum free energy condition is given by

$$\sum_{i=1}^{n} \sigma_i F_i \text{ is a minimum}$$

where σ_i represents the surface free energy of the i^{th} face of area F_i. The above relation holds for the case where the crystal surface is in equilibrium with its vapour.

Curie [2] and Wulff [3] developed the criterion of minimum free energy. If D_i is the perpendicular distance of the i^{th} face of the crystal from a fixed point inside the crystal, then the volume of the crystal can be written as

$$V = 1/3 \sum_{i=1}^{n} D_i F_i \qquad (2.1)$$

The total energy of the crystal is given by the summation

$$E = \sum_{i=1}^{n} \sigma_i F_i \qquad (2.2)$$

For a very small change in volume

$$dV = \sum_{i=1}^{n} F_i dD_i \qquad (2.3)$$

where one set of faces is assumed to grow at the expense of another.

From equation 2.1

$$dV = 1/3 \sum_{i=1}^{n} (F_i dD_i + D_i dF_i) \qquad (2.4)$$

If the volume is kept constant, dV = 0 and from equations 2.3 and 2.4 we get the relation

$$\sum_{i=1}^{n} D_i dF_i = 0 \qquad (2.5)$$

In the minimum energy criterion if the total free energy is constant and any variation of σ with F is neglected

$$\sum \sigma_i dF_i = 0 \qquad (2.6)$$

and from equations 2.5 and 2.6 we get the relation, $D_i \alpha \sigma_i$, which means that the crystal should form a polyhedron such that the perpendicular distances from a point within the crystal are proportional to the specific free energies of the

appropriate faces. The above theory also implies that on a crystal, the velocities of growth of different faces in the directions of the normals are proportional to the appropriate specific surface free energies.

According to Bravais [4], the velocities of the growth of the different faces of crystal would depend upon the densities of lattice points in various planes, i.e. the reticular density. He also suggested that the velocity of growth in a direction normal to a face would be the slowest for the plane of maximum density. The Bravais theory was further developed to take into account of the effect of symmetry operations on Miller indices and to explain crystal morphology. After the theories of Gibbs and Curie [1, 2], Soehncke [5] introduced the ideal of surface energies by postulating that the faces which possess the greatest reticular densities are those with minimum surface energies, and hence have minimum velocities of growth.

For the purpose of illustration of the growth of a perfect crystal, a model was suggested by Kossel [6] in which the molecules are taken to be cubes stacked face to face. Each cube is attracted equally by all its six neighbours. In the Kossel model, at absolute zero, the low index faces of a crystal have a completely flat surface partially covered by another layer. There are incomplete steps on the surface having exchange sites called kinks. As the temperature is raised, some of the molecules leave the crystal surface acquiring sufficient energy to overcome the binding energy, while some molecules arrive at the surface, leading to an equilibrium state.

A molecule adsorbed on an atomically smooth crystal surface often migrates considerable distances before it becomes a part of the crystal. The distance through which an adsorbed molecule migrates is given by Einstein's formula.

$$x_s^2 = D_s T_s \qquad (2.7)$$

where D_s represents the diffusion coefficient and T_s the mean life period on the surface. In model suggested by Kossel-Stranski

$$x_s \cong a \exp(3\phi/2kT) \qquad (2.8)$$

where a is the intermolecular distance, ⊔ is the strength of the nearest neighbour bond, k is the Boltzmann constant and T is the absolute temperature. In the above expression the second and higher order neighbour bonding is neglected.

The migrating molecules adhere to the kink sites on the steps. BCF theory [7] has shown that at any temperature there exist a finite number of kinks on the steps. The mean, x_0 between the kinks is given by the relation

$$x_0 = \tfrac{1}{2}\, a \exp(\phi / 2kT) \qquad (2.9)$$

As the super saturation is increased more and more molecules join kinks and so the step advances. The rate of advance of a straight step is given by the relation

$$V_d = (\alpha - 1)\, x_s\, \gamma e^{-W/kT} \qquad (2.10)$$

where α is saturation ratio, x_s is the mean distance of diffusion of the adsorbed molecule, γ is a frequency factor which is of the order of atomic frequency of vibration $\approx 10^{13}$ sec^{-1} in the case of monatomic substances, W is the total evaporation energy.

Qualitatively the above equation implies that all molecules which hit the surface in the zone of width $2x_s$ will reach the advancing step and since the concentration of kinks in the step is fairly large, they will be adsorbed.

A curved step with a radius of curvature ρ advances with a velocity

$$v_\rho = v_\infty (1 - \rho_c / \rho) \qquad (2.11)$$

where ρ_c is the critical radius of curvature defined by the relation

$$\rho_c = a\phi / 2kT \ln \alpha) \qquad (2.12)$$

where α is the supersaturation.

On the perfect crystal surface steps are created by thermodynamic fluctuations. Once the step has covered the whole surface, a new layer is to be

initiated. This involves a process by which a monomolecular island is formed on the edges of which growth proceeds. The nucleation of monomolecular island requires additional energy. If it is assumed that only a single nucleus of monomolecular height is formed having a circular shape with radius r then the excess free energy f of the system is given by

$$f(r) = -kT \ln\alpha \, \pi r^2/a^2 + T_s 2\pi r/a \qquad (2.13)$$

where α is the supersaturation and T_s is the surface tension at the interface. Once the nucleus is formed due to thermodynamic fluctuations it will spread and again leave the surface smooth. For further growth a fresh nucleus is to be formed. The growth rate of crystals is governed by nucleation rate rather than the growth velocity of surface steps.

A rigorous analysis of nucleation [7] shows that the nucleus is not circular, and the free energy per unit length of the edge varies with crystallographic direction. The rate of formation of nuclei is given by

$$Z(S/s_0) \exp(-F_0/kT) \qquad (2.14)$$

where Z gives the rate of arrival of fresh molecules at single surface lattice sites, S is the surface area of crystal face under consideration and s_0 is the area per molecule in the layer. F_0 is the maximum surface free energy at critical radius of the nucleus. Substitution of typical values for the different terms in equation 2.14 brings one to the conclusion that nucleation rate is a sensitive function of supersaturation and below a supersaturation of 25-50percent, the probability of nuclei formation is negligible. This was not in agreement with experimental observations [8], where the growth rate was found to be proportional to supersaturation down to values much lower than the critical supersaturation as calculated from the surface nucleation theory. This, therefore, led to the conclusion that the growth of crystals at low supersaturations could only be explained by the fact that real crystals differ from ideal crystals.

2.3.2 Growth of real crystals

It was Smekal [9] who first pointed out that an important difference in the properties of crystals is related to the distinction between ideal and real crystals. Certain properties independent of crystal defects were designated by him as structure –insensitive while those dependent on crystal defects were termed structure – sensitive. The imperfections that explained the structure sensitive properties were lattice flaws, interstitial atoms and dislocations.

A revolutionary breakthrough in the field of crystal growth was presented by Burton et al. [7]. The success of their paper was due to the application of concepts, results and methods of theoretical physics to crystal growth. They gave the existing theories a stronger statistical mechanical foundation and proposed the famous spiral growth theory. The mathematical treatment of the spiral growth theory is summarised as follows. If ω is the rotational velocity, the growth rate is given by the relation

$$R = (\omega / 2\pi)\, h_s \qquad (2.15)$$

where h_s is the step height of the spiral step. Assuming this velocity to be constant with time, the step velocity of the curved step is obtained as

$$V_r = V_s\,(1 - r_c/r) \qquad (2.16)$$

where r_c and r are the radii of the critical and real nuclei respectively and V_r and V_s are velocities of the curved and straight step respectively.

The radius of curvature r of the steps is derived in Cartesian co-ordinates by considering a portion of a circular step, y = f(x) as

$$r = [1 + (y')^2]^{3/2} / y'' \qquad (2.17)$$

The velocity normal to a rotation spiral step is given by the relation

$$V_r = r_0\omega / [1 + r_0^2\,(d\theta/dr_0)^2]^{1/2} \qquad (2.18)$$

where ω is the rotational velocity, r_o is the radius vector and $d\theta$ is an infinitesimal rotation during which the radius changes by dr_o

The velocity of the growing step along the radius of curvature V_r is related to the velocity of a straight step on the surface by (2.16) and therefore

$$V_s(1-r_c/r) = r_o\omega/[1+r_o^2(d\theta/dr_o)^2]^{1/2} \qquad (2.19)$$

which for large values of r_o reduces to give

$$\theta = (\omega/V_s)\, r_o + \text{constant} \qquad (2.20)$$

and for small values of r

$$\theta = (1/2\, r_c)\, r_o + \text{constant} \qquad (2.21)$$

Equations 2.20 and 2.21 represent spiral with constant step spacing, $S_c = 19r_c$. The spiral growth mechanism was shown to be favourable for the rate versus supersaturation data for growth from vapour measured by Volmer and Schultz [8]. Growth spirals are said to have been observed [10] on paraffin crystals by Heck, although these were not recognized as growth spirals because this concept was not then developed. Griffin [11] and later a number of others observed growth spirals through optical and electron microscopic observation techniques [12, 13]. Growth spiral concept is now generally known in crystal growth community and among scientists working in areas where crystallization plays an essential role.

The recent developments in the theory of crystal growth using as a frame of reference the BCF paper [7], have been mentioned in a recent review by Bennema [14]. It is shown here how and where the BCF theory contributed to a narrowing of the gap between theory and experiment.

2.4 GROWTH OF CRYSTALS FROM SOLUTIONS

2.4.1Growth from Pure Solutions

During the growth from pure solutions a solute molecule must break the bonds it has with the solvent and make new bonds in the crystal. It is believed that

new molecules are added only at kinks in steps present on the close packed faces of a growing crystal after a crystal has been growing steadily for some time. The kinks on the monomolecular steps are so numerous [7] that the steps behave as continuous line sinks with a velocity independent of crystallographic orientation and a more or less circular shape indicating the location of the source from which they originated.

The path taken by the solute molecules from the solution to a kink site is not certain. Deposition may either occur directly at the step via volume diffusion or solute molecules may become adsorbed on the surface and migrate to the steps by surface diffusion. Both processes are considered to be active in most cases. Their relative importance should depend on the ratio, $D_vC_{ve}a/D_sC_{se}$, where D_v and D_s are the volume and surface diffusion coefficients, C_{ve} and C_{se} are the equilibrium concentrations of solute in the solution and adsorbed on the surface, and a is the height of a step. The kinetics of crystal growth can be considered in terms of (a) the creation of steps at certain sources and (b) their motion away from the sources. Since the flow of steps away from a source has an influence on the rate of step creation, the latter part is considered first.

Flow of steps

It is clear that the velocity of a step will depend on the proximity of other steps on the surface, for; nearby steps absorb some of the solute. Consider, for example, a series of uniformly spaced straight steps of height, a, separated by distances n^{-1}, where, n is the density of steps normal to their direction of motion. When the steps are very far apart, the velocity of each will be maximum. As the spacing between steps decreases their velocity decreases, becoming a minimum for na= 1. In order to understand whisker growth and morphology changes it is also necessary to consider steps which have a step height equal to a multiple of the lattice spacing.

Sources of steps

Two main types of sources of steps can be distinguished: 1) points of the crystal surface where dislocations with Burger vector having non-zero component

normal to the surface terminate and 2) surface nucleation at any point on a perfect crystal surface.

According to Cabrera and Levine [16], dislocations should be the only possible sources at very low supersaturations when there is no diffusion field near the source. Under these conditions, the rate of formation of new steps at the source

$$\gamma_o = \gamma_\alpha / 19\ \rho_c \qquad (2.22)$$

Where ρ_c is the medium radius of curvature of the step corresponding to the supersaturation σ and is given by

$$\rho_c = \gamma\Omega/KT \ln(1+\sigma) \approx \gamma\Omega/KT\sigma \qquad (2.23)$$

where γ is the surface energy of the edge of the step and Ω is the volume of crystal per molecule. Under steady state conditions the step winds itself into a spiral so that the density of steps away from the source satisfies $\gamma_o = \gamma$ and hence

$$n = 1/19\ \rho_c \qquad (2.24)$$

Since γ_α and ρ_c^{-1} are both proportional to σ, γ_o is proportional to the square of the supersaturation.

For surface nucleation at any point on a perfect crystal surface, new steps must arise by repeated nucleation on the perfect surface of the crystal. Such a process generally requires a very large supersaturation and is observed only rarely.

Two important conclusions of the theory regarding growth in pure solutions are that a single dislocation should be sufficient to grow a large crystal and no mechanism is available for the introduction of further dislocations. But, the presence of a small concentration of impurities provides a simple mechanism for the introduction of dislocations during growth.

2.4.2 Growth from impure solutions

The growth of crystals from solutions containing other solutes, colloidal particles or suspended material is much more complicated than growth from pure solutions. However, the growth of real crystals generally occurs in such solutions, and to grow useful crystals it is very often necessary to make minor additions to the growth solution in order to influence the growth in some desirable way. An understanding of impurity effects is thus of great interest. The effect of impurities on growth kinetics is briefly discussed below.

The rate of growth is often altered by the presence of impurities, usually by way of reducing the growth velocity at a given supersaturation. The effectiveness of an impurity in reducing the growth rate decreases with temperature [17]. In certain cases addition of impurities results in the increase of growth rate at a given supersaturation. For example, halide ions are known to facilitate reactions at mercury electrodes [18] and an increase in the rate of growth in thickness of thin plates of lithium fluoride is brought about by additions of 2×10^{-6} mole fraction of ferric fluoride [19].

If the impurity molecules are immobile on the surface so that they will remain at the points where they reached the surface, the average velocity of advancing step is reduced by the impurities. It is shown that there is a critical supersaturation below which growth is extremely slow. Behind regions of very high impurity content, bunching of steps occurs producing dislocations. In the case of mobile adsorbed impurities, the decrease in velocity due to the impurities will be small. Thus immobile impurities are more effective than mobile ones in retarding and in ultimately stopping the flow of steps and consequently the growth of large crystals.

2.5 BASICS OF NONLINEAR OPTICS

2.5.1 Nonlinear Polarization

Light is transverse electromagnetic (EM) wave. EM field is a vector field. Therefore, in principle, when interaction of light with matter is formulated, the effect of the electric field (E) and magnetic field (B) as well as their directional nature must

be considered. Besides, spatial and temporal variation of E & B is also to be taken into account [20]. However, light- matter interaction in nonmagnetic materials is described in terms of E only. In non-magnetic materials, B is neglected [23]. Magnitude of B is less than that of E.

Based on the concept of harmonic oscillator, the basic Physics of the light matter interaction can be summarized briefly as follows. E of light can interact with charged particles in the matter, mainly electrons and hence distort the equilibrium charge distribution, which results in the separation of unlike charges to produce an electric polarization. The polarization thus generated is related to externally applied electric field through a characteristic property of the medium, called optical susceptibility [21]. It determines the magnitude as well as the direction of induced electric polarization for a given field strength, at a particular wavelength. The magnitude of optical susceptibility depends on various factors such as molecular and atomic structure of the materials, wavelength of excitation and intensity of light [22]. It has been found that when excitation intensity is increased, induced polarization becomes a non-linear function of applied electric field strength [20, 22-24]. The consequences of the nonlinear relationship between E and $\vec{P}$ are that at very high values of light intensity, a number of new and interesting phenomena begin to manifest macroscopically.

In this context, it is highly desirable to examine the strength E associated with light obtained from various sources used for optical excitation and compare the same with interatomic field. E associated with conventional light sources such as Xenon lamp and Mercury lamp, which are mainly used to excite samples in the pre-laser era, is very low in comparison with inter atomic electric field. Because of its low electric field strength, light from conventional sources cannot appreciably perturb the molecular charge distribution. For instance, atomic field is of the order of 10^8 or 10^9 VCm^{-1}[20, 24, 27], whereas electric field strength associated with conventional sources is 10^2-10^5 VCm^{-1}. Under the action of such a low electric field, electrons bound to the nucleus are displaced only by about 10^{-18} m, which is very small in comparison with inter-atomic distance, which is of the order of 10^{-10} m [22]. Therefore, it can be said that this small displacement is within the elastic limit and

hence, there is no anharmonicity in the oscillation of induced polarization. Hence, measurements using conventional light sources give a polarization, $\vec{P}$ which is linearly dependent on electric field strength. $\vec{P}$, in this case can be written as [22]

$$\vec{P} = \varepsilon_0 \chi^{(1)} \vec{E} \qquad (2.25)$$

where ε_0 is the susceptibility of vacuum. This domain of interaction of electric field with matter is referred to as linear optics. Linear effects, also called first order effects, include linear optical properties such as refractive index, linear absorption and birefringence.

With the invention of lasers, which have high degree of spectral purity, coherence and directionality, it has become possible to irradiate atoms and molecules with $\vec{E}$ that is comparable to inter-atomic field. This is because of the fact that lasers can be focused to a very small spot size, of the order of its wavelength, giving very large intensity and consequently extremely high electric field strength, at the focal region. This results in a considerable distortion of the equilibrium charge distribution, which gives rise to a large displacement of electrons with respect to their equilibrium position. Consequently, vibration of the electrons becomes highly unharmonic. It is also interesting to note that, when laser beam is tightly focused, photon density at the focal region approaches atomic density. In such cases, the potential which electrons experience cannot be approximated to a parabolic one. Consequence of this unharmonicity is that unlike in eq.(2.25), induced polarization becomes a function of higher powers of electric field too, i.e. nonlinear dependence on electric field strength. In such cases the polarization is expressed as a power series in the applied field as [26].

$$\vec{P}_{NL} = \varepsilon_0 (\chi^{(1)} E + \chi^{(2)} E^2 + \chi^{(3)} E^3 + \ldots\ldots) \qquad (2.26)$$

Here, $\chi^{(2)}$ and $\chi^{(3)}$ correspond to second order and third order susceptibilities respectively[26]. In the nonlinear optical regime a number of interesting phenomena that are conspicuous by their absence in linear regime emerge. One significant difference between linear and nonlinear optical interactions is that unlike in the linear case, in nonlinear optical processes two light beams can interact and exchange

energy through induced nonlinear polarization of the medium [20]. In the case of very intense laser beams, even air itself can act as nonlinear medium. It is well known that femtosecond laser pulses get self-focused in continuum (white light), which occurs when some materials are irradiated with terra watts of power. Many of these nonlinear optical effects have important scientific and technological relevance. Therefore, study of nonlinear effects is very important. It helps us to understand the mechanism of nonlinearity as well as its spatial and temporal evolution. Besides, detailed knowledge of NLO processes and their dynamics is also essential for the implementation of these techniques in appropriate areas of technology such as optical switching [28], optical communication [29], passive optical power limitation [30-32], data storage [33] and design of logic gates [34-36].

The wavelength at which nonlinear parameters are measured is also important. If the wavelength of excitation is close to one, two or three-photon resonance, resonant enhancement of nonlinearity will occur. At and near resonant frequencies, refractive index becomes a complex quantity. If wavelength of the light interacting with matter is at or near resonance, the power series expansion as in eq.(2.26) is not relevant. In the case of resonant excitation [20] (one photon, two-photon or three-photon), the nonlinear susceptibility term corresponding to resonant absorption can have enormously large magnitude. Generally, resonant nonlinearity has large magnitude but slow response, whereas non-resonant nonlinearity has large magnitude but slow response. Usually, observed nonlinear susceptibility is due to the response of weakly bound outer most electrons of atoms or molecules. However, if the wave length of excitation is valid, the corresponding nonlinearity is called weak nonlinearity. On the other hand, if the frequency of excitation is very close to resonance, power series expansion as in eq. (2.26) is not correct. Such nonlinearity is called strong nonlinearity [20].

2.5.2 Second Harmonic generation

In second harmonic generation, radiation at an incident frequency ω_1 is convened to radiation at twice the frequency of the incident radiation i.e.

$$\omega_2 = 2\omega_1 \qquad (2.27)$$

It is observed only in non-centro symmetric crystals and the constitutive equation typical to second order process under dipole approximation, is given by [23]

$$P_i^{2\omega} = \sum_{j,k=x,y,z} d_{ijk}^{2\omega} E_j^{(\omega)} E_k^{(\omega)} \qquad (2.28)$$

Efficiency of SHG is proportional to phase mismatch parameter Δk as given by the relation [23]

$$\eta_{SHG} \propto \frac{\sin^2(\Delta kl/2)}{(\Delta kl/2)^2} \qquad (2.29)$$

It is obvious that as Δk deviates from zero, the conversion efficiency steadily decreases.

2.5.3 Self Action Effects

Self-action effects are those that affect the propagation characteristics of the incident light beam. They are due to nonlinear polarizations that are at the same frequency as that of the incident light wave. Depending on the particular effect they can change the direction of propagation, the degree of focusing, the state of polarization or the bandwidth of the incident radiation. Self-action effects can also change the amount of absorption of the incident radiation, and sometimes one of these effects can occur alone but more commonly two or more of them occur simultaneously. The most common self-action effects arise from third order interactions. The various types of self-action effects depend on whether the susceptibility is real or imaginary and on the temporal and spatial distribution of the incident light. The real part of the nonlinear susceptibility gives rise to the spatial effects of self-focusing, self-defocusing, spectral broadening and changes in the polarization vector. The imaginary part of the susceptibility causes nonlinear absorption. The important self-action effects are self focusing, self-defocusing, self-phase modulation, nonlinear absorption and saturable absorption.

(a) Self-Focusing

The real part of the third order susceptibility causes a change in the index of

refraction of the material according to the relation

$$n = n_1 - n_2\left\langle E^2 \right\rangle \tag{2.30}$$

Where

$$n_2 = \left(\frac{3}{4n_1}\right)\chi' \tag{2.31}$$

In Eq 2.30 and 2.31 $\left\langle E^2 \right\rangle$ is the time average of the square of the total electric field which is proportional to the intensity, n_1 and n_2 are the linear and nonlinear refractive indices and χ' is the real part of χ. Self-focusing occurs as a result of a combination of a positive value of n_2 and an incident beam that is more intense in the center than at the edge. In this situation the refractive index at the center of the beam is greater than that at its edge and the optical path length at the centre is greater than that for rays at the edge. This is the same condition that occurs for propagation through focusing lens and as result the light beam creates its own positive lens in the nonlinear medium. As the beam gets focused the strength of the nonlinear lens increases causing stronger focusing and increasing the strength of the lens still further. This behaviour results in catastrophic focusing in which the beam collapses to a very intense small spot in contrast to the relatively gentle focusing that occurs for normal lenses. Self-focusing can occur in any transparent material at sufficiently high intensities and has been observed in a wide range of materials including glasses, crystals, liquids, gases and plasmas [24].

(b) Self-defocusing

Self-defocusing results from a combination of a negative value of n_2 and a beam profile that is more intense at the center than at the edge. In this situation the refractive index is smaller at the center of the beam than at the edge, resulting in a short optical path for rays at the center than for those at the edge. This is the same condition that exists for propagation through a negative focal length lens and the beam gets defocused.

(c) Self-Phase Modulation

Self phase modulation results from a combination of a material with a nonlinear refractive index and incident field amplitude that varies in time. Because the index of refraction depends on the optical intensity, the optical phase given by

$$\phi = kz - \omega t = \frac{2\pi}{\lambda}\left[n_0 - \frac{1}{2}n_1|A(t)|^2\right]z - \omega t \qquad (2.32)$$

develops a time dependence that follows the temporal variation of the optical intensity. The phase shift incurred by an optical beam of power P and cross sectional area 'A' traveling a distance in the medium is given by

$$\Delta\phi = 2\pi n_1 \frac{1}{\lambda_0 A} P \qquad (2.33)$$

which is proportional to the optical power P. Self phase modulation is useful in applications in which light controls light. For example it can be used for compression of optical pulses in a manner similar to pulse compression in chirped radar. Pulse compression of factors of 10 or more have been achieved with self phase modulation of pulses propagated freely in nonlinear media resulting in the generation of sub picosecond time range.

(d) Nonlinear Absorption

Self action effects can also change the transmission of light through a material. Nonlinear effects can cause materials that are strongly absorbing at low intensities to become transparent at high intensities in an effect termed 'saturable absorption' or they can cause materials that are transparent at low intensities to become absorbing at high intensities in an effect termed 'multiphoton absorption'. The multiphoton absorption can occur through absorption of two, three or more photons. The photons can be of the same or different frequencies. When the frequencies are different the effect is termed sum frequency absorption.

(e) Saturable absorption

Saturable absorption involves a decrease in absorption at high optical intensities and it is usually observed in materials that are strongly absorbing at low light intensities. Saturable absorption occurs when the upper state of the absorbing transition gains enough population to become filled, preventing the transfer of any more population into it. Saturable absorption is used to mode lock solid state and pulsed dye lasers [25]. It can also be used with four wave-mixing interactions to produce optical phase conjugation [26].

2.6 PHYSICS OF NLO BEHAVIOUR IN ORGANIC MOLECULES

The absorption of radiation in molecules results in the excitation of electrons from their lower occupied states to higher molecular states. There are number of different possible path ways for de-excitation from these higher energy states to the lower states. The most favourable de-excitation path way depends on the type of the molecules and nature of electronic states involved in the process [37]. One of the interesting properties of electronically excited molecules is their tendency to re-emit radiation on returning to the ground state. By the light absorption two excited electronic states can be derived from electronic orbital configuration. In one state, the electron spins are paired and in the other the electron spins are unpaired. A state with paired spins remains as a single state in the presence of a magnetic field and is termed as singlet states. But a state with paired spins can interact with magnetic fields and splits into three quantized states and is termed as triplet states. An energy state is a display of the relative energies of these energy states of a molecule for a given fixed nuclear geometry [38].

The electronic ground state of a molecule is a singlet state and is denoted as S_0. The higher singlet states are denoted as S_1, S_2, S_3 ... S_n. Similarly the higher triplet states are denoted as T_1, T_2, T_3 ...Tn. Each electronic state has a broad continuum of levels and the optical transitions between these continua lead to broad absorption and emission spectra. Transition between singlet states are spin allowed and gives rise to strong absorption bands. Transitions between the ground level of one energy state and the higher vibrational states of the same level are also possible

and these transitions occur within a few picosecond time duration. Decay process included in this type of transitions is non-radiative in nature. From the first excited singlet state S_1 the molecule can relax back radiatively or non-radiatively to the ground state S_0, or cross over to the triplet state. The spontaneous radiative decay from S_1 to S_0 is known as Fluorescence and is governed by the life time of S_1 state. The non-radiative transition from S_1 to S_0 state is known as internal conversion and transition from S_1 to T_1 state is known as intersystem crossing. Similarly the decay from T_1 to S_0 can also be radiative or non-radiative. If this transition is radiative it is termed as Phosphorescence. Typical phosphorescence life times are in the range milliseconds to microseconds and the life time of triplet state is generally large since the triplet-singlet transition is dipole forbidden. Under special experimental conditions the molecules in the ground state S_0 can be excited to higher energy state S_n. These higher states relax back to the S_1 state on a very fast time scale and generally this is of the order of few femto seconds. In certain cases, the T_1 state can be populated by the intersystem crossing. Similarly the higher triplet states can also be populated under suitable conditions through the intersystem crossing in the upper states. Therefore, even though the direct absorption form singlet state to triplet state is forbidden by selection rule it can be populated indirectly and these types of transitions between the energy levels are responsible for most of the nonlinear phenomena observed in organic molecules.

2.7 REFERENCES

[1] J.G.Gibbs, "Collected works", Longman's Green and Co,1928.

[2] P.Curie, Bull. Soc. franc. Miner. 8,145(1885).

[3] W.Wulff, Z. Kristallogr. 34,449(1901).

[4] A.Bravais, " A Etudes Cristallosraphiques" Gauthier Villara, Paris, 1866.

[5] L.Soehncke, " Entwickelung einer Theorie de. Kristallstructur", Leipzig, 1879.

[6] W.Kossel, Nachr. Ges. Wiss. Gottingen, Math-Physik., Kl., 135(1927).

[7] W.K.Burton et al., Phil, Trans. Roy. Soc. London A 243, 299(1951).

[8] M.Volmer and W.Shultz, Z. Phys. Chem. A 156,1(1931).

[9] A.Smekal, Handb. Phys 24,795(1933).

[10] F.C.Frank, " Growth and perfection of crystals" Wiley, N.Y., 1958.

[11] L.J.Griffin, Phil. Mag. 41,196(1950).

[12] A.L.Varma, " Crystal growth and dislocations, Butterworths, London, 1953.

[13] W.Dekeyser , S.Amelinckx, "Les—Dislocations at Ia Croissance Cristalline", Paris, 1955.

[14] P.Bennema, J. Cryst. Growth 69,182(1984).

[15] N.Cabrera, D.A.Vermilyea, " Growth and perfection of crystals", Wiley, N.Y, 1958.

[16] N.Cabrera, M.M.Levine, Phil. Mag. 1,450(1956).

[17] H.C.Buckley, " Crystal growth "Wiley, N.Y.,1958.

[18] J.E.B.Randler, K.W.Somerton, Trans. Far. Soc. 52,951(1948).

[19] G.W.Sears, .J. Chem. Phys. 24, 868(1956).

[20] P. N. Butcher, D. Cotter, The elements of nonlinear optics, Cambridge University Press, Cambridge,1990 .

[21] T. H. Maimnan, Nature 187,493(1960).

[22] P. A. Franken, A. F. Hill, C. W. Peters, Phys.Rev.Lett.7,118(1961)

[23] N. Bloembergan, Nonlinear Optics, World Scientific, Singapore (1996).

[24] E.G. Sauter, Nonlinear optics. John Wiley& Sons Inc, Newyork (1996).

[25] Y. R. Shen, Principles of nonlinear optics, John Wiley and Sons, Newyork.

[26] L. Wood, F. J. Sharp, Nonlinear Optics& Electro-Optics hand book, McGraw Hill Inc. New York, (1994),

[27] Encyclopedia of lasers and optical technology, Elsevier, London.

[28] V.V. Rampal, .Photonics Elements and devices, Wheeler publishers, Allahabad.

[29] R. A. Fisher (Ed.), Optical Phase Conjugation, Academic press, 1983.

[30] B. L. Davies,M. Samoc, Current Opinion in Solid State and Mater science, p. 213, (1997),

[31] W. Yau, C. H. Lee, I. Wang. J. Opt. Soc. Am. B. 17,1626 (2000) .

[32] M. Tadakuma, S. Namiki, Furukawa Review, 19, 63 (2000).

[33] D Dini, M. Barthel, H. Hanack, Eur. J. Org. Chem.p3759 (2001).

[34] G.H. He, C Weder, P Smith and P N Prasad,. IEEE.J.OE, 34,2279 (1998).

[35] H. Ditlbacher, S. R. Krenn, B. Lamprecht, A. Leitner, Opt.Lett.25,653(2000).

[36] A. Bhardwaj, K. Vahala,, J. Opt. Soc. Am. B 18,657 (2001).

[37] K.K.R.Mukherjee, Fundamentals of Photo- Chemistry, Wiley Eastern Ltd., New Delhi, (1992).

[38] S Venugopal Rao, Ph.D. Thesis, School of physics, University of Hyderabad, India.

****ꕥ****

Chapter 3

CHARECTERISATION TOOLS AND TECHNIQUES

Chapter 3

CHARACTERISATION TOOLS AND TECHNIQUES

3.1 INTRODUCTION

The advent of sophisticated instruments has improved in analysing materials for their chemical and physical properties. The aim of this section is to present a comprehensive description on the techniques that are followed to characterise the crystal samples in the present research work. The instrumentation used in each case is basically described, without entering into details.

3.2 X-RAY POWDER DIFFRACTION

Much of what we know about the architecture of molecules is derived from studies on the diffraction of X- rays by crystals. This method was first used by Bragg in 1913. Since then X-ray and neutron diffraction techniques have helped to establish detailed features of the molecular structure of every kind of stable chemical species in a crystalline form, from the simplest to those with many thousands of atoms [1-4].

An X-ray incident upon a sample will either be transmitted, in which case it will continue along its original direction, or it will be scattered by the electrons of the atoms in the material. All the atoms in the path of the X-ray beam scatter X-ray. In general, the scattered waves destructively interfere with each other, with the exception of special orientations at which Bragg's law given by the equation $N\lambda=2d\sin\theta$ is satisfied. The phenomenon of diffraction occurs when penetrating radiation, such as X-rays, enters a crystalline substance and is scattered. The direction and intensity of the scattered (diffracted) beams depend on the orientation of the crystal lattice with respect to the incident beam. Any face of a crystal lattice

consists of parallel rows of atoms separated by a unique distance (d – spacing), which are capable of diffracting X – rays. In order for a beam to be 100% diffracted, the distance it travels between rows of atoms at the angle of incidence must be equal to an integral multiple of the wavelength of the incident beam.

An X – ray diffractometer (Rigaku, Japan) utilizes a powdered sample [5, 6], a goniometer and a fixed – position detector to measure the diffraction pattern of unknowns. The powdered sample provides (theoretically) all possible orientations of the crystal lattice, the goniometer provides a variety of angles of incidence and the detector measures the intensity of the diffracted beam. The resulting analysis is described graphically as a set of peaks with percentage intensity on the Y axis and goniometer angle on the X axis. The exact angle and intensity of a set of peaks is unique to the crystal structure being examined. The X – ray diffraction method is most useful for qualitative, rather than quantitative analysis (although it can be used for both). The monochromator is used to ensure that a specific wavelength reaches the detector, eliminating fluorescent radiation. The resulting trace consists of a recording of the intensity Vs counter angle (2θ). The trace can then be used to identify the phases present in the sample. Diffracted data from many materials has been recorded in a computer searchable Powder Diffraction file (JCPDS file. Matching the observed data allows the phases in the sample to be identified.

In the present study we have employed a Bruker D8 advance diffractometer, operating at 40 KV and 50mA, using Cu target and graphite monochromator. The intensity data is recorded by continuous scan from 5° to 60° with a step size of 0.02°and scan speed of 4°/minute. The structure is refined by Pawley method [7] using the TOPAZ R version 3 program [8].

3.3 ELEMENTAL ANALYSIS

3.3.1 CHN analysis

The elemental analysis of a compound is particularly useful in determining the empirical formula of the compound. The empirical formula is the formula for a compound that contains the smallest set integer ratios for the elements in the compound that gives the correct elemental composition by mass. The most common

form of elemental analysis, CHN analysis, is accomplished by combustion analysis. In this technique, a sample is burned in an excess of oxygen, and various traps collect the combustion products — carbon dioxide, water, and nitric oxide. The weights of these combustion products can be used to calculate the composition of the unknown sample.

The analysis of results is performed by determining the ratio of elements from within the sample, and working out a chemical formula that fits with those results. This process is useful as it helps to determine if the sample examined has the desired composition and confirms the purity of a compound. The accepted deviation of elemental analysis results from the calculated is 0.4%.

In our study, chemical composition of the grown crystals determined by carbon, hydrogen, nitrogen (CHN) analysis using VarioEL III CHNS serial number 11035060 is compared with the theoretical values of carbon, hydrogen and nitrogen present in the crystals.

3.3.2 Energy dispersive X-ray (EDX) analysis

It is a technique used for identifying the elemental composition of the specimen. The EDX analysis system works as an integrated feature of a scanning electron microscope (SEM), and cannot operate on its own without the latter [9, 10]. During EDX Analysis, the specimen is bombarded with an electron beam inside the scanning electron microscope. The bombarding electrons collide with the specimen atom's own electrons, knocking some of them off in the process.

The EDX spectrum is a plot of intensity of X-rays vs energy of the emitted X-rays. An EDX spectrum normally displays peaks corresponding to the energy levels for which the most X-rays have been received. Each of these peaks is unique to an atom, and therefore corresponds to a single element. The higher the intensity of peak in a spectrum, the more concentrated is the element in the specimen. An EDX spectrum plot not only identifies the element corresponding to each of its peaks, but the type of X-rays to which it corresponds as well. For example, a peak corresponding to the amount of energy possessed by X-rays emitted by an electron in

the L-shell going down to the K-shell is identified as a K_α peak. The peak corresponding to X-rays emitted by M-shell electrons going to the K-shell is identified as a K_β peak as shown in figure 3.1

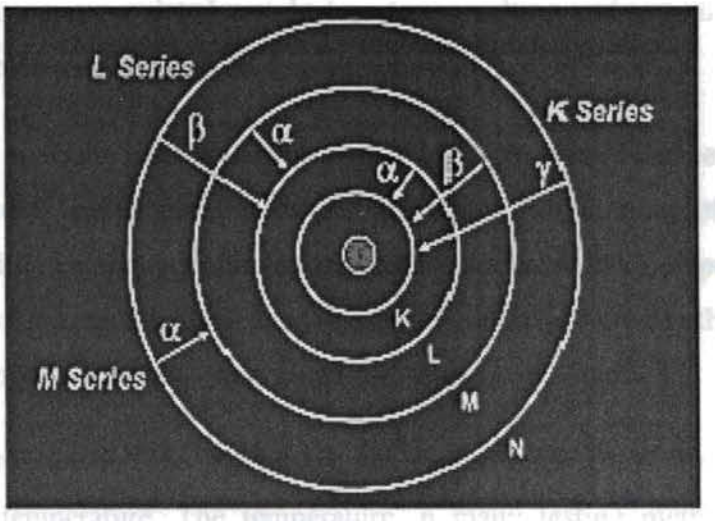

Figure.3.1 Electronic transitions showing the emission of X- rays

3.4 THERMAL CHARECTERISATION

3.4.1 TGA/DTA analysis

Thermo gravimetric Analysis (TGA) is a type of thermo analytical testing performed on materials to determine changes in weight in relation to changes in temperature. TGA relies on a high degree of precision in three measurements: weight, temperature, and temperature change. As many weight loss curves look similar, the weight loss curve may require transformation before results may be interpreted. A derivative weight loss curve can be used to tell the point at which weight loss is most apparent. TGA is commonly employed in research and testing to determine characteristics of materials, to determine degradation temperatures, absorbed moisture content of materials, the level of inorganic and organic components in materials, decomposition points of explosives, and solvent residues.

A simultaneous TGA-DTA measures both heat flow and weight changes in a material as a function of temperature or time in a controlled atmosphere. Simultaneous measurement of these two material properties not only improves productivity but also simplifies interpretation of the results. The complimentary information obtained allows differentiation between endothermic and exothermic events which have no associated weight loss (e.g., melting and crystallization) and those which involve a weight loss (e.g., degradation).

A TGA analyser usually consists of a high-precision balance with a pan (generally platinum) loaded with the sample. The pan is placed in a small electrically heated oven with a thermocouple to accurately measure the temperature. The atmosphere may be purged with an inert gas to prevent oxidation or other undesired reactions. A computer is used to control the instrument.

Analysis is carried out by raising the temperature gradually and plotting weight against temperature. The temperature in many testing methods routinely reaches 1000°C or greater, but the oven is so greatly insulated that an operator would not be aware of any change in temperature even if standing directly in front of the device. After the data is obtained, curve smoothing and other operations may be done such as to find the exact points of inflection.

A method known as hi-res TGA is now often employed to obtain greater accuracy in areas where the derivative curve peaks. In this method, temperature increase slows down as weight loss increases. This is done so that the exact temperature at which a peak occurs can be more accurately identified. Several modern TGA devices can vent burn off to a Fourier-transform infrared spectrophotometer to analyze composition.

In Differential thermal analysis (DTA), the material under study and an inert reference are made to undergo identical thermal cycles, while recording any temperature difference between sample and reference [11]. This differential temperature is then plotted against time, or against temperature (DTA curve or thermogram). Changes in the sample, either exothermic or endothermic, can be detected relative to the inert reference. Thus, a DTA curve provides data on the

transformations that have occurred, such as glass transitions, crystallization, melting and sublimation. The area under a DTA peak is the enthalpy change and is not affected by the heat capacity of the sample.

A DTA consists of a sample holder comprising thermocouples, sample containers and a ceramic or metallic block, a furnace, a temperature programmer, and a recording system. The key feature is the existence of two thermocouples connected to a voltmeter. One thermocouple is placed in an inert material such as Al_2O_3, while the other is placed in the sample of the material under study. As the temperature is increased, there will be a brief deflection of the voltmeter if the sample is undergoing a phase transition. This occurs because the input of heat will raise the temperature of the inert substance, but be incorporated as latent heat in the material changing phase [12].

We have used a Perkin Elmer simultaneous TGA/DTA instrument for the thermal analysis of the grown crystals.

3.4.2 Differential scanning calorimetry

Differential scanning Calorimetry (DSC) is a dynamic thermal analysis technique, with which thermal behaviour of any sample can be studied over a wide temperature range, under non isothermal conditions. Whenever a material under goes a change in its physical state such as melting or transition from one crystalline form to another or whenever it reacts chemically, heat is either absorbed or liberated. Many such processes can be initiated simply by raising the temperature of the material. In DSC, the enthalpies of these processes are determined by measuring the differential heat flow required to maintain a sample material and an inert reference at the same temperature. This temperature is usually programmed to scan a temperature range by increasing linearly at a predetermined rate. Thermal changes in a sample are due to exothermic or endothermic enthalpic transitions or reactions. Such enthalpic changes can be caused by phase changes, fusion, crystalline inversions, boiling, sublimation, vaporization, oxidation, reduction or other chemical reactions. Generally, phase transitions, dehydration, reduction and some decomposition reactions are endothermic in nature, whereas crystallization, oxidation and some

decomposition reactions are exothermic. The phenomenon of glass transition exhibits itself in a DSC curve as an endothermic baseline shift. Although DSC yields data, which are inherently more qualitative and more amenable to theoretical interpretation than the differential thermal analysis (DTA) data, it does not seem to have been used as widely as the latter. The DSC technique has been applied, however, to diverse types of compounds and reviews on the application of DSC to petroleum products, plastics, biological systems and metal complexes, single crystals, etc. have appeared [13- 15] in literature.

The relative advantages of the DSC over conventional calorimetric technique are [16] (i) rapidity in the determination of thermal properties over a wide temperature range (ii) small amounts of sample required for measurements (iii) easy data analysis procedure and (iv) ability to study many different types of reactions. The main disadvantages of this technique are (i) relatively low accuracy and precision (5—10% accuracy), (ii) inability to conveniently determine the ΔH of overlapping reactions and (iii) inaccuracy in the determination of peak areas due to baseline changes during the transition or reaction.

We have used a Perkin-Elmer differential calorimeter in the present study. Usually, the differential scanning calorimeter is programmed to scan a temperature range by changing at a linear rate over a temperature ramp for the study of the endothermic and exothermic reactions. With the liquid nitrogen the temperature can be varied from $\approx$ 77 K to 1000 K. Before any quantitative measurements are made the calorimeter must be calibrated and fix the temperature scale accurately. Correct sampling techniques must also be used. High purity metals with accurately known enthalpies of fusion are generally used as calibration standards. The most commonly used calibrants are Indium and Zinc, which can be used to calibrate the instrument over a wide temperature range.

Differential scanning calorimetry can also be used to measure the specific heat C_p of materials. When a sample material is subjected to a linear temperature increase, the rate of heat flow into the sample is proportional to the instantaneous specific heat. By measuring this rate of heat flow as a function of temperature and comparing it with a standard material under the same conditions, one can obtain the

specific heat Cp as a function of temperature [16, 17].

The procedure is briefly described as follows. Empty aluminium pans are placed in the sample and reference holders. An isothermal base line is recorded at the lower temperature and the temperature is then programmed to increase over a range. An isothermal baseline is then recorded at the higher temperature as indicated in the lower part of Fig. 3.2. The two isothermal baselines are used to interpolate a baseline over the scanning section as shown in the upper part of Fig. 3.2. The procedure is repeated with known mass of sample in the sample pan and a trace of dH/dt against time is recorded. There is a pen displacement due to the absorption of heat by the sample, then

$$dH/dt = m\, C_p\, dT_p/dt \qquad (3.1)$$

where m is the mass of the sample in grams, C_p, is the specific heat and dT_p/dt is the programmed rate of temperature increase.

This equation could be used to obtain values of C_p directly, but any errors in ordinate read-out dH/dt, and in programming rate dT_p/dt, would reduce the accuracy. To minimize these errors the procedure is repeated with a known mass of sapphire, the specific heat of which is well established [17] and a new trace is recorded. Thus at any temperature T,

$$K\, y = m\, C_p\, dT/dt \qquad (3.2)$$

$$K\, y' = m' C_p'\, dT/dt \qquad (3.3)$$

where y and y' are the ordinate deflections due to the sample and the standard respectively, m' and C_p' are the mass and specific heat of the standard, and K is the calibration factor in Joules cm^{-1} sec^{-1}.

Dividing equation (3.2) by equation (3.3) and rearranging terms

$$C_p / C_p' = m'y/my' \qquad (3.4)$$

Thus the calculation requires only the comparison of two ordinate deflections at the

same temperature.

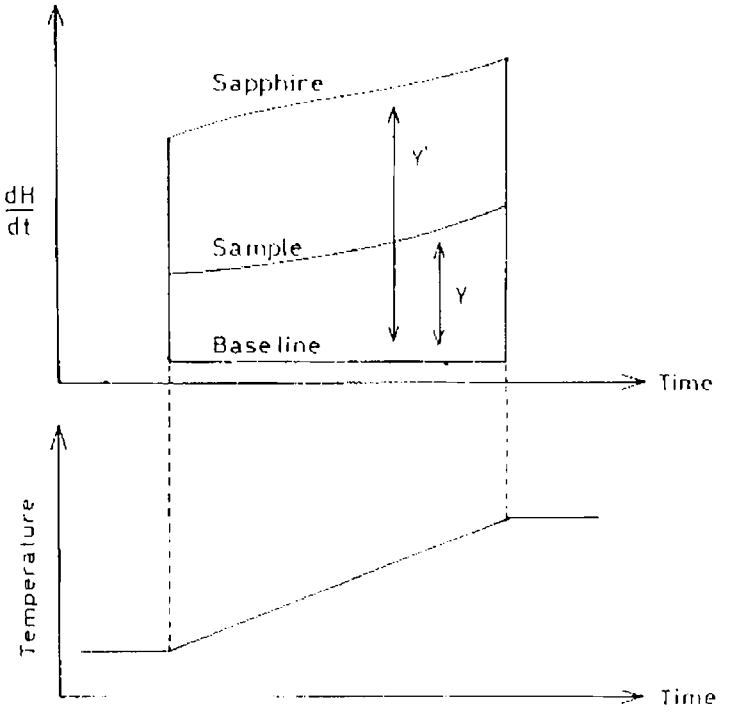

Fig 3.2 specific heat determination by ratio method

3.5 OPTICAL CHARACTERISATION

3.5.1 UV/VIS/NIR absorption spectroscopy

A number of different optical phenomena may be associated with the incidence of light on a crystalline solid, including reflection, refraction, absorption, and transmission. A variety of electronic processes may contribute to these observed phenomena. Figure 3.3 shows a schematic representation of optical absorption as a function of wavelength of the incident electromagnetic radiation [18- 22]. From higher to lower energies the processes involved are optical excitation (1) to and from energy bands with greater energy separation than the uppermost occupied band and the next-higher-lying empty band, (2) of excitons, (3) from the uppermost occupied levels to the next-higher-lying empty band, (4) from an imperfection to a band, from a band to an imperfection, or within the energy levels of an imperfection, (5) of free

carriers to a higher energy state in the same band, and (6) of a Reststrahlen mode of the lattice vibrations.

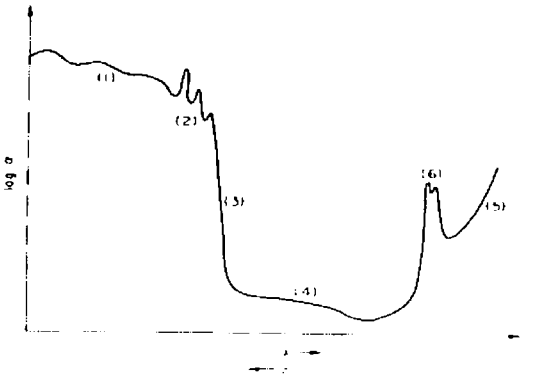

Fig 3.3 Schematic display of different types of optical absorption typically found in crystals. (1) Transition to high-lying bands, (2) excitons, (3) absorption edge for valence-band-to-conduction-band transition, (4) imperfection, (5) free-carrier absorption, and (6) Reststrahlen absorption.

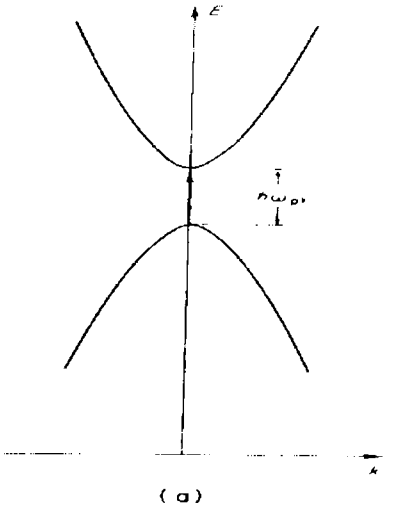

Fig 3.4 Direct optical transition between two bands with extrema at K=0

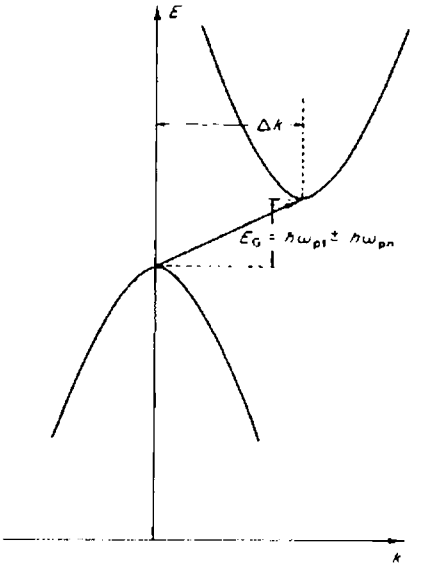

(b)

Fig 3.5 Indirect optical transition from the top of the valence band at k=0 to the bottom of the conduction band at some finite value of k.

Information about the band structure of a material can be obtained if accurate measurements can be made of optical absorption for photon energies near that of the absorption edge. This is because a band structure with extrema at the same point in k space involves optical absorption without the emission or absorption of phonons, whereas a band structure with the conduction and valence band extrema at different points in k space requires absorption or emission of phonons in the optical absorption process. Since a direct transition, the one not involving phonons, has a different dependence on photon energy from that of an indirect transition, which is the one involving phonons, it is possible in principle to deduce which is present in a given material by optical absorption measurements [24- 26].

The direct transition is a first-order process and therefore has larger values of the absorption constant than are found for the indirect transition, which is a second-order process. Since the indirect transition can involve a distribution of states in

conduction and valence bands, the difference in absorption constant between the two types of transition is not as large as might be expected.

The photon absorption in many crystalline materials is found to obey the Tauc relation given by,

$$(\alpha h\upsilon) = A (h\upsilon - E)^{n}$$

Here α is the absorption coefficient in eVm^{-1}, $h\upsilon$ the photon energy, A is a constant and the index n is connected with the distribution of the density of states. For direct allowed transition energy gap, n=1/2 and for indirect allowed transition energy gap, n=2.

In the present work we have used Jasco V 570 UV/VIS/NIR Spectrometer for charting the diffuse reflectance spectrum of the sample. It has a spectral range of 180 – 2500 nm. The experimental set up of a generic UV/ VIS/ NIR spectrometer is as shown in Fig.3.6.

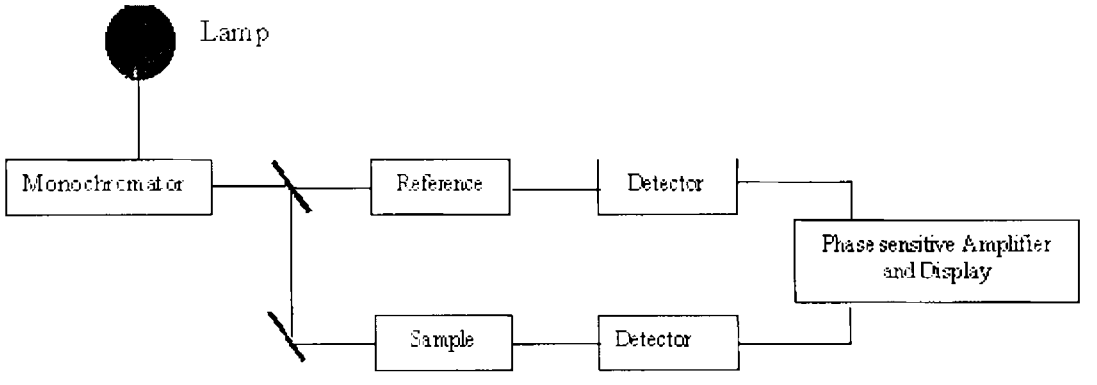

Fig 3.6 Schematic plot of a UV/Vis/NIR spectrophotometer

The refractive index (n) and the extinction coefficient (k) and the absorption coefficient (α) are determined from the transmission (T) and reflection (R) spectrum of the samples [20, 24]

$$T = (1-R)^{2} \exp(-\alpha t) / 1-R^{2} \exp(-\alpha t) \qquad (3.5)$$

where t is the thickness of the sample and the absorption coefficient α is related to extinction coefficient K (absorption index) by

$$K = \alpha \lambda / 4\pi \quad (3.6)$$

For semiconductors and insulators ($k^2 << n^2$), there exists a relationship

$$R = (n - 1)^2 / (n + 1)^2 \quad (3.7)$$

The relationship between dielectric constant ε and k is given by [27]

$$\varepsilon = \varepsilon_r + i\varepsilon_i = (n + ik)^2 \quad (3.8)$$

$$\varepsilon_r = n^2 - k^2 \quad (3.9)$$

$$\varepsilon_i = 2nk \quad (3.10)$$

Hence by analysing the UV/VIS/NIR spectrum, we can obtain the variation in the refractive index, dielectric constant, extinction coefficient with wavelength or energy.

3.5.2 Photoluminescence studies

Photoluminescence is a process in which a chemical compound absorbs a photon with a wavelength in the range of visible electromagnetic radiation, thus transitioning to higher electronic energy state, and then radiates a photon back out, returning to a lower energy state. The period between absorption and emission is typically extremely short, of the order of 10 nanoseconds. Photoluminescence spectroscopy is a contactless, nondestructive method of probing the electronic structure of materials. Light is directed on to a sample, where it absorbs and imparts excess energy into the material in a process called "photo-excitation". One way this excess energy can be dissipated by the sample is through the emission of light, or luminescence. In the case of photo excitation, this luminescence is called "photoluminescence". The intensity and spectral content of this photoluminescence is a direct measure of various important material properties [28].

Specifically, photo-excitation causes electrons within the material to move into permissible excited states. When these electrons return to their equilibrium states, the excess energy is released and may include the emission of light (a radiative process) or may not (a non radiative process). The energy of the emitted light—or photoluminescence—is related to the difference in energy levels between the two electron states involved in the transition—that is, between the excited state

and the equilibrium state. The quantity of the emitted light is related to the relative contribution of the radiative process.

In the present study we have used a Flurolog 3 Spectrofluorometer (model FL 3-22) having double excitation and emission spectrometers, with a source of 450 W xenon lamp and the detector employed is a photo multiplier tube.

3.6 SURFACE ANALYSIS

3.6.1 Optical microscopy

Structural and geometrical investigation of the surface features of a crystal is the most fundamental step in characterizing a crystal. The surface studies also provide information regarding the nature and distribution of imperfections in a crystal.

The surface features and etch patterns of the grown crystal is studied using an optical microscope attached to personal computer for viewing the microstructure of the crystal surface. It has a large binocular polarizing microscope with versatile functions. It can be used for bright field, dark field, polarizing light and phase contrast. The lamp housing can be adjusted for reflected or transmitted position along with the filter. Magnifications of 50, 100,200, 1000 times are possible with adjustable objectives.

3.6.2 Scanning electron microscope (SEM)

The Scanning Electron Microscope (SEM) is a microscope that uses electrons rather than light to form an image [9]. The SEM has a large depth of field, which allows a large amount of the sample to be in focus at one time. It also produces images of high resolution, which means that closely spaced features can be examined at a high magnification. Preparation of the samples is relatively easy since most SEMs only require that sample should be conductive. The combination of higher magnification, larger depth of focus, greater resolution, and ease of sample observation makes the SEM one of the most heavily used instruments in current research and development. The electron beam comes from a filament, made of a loop

of tungsten that functions as the cathode. A voltage is applied to the loop, causing it to heat up. The anode, which is positive with respect to the filament, forms powerful attractive forces for electrons. This causes electrons to accelerate toward the anode. The anode is arranged, as an orifice through which electrons would pass down to the column where the sample is held. The streams of electrons that are attracted through the anode are made to pass through a condenser lens, and are focused to very fine point on the sample by the objective lens. The electron beam hits the sample, producing secondary electrons from the sample. These electrons are collected by a secondary detector or a backscatter detector, converted to a voltage, and amplified. The amplified voltage is applied to the grid of the CRT that causes the intensity of the spot of light to change. The image consists of thousands of spots of varying intensity on the face of a CRT that corresponds to the topography of the sample.

Figure 3.7 shows the interaction of electrons with matter in a scanning electron microscope.

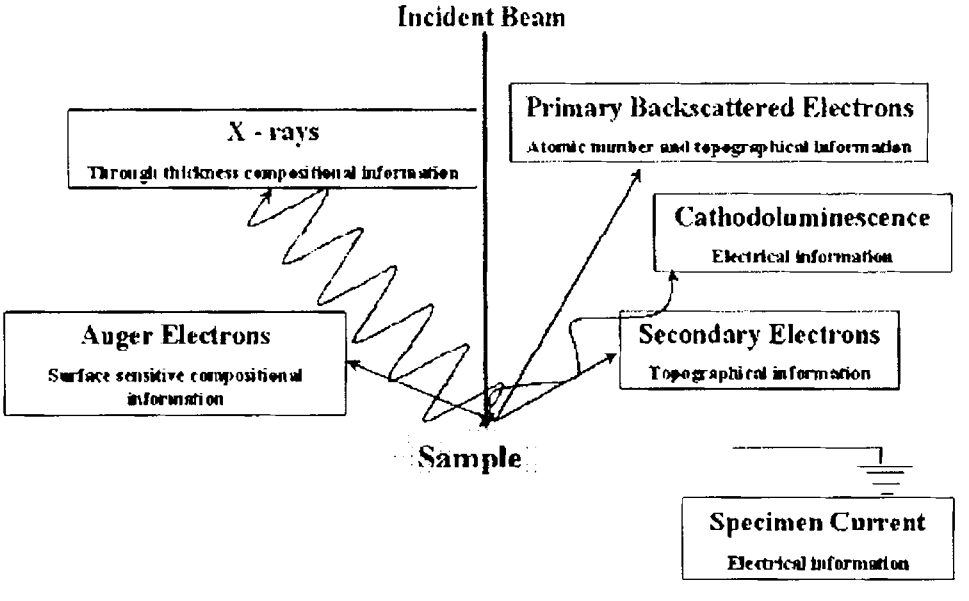

Figure. 3.7 In a SEM, interaction of electron with the sample produces both photons and electrons

3.7 VIBRATIONAL SPECTRAL ANALYSIS

3.7.1 Fourier transform infrared spectroscopy

Infrared spectroscopy is a very useful technique for characterisation of materials that gives information about the composition and the structure of molecules. The advantages of infrared spectroscopy include wide applicability, nondestructiveness, measurement under ambient atmosphere and the capability of providing detailed structural information. Infrared spectroscopy by Fourier transform (FTIR) has additional merits such as: higher sensitivity, higher precision, quickness of measurement and extensive data processing capability[29-33].

IR spectra originate in transitions between two vibrational levels of a molecule in the electronic ground state and are usually observed as absorption spectra in the infrared region. For a molecule to present infrared absorption bands it is needed that it has a permanent dipole moment. When a molecule with at least one permanent dipole vibrates, this permanent dipole also vibrates and can interact with the oscillating electric field of incident infrared radiation. In order for this normal mode of vibration of the molecule to be infrared active, that is, to give rise to an observable infrared band, there must be a change in the dipole moment of the molecule during the course of the vibration.

If the vibrational frequency of the molecule, as determined by the force constant and reduced mass, equals the frequency of the electromagnetic radiation, then adsorption can take place. As the frequency of the electric field of the infrared radiation approaches the frequency of the oscillating bond dipole and the two oscillate at the same frequency and phase, the chemical bond can absorb the infrared photon and increase its vibrational quantum number by +1, or what is the same, increase its vibrational state to a higher level.

As a first approximation, the larger the strength of the bond the higher the frequency of the fundamental vibration. In the same way, the higher the masses of the atoms attached to the bond the lower the wave number of the

fundamental vibration. As a general guide, the greater the number of groups of a particular type and more polar the bond, the more intense is the band.

The infrared spectrum can be divided into two regions, one called the functional group region and the other the fingerprint region. The functional group region is generally considered to range from 4000 to 1500 cm^{-1} and all frequencies below 1500 cm^{-1} are considered characteristic of the fingerprint region. The fingerprint region involves molecular vibrations, usually bending motions, that are characteristic of the entire molecule or large fragments of the molecule [35, 36]. Thus these are used for identification of the material. The functional group region tends to include motions, generally stretching vibrations, which are more localised and characteristic of the typical functional groups, found in organic molecules. While these bands are not very useful in confirming identity, they do provide some very useful information about the nature of the components that make up the molecule.

Basically an IR spectrometer is composed by the source, the monochromator and the receptor. The ideal IR source would be one that would give a continuous and high radiant energy output over the entire IR region [34]. The two sources in most common use are the Nernst Glower (heated up to 2200K) and the Globar (heated to about 1500K). In general, in all IR sources the radiant energy, which depends upon the temperature of the source, is low in the far infrared, and to obtain sufficient energy the slit width of the source has to be opened considerably with a corresponding decrease in resolution.

Between the source and the detector there must be some kind of device to analyse the radiation so that intensity can be evaluated for each wavelength resolution element. There are two basic types, namely, monochromators, used in dispersive instruments, and interferometers used in Fourier transform instruments. In a monochromator, a prism or a diffraction grating is used, separating the components of polychromatic radiation. For spectroscopic work a prism must be transparent to the particular wavelength region of interest and the dispersion of the prism must be as large as possible.

The final part of the spectrometer is the detector. The IR detector is a device that measures the IR energy of the source that has passed through the spectrometer. Their basic function is to change radiation energy into electrical energy, which can be generated to process a spectrum.

In the case of FTIR spectroscopy the spectra are recorded in the time domain followed by computer transformation into the frequency domain, rather than directly in the frequency domain, as is done by dispersive IR spectrometers. To record in the time domain, interference has to be used to modulate the IR signal at a detectable frequency. This is done by means of the well known Michelson interferometer, which is used to produce a new signal (interferogram) of a much lower frequency which contains the same information as the original IR signal.

Figure 3.8 gives the schematic representation of a FTIR spectrometer. In the FTIR instrument, the sample is placed between the output of the interferometer and the detector. The sample absorbs radiation of particular wavelengths. Therefore, the interferogram contains the spectrum of the source minus the spectrum of the sample. An interferogram of a reference (sample cell and solvent) is needed to obtain the spectrum of the sample. After an interferogram has been collected, a computer performs a fast Fourier transform, which results in a frequency domain trace (i.e. intensity vs. wave number).

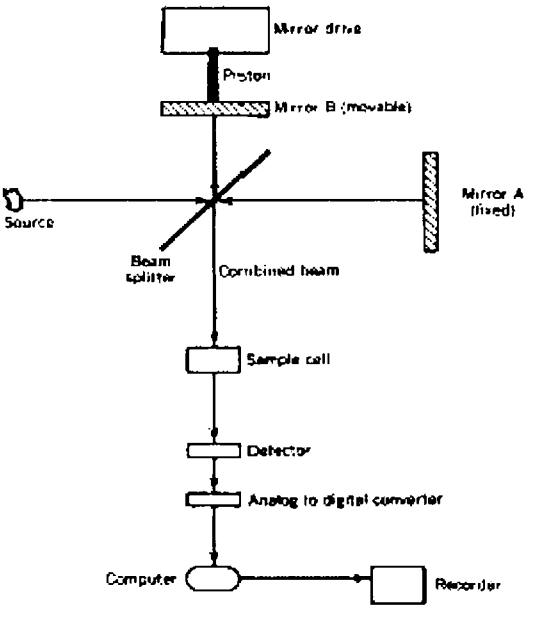

Fig.3.8 Schematic representation of FTIR spectrometer

Fourier transform infra red spectrum of the crystal is taken with AVTAR 370 system with a resolution of $4cm^{-1}$ in the range 400-$4000cm^{-1}$.

3.7.2 Raman spectroscopy

The energy of a molecule or ion consists in four components that for a first approximation can be treated separately : the translational energy, the rotational energy, the vibrational energy and the electronic energy. When the molecule is placed in an electromagnetic field, a transfer of energy from the field to the molecule will occur only when the difference in energy between two quantified states equals hυ, h being the Planck's constant and υ the frequency of light.

When a molecule has n atoms there are 3n-6 independent vibrations (3n degrees of freedom minus the three coordinates related to translational and rotational movement). For linear molecules, there are 3n-5 independent vibrations. These so-called normal vibrations can be observed by different techniques but especially by infrared and Raman scattering. Both rotation and vibration of molecules are involved in the absorption of infrared radiation, but since molecular rotation is not usually resolved in most infrared and Raman spectra, we will ignore this additional consideration [35].

Raman spectroscopy is an invaluable technique for characterisation of materials. Because of its higher resolution with respect to FTIR spectroscopy and its versatility and simplicity in terms of sample handling and the possibility of acquisition of the whole spectra (4000 to 10 cm^{-1}) with the same instrument, Raman, and specially micro-Raman spectroscopy has actually an increasing use versus other similar spectroscopic techniques.

Raman spectra originate in the electronic polarisation caused by UV or visible light. The mechanism by which the incident radiation interacts with the molecular vibrational energy levels has its origins in the general phenomenon of light scattering, in which the electromagnetic radiation interacts with a pulsating deformable (polarisable) electron cloud, this interaction is being modulated by the

molecular vibrations, i.e., it depends on the chemical structure of the molecules responsible for the scattering.

If a molecule is irradiated by monochromatic light of frequency υ having electric field strength E, because of the electronic polarisation induced in the molecules by this incident light, it presents an induced dipole moment P that, at low E values, can be expressed as:

$$P = \alpha E$$

Where α is the polarizability tensor.

In normal Raman scattering the polarizability tensor is symmetric ($\alpha_{xy} = \alpha_{yx} = \alpha_{zy}$). In molecules α is not constant since certain vibrations and rotations can cause α to vary. The intensity of a Raman band depends on the polarizability of the molecule, the source intensity, the concentration of active groups, and other factors. Without absorption, the intensity of the Raman emission rises with the fourth potence of the source frequency. The Raman intensities are directly proportional to the concentration of active species [37].

Since Raman lines represent frequency differences from the incident frequency, they are also called Raman shifts and are designated in cm^{-1}. They are independent of the excitation wavelength. As a result, the anti-Stokes lines are weaker than the red shifted spectrum where they appear as Stokes lines. The ratio of the intensities of equivalent pairs of lines $I_{anti\text{-}Stokes}/I_{Stokes}$ falls as the vibrational frequency increases, and decreases with temperature [38].

A typical current Raman spectrometer incorporates (fig.3.9):

1. The illumination source composed of an Nd-YAG laser, sometimes coupled to a dye laser or a solid state titanium sapphire laser providing tunable radiation.

2. A macro sample chamber and a classical optical microscope for microanalysis.

3. A dispersive system composed of a double monochromator and a spectrograph. The two monochromators can be used either in subtractive mode to provide a wide field to the spectrograph or in additive mode when higher resolution is required. The double monochromator has one or two slits in between the first and second stage monochromators.

4. The detection system, which includes a multichannel detector (a linear diode array) and a photomultiplier connected to a single photon counter.

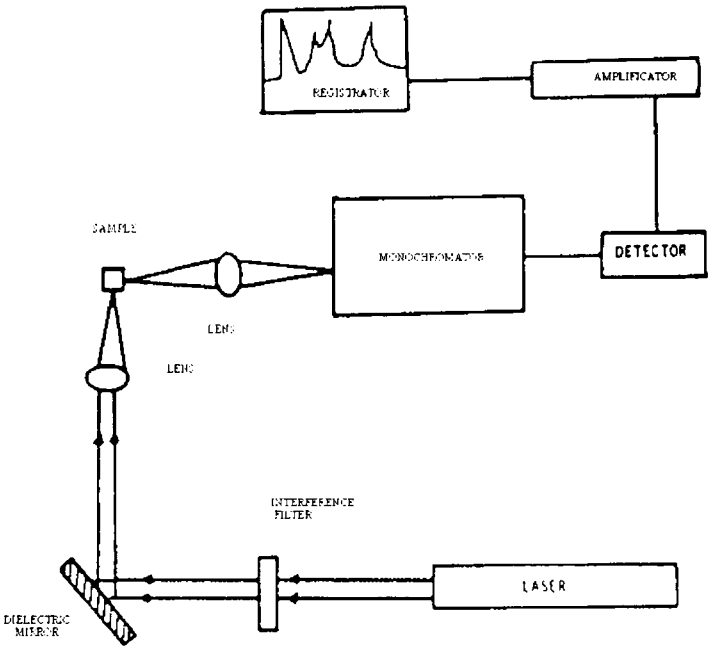

Fig. 3.9. *Schematic representation of a Raman spectrometer.*

3.8 MICRO HARDNESS STUDIES

The term hardness has different meanings to different people, depending upon their area of interest. It is the resistance to penetration to a metallurgist, the resistance to cutting to a machinist, the resistance to wear for a lubrication engineer and a measure of flow stress of the material. Micro hardness studies have been applied to understand the strength and deformation characteristics of a material, since

the hardness properties are basically related to the crystal structure of the material [39]. Several investigators have used the microhardness indentation technique to study anisotropy, deformation, glide, state of dispersions of impurity, quench hardening, effect of irradiation and environment of dislocation mobility. Attempts were made by various researchers to relate the hardness of a crystal with other physical properties such as vibrational frequencies, atomic concentrations, impurities, surface energy and lattice energy [40]. Part of the energy absorbed during indentation is used in producing plastic deformation and the rest increases the surface free energy. The microhardness method is employed to study the individual structural constituent element of metallic alloys, artificial abrasives, glasses, minerals and enamels.

Hardness value depends not only on the properties of the materials under test but also on the conditions of measurement. In metals, polymers and organic molecular solids, an indentor is pressed into the surface and the size of the permanent indentation mark produced is measured. In certain materials, an indentor is pressed into the material and the hardness is determined by the extent to which it has penetrated under load [42]. In the case of minerals and brittle solids, the scratch produced in one material by another of specific hardness number is used to calculate hardness. No method of measuring hardness is dependent on a single physical property since the hardness of a material depends on its elastic and plastic deformation characteristics. Hardness property of a material may change appreciably as the test is applied.

In an indentation test, the initial penetration of the indentor increases the resistance of the material to further indentation. In a wear test, the surface may become work hardened and offer more resistance to further abrasion. Materials having the same hardness number may have varying physical properties like forging, drawing, stretching or rolling. Chemical forces in a crystal also resist the motion of dislocation as it involves the displacement of atoms. Such resistance is known as the intrinsic hardness of a crystal [41, 43].

The theory that hardness is independent of load is valid only for high load indentations. For small loads, the hardness number of some materials may increase

with load, since less number of dislocations becomes available for slip in such small volumes of the crystal. If more than one slip system exists, increasing the load may activate a secondary system, thereby decreasing the hardness of the material. Hardness also depends on time, especially for ductile materials. If stress is applied to such a material over long period of time, creep processes come into play. Hence contact time must remain constant form one indentation test to another.

To account for the deformation below an indenter, two models have been postulated – skip line field and the elastic theory. The slip theory was first explained by Prandtl, who calculated the mean stress for the onset of plastic flow upon indentation. This theory assumes the existence of a plastic region below the indentor, surrounded by a rigid material [44- 46]. The upward flow in the material accounts for the volume displaced by the indentor.

The development of an elastic region beyond the plastic boundary is predicted by the elastic theory. The displaced materials are accounted for, by an elastic decrease in the volume of the material. When the indentation load is removing, there is a second plastic action over a smaller volume in the opposite direction. This theory corresponds more closely to the flow pattern of blunt indentor. The stress field which develops around an indentor is complex. But the understanding of the mechanism of slip is simplified by the fact that hydrostatic pressure plays no part in the mechanism of slip

sA hardness tester, Leitz Miniload fitted with a diamond pyramidal indentor attached to an incident light microscope is used for the present study. The diamond indentor is in the form of a square pyramid, opposite face of which make an angle of 136^0 with one another (Figure 3.10). Indentation can be done with different loads from 5 to 250 g. The impression is of a square pyramid and has a superficial area $d^2/2 \sin 68^0$, where d is the length of the diagonal of the indentation square in micrometers.

Vicker's hardness number [H_v] is calculated using the relation [40].

$$H_V = \text{load/ area of impression} = 2P\sin 68^0 / d^2 \ g\mu m^{-2} = \frac{1.8544\ P}{d^2} \ kg/mm^2 \qquad (3.11)$$

where P is the applied load in kilograms and d is the mean diagonal length of the indentation impression in mm.

The data obtained for P and d can be analysed by Mayer's equation [43].

$$P = k_1 d^n \tag{3.12}$$

where k_1 and n are constants for the material. The constant k_1 is usually referred to as the standard hardness. Mayer index (n) which represents work hardening capacity of the material can be determined by plotting log p Vs log d.

The dependence of Vicker's hardness number on applied load shows different behaviour on different materials [41-43]. In certain cases, microhardness increases with applied load and reaches a constant value at higher loads [44-46]. Microhardness is found to decrease with increasing load and attains a constant value after a particular load for certain crystals. For certain materials, H_V is found to have complex load dependence. Combining Equations (3.11) and (3.12), we have

$$Hv = 1.8544\, k_1 d^{n-2} \tag{3.13}$$

or,

$$Hv = 1.8544\, k_1^{(1+2/n)} P^{(1-2/n)} \tag{3.14}$$

Or,

$$Hv = b\, P^{(n-2)/n} \tag{3.15}$$

where $b = 1.8544\, k_1^{(1+2/n)}$, a new constant. The above expression shows that *Hv* should increase with increase in *P* if $n > 2$ and decrease with the same if $n < 2$. According to Onitsch [44] and Hanneman [45] *n* should lie between 1 and 1.6 for hard materials and above 1.6 for softer ones.

According to Hays and Kendall's theory of resistance pressure [46], there is a minimum level of indentation load (*W*), also known as resistance pressure, below which no plastic deformation occurs. Hays and Kendall have proposed a relationship between indentation test load and indentation size by modifying Kick's law [47] as

$$(P = k_2 d^2) \tag{3.16}$$

$$P - W = k_2 d^2 \qquad (3.17)$$

where k_2 is a new constant and $(P-W)$ is the effective indentation test load considered in the microhardness calculations. Combining expressions (3.16) and (3.17) we get:

$$W = k_1 d^n - k_2 d^2 \qquad (3.18)$$

Or,

$$d^n = W/k1 + (k_2/k_1)\, d^2 \qquad (3.19).$$

The plot of d^n versus d^2 is a straight line having slope k_2/k_1 and intercept W/k_1.

Elastic stiffness constant (C_{11}) of a material can be calculated from the Wooster's empirical relation [48] as

$$C_{11} = Hv^{7/4} \qquad (3.20)$$

If the stiffness constant C_{11} is high, it reveals that the binding forces are quite strong.

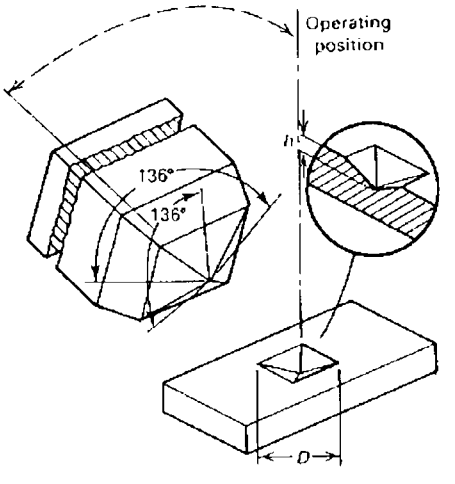

Fig. 3.10 Operation of a pyramidal indentor

3.9 CHEMICAL ETCHING STUDIES

When a crystal is placed in contact with a solvent, it dissolves chemically or physically in such a way as to be consistent with its symmetry. This phenomenon is known as chemical etching. Due to anisotropy of the crystal, the dissolution rates are different in different directions giving rise to conical depressions with regular known as etch pits. The sites where dislocations emerge on the surface may become such preferential sites with appropriate choice of the solvent. Of course, probably the only other preferential sites may be those provided by impurities on the surface. Many workers have experimentally proved that dislocations can be revealed in the form of etch –pits. Gilman and Johnston [49] have shown this in the most striking way in the case of LiF single crystals.

The chemical etching of a crystal surface involves the following sequence:

The reactant/s

a) Approach the surface
b) Interact with the surface and
c) React chemically.
d) Disengage themselves from the surface.
e) Move away from the surface.

If the solvent is weak, or permitted to act only briefly, it is often observed that it attacks the crystal at a number of isolated points, producing minute pits, called etch pits, at these points. The shape of such a pit is consistent with the symmetry of the crystal at that point, and etch pits can therefore be used to reveal the symmetry of the crystal.

According to Gilman, when a perfect crystal face is exposed to a solvent, dissolution probably begins by the nucleation of 'unit pits' of one molecule depth. On a real crystal, dislocations may be preferential sites for nucleation of unit pits and repeated nucleation at a dislocation site leads to the formation of an etch pit. Different nucleation theories have been formulated to explain the etching

phenomenon. Nucleation of etch pits at dislocation has been attributed to the elastic strain associated with the dislocation which causes a decrease in the activation energy for nucleation [50]. The screw dislocation has a shear stress field which vanishes at the surface except at the core; whereas strain energy associated with an edge dislocation is retained at the surface and extends to a considerable distance beyond core.

The morphology of dislocation etch pits depends on the nature of dislocation and on the angle at which dislocation line intersects the surface. The dislocation perpendicular to the surface will produce symmetrical pits while any deviation from it produces asymmetry. If the dislocations are parallel or almost parallel to the surface, etch grooves or pits elongated in the direction of dislocation will result [51]. If the dislocation moves from its position during etching, as in the case of shallow dislocation half loops or as a result of applied stress, then the bottom of pit becomes flat and upon continued non preferential etching, pit is eliminated. The formation of visible dislocation etch pit is influenced by etching rates along the dislocation line, parallel to the surface and perpendicular to the surface, the morphology of the etch pit will change.

Etch pits formed during etching do not necessarily correspond to dislocations. Precipitates or impurity inclusions, clusters of point defects etc., may also lead to etch pit formation. The reliability of an etchant as a dislocation etchant is usually judged by one or more of the following tests.

1. Alternate application of the etchant followed by mechanical or chemical polishing: Etch pits associated with individual dislocations reappear after each successive polishing and etching since a dislocation line cannot terminate inside a crystal.
2. When cleavage is possible, etch patterns produced by the etchant on the two oppositely cleaved surfaces should appear as mirror images of each other. However, Sagar and Faust [52] and Bhatt and Pandya [53] have shown that branching and bending of dislocations at the cleavage may result in deviations from one-to-one correspondence of etch pits on oppositely matched cleavage surfaces. Thus, deviation from one-to-one correspondence

of etch pits on oppositely cleaved surfaces does not always indicate unreliability of the etchant as a dislocation etchant.

3. Wherever possible, the etch pit density should show a reasonable agreement with the theoretically estimated dislocation density.
4. The comparison of measured distance between pits on a lineage line to those calculated from X-ray orientation differences across the boundary may also help in judging the reliability of the etchant as a dislocation etchant.
5. Any plastic deformation of the crystal should result in increase of etch pit density at least in the vicinity of the region of deformation, since plastic deformation always involves creation and motion of dislocations.

Thus chemical etching is not always an assured way of revealing dislocations, though it has been widely used with good success. The most firmly established dislocation etchants are probably those for ADP [54] among salts, LiF and NaCl [55] among alkali halides, molybdenum [56] among metals, CdS [57] among chalcogendies, and Silicon [58] and Ge [59] among semiconductors.

Etching processes are generally very complex and their detailed mechanisms are not quantitatively understood. The etching techniques are still based on qualitative or empirical bases. Developing a dislocation etchant for a given material still remains a trial and error process. Etching can be effectively used.

1. to decide whether a given solid is a single crystal, a polycrystal or an amorphous body
2. to distinguish between different faces of a crystal
3. to reveal the history of growth of crystal
4. to determine density of dislocations
5. to determine impurity distribution in crystalline bodies.

In addition, with a highly 'qualified' dislocation etchant, dislocation mobility and nature and structure of dislocations can also be studied.

3.10 DIELECTRIC STUDIES BY MICROWAVE CAVITY PERTURABTION METHOD

Nowadays electromagnetic cavity has been identified as one of the most popular tools to study the dielectric properties of materials. Various techniques have been invented in using cavities for this purpose in the last 30 years. This is mainly due to the existence of infinity of resonance frequencies in a single cavity, representing every one of them in its own mode. The mode with the lowest resonance frequency is called the fundamental mode and the rest are called the higher modes. Every single mode of the cavity has in general its own distribution or form of fields in the cavity, giving birth to infinity of possibilities in introducing the material whose properties are to be studied.

The cavity perturbation technique is an accurate and precise method for complex permittivity measurements. In the present work, the non destructive, microwave cavity perturbation technique [60- 63] in the S band is employed.

Closed section of a waveguide constitutes a waveguide cavity resonator. The cavity resonator can be of transmission or reflection type. Electromagnetic energy is coupled to the cavity through coupling holes at the ends of the cavity. A nonradiating slot is provided at the broad wall of the cavity for the introduction of the sample. The cavity resonates at different frequencies depending on its dimensions. The schematic diagram of the transmission type cavity is shown in Fig.3.11.

The experimental set-up consists of a transmission type S-band rectangular cavity resonator, HP 8714 ET network analyser and an interfacing computer as shown in Fig.3.12. The cavity resonator is excited in the TE10p mode. A typical resonant frequency spectrum of the cavity resonator is shown in Fig. 3.13. Initially, the resonant frequency f_0 and the corresponding quality factor Q_0 of each resonant peak of the empty cavity are determined. Samples prepared in the form of thin strips are introduced into the cavity resonator through the nonradiating slot. One of the resonant frequencies of the loaded cavity is selected and the position of the sample is adjusted for maximum perturbation (i.e. maximum shift of resonant frequency with minimum amplitude for the peak). The new resonant frequency fs and 3-dB

bandwidth and hence, the quality factor Qs are determined. The procedure is repeated for other resonant frequencies.

The basic principle involved in the technique is that the field within the cavity resonator of volume V_0 is perturbed by the introduction of the dielectric sample of volume V_s through the non-radiating slot. Dielectric material interacts only with electric field and the contribution of magnetic field for the perturbation is minimum. The resonant frequency and the quality factor of the cavity get shifted by the perturbation. The shift in the frequency is a measure of dielectric constant and that in quality factor gives the loss factor [63]. The conductivity of the sample can be found out from the loss factor.

The real part ε_r', of the complex permittivity is usually known as dielectric constant. The imaginary part ε_r'', of the complex permittivity is associated with dielectric loss of the material. The effective conductivity σ is given by

$$\sigma = \omega\varepsilon'' = 2\pi f\varepsilon_0\varepsilon_r'' \quad (3.21)$$

$$\varepsilon_r' - 1 = (fo-fs/2fs)\,(V_0/V_s) \quad (3.22)$$

$$\varepsilon_r'' = (Vo/4V_s)\,(Q_0-Qs/Q_0Qs) \quad (3.23)$$

The dielectric loss or loss tangent or $\tan\delta = \varepsilon_r'/\varepsilon_r''$ (3.24)

Absorption coefficient $\alpha_f = \varepsilon r''fs/(\varepsilon_r'^2 + \varepsilon_r''^2)^{1/2}\,C$ (3.25)

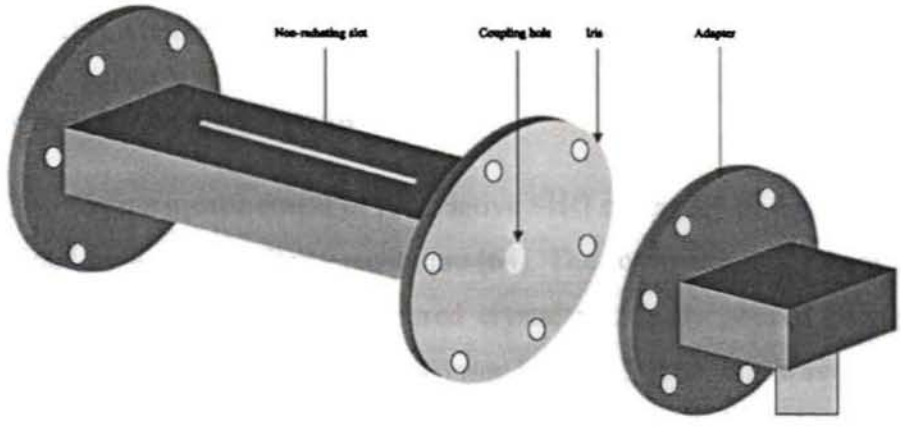

Fig. 3.11. Schematic diagram of the cavity resonator.

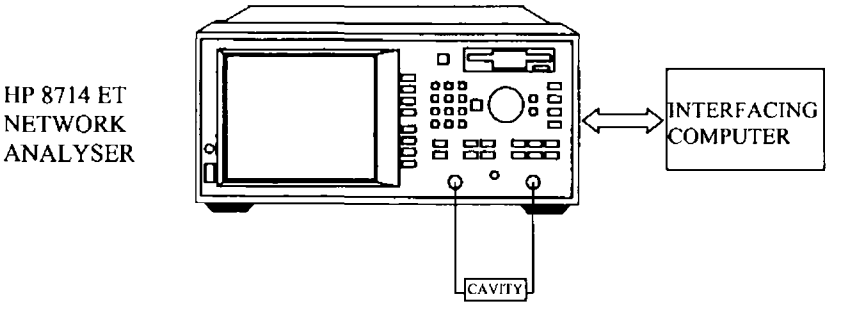

Fig. 3.12. Experimental set-up.

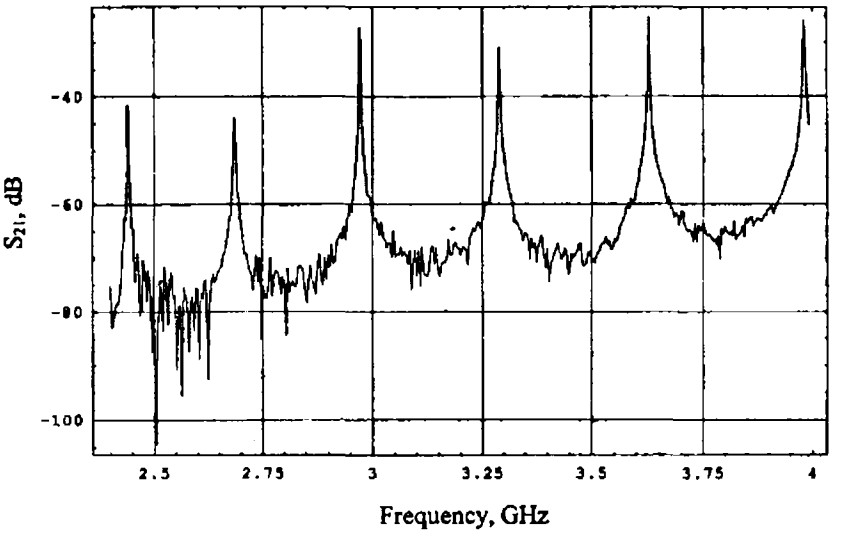

Fig. 3.13 Resonant frequency spectrum of cavity resonator.

3.11 NONLINEAR OPTICAL CHARECTERISATION

3.11.1 Second harmonic generation (SHG)

Quantitative measurement of the relative SHG efficiency of the grown crystal is determined by Kurtz and Perry technique [64]. The schematic of the experimental setup is shown in figure 3.14. Powdered crystal is densely packed between two transparent glass slides. A fundamental laser beam of 1064 nm wavelength (7ns pulse width with 10Hz pulse rate) from an Nd-YAG laser is made to fall normally on the sample cell. The energy/pulse of the incident beam is measured using an energy meter. The transmitted fundamental wave is passed over a monochromator which

separates 532 nm (second harmonic signal) from 1064 nm and is passed through two successive IR filters which remove the residual 1064nm fundamental beam and is focused to a photomultiplier tube which gives the second harmonic wave generated by the crystal. KDP crystal, powdered to the identical size is used as reference material. The SHG efficiency of a crystal can then be found by the formula [65],

$$\text{SHG efficiency, } \eta = I^{2\omega}{}_{sample} / I^{2\omega}{}_{KDP} \qquad (3.26)$$

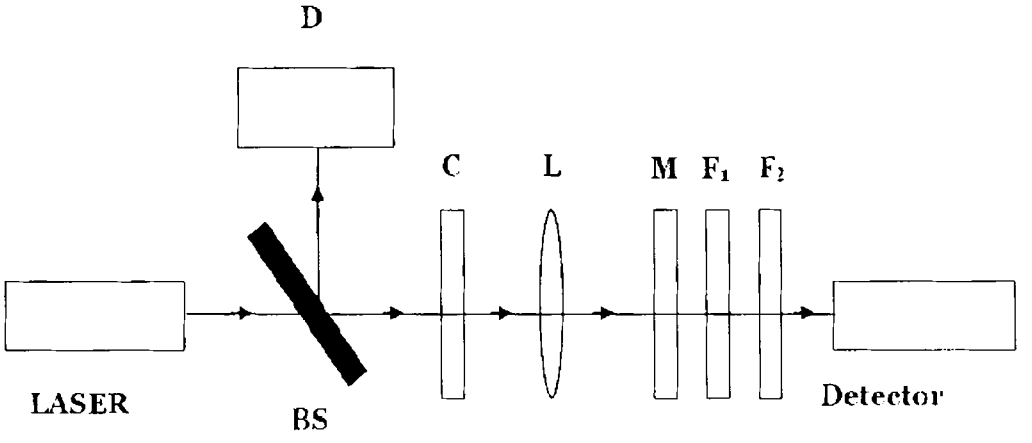

Fig.3.14 schematic diagram of the SHG set up.
D- detector, C-crystal, L-lens, M- monochromator; F_1, F_2-IR filters

3.11.2 Laser damage threshold studies

A Q-switched Nd: YAG (yttrium aluminum garnet) Quanta Ray laser of pulse width 7 ns and 10 Hz repetition rate operating in TEM_{00} mode is used as the source. The energy per pulse of 1064 nm laser radiation is reduced by means of a variable attenuator and is measured using an energy meter (Rj-7620, Laser Probe Inc.).

For surface damage, the sample is placed at the focus of a plano-convex lens of focal length of 100 mm. The diameter of the focused spot, calculated for 1064 nm is 44 μm using the equation

$$d' = 2.44f\lambda/d \qquad (3.27)$$

where d' is the diffraction limited beam diameter, f is the focal length of the lens at which the sample is placed, and d is the beam diameter at the output aperture of the laser.

The onset of damage can be determined by various means, viz., by observing it with microscope, by visual incandescence, or by observing the scattering of helium-neon laser beam passing through the damaged volume. In the present investigation, the resulting damage pattern is characterized by observing it with an optical microscope and by scanning electron microscope. In our work, the damage almost always occurred by the formation of white spark accompanied by an audible tick sound.

Laser can be operated in two modes. In the single-shot mode the laser emits a single 7 ns pulse. In the multi-shot mode the laser produces a continuous train of 7 ns pulses at a repetition rate of 10 Hz. To determine the single shot damage threshold, the sample is irradiated at different spots on the same crystal at different pulse energies. This is done to avoid the cumulative effects resulting from multiple exposures [66, 67]. Once the single shot damage threshold (P_1) is determined, the multiple shot experiment is carried out by keeping the power level slightly lower than the single shot value and subjecting the same point of the sample for exposure until damage occurred. According to Nakatani et al., [68] the multiple shot damage threshold (P_n) value is determined as the maximum power level at which the crystal remains undamaged even after exposing it to 1800 pulses.

3.11.3 Z Scan measurement of optical nonlinearity

There is considerable interest in finding materials having large yet fast nonlinearities. This interest is driven primarily by the search for materials for all-optical switching and sensor protection applications, which concerns both nonlinear absorption (NLA) and nonlinear refraction (NLR).

The Z-scan technique is a method which can measure both NLA and NLR in solids particularly in liquids and liquid solutions [69, 70]. It has gained rapid acceptance as a standard technique for separately determining the nonlinear changes in index of refraction and changes in absorption. This acceptance is primarily due to the simplicity of the technique as well as the simplicity of the interpretation. The index change, Δn, and absorption change, $\Delta\alpha$ can be determined directly from the data without resorting to fitting.

In a typical z-scan experimental setup (Fig.3.15), a laser beam with a Gaussian profile is initially focused by a lens. The sample is then moved along the axial direction of the focused beam in such a way that it moves away from the lens, passing through the focal point. At the focal point the sample experiences the maximum pump intensity, which will progressively decrease in either direction of motion from the focus. If a light detector is placed in the far field and the transmitted intensity is measured as a function of the position of the sample, one obtains an "open aperture" z-scan curve, the shape of which will reveal the presence of any absorptive nonlinearity in the sample. On the other hand, if a properly chosen aperture is placed in front of the detector, a "closed aperture" z-scan curve is obtained which will reflect the occurrence of refractive nonlinearities.

In the present work, the second harmonic output of a hybrid mode-locked Nd: YAG laser operating at 10 Hz repetition rate having output 532nm is used. The crystal is fixed on a microprocessor controlled translation stage that has a range of 30 cm and a resolution of 2 microns, so that it can be accurately moved through the focal region of the laser beam. A fast photodiode monitors the input laser energy, and a large area photodiode collects the transmitted beam. For the closed aperture measurements, a suitable aperture is placed in front of the photo diode. Data acquisition is facilitated in real time by the use of a PC.

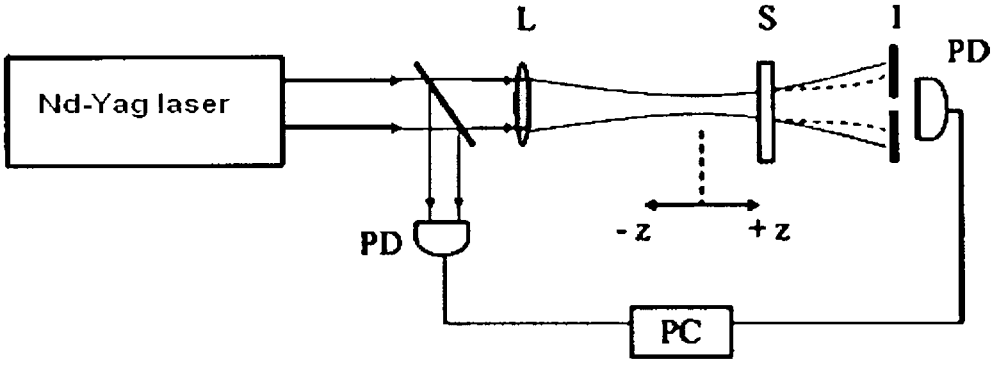

Fig.3.15 Z scan experimental set up

There are two type of nonlinear absorption present in NLO materials. One is saturable absorption (SA) and the other one is reverse saturable absorption (RSA). In SA, open aperture Z scan curve result in a peak at the focus (Z=0) and in RSA, a valley results at the focus.

The intensity dependent nonlinear absorption coefficient $\alpha(I)$ can be written in terms of linear absorption coefficient α and two photon absorption (TPA) coefficient β as [71]

$$\alpha(I) = \alpha + \beta I \qquad (3.28)$$

The RSA coefficient β can be obtained from a best fitting performed on the experimental data of the OA measurement with the equations (3.29) and (3.30) where τ is the time, I(z) is the irradiance and L is the optical path length.

$$T(Z) = \frac{1}{Q(z)\sqrt{\pi}} \int_{-\infty}^{+\infty} \ln [1 + Q(z)] e^{-\tau^2} d\tau \qquad (3.29)$$

$$Q(Z) = \beta I(Z) \frac{1-e^{-\alpha L}}{\alpha} \qquad (3.30)$$

where $\frac{1-e^{-\alpha L}}{\alpha}$ is the effective path length L_{eff}

In a closed aperture (CA) Z scan, the resulting peak-valley configuration suggests that nonlinear refractive index is negative. In other words, if the nonlinear refracive index is positive, CA curve represnts a valley followed by peak.

The nonlinear refraction coefficient n_2 (m^2/W) is obtained through the following equation

$$\Delta\Phi_0 = k n_2 I_0 L_{eff} \qquad (3.31)$$

In the above equation the phase shift $\Delta\Phi_0$ is equal to $2\pi/\lambda\ n_2\ I_0\ L_{eff}$.

The difference between the normalized transmittance at the peak and valley is related to $\Delta\Phi_0$ by the relation

$$\Delta T_{P\rightarrow V} = 0.406\,(1-S)^{0.25}\,\Delta\Phi_0 \qquad (3.32)$$

The molecular hyperpolarizability, γ, may be obtained with the equation below [72]

$$\gamma = 40\pi\, n_2 / cn_0 \qquad (3.33)$$

The real and imaginary parts of the $\chi^{(3)}$ of the sample can also be calculated by the following equations [73, 74]

$$\text{Re}\,\chi^3\,(\text{esu}) = (cn_0^2/\,120\pi^2)\,n_2, \qquad (3.34)$$

$$\text{Im}\,\chi^3\,(\text{esu}) = (cn_0^2\varepsilon_0\lambda\,/2\pi)\,\beta \qquad (3.35)$$

Introducing the coupling factor ρ, the ratio of imaginary part to real part of third-order nonlinear susceptibility,

$$\rho = \text{Im}\,\chi^3 / \text{Re}\,\chi^3 \qquad (3.36)$$

If the observed value of coupling factor is seen to be less than 1/3, it indicates that the nonlinearity is electronic in origin [75].

3.12 REFERENCES

[1] B.D. Cullity and S.R. Stock, Elements of X ray diffraction, Prentice Hall, N. J,2001

[2] Sheldrick, G. M. Acta Cryst. A46, 467(1990).

[3] Subha Nandhini, M., Natarajan, S. Acta Cryst.C57, 115(2001).

[4] Venkatraman, J., Prabu, M. M. & Vijayan, M. J. Pept. Res. 50, 77 (1997).

[5] Vijayan, M. Prog. Biophys. Mol. Biol. 52, 7(1988).

[6] Krishan Lal and G. Bhagavannarayana, J. Appl. Cryst. 22, 209 (1989).

[7] G. S. Pawley, J. Appl. Cryst 14, 357(1981).

[8] Sheldrick, G. M. TOPAZ- R, Ver.3,. University of Goettingen, Germany, (1997).

[9] D. K. Schroder, Materials and Device Characterization, Wiley-Interscience, N .Y, 1998.

[10] P. E .J. Flewit and R. K. Wild, Physical methods for material characterization, IOP publishing, London, 2003.

[11] P. N. Kotru, K. K. Raina, and M. C Koul, Indian J. Pure. Appl. Phys. 25, 220 (1987).

[12] S. Joseph and M. J. Joshi, Indian J. Phys. 71A, 183 (1997).

[13] R. M. Dabhi and M. J. Joshi, Indian J. Phys. 76A, 211 (2002).

[14] A.W. Coates and J. P. Redfern, Nature 201, 68 (1964).

[15] K. J. Laidler, Chemical Kinetics, 3rd Ed., Harper and Row, New York, 1987.

[16] M.J. O' Neill, Anal.chem.38, 1331(1966).

[17] K.Nandakumar, PhD thesis, Cochin University of science and technology, India (1992).

[18] I. M. Tsidilkovsk, Band structure of semiconductors, Pergamon Press, Oxford (1982).

[19] J. I. Pankove, Optical processes in semiconductors, Prentice-Hall, New York (1971).

[20] A. Ashour, H.H. Afifi and S.A. Mahmoud, Thin Solid Films,248, 253(1994).

[21] K. Yamaguchi, N. Nakayama, S. Ikegami, Jpn. J. Appl. Phys., 16, 1203(1977)

[22] O.P. Agnihotri and B.K. Gupta, Jpn. J. Appl. Phys., 18, 317(1979).

[23] D. R. E. Campbell and R. D. Tomlin, J. Phys. D 5, 852 (1972).

[24] A. A. El-Kadry and N. Mahmoud, Thin Solid Films 269, 117 (1995).

[25] I. C. Ndukwe, Sol. Ener. Mater. Sol. Cells, 40, 123(1996).

[26] Janai, M., D. D. Alfred, D. C. Booth and B.O. Seraphin, Sol. Ener. Mater. 1,11(1979),.

[27] J. I. Pankove, Optical processes in semiconductors, Prentice-Hall, New York (1971).

[28] D.R.Vij (Ed.) Luminescence of solids, Plenum Press, New York, 1998.

[29] Fately,W.G., Mc Devit,N., Bentely,F.F.: Appl.Spectrosc., 25 (1971) 155

[30] Halberstadt, E.S., Henish, H.K.: J.Crystal Growth, 3 (1968) 363

[31] Hobden, M.V.: J.Appl.Phys., 38, 4365 (1967)

[32] Kaneko, N., Kaneko, M., Takanashi, H. : Spectrochim. Acta Part A, 40, 33 (1984)

[33] Lippincott, E.R., Schroeder, R .: J.Chem.Phys., 23, 1099 (1955)

[34] Sonin, A.S., Filimunov, A.A., Suvorov, V.S.: Soviet Physics-Solid State, 10, 1481 (1968)

[35] Srivastava, G.P., Mohan, S., Jain, Y.S.: J.Raman Spectroscopy, 13, 25 (1982)

[36] Stuart, A.V., Sutherland, G.B.M.: J.Chem.Phys., 24, 559 (1956)

[37] Taylor, W., Lockwood, D.J., Labbe, H.J.: J.Phys., C17, 3685 (1984)

[38] Tobin, M.C. : Laser Raman Spectroscopy, Wiley Interscience, New York, 1971.

[39] Meyer, Some aspects of the hardness of materials, PhD thesis, Dreft, (1951).

[40] P. N. Kotry, A. K. Razdan, B. M. Wnakyn, J. Mater. Sci. 24, 793(1989).

[41] J. N. Sherwood, Pure & Appl. Opt. 7, 229 (1998).

[42] I. V. Kityk, B. Marciniak, A. Mefleh, J. Phys. D:Appl.Phys. 34, 1 (2001).

[43] E. Meyer, Z. ver. Deut. Ing. 52,645(1908).

[44] E.M. Onitsch, Mikroscopia 2,131(1947).

[45] M. Hanneman, Metall. Manchu. 23,135(1941)

[46] C. Hays, E.G. Kendall, Metallurgy 6,275(1973).

[47] F. Kick, Das Gasetzder, Proportionalen Widerstande Und Science Anwendung, Felix, Leipzig, 1885

[48] W.A. Wooster, Rep. Progr. Phys. 16,62(1953).

[49] Gilman. J., Jhonston.E.J, J.Appl.Phys, 31, 936(1960).

[50] N.Cabrera, The surface chemistry of metals and semiconductors, John Wiley, Holland, 1960.

[51] S.Amlenikx, Direct observation of dislocations, vol.6, Academic press, New York, 1964.

[52] Sagar.A, J.Faust, J.Appl.Phys, 38,482,1967.

[53] Bhatt.V.P, Pandya.A.R, J.Phys.C. 6, 36, 1973.

[54] Patel.A.R and Bhatt.H.L, J.Cryst.growth, 12, 288,(1972) .

[55]. Patel,A.R, Arora,S.KJ.Cryst.growth, 18, 199(1973) .

[56]. Blank.Z J.Cryst.growth, 18, 281,(1973) .

[57]. Boulin.D and Ellis.W.C, J.Cryst.growth, 6, 290,(1970) .

[58]. Hatschek,kolloidzeit Schr, 10,77, (1912) .

[59]. Garrett.D.E, Br.Chem.Eng.,4,673,(1956) .

[60] K.T. Mathew, U. Raveendranath, Sensors Update (Ger.) 7 (1999) 185.

[61] U. Raveendranath, K.T. Mathew, J. Mol. Liq. 68 (1996) 145.

[62] W.J. MacKnight, R.D. Lundberg, Thermoplastic Elastomers (Munich), 1987.

[63] J.S. Tan, NATO ASI Series C: Mathematical and Physical Sciences, vol. 198, 1987, p. 439.

[64] S. K. Kurtz and T. T. Perry, J. Appl. Phys. 39, 3798 (1968).

[65] A. Aravindan, P. Srinivasan, N. Vijayan, Cryst. Res. Technol. 42, No. 11, 1097 (2007).

[66] N. L. Boling, M. D. Crisp, and G. Dube, Appl. Opt. 12, 650 ,1973.

[67] E. de Matos Gomes et al., Synth. Met. 115, 225 ,2000.

[68] H. Nakatani, W. R. Bosenberg, L. K. Cheng, C. L. Tang, Appl. Phys. Lett. 53, 2587,1988.

[69] M. Sheik-Bahae, A.A. Said, and E.W. Van Stryland, Opt. Lett. 14, 955(1989).

[70] M. Sheik-Bahae, A. A. Said, , E. W.Van Stryland, IEEE J. Quantum Electron. 26, 760 (1990).

[71] G. Yang, W. T. Wang, L. Yan, H. B. Lu, and Z. G. Chen, Opt. Comm. 209, 445 (2002).

[72] Seetharam.S, G. Umesh, K. Chandrasekharan, B.K. Sarojini, Opt. Mater. 30 1297(2008)

[73] Lee W. Tutt, Thomas F. Boggess, Prog. Quant. Electron. 17, 299(1993).

[74] P.N. Prasad, D.J. Williams, Introduction to Nonlinear Optical Effects in Molecules and Polymers, Wiley, New York, 1991.

[75] Seetharam.S, G. Umesh, K. Chandrasekharan, B.K. Sarojini, Opt. Mater. 30 1297(2008).

****ಜಿಆರ್****

Chapter 4

GROWTH AND CHARACTERISATION OF GLYCINIUM OXALATE SINGLE CRYSTALS FOR NONLINEAR OPTICAL APPLICATIONS

Chapter **4**

GROWTH AND CHARACTERISATION OF GLYCINIUM OXALATE SINGLE CRYSTALS FOR NONLINEAR OPTICAL APPLICATIONS

4.1 INTRODUCTION

In recent years, one has witnessed increasing interest in the study of amino acids and their derivative crystals. This interest has been stimulated by the perspective of understanding a system where the hydrogen bonding plays a fundamental role and, as a result of this understanding, a better knowledge of some important biological molecules can be achieved. Amino acid crystals usually display large nonlinear optical (NLO) response and are potential candidates for applications in the emerging areas of photonics [1]. Molecules that show asymmetric polarization induced by electron donor and acceptor groups are responsible for electro optic and NLO properties [2].

Glycine (NH_2CH_2COOH amino acetic acid) is the simplest amino acid, which is hydrophilic polar in nature. It is the only protein- forming amino acid without a center of chirality. Glycine helps to trigger the release of oxygen to the energy requiring cell-making process. It is necessary for the manufacture of hormones in the human biological system that builds a strong immune system [3]. Glycine exhibits polymorphism. It grows in many forms; such as the stable α form- and γ- form (optically active showing SHG) and the unstable β- form [4]. The single crystals of γ-glycine and α-glycine may be obtained by slow cooling of aqueous solution of glycine [3, 4]. The crystal of α- form is metastable in aqueous solution and it transforms into γ-form spontaneously [5]. While glycine can exist as a neutral molecule in the gas phase, it exists as zwitterions in solution and in the solid

4.2.2 CHN analysis

The chemical composition of the grown GLO crystal determined by carbon, hydrogen, nitrogen (CHN) analysis using VarioEL III CHNS serial number11035060 is compared with the theoretical values of carbon, hydrogen and nitrogen present in the crystal and is shown in Table 4.1. From the results, the composition of the material is established as $C_4H_7NO_6$.

Table 4.1. CHN analysis data.

Element	Theoretical composition (%)	Measured composition (%)
Carbon	29.07	28.72
Hydrogen	4.24	4.42
Nitrogen	8.48	8.50

4.2.3 X-ray powder diffraction studies

The powder X-ray diffractogram of the GLO crystal shown in Fig.4.2 is registered with Bruker D8 advance diffractometer operated at 40 KV and 50mA, using Cu target and graphite monochromator. The intensity data is recorded by continuous scan from 5° to60° with a step size of 0.02°and scan speed of 4°/minute. The structure, refined by Pawley method [7] using the TOPAZ R version 3 program is given in table 4.2, which agrees well with the reported values [6].

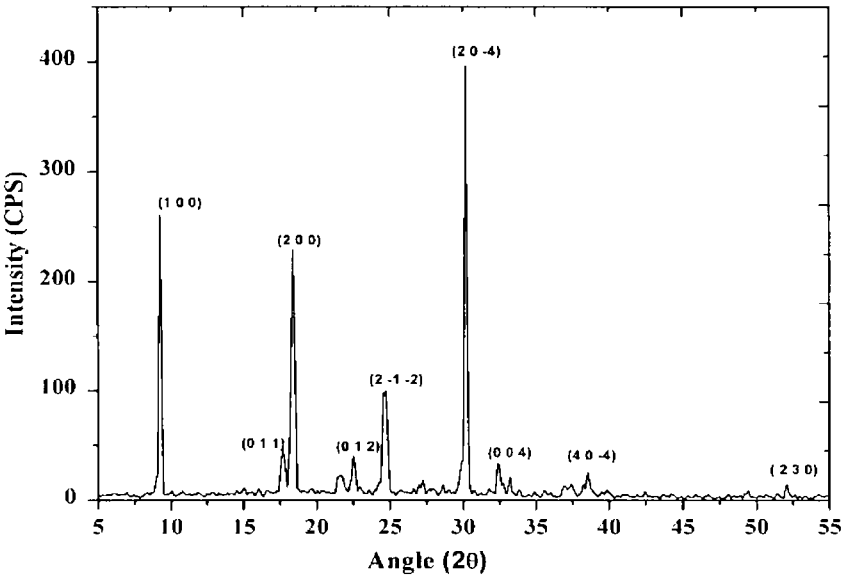

Fig 4.2 Powder XRD pattern of GLO crystal

Table 4.2 XRD data of GLO crystal

Symmetry cell	monoclinic
Space group	$P2_1$ / C
Crystallite Size(nm)	200.2
Lattice parameters	
a (Å)	10.50
b (Å)	5.65
c (Å)	12.04
$\alpha = \gamma$	90
beta(°)	113.57
Volume(Å^3)	715.68

4.2. 4 UV/Vis/NIR spectrum and evaluation of linear optical constants

The UV/Vis/ NIR spectrum plays a vital role in identifying the potential of a NLO material because a given NLO material can be of utility only if it has a wide transparency window without any absorption at the fundamental and second harmonic wavelengths [8]. The UV-Vis-NIR spectrum of the sample in the range

200nm- 2500nm is recorded with Hitachi U3140UV-VIS-NIR spectrophotometer and is shown in Fig.4.3. It is evident that the crystal has a transparency window from 324nm to 2500 nm making it suitable for applications in the whole region for higher harmonic generation. The absence of absorption of light in the visible region is an intrinsic property of all the amino acids [9].

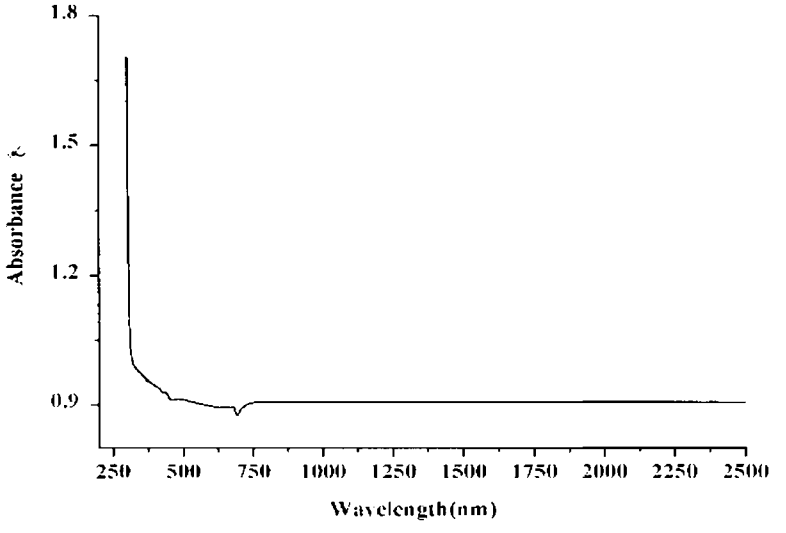

Fig 4.3 UV/VIS/NIR Spectrum of GLO

The absorption coefficient α which depends on the wavelength λ can be obtained by using the following relation. When scattering effects are neglected, the absorption coefficient may be expresses by

$$\alpha h\upsilon = A\,(\alpha h\upsilon - Eg)^{n}$$

where A is a constant nearly independent of photon energy and Eg is the optical band gap. For the indirect allowed transitions n = 2, but, for the direct allowed transitions n = 0.5 [10]. The plot of $(\alpha h\upsilon)^2$ versus hν for the GLO crystal is shown in fig(4.4) . The X-axis intercept of the plot will give the band gap energy. The band gap of GLO crystal is found to be 3.9 eV.

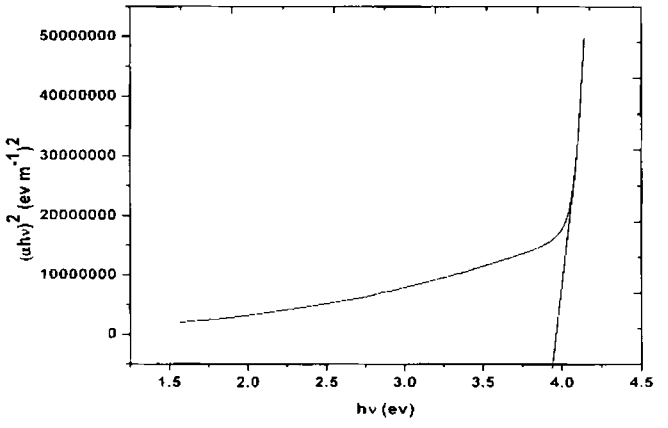

Fig.4.4 Plot of $(\alpha h\upsilon)^2$ versus hν for the GLO crystal

The optical constants such as refractive index (n) and the extinction coefficient(k) and the absorption coefficient(α) are determined from the transmission (T) and reflection (R) spectrum based on the following relations [11, 12].

$$T = (1-R)^2 \exp(-\alpha t) / 1-R^2 \exp(-\alpha t) \quad (4.1)$$

where t is the thickness and the absorption coefficient α is related to extinction coefficient k (absorption index) by

$$K = \alpha \lambda / 4\pi \quad (4.2)$$

For semiconductors and insulators (where $k^2 << n^2$) there exists a relationship between R and n (refractive index) given by [13, 14]

$$R = (n-1)^2/(n+1)^2 \quad (4.3)$$

The relationship between ε and k is given by [15] $\varepsilon = \varepsilon_r + i\varepsilon_i = (n+ik)^2$ (4.4)

The real part ε_r and imaginary part ε_i of the dielectric constant is given by

$$\varepsilon_r = n^2-k^2 \quad (4.5)$$

$$\varepsilon_i = 2nk \quad (4.6)$$

The variation of refractive index, extinction coefficient and dielectric constant with energy in the range 1-6 ev is shown in figures 4.5, 4.6 and 4.7 respectively. The linear optical constants evaluated using the present study are utilised for the determination of the nonlinear optical constants of the crystal.

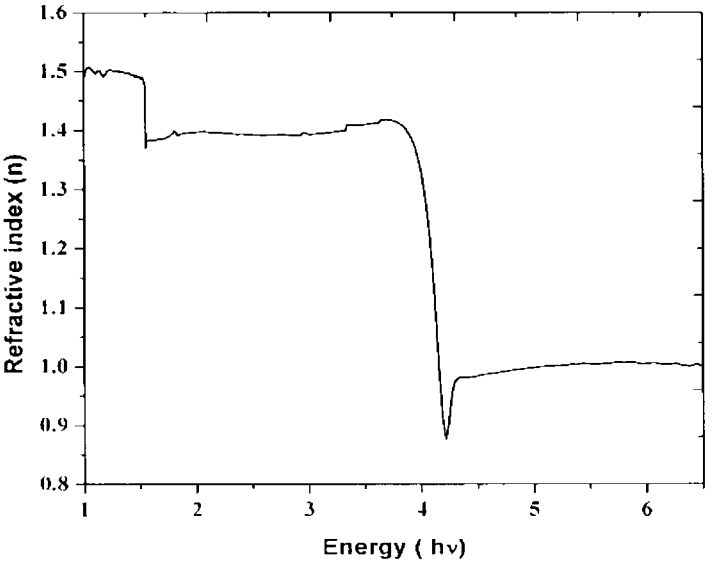

Fig. 4.5 Plot of variation of n with energy

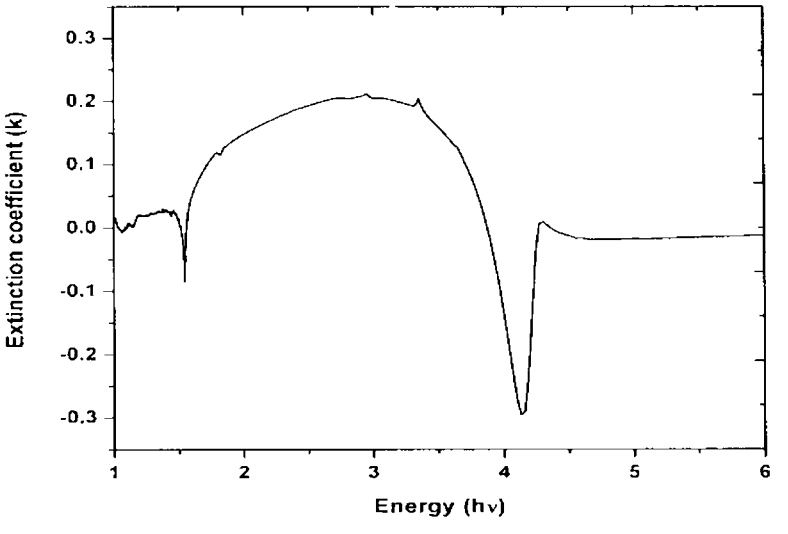

Fig. 4.6 plot of variation of k with energy

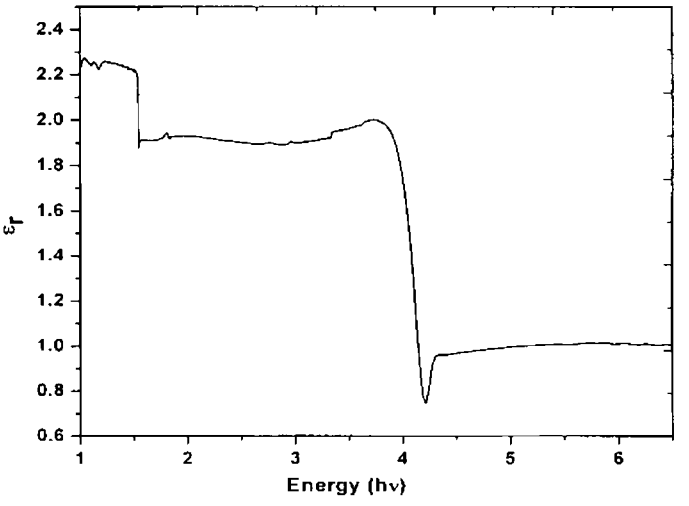

Fig. 4.7 Plot of variation of ε_r with energy

4.2.5 FTIR and FT Raman spectral analysis

The FTIR spectrum of the grown crystals, recorded in the wave number range from 400cm^{-1} to 4000cm^{-1} using Thermo-Nicolate Avatar 370 system is shown in figure (4.8). The FT Raman spectrum of the powdered sample (Fig.4.9) is recorded with BRUKER RFS100/S system with a resolution of 4 cm^{-1} using a standard InGaAs detector with a laser source of 150 mW with a resolution of 4cm^{-1} in the range 400-4000cm^{-1}.

The vibrational analysis of glycinium oxalate is performed on the basis of vibrations of the glycinium ion consisting of amino, methylene, carboxylic groups and the oxalate ion and is given in table 4.3.

For saturated amines, it is established that the asymmetric NH_2 stretch will give rise to a band between 3380 and 3350 cm^{-1}, while the symmetric stretch will appear between 3310 and 3280 cm^{-1} [16]. But the protonation of NH_2 group can produce a shift in band position towards the range 3300–3100 cm^{-1} for

asymmetric stretch and 3100–3000 cm^{-1} for symmetric stretch as appeared in glycine derivatives [17, 18]. Further, the NH_3^+stretching bands are broader and weaker in IR than those arising from the uncharged NH_2 groups [19, 20]. The infrared spectrum shows a very broad intense band observed at 3224 cm^{-1}corresponding to NH_3^+ asymmetric stretching mode. The position and broadness of this band clearly indicate the presence of NH_3^+group in the crystal. Thus, the protonation of the amino group can be inferred from the vibrational spectra. The NH_3^+symmetric stretching frequencies are overlapping with vibrations of CH_2 group.

The NH_3^+ asymmetric and symmetric deformation modes appear in the regions 1625–1560 cm^{-1} and 1550–1505 cm^{-1} respectively [21]. The strong bands at around 1623 cm^{-1} and band at 1593 cm^{-1} in IR and corresponding Raman bands at 1621 cm^{-1} and at 1595 cm^{-1}, are assigned to the parallel and perpendicular asymmetric NH_3^+deformation modes, respectively [17]. The NH_3^+ symmetric deformation mode occurs in the IR spectrum as a very strong band at 1507 cm^{-1}. The corresponding Raman bands of NH_3^- are also observed in the same region. The NH_3^+ rocking modes occur at frequencies around 1100 cm^{-1} for glycine and its derivatives and exact band position depends, on the position and strength of the hydrogen bond [22]. The IR bands at around 1090 and at 964 cm^{-1} and the corresponding Raman bands at around 1099 and at 962cm^{-1} are assigned to parallel and perpendicular NH_3^+ rocking modes, respectively [17]. The medium intense band in IR at 480 cm^{-1} is assigned to the NH_3^+ torsion mode.

For amino acids, the asymmetric CH_2 stretching vibrations are generally observed in the region 3100–3000 cm^{-1}, while the symmetric stretch will appear between 3000 and 2900 cm^{-1} [24-26]. The CH_2 asymmetric vibrations are observed as strong band in Raman spectrum at 3033 cm^{-1} and medium shoulder in IR at 3032 cm^{-1}. The symmetric stretching also observed as an intense sharp band in Raman at 2975 $cm^{-1}$and medium intense shoulder in IR at 2979 cm^{-1}. The bands

corresponding to scissoring, wagging and rocking vibrations of CH_2 appear at 1433, 1322 and 1042 cm^{-1} in the IR spectrum. The frequencies at 1434, 1321 and 1039 cm^{-1} in Raman spectrum are assigned to CH_2 scissoring, wagging and rocking modes, respectively, which are supported by the results reported on glycine derivatives [26-29].

The Carbonyl stretching vibrations are found in the region 1780–1700 cm^{-1} [16, 21]. The sharp intense band in IR spectrum at 1713 cm^{-1} can be assigned to C=O stretching vibration, which is also observed in Raman at 1710 cm^{-1} as a strong band. The COO bending, wagging and rocking vibrations are observed as intense bands in the IR spectrum in the expected regions [24] at 712, 579 and 519 cm^{-1}, respectively. The less intense Raman band arising from bending is also found at707 cm^{-1}. This mode has been assigned to the COO wagging mode in literature [23-26]. The absorption bands arising from C–N and C–C stretching vibrations are usually observed in the region 1150–850cm^{-1} [21]. The C–C stretching is observed as an intense band at 864 cm^{-1} in IR spectrum and the corresponding Raman band at 873 cm^{-1}. It is assigned that the NH_3 rocking, CH_2 rocking and C –C stretching modes overlap to give the most intense band observed at 897 cm^{-1} in IR and at 893 cm^{-1} in Raman, respectively. Earlier reports [22, 23–26] have given this mode as C–C stretching. However, deuterated studies [30] have indicated that this band has undergone shift on deuteration of NH_3 group. Hence it is reasonable to assume that the vibrational interaction involving NH_3 rocking, CH_2 rocking and C –C is responsible for the most intense Raman band at 893 cm^{-1} and not the pure C –C stretching as reported in literature.

The stretching vibration of the hydroxyl group of oxalate appears as a very weak shoulder in IR at 3589 cm^{-1}. The hydroxyl bending mode at 1370 cm^{-1} in Raman and 1371 cm^{-1} in IR arises due to the O–H bending of carboxylic group of oxalates while, the weak band at 1412 cm^{-1} in Raman spectrum corresponds to the O–H bending of glycinium.

The present study highlights the presence of NH_3^+ ion in the crystal confirming protonation of the amino acid group leading to the formation of glycinium oxalate molecule. Noncentrosymmetry is one of the decisive criterion for a material to be NLO active, particularly SHG active. For a noncentrosymmetric material, there exists an exact match between the infrared and Raman wave numbers. In the vibrational spectra of GLO, there is excellent matching between vibrational bands of the infrared and Raman spectra. The result of the XRD analysis also reveals that the material is noncentrosymmetric. Thus the NLO activity of GLO crystal is confirmed from the vibrational spectrum.

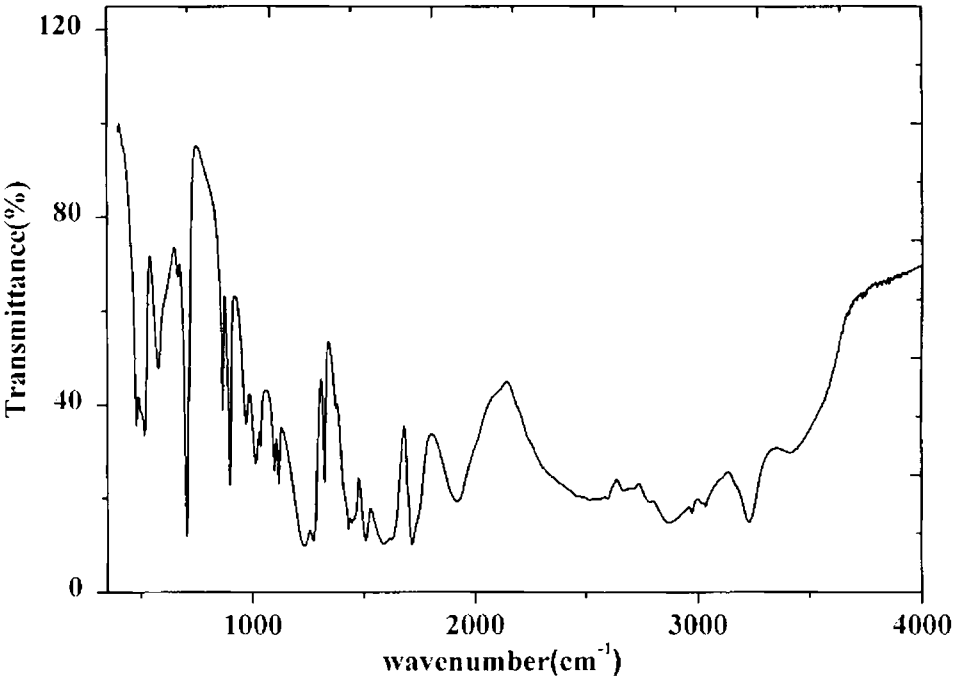

Fig. 4.8 FTIR spectrum of GLO crystal

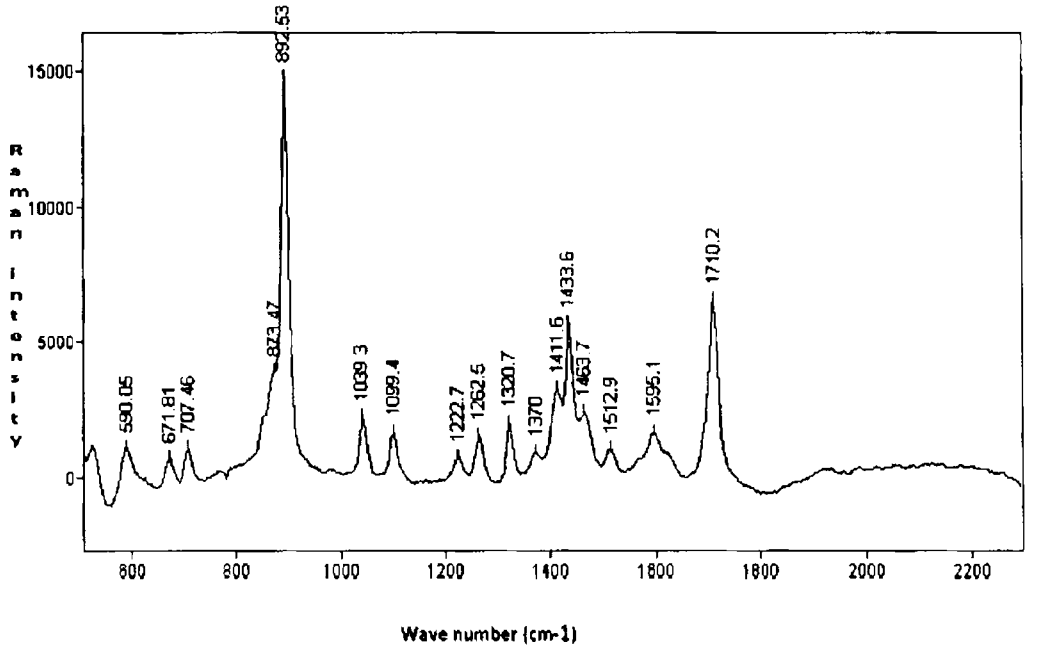

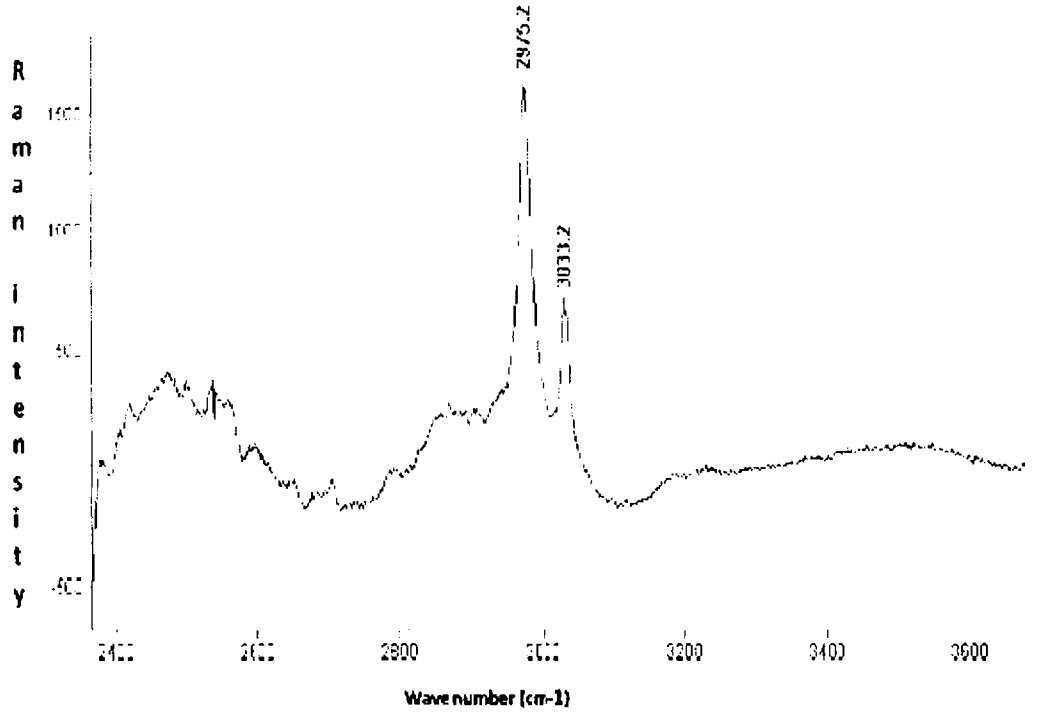

Fig.4.9 FT Raman spectrum of GLO crystal

IR band Positions (cm^{-1})	Raman band Positions (cm^{-1})	Assignment of vibrations
481		NH_3^+ torsion mode.
518		COO rocking mode.
582	590	COO wagging mode/CH_2 out of plane bend
670	672	COO out of plane bending
708	707	COO in plane bending mode.
869	873	C- C stretching mode.
901		NH_3 rocking/CH_2 rocking in
972	962	NH_3 rocking
1015		O-H-O stretching mode.
1037	1039	CH_2 rocking out vibration.
1098	1099	⊥ NH_3^+ rocking mode.
1118		C-N stretching mode
1231	1223	C-O stretch/O-H in plane bend
1322	1321	CH_2 wagging vibration.
1429	1434	CH_2 bending deformation.
1509		NH_3^+ symmetric stretching mode.
1594	1595	NH_3^+ assymmetric deformation
1716	1710	C=O stretching mode.
1922		C-C overtone
2873	2873	O-H stretching
2974	2975	CH_2 symmetric stretching mode.
3033	3033	CH_2 assymetric vibration
3229		NH_3^+ assymetric stretching mode.

Table 4.3 Vibrational assignments

4.2.6 THERMAL ANALYSIS

The thermal properties of the GLO crystal are studied using thermo gravimetric analysis (TGA) / differential thermal analysis (DTA) and differential scanning calorimetry (DSC). Powdered sample of 6.945 mg glycinium oxalate is analyzed in N2 atmosphere by using Perkin Elmer Diamond TGA / DTA equipment. The analysis is carried out simultaneously in air at a heating rate of 10°C / min for a temperature range of 28°C to 810°C. The TGA/DTA curve is shown in Fig. 4.10. Quite interesting and important point to be noticed is the very good thermal stability of the material up to 190°C. The absence of water of crystallization in the molecular structure is indicated by the absence of weight loss around 100°C. The endothermic peak in the DTA curve at 179°C represents the melting point of the sample. Another important observation is that there is no phase transition till the material melts and this aspect enhances the temperature range for the utility of the crystal for NLO applications. Further there is no decomposition up to the melting point. This ensures the suitability of the material for possible applications in lasers, where the crystals are required to withstand high temperatures. After 190°C, there is decomposition, illustrated by the loss of mass in the temperature range 190°C to 240°C. In this region the gaseous fragments like carbon dioxide and ammonia might be librated.

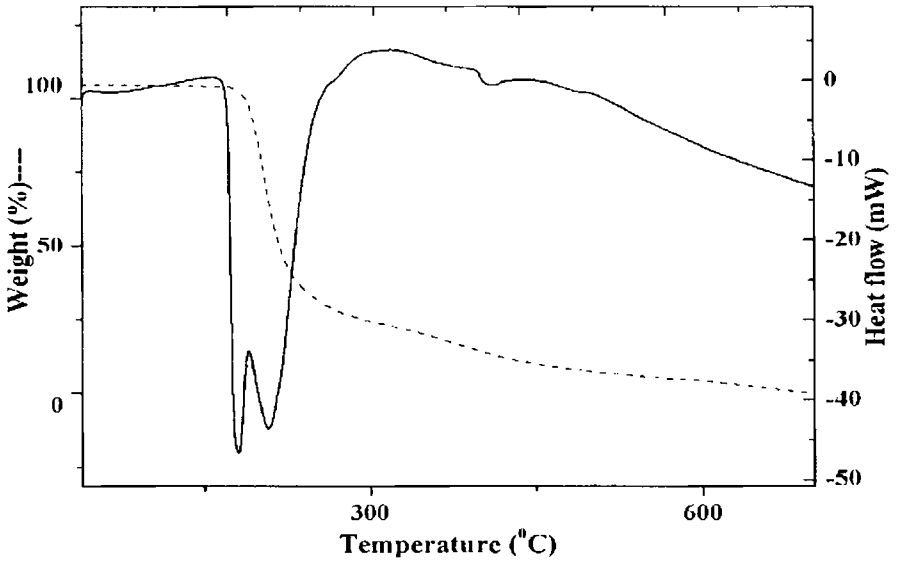

Fig.4.10 TGA/DTA curve of GLO crystal

The specific heat at constant pressure Cp of the crystal is estimated from the DSC curve using the ratio method [31]. In this method, base line corresponding to the temperature range of interest is first obtained. After this, two independent DSC runs are performed under identical conditions; one with weighed quantity (m') of α-Al_2O_3 and the other with a weighed quantity (m) of the sample. Then the specific heat Cp of the sample can be determined by using the relation

$$Cp/Cp' = m'y / my' \quad (4.7)$$

where Cp' is the specific heat of α-Al_2O_3, y and y' are the ordinate deflections of the sample and reference standard respectively. Figure 4.11 depicts the DSC runs performed for the baseline, reference standard and the sample under the same heating conditions and figure 4.12 gives the variation of specific heat of the sample within the temperature range of interest.

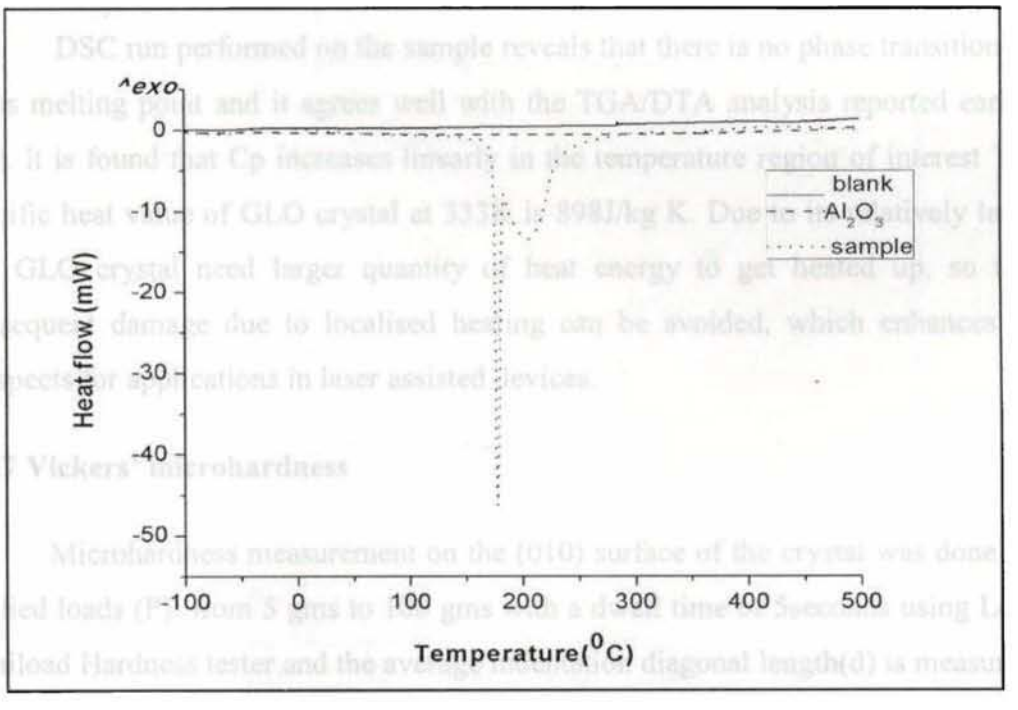

Fig. 4.11 DSC thermogram

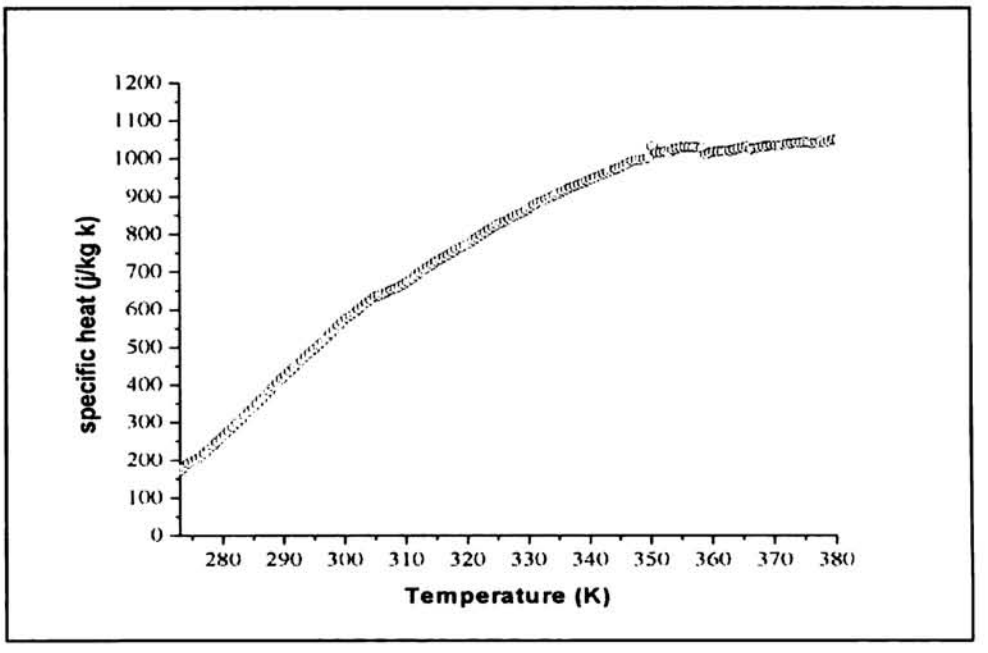

Fig.4.12 Temperature dependendnce of specific heat

DSC run performed on the sample reveals that there is no phase transition up to its melting point and it agrees well with the TGA/DTA analysis reported earlier [32]. It is found that Cp increases linearly in the temperature region of interest The specific heat value of GLO crystal at 333K is 898J/kg K. Due to its relatively large Cp, GLO crystal need larger quantity of heat energy to get heated up, so that consequent damage due to localised heating can be avoided, which enhances its prospects for applications in laser assisted devices.

4.2.7 Vickers' microhardness

Microhardness measurement on the (010) surface of the crystal was done for applied loads (P) from 5 gms to 100 gms with a dwell time of 5seconds using Leitz Miniload Hardness tester and the average indentation diagonal length(d) is measured. Figure (4.13) illustrates the Vicker's micro hardness profile [33] of the crystal calculated using the formula

$$H_v = 1.8544\ P/d^2\ Kg/mm^2 \qquad (4.8)$$

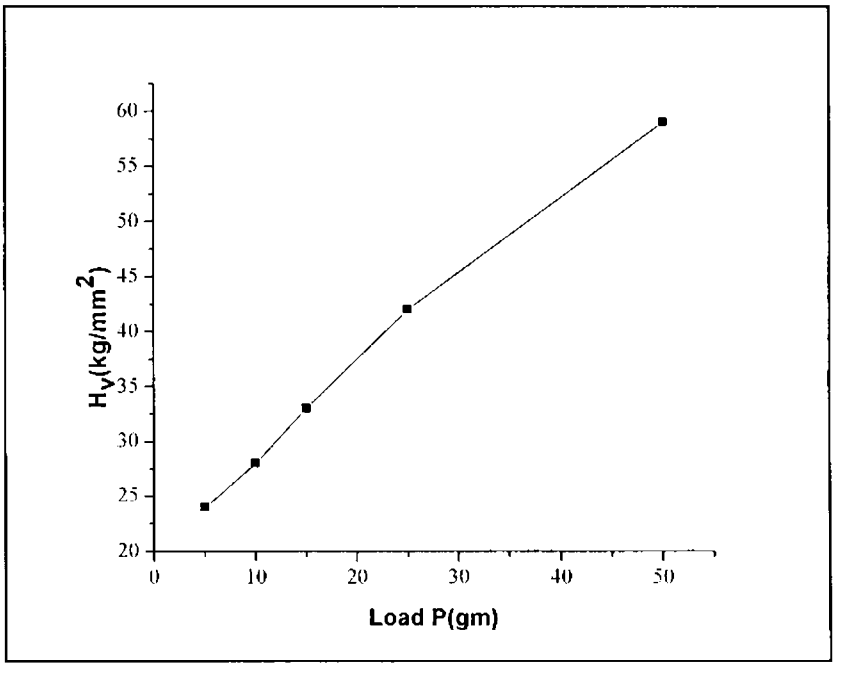

Fig.4.13. Plot of Vickers hardness number vs. load.

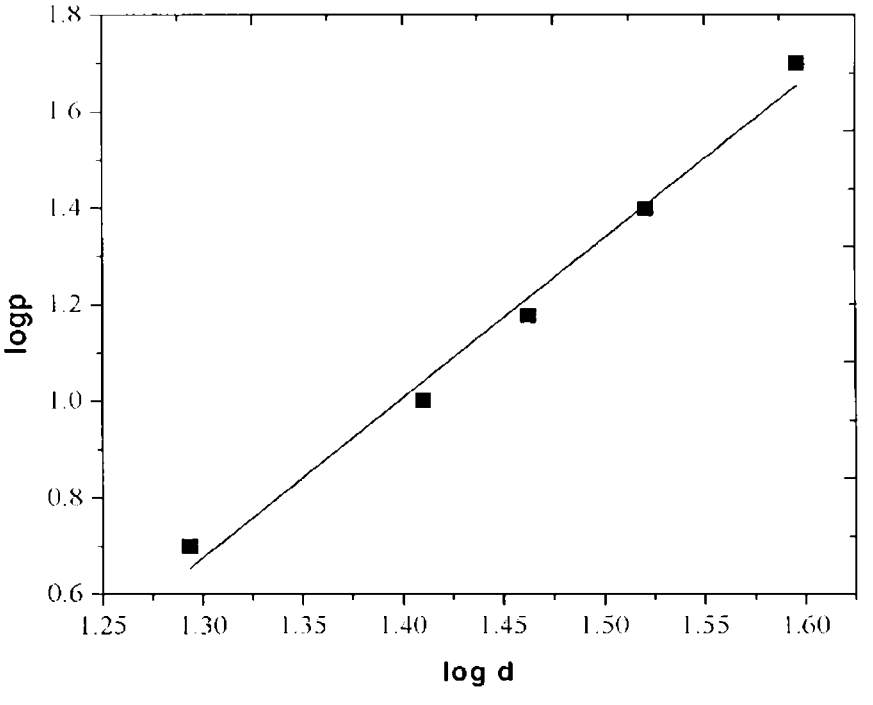

Fig. 4.14. Plot of log P vs. log d.

Increase in microhardness with increase of load in the low load region can be attributed to the heaping up of material at the edges of impression made by the indentor due to the slipping of layers [34]. At higher loads, slipping of layers stops which in turn hardens the crystal. Since crack initiation and material chipping become significant beyond 50 g of the applied load, hardness test could not be carried out above this load. Elastic stiffness constant C_{11} for various loads, which gives an idea about the tightness of bonding between neighboring atoms, is calculated using Wooster's empirical formula [35] and is given in table 4.4.

$$C_{11} = (H_v)^{7/4} \quad (4.9)$$

Table 4.4 Variation of C_{11} with load.

Load(gm)	Hv (kg/mm^2)	C_{11} (GPa)
5	24	1.1466
10	28	3.373
15	33	10.65
25	42	57.63
50	59	62.21

The slope of the Mayers' plot of log P versus log d shown in figure 4.14 yields the Mayers' index number 'n' which in the present case is found to be equal to 3.3. According to Onitsch [36] and Hanneman [37] 'n' should lie between 1 and 1.6 for hard materials and above 1.6 for softer ones. Hence GLO belongs to softer material category. According to Hays and Kendall's theory of resistance pressure [38], there is a minimum level of indentation load (W) also known as resistance pressure below which no plastic deformation occurs. 'W' can be found out by drawing a graph between d^n and d^2 which yields a straight line as shown in figure 4.15 according to the equation

$$d^n = w/k_1 + (k_2/k_1)\, d^2 \quad (4.10)$$

Where k_1 and k_2 are material constants. The value of W is calculated as 19.2 gm.

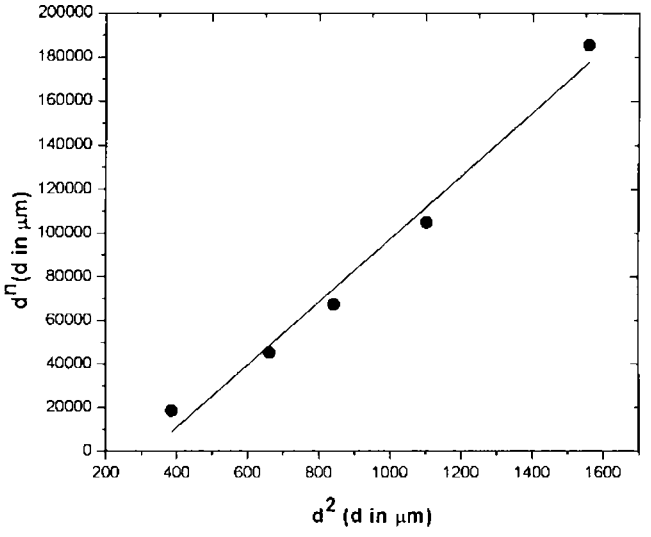

Fig. 4.15 Plot of d^n vs. d^2.

Vickers microhardness study on solution grown GLO crystals reveals that the Vickers hardness number Hv increases with increase in load and the sample belongs to soft material category as Meyer's index number 'n' is greater than 1.6. From Hey and Kendall's theory of resistance pressure, the minimum load that induces plastic deformation in GLO crystal is 19.2 gm which shows that the mechanical property of the crystal is quite good. The stiffness constant C_{11} is quite high, revealing that the binding forces between the ions are quite strong.

4.2.8 Chemical etching studies

Good optical quality crystals free from defects are used for micro topographical studies using Leica Q Win Systems metallurgical microscope to check the presence of features like spirals, hillocks, slip lines.....etc as they yield considerable information about the growth mechanism [39,44]. We have observed two dimensional growth layers of small step height on the free surface of almost all the crystals (Fig.4.16.a). Patterns like spirals, striations, slip bands, etc. are absent in the present study. The transmission photomicrograph of the inclusions present in the crystal is shown in Fig.4.16.b. A variety of parameters such as non-uniform growth rates, variation in super saturation during growth due to transition from dissolution to

growth are responsible for these types of patterns. Kitamura et al. [40] pointed out that liquid inclusions getting trapped parallel to the interfaces are due to drastic changes in growth conditions. GLO crystals show sharp cleavage on (010) plane, which shows river patterns and rivulets.

Chemical etching studies are carried out on the as grown and cleaved GLO crystals to study the symmetry of the crystal face from the shape of pits and the distribution of structural defects. First, the crystal is completely immersed in the etchant and then cleaned and dried and the etch figures are observed in the reflection mode. A mixture of n-propyl alcohol and distilled water is used as chemical polishing agent. Fig.4.16.c shows the pyramidal hillock with a circle at the middle portion formed by etching with dilute propionic acid. When the surface dissolution is low, the surface is smooth and the increased dissolution at dislocations can lead to terracing [41,45]. A composition of water in acetone in the ratio 1:5 volume is found to produce triangular etch pattern on the (010) surface when etched for 5-10 seconds is shown in Fig.4.16.d. When etched with water, fast dissolution layers are formed and are shown in figure 4.16.e. When etched with a mixture of acetic acid, methanol and distilled water circular etch pits are formed Fig.4.16.f. On successive etching no spurious development of pits is observed which suggests that etch pits are produced at the emergence of dislocation. It was found that propionic acid (50%) and formic acid (60%) and sulphuric acid in the volume ratio 8: 1:1 produces etch pits with their sides parallel to [010] and [110] directions(fig.4.16.g). The shape of etch pits reflects the slow dissolution rate along the directions parallel to the sides of the pits [42, 43]. Thus the dissolution rate along a [110] direction is faster than that along a [010] direction as seen from the structure of etch pits produced by this etchant. A hackle like pattern observed on the figure upon cleavage is shown in fig. 4.16.h. When the grown crystal is taken out from the solution and dried quickly, tree like structures are formed (fig.4.16.i). These dendrites are due to fast evaporation, which cause uneven growth resulting into the formation of dendrites. An indentation fracture pattern is represented by the photomicrograph 4.16.j. Slip bands and fracture lines are clearly visible in the figure. Following interesting features are noteworthy regarding the pattern observed in dynamic indentation. It can be seen that there are four prominent cracks forming a shape of letter 'V' on two opposite sides of the indentation mark

occupied by the regions of twin bands; whereas, on two other sides there are, no such prominent cracks. The cracks observed in the regions devoid of twin bands are quite short, less prominent in appearance and frequently curved as is seen in the photograph. The cracks forming the 'V' shape also run mostly along the terminations of the twin bands indicating the way in which the crack nucleate and propagates.

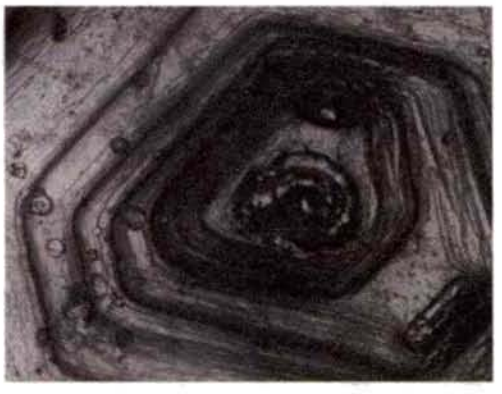

Fig. 4.16.a. 2D layers (×100)

Fig.4.16.b Inclusions (×100)

Fig.4.16.c pyramidal etch hillock (×100)

Fig.4.16.d triangular etch pits (×100)

Fig.4.16.e. Fast dissolution layers (×100)

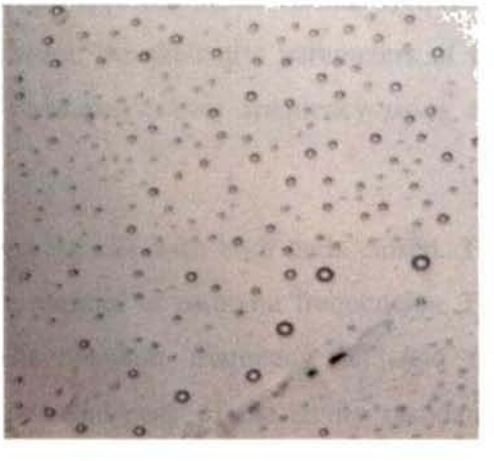

Fig.4.16.f. Circular etch pits (×100)

Fig.4.16.g. Elongated etch pits (×100)

Fig.4.16.h. Hackle like pattern (×100)

Fig.4.16.i Tree like dendrites (×100)

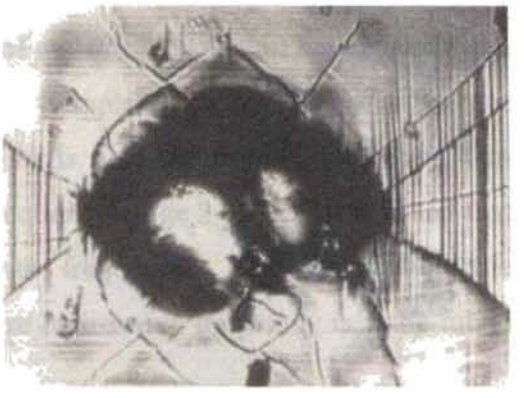

Fig.4.16.j. Indentation fracture (×100)

4.2.9 Microwave dielectric studies

Very little is known about the microwave absorption characteristics of NLO organic crystals. An understanding of the dielectric properties of the nonlinear optical GLO crystal is essential as far as device applications at various frequency ranges are concerned. Hence in the present work, the dielectric parameters of the GLO single crystals are investigated at S band microwave frequency using the resonant cavity perturbation method [46, 47].

The cavity is made from a S-band wave-guide with both ends closed. The length of the resonator cavity determines the number of resonant frequencies. The resonator is excited in the TE_{10p} mode. The resonant frequency 'f_0' and the corresponding quality factor 'Q_0' of each resonant peak of the cavity resonator, without sample placed at the maximum of the electric field, are noted. The

sample is introduced into the cavity resonator through the non-radiating slot. The resonant frequencies of the sample loaded cavity are selected and the position of the sample is adjusted for maximum perturbation (that is, maximum shift of resonant frequency with minimum amplitude for the peak). The new resonant frequency f_s and quality factor Q_s are determined. The procedure is repeated for other resonant frequencies. The frequency dependence of effective conductivity, dielectric constant and dielectric loss and absorption coefficient are plotted in figure.4.17

From the figure it is clear that variation of dielectric constant with increase in microwave frequency in the S band is negligible. Dielectric loss is very negligible throughout the S band. The very low value of dielectric loss is an indication of the better crystallinity of the crystals formed [48]. Samples with low dielectric loss are needed for device applications. Conductivity is also very small indicating that sample is an insulator to microwaves in the frequency range 2-3 GHz. It is found that absorption coefficient increases slightly with frequency. The exact dielectric behaviour of the material throughout the entire microwave frequency is to be found out.

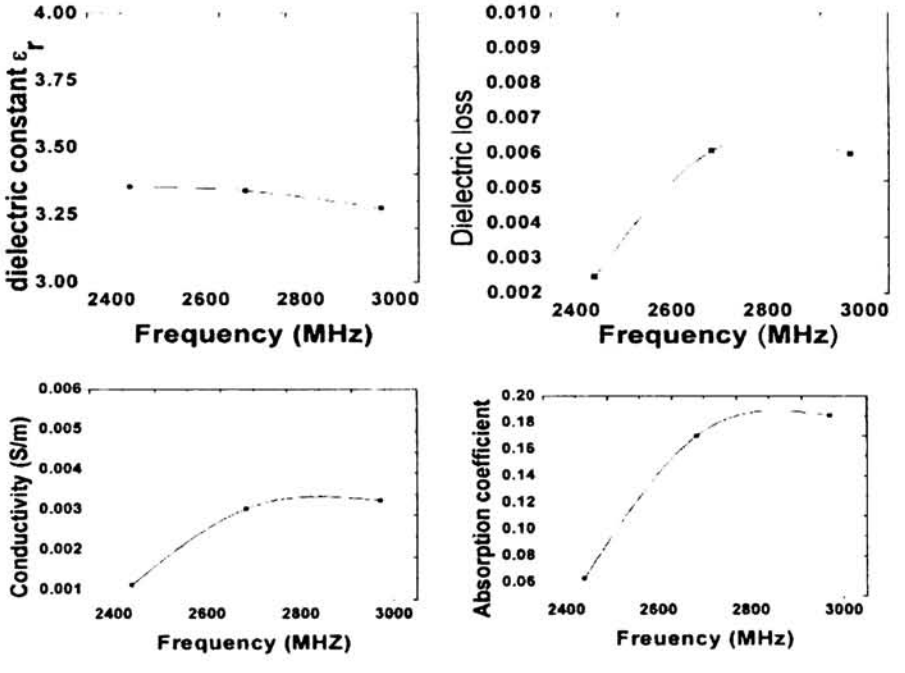

Fig. 4.17 Frequency dependence of the various dielectric parameters

4.2.10 Photoluminescence studies

Photo-luminescence spectrum (PL) is recorded with a Jobin Yvon Spectrofluorometer (Model FL3-22). A 450 W xenon lamp is used as the source and PMT (Model R928P) as the detector. Double gratings are used for the excitation and emission spectrometers. Excitation wavelength used is 260 nm. PL spectrum of GLO crystal recorded is shown in figure 4.18.

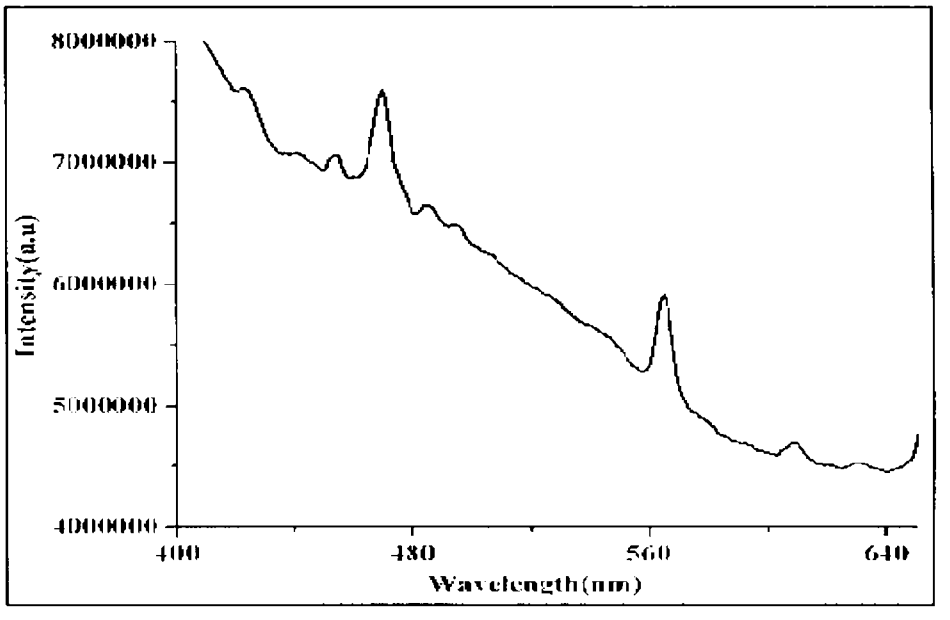

Fig. 4.18 PL spectrum of GLO

The main contribution to the HOMO state comes from the mono ionised oxalate ions, while to the LUMO state comes from the NH_3+ ions. In GLO molecular chains, these two molecular orbitals are at opposite extrema. So, in the interband transitions, the electron has to cross the whole chain, loosing energy to the vibrational modes of the crystal, contributing to the luminescence. Peaks in the visible region can be assigned to lattice related processes, while the peaks in the UV region can be due to the relaxation of excited molecular states. The maximum intensity peak at 470nm is assigned to a lattice related process. The intense PL emission observed at 470nm is significant from the view point of application of this material as bio compatible capping agents for nano particles in bio medical imaging and targeted drug delivery applications [49].

4.2.11 SHG in GLO crystal

The second harmonic generation behaviour of the powdered material is tested using Kurtz and Perry method [50]. A high-intensity Q switched Nd: YAG laser (λ =1064 nm) with pulse duration of 7 ns and frequency repetition of 10 Hz is passed through the sample. The SHG behaviour is confirmed from the output of the laser beam having the bright green emission (λ = 532 nm) from the specimen. The second harmonic signal of 110 mV was obtained for an input energy of 3.0 mJ/ pulse, while the standard KDP give a SHG signal of 120 mV for the same input energy. The second order nonlinear efficiency will vary with the particle size of the powder sample [51]. It has been found that vacancies influence the nonlinear optical properties of organic crystals, particularly the SHG [52].

It has been generally understood that the second-order molecular nonlinearity can be enhanced by systems with strong donor and acceptor groups [53,54]. Since a large molecular hyperpolarizability γ is the basis of a strong second harmonic generation (SHG) response, organic molecules that usually exhibit large γ values are certainly candidate molecules for NLO applications.

Table. 4.5 gives a comparison of the second harmonic generation in the GLO crystal with KDP crystal for different laser inputs.

Table 4.5 SHG data

Laser input	KDP	GLO crystal
3.0 mJ	120mV	110mv
5.0 mJ	211mV	198mv

4.2.12 Laser damage threshold studies

One of the decisive criteria for a NLO crystal to perform as a device is its resistance to laser damage, since high optical intensities are involved in nonlinear processes [55].

The laser damage threshold measurement is made on cleaved GLO single crystal (010) surface using a Q-switched Nd: YAG laser for 7 ns laser pulses operating in (TEM_{00}) mode at a wavelength of 1064 nm. The output intensity of the laser is controlled with a variable attenuator and delivered to the test sample located at the near focus of the converging lens. The lens with a focal length of 10 cm is used, which is useful in setting the spot size to the desired value according to the equation.

$$d' = 2.4\, f\lambda / d \qquad (4.11)$$

where d' is the diffraction limited beam diameter, f is the focal length of the lens at which the sample is placed, and d is the beam diameter at the output aperture of the laser.

The sample is mounted on a holder which is used to position the different sites in the beam. Single and multiple laser damage measurements are made on the cleaved face of the grown crystal. In the present study, the laser damage threshold energy density for the single shot is found to be 15.5 GW/cm^2 and that for the multiple shot is found to occur at laser power of 11.5 GW/cm^2. The laser damage threshold value is lower when the crystal is subjected to multiple shots. It reveals the fact that single shot damage threshold is higher than multiple shot damage. Figure 4.19 (a) and (b) depicts the laser damage pattern observed on the (010) crystal surface for single shot and multiple shot. Striation pattern of unequal width observed on the surface is depicted in figure 4.19 (c); the cause of which can be attributed to be of thermal origin. Since GLO has a room temperature specific heat of 898 J kg^{-1} K^{-1}, one can expect a high threshold value for laser damage and that is what we have observed in our investigation. Apart from the thermal effect, multiphoton ionization is an important cause of laser-induced damage [56]. For the pulse widths of several nanoseconds, the thermal effects are unavoidable, while for the picosecond pulse widths, the thermal effects are negligible. This is because the thermal effects take several nanoseconds to buildup and could take several milliseconds to decay [57]. The observed damage threshold value is greater than that of other known NLO organic single crystals [58-60].

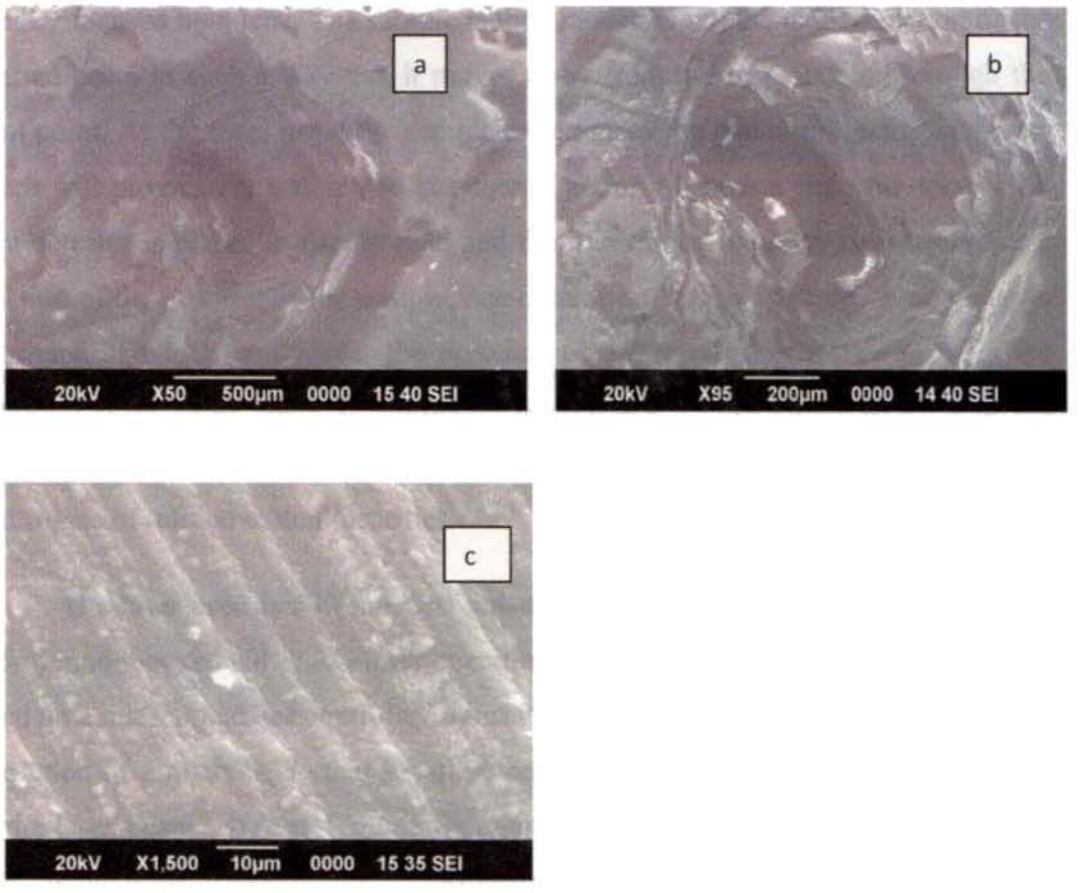

Fig.4.19 (a) single shot damage (b) multiphoton damage (c) Thermal striation pattern

4.2.13 Z Scan measurement of the optical non linearity

There is considerable interest in finding materials having large yet fast nonlinearities. This interest is driven primarily by the search for materials for all-optical switching and sensor protection applications, which concerns both nonlinear absorption (NLA) and nonlinear refraction (NLR).

The Z-scan technique is a method which can measure both NLA and NLR in solids, particularly in liquids and liquid solutions [61, 62], and has gained rapid acceptance as a standard technique for separately determining the nonlinear changes in index of refraction and changes in absorption. This acceptance is primarily due to the simplicity of the technique as well as the simplicity of the interpretation. The index change, Δn, and absorption change, $\Delta\alpha$ can be determined directly from the data without resorting to fitting.

In a typical *z*-scan experimental setup, a laser beam with a Gaussian profile is initially focused by a lens. The sample is then moved along the axial direction of the focused beam in such a way that it moves away from the lens, passing through the focal point. At the focal point the sample experiences the maximum pump intensity, which will progressively decrease in either direction of motion from the focus. If a light detector is placed in the far field and the transmitted intensity is measured as a function of the position of the sample, one obtains an ''open aperture'' *z*-scan curve, the shape of which will reveal the presence of any absorptive nonlinearity in the sample. On the other hand, if a properly chosen aperture is placed in front of the detector, a ''closed aperture'' *z*-scan curve is obtained which will reflect the occurrence of refractive nonlinearities.

The laser used is 532 nm, 7ns pulses from the second harmonic output of a hybrid mode-locked Nd: YAG laser operating at 10 Hz repetition rate. The crystal is fixed on a microprocessor controlled translation stage that has a range of 30 cm and a resolution of 2 microns, so that it can be accurately moved through the focal region of the laser beam. A fast photodiode monitors the input laser energy, and a large area photodiode collects the transmitted beam. For the closed aperture measurements, a suitable aperture is placed in front of the photo diode. Data acquisition is facilitated in real time by the use of a PC.

In the open aperture *z* scan, the open aperture transmission normalized to the linear transmission of the sample is plotted against the sample position measured relative to the beam focus is shown in figure 4.20. Nonlinear absorption in the present study is indicated by a smooth valley-shaped curve, symmetric about the focal ($z = 0$) position. The RSA coefficient β (m/W) can be obtained from a best fitting performed on the experimental data of the OA measurement with the equations (4.12) and (4.13)[70] where α and β are the linear and effective third order NLO absorption coefficients, respectively, τ is the time, I(z) is the irradiance and L is the optical path length.

$$T(Z)= \frac{1}{Q(z)\sqrt{\pi}} \int_{-\infty}^{+\infty} \ln [1 + Q(z)]e^{-\tau 2}\, d\tau \qquad (4.12)$$

$$Q(Z)= \beta I(Z) \frac{1-e^{-\alpha L}}{\alpha} \quad (4.13)$$

where $\frac{1-e^{-\alpha L}}{\alpha}$ is the effective path length L_{eff}

The value of the non linear absorption coefficient β is found to be equal to be 7.429 cm/ GW.

Figure 4.21 shows a typical closed aperture *z* scan, obtained for glycinium oxalate crystal. The peak-valley structure of the curve is a clear indication of a negative refractive nonlinearity exhibited by the medium [62]. The nonlinear refraction coefficient n_2 (m^2/W) is obtained through the following equation

$$\Delta\Phi_0 = k n_2 I_0 L_{eff} \quad (4.14)$$

In the above equation the phase shift $\Delta\Phi_0$ is equal to $2\pi/\lambda\ n_2\ I_0\ L_{eff}$.

The difference between the normalized transmittance at the peak and valley is related to $\Delta\Phi_0$ by the relation

$$\Delta T_{P-V} = 0.406\ (1-S)^{0.25}\ \Delta\Phi_0 \quad (4.15)$$

The value of n_2 is calculated to be equal to $-1.689\times10^{-13} m^2/W$.

The molecular second hyperpolarizability, γ, may be obtained to be 4.0424×10^{-24} esu with the equation below [71]

$$\gamma = 40\pi\ n_2/\ c n_0 \quad (4.16)$$

The real and imaginary parts of the χ (3) of the sample can also be calculated by the following equations [63- 68]

$$\text{Re}\ \chi^3\ (\text{esu}) = (c n_0^2/\ 120\pi^2)\ n_2, \quad (4.17)$$

$$\text{Im}\ \chi^3\ (\text{esu}) = (c n_0^2 \varepsilon_0 \lambda\ /2\pi)\ \beta \quad (4.18)$$

The value of the real part of nonlinear susceptibility Re χ^3 (esu) and imaginary part Im χ^3 (esu) is found to be equal to 1.474 $\times 10^{-11}$ esu and 0.40854$\times 10^{-11}$ esu respectively.

Introducing the coupling factor ρ, the ratio of imaginary part to real part of third-order nonlinear susceptibility,

$$\rho = \text{Im } \chi^3 / \text{Re } \chi^3 \qquad (4.19)$$

The value of ρ in this case is found to be equal to 0.27

The observed value of coupling factor is seen to be less than 1/3, which indicates that the nonlinearity is electronic in origin [71].

The open aperture curve demonstrates a nonlinear absorption and the characteristic pattern of the curve shows that the nonlinear absorption is reverse saturation absorption (RSA) implying that the crystal can be effectively used for optical limiting applications. The peak to- valley configuration of the closed aperture curve suggests that the refractive index change is negative, exhibiting a self defocusing effect [69]. The experimental results exhibit that the GLO crystal possesses a large third-order NLO properties. The reason for the large value of RSA coefficient may be due to the delocalization resulting from the protonation of amino group leading to the formation of glycinium oxalate molecule.

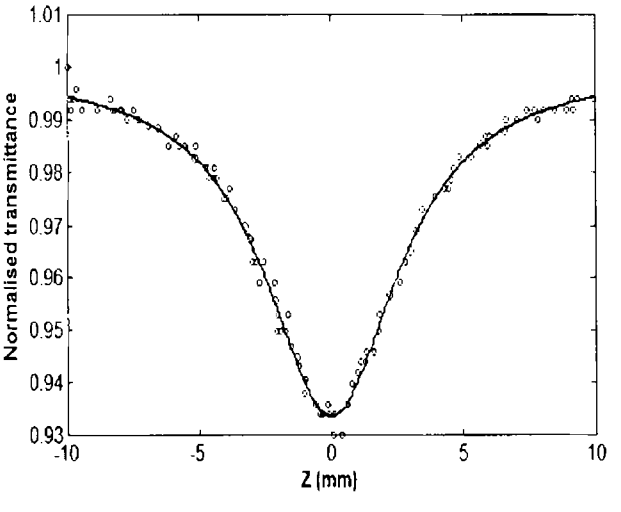

Fig. 4.20 open aperture Z scan curve of GLO

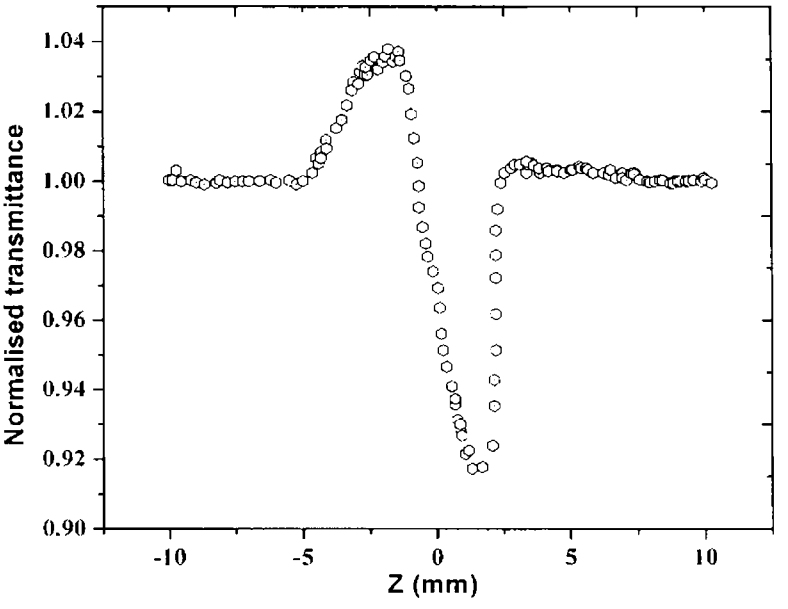

Fig.4.21 closed aperture Z scan curve of GLO

4.3 CONCLUSIONS

Glycinium oxalate single crystals are grown from the saturated solution at ambient temperature. Powder XRD study on the grown crystal agrees well with the reported single crystal XRD data. CHN analysis confirms the molecular formula as $C_4H_7NO_6$. The vibrational analysis carried out using the FTIR and FT Raman spectroscopy shows the presence of NH_3^+ ion confirming the protonation of amino group leading to the formation of glycinium oxalate molecule. The non centrosymmetry in the grown crystals of glycinium oxalate is established on the basis of the excellent match between the various vibrational frequencies in the vibrational spectra. Thermal studies carried out employing TGA/DTA and DSC techniques, establish that the crystal has thermal stability up to 180^0C. Vickers' microhardness analysis carried out on the material suggests that the material belongs to soft material category. The value of load independent resistance to deformation is calculated as 19.2 g. Dislocation density for solution grown GLO, in the present study is about $10^4/cm^2$ which is quite small compared with many other solution grown inorganic semiconductors. It is established that growth mechanism of GLO single crystals in

the present work is 2D nucleation and subsequent spreading of layers. It is seen that the GLO crystal has a wide transparency window ranging from 324 nm to 2500nm and the absorption throughout this range is very small. This aspect highlights its prospects of applications as a material for higher harmonic generation in nonlinear optics. The value of the linear optical constants, α, n and k are evaluated and these values are used to compute the non linear optical parameters from the Z scan studies. The value of dielectric loss found by microwave cavity perturbation technique for this crystal is very small which is of the order of 0.006, and is an indication of the crystalline perfection of the grown crystal. The intense emission peak at 470 nm in the PL spectrum observed in GLO crystal extends ample scope for further detailed investigations in this direction. The SHG efficiency of the crystal is found to be 0.92 times that of KDP by Kurtz and Perry technique. The single shot (P_1) and multiple shot (P_n) laser damage threshold values for (010) cleaved face of GLO are found to be 15.5 and 11.5GW cm^{-2}, respectively for 1064 nm, pulsed Nd: YAG laser radiation. Open aperture Z scan studies carried out using 532nm radiation of the pulsed Nd: YAG laser of 7ns pulse width shows that there is reverse saturable absorption (RSA) in the material and two photon absorption is the mechanism responsible for RSA. The peak-valley structure of the curve obtained in the closed aperture Z scan studies is a clear indication of a negative nonlinear refraction exhibited by the crystal.

4.4 REFERENCES

[1] J. Badan, R. Hierle, A. Perigaud, NLO properties of organic molecules and polymeric materials, American Chemical Society, Washington,1993.

[2] P.N. Prasad, D.J. Wollians, Introduction to Nonlinear Optical Effects in Molecules and Polymers, Wiley, New York, 1991.

[4] S.B. Monaco, L.E. Davis, D. Eimerl, A.J. Zalkin, J. Cryst. Growth, 85, 252(1987).

[3] D.K. Hakerston, Biochemistry, Wiley, Singapore, 1990.

[5] B. N. Moolya, S.M. Dharmaprakash, J. Cryst. Growth, 280, 581(2005).

[6] M. Subhanadinini, R. V. Krishnakumar, S. Natarajan, Acta. Cryst. C57, 165(2001).

[7] G. S. Pawley, J. Appl. Cryst 14, 357(1981).

[8] M. Toulemonde, C. Dufour, E. Parrmier, Phys. Rev. B,4, 14362, (1992) .

[9] R. Silverstein, G. C. Bassler, Spectrometric identification of organic compounds, Wiley& sons, New York, (1981).

[10] N. Daude, C. Gout, and C. Jounain, Phys.Rev. B. 15, 3229 (1977).

[11] D. R. E. Campbell and R. D. Tomlin, J. Phys. D 5, 852(1972).

[12] A. A. El-Kadry and N. Mahmoud, Thin Solid Films 269, 117(1995).

[13] I. C. Ndukwe, Sol. Ener. Mater. Sol. Cells, 40, 123(1996).

[14] Janai, M., D. D. Alfred, D. C. Booth and B.O. Seraphin, Sol. Ener. Mater, 1, 11(1979).

[15] J. I. Pankove, Optical processes in semiconductors, Prentice-Hall, New York, 1971.

[16] B. Smith, Infrared Spectral Interpretation: A Systematic Approach, CRC press, Washington, DC, 1999.

[17] J. Baran, A.J. Barnes, H. Ratajczak, Spectrochim. Acta A, 51,197(1995).

[18] A. Novak, Struct. Bonding 18,177(1973).

[19] T. Edsall, H. Scheinberg, J.Chem. Phys. 8, 520(1940).

[20] L.J. Bellamy, The Infrared Spectra of Complex Molecules, Chapman and Hall, London, 1980.

[21] N.B. Colthup, L.H. Daly, S.E. Wiberley, Introduction to Infrared and Raman Spectroscopy, Academic Press, New York, 1990.

[22] I. Hubert Joe, G. Aruldhas, P. Ramasamy, J. Cryst.Res.Technol. 29, 685(1994).

[23] J. Lia, Y. Wu, S. Hu, G. Lan, J. Zheng, J. Mol. Struct. 446,109,(1998).

[24] G. Litvinov, Proceedings of the XIIIth International Conference on Raman Spectroscopy, Wurzburg, Germany, 1992.

[25] K. Furic, V. Mohacek, M. Bonifacic, I. Stefanic, J. Mol. Struct. 267, 39,(1992).

[26] G. Lan, H. Wang, Spectrochim. Acta A,46,1211(1990).

[27] K. Machida, A. Kagayama, Y. Saito, T. Uno, Spectrochim. Acta A,33,569(1977).

[28] F.R. Dollish, W.G. Fateley, F.F. Bentley, Characteristic Raman Frequencies of Organic Compounds, Wiley, New York, 1974.

[29] B. Borut Lavrencic, V.S. Robin, Ferroelectrics 88,37(1988).

[30] L. Santra, A.L. Verma, B. Hilczer, P.V. Huong, J. Phys.Chem. Solids 55,405(1994).

[31] M.J.O'Neill, Anal. Chem., 38, 1331(1966).

[32] Arun.K.J, S.Jayalekshmi, Optoelectron. Adv. Mater (RC), Vol. 2(11), 701, (2008).

[33] Meyer, Some aspects of the hardness of materials, PhD thesis, Dreft, 1951.

[34] M. Hanneman, Metall. Manchu. 23,135(1941).

[35] C. Hays, E.G. Kendall, Metallurgy 6, 275(1973).

[36] E.M. Onitsch, Mikroscopia 2, 131(1947).

[37] F. Kick, Proportionalen Widerstande Und Science Anwendung, Felix, Leipzig, 1885.

[38] W.A. Wooster, Rep. Progr. Phys. 16, 62(1953).

[39] M. S. Joshy, A. S. Vagh, Ind. J. Pure & Appl.Phys, 5,318(1967).

[40] M. Kitamura, A. Kouchi, J. Miner, 3, 119 (1982).

[41] K. Sangwal, Etching of crystals, North Holland Physics Publication, Amsterdam, 1987.

[42] Barber D J, J. Appl. Phys. 33 3141 (1962).

[43] Hari Babu V, Sirdeshmukh D and Bansigir K.G, Phil. Mag. 14 1067 (1966).

[44] K.Kishan Rao, V.Surender, Bull. Mater.Sci. 24, 6 (2001).

[45] Binay Kumar, Nidhi Sinha., Cryst.Res.Technol.40, 9(2005).

[46] K.T. Mathew, U. Raveendrnath.K, Sensors Update (Ger.) 7, 185(1999).

[47] K.T. Mathew, U. Raveendrnath.K, K.G. Nair, Micro. Opt. Tech. Letts. 6,104(1993).

[48] Jaimon Yohannan, K. Nandakumar, Nuclear Instru. Meth. Phys. Res. B, 156, 227(1999).

[49] Ju Ho Lee, Yong Kim, Kimoon Kim, Bull. Korean Chem. Soc., 28(7), 1091(2007).

[50] S.K. Kurtz, T.T. Perry, J. Appl. Phys. 39, 3798(1968).

[51] F. Joseph Kumar, D. Jayaraman, P. Ramasamy, J. Cryst. Growth 137, 535 (1994).

[52] I.V.Kityk, B.Marciniak, A.N.Mefleh, J.Phys.D 34, 1 (2001)

[53] N. Ponpandian, P. Balaya, and A. Narayanasamy, J. Phys: Cond. Matter 14, 3221 (2002).

[54] C. V. Kannan, C. Subramanian, P. Ramasamy, Cryst. Res. Technol. 37, 1180 (2002).

[55] A. J. Glass and A. H. Guenther, Appl. Opt. 12, 637 (1973).

[56] B. C. Stuart, M. D. Feit, A. M. Rubenchik, M. D. Perry, Phys. Rev. Lett. 74, 2248 (1995).

[57] F. Mauro, J. Opt. A: Pure Appl. Opt. 1, 662 (1999).

[58] Bhat, H. L. Bull. Mater. Sci., 17, 1233(1994) .

[59] Boomadevi, S.; Dhanasekaran, R. J. Cryst. Growth 261, 70 (2004).

[60] S. S. Gupte, R. D. Pradhan, C. F. Desai J. Appl. Phys. 91, 3125 (2002).

[61] M. Sheik-Bahae, A.A. Said, and E.W. Van Stryland, Opt. Lett. 14, 955(1989).

[62] M. Sheik-Bahae, A. A. Said, T. H. Wei, D. J. Hagan, E. W.Van Stryland, IEEE J. Quantum Electron. 26, 760 (1990)

[63] W. A.Schoonweld, J. Wildeman, D. Fichou, Nature 404, 977(2000)

[64] J. Zyss, J. F. Nicoud, Curr. Opin. Solid State Mater. Sci. 1, 533 (1996).

[65] M. Subhanadinini, R. V. Krishnakumar, S. Natarajan, Acta. Cryst. C57, 165 (2001).

[66] N. Sandhyarani and T. Pradeep, Chem. Mater. 12, 1755 (2000).

[67] M. Sheik-Bahae, A. A. Said and E. W. Van Stryland, Opt. Lett., 14, 955 (1989).

[68] G. Yang, W. T. Wang, L. Yan, H. B. Lu, and Z. G. Chen, Opt. Comm. 209, 445 (2002).

[69] S.F. Wang, W. T. Huang, T. Q. Zhang, and Y. F. Miura, Appl. Phys. Lett. 75, 1845 (1999).

[70] S. Hughes, B. Wherret, Phys. Rev. A 54, 3546 (1996).

[71] Seetharam.S, G. Umesh, K. Chandrasekharan, B.K. Sarojini, Opt. Mater. 30 1297(2008)

****ꕥ****

Chapter 5

GROWTH AND CHARECTERISATION OF NONLINEAR OPTICAL SINGLE CRYSTALS OF L-ALANINIUM OXALATE

Chapter 5

GROWTH AND CHARACTERISATION OF NONLINEAR OPTICAL SINGLE CRYSTALS OF L-ALANINIUM OXALATE

5.1 INTRODUCTION

In the modern world, the development of science in many areas has been achieved through the growth of single crystals. Large sized single crystals are essential for device fabrication and efforts are taken to grow large single crystals in short duration with less cost.

Over the past two decades much attention has been paid to the search of novel high quality NLO materials that can generate high second order optical nonlinearities which is important for potential applications including telecommunication, optical computing, and optical data storage and processing. [1] – [6]. Organic NLO materials are formed by weak Van der Waals and hydrogen bonds with conjugated π electrons and are more advantageous than their inorganic counterparts due to high conversion efficiency for second harmonic generation and transparency in the visible region, high resistance to optical damage and so on. They also offer the flexibility of molecular design and the promise of virtually an unlimited number of crystalline structures. Traditionally, crystals of organic materials have been grown from the melt or from vapor or solution.

The α amino acid L alanine can be considered as the fundamental building blocks of more complex amino acids which show strong non linear behaviour and anomalous phonon coupling and is a system exhibiting vibrational solitons [7].

In the present work, an attempt is made to synthesize and grow an organic charge transfer complex NLO material L alaninium oxalate (LAO) using L alanine and oxalic acid. The top seeded, aqueous solution grown crystals of LAO by slow

evaporation are characterized by powder XRD, TGA/DTA, DSC, FTIR, FT Raman, CHN analysis, UV/Vis/NIR absorption spectroscopy, Vickers' microhardness analysis, chemical etching studies, photoluminescence studies and the results are reported. The second and third order NLO response and laser damage threshold are tested by using a pulsed Nd: YAG laser and are discussed in detail.

5.2 SYNTHESIS AND GROWTH

L alaninium oxalate is synthesized from equimolar solution of L alanine and L oxalic acid by evaporation preventing decomposition. Synthesized samples are crystallized repeatedly to get a pure, colorless, crystalline powder. Good quality seed crystals are prepared using this powder. One or two seed crystals are then placed in its supersaturated solution kept in a bath at ambient temperature. Seed crystals are grown to big crystals by slow evaporation to a size of about 40x 15 x 8 mm^3 with good transparency in a time of about three weeks [fig.5.1] as reported by the authors[8,9].

Fig.5.1 LAO single crystal

5.3 CHARECTERISATION METHODS

5.3.1 Powder X ray diffraction studies

Powdered XRD spectrum of the crystals is recorded using Rigaku X ray diffractometer using Rigaku x ray diffractometer with CuKα radiation to identify the compound and structure

From the XRD data, it is found that L-alaninium oxalate belongs to the orthorhombic system with a = 5.65A°, b= 7.26 A° and c= 19.69 A°, the space group being $P2_12_12_1$ and has four molecules in the unit cell with a volume of 808.37 A°. The close agreement with the observed, calculated and reported d values [10] confirm the identity of the grown crystal. The recorded powder XRD pattern is given in Figure 5.2. In the layered crystal structure of LAO (Fig.5.3), the amino group of the L-alaninium cation forms three N– H...O hydrogen bonds with the oxygen of semi oxalate group and a symmetry-related alanine cation. There also exists two O–H...O hydrogen bonds. The alaninium and semi-oxalate ions form alternate columns leading to a layered arrangement parallel to the a.c. plane and each such layer is interconnected to the other through N–H...O hydrogen bonds. Two short C...O contacts involving the carboxyl oxygen of the alaninium ion [C1....O2 (1/2 + x, 3/2 – y, – z) = 2.931(3) Å and C2...O2 (– 1/2 + x, 3/2 – y, – z) = 2.977(3) Å] are also observed in these layers. The slight difference observed in the bond lengths of C5–O5 [= 1.219(2) Å] and C5–O6 [= 1.235(2) Å] in the carboxylate group of the semi-oxalate ion may be attributed to the difference in strengths of the N–H...O hydrogen bonds in which both O5 and O6 are involved.

Powder XRD data recorded is given in table 5.1. Using Pawley method [11], 320 diffraction peaks are identified for L alaninium oxalate crystal from the powder x-ray diffraction.

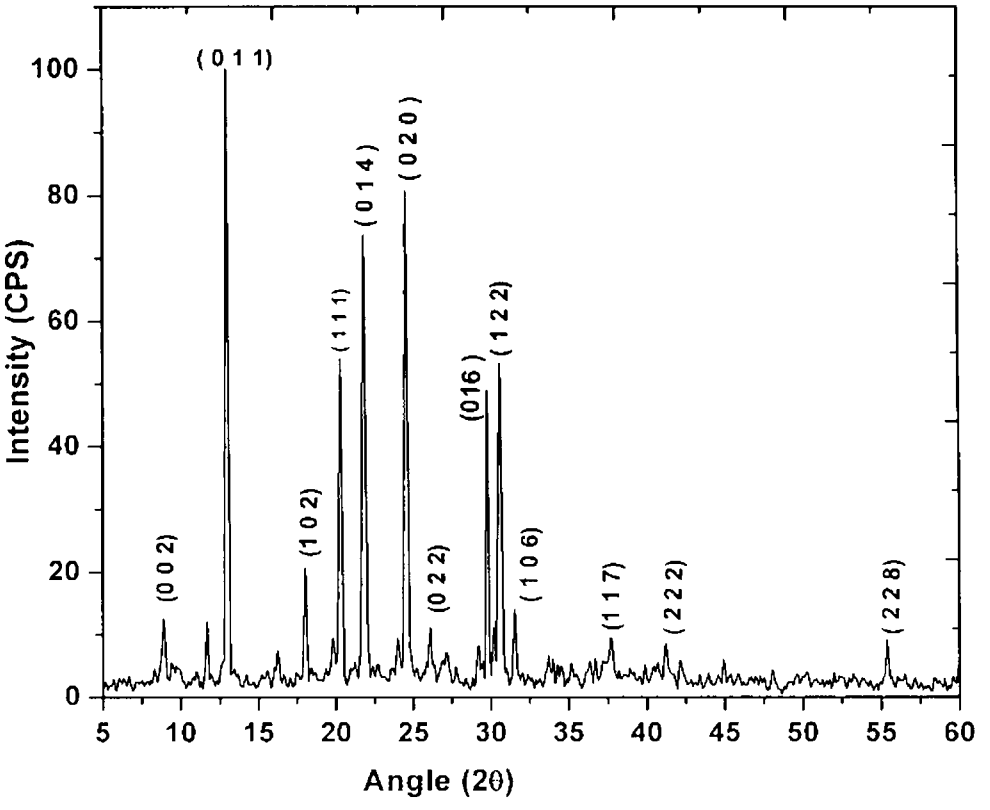

Fig. 5.2 Powder XRD spectrum of LAO

Space group	**$P2_12_12_1$**
Cry. Size Lorentzian(nm)	322.6
Lattice parameters	
a (Å)	5.65
b (Å)	7.26
c (Å)	19.69
Volume(Å^3)	808.37

Table 5.1 unit cell parameters of LAO crystal

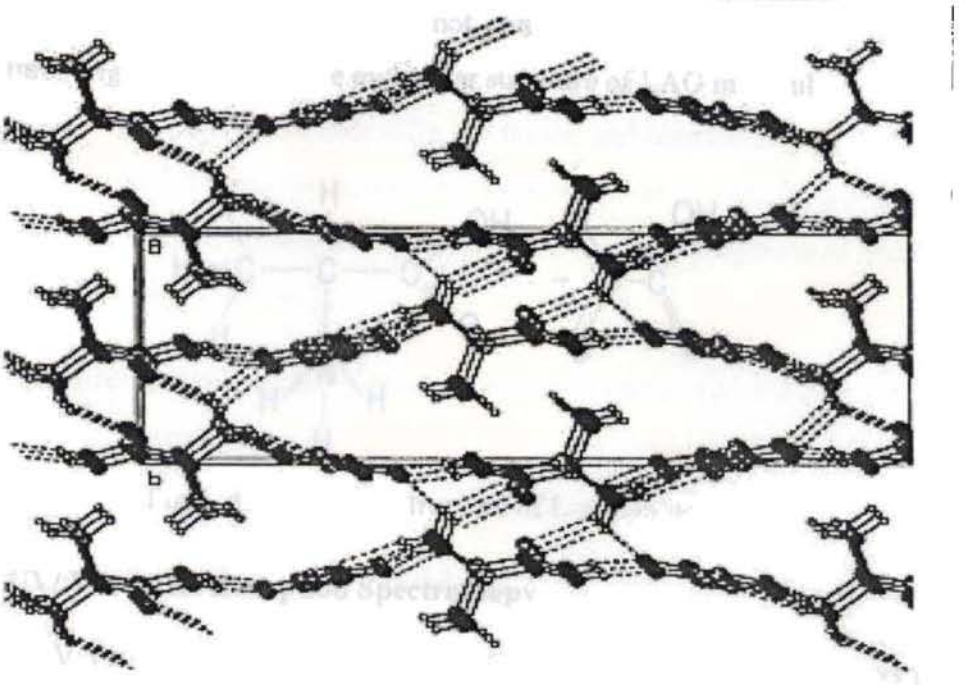

Fig 5.3. Layer structure of LAO crystal

5.3.2 Measurement of Density

The measurement of density is one of the important methods to study the purity of crystals. The most sensitive method to find the density of the crystal, namely, the swim or sink method [10] is used in the present study. In this analysis, theoretical density value is found using the formula, density = $(MZ)/(NV)$; where M is the molecular weight, Z is the number of molecules per unit cell, N is the Avogadro number, and V is the volume of the unit cell. The density values are experimental: 1.35 g/ cm^3; and theoretical: 1.37 g/ cm^3.

5.3.3 CHN Analysis

The chemical composition of the grown crystal determined using CHN analysis reveals that it contains 33.18% carbon (33.51%), 4.96% hydrogen (5.02%), 7.79% nitrogen (7.82%) where the figures in bracket represent the theoretical composition. Thus the molecular formula of the compound L alaninium oxalate is

established as $C_5H_9NO_6$ and it does not contain any water of crystallisation in its structure. Figure 5.4 shows the molecular structure of LAO molecule.

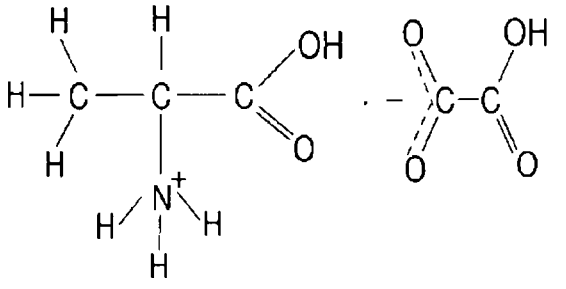

Fig.5. 4. Molecular structure of L-alaninium oxalate.

5.3.4 UV/ Vis/ NIR Absorption Spectroscopy

UV/Vis/NIR absorption spectrum [Fig.5.5] shows that LAO crystal has a wide transparency window without any absorption in the UV, visible and near IR regions, ranging from 318 nm to 1524 nm suggesting its suitability for second and third harmonic generations of the 1064 nm radiation and other applications in the blue – violet region.

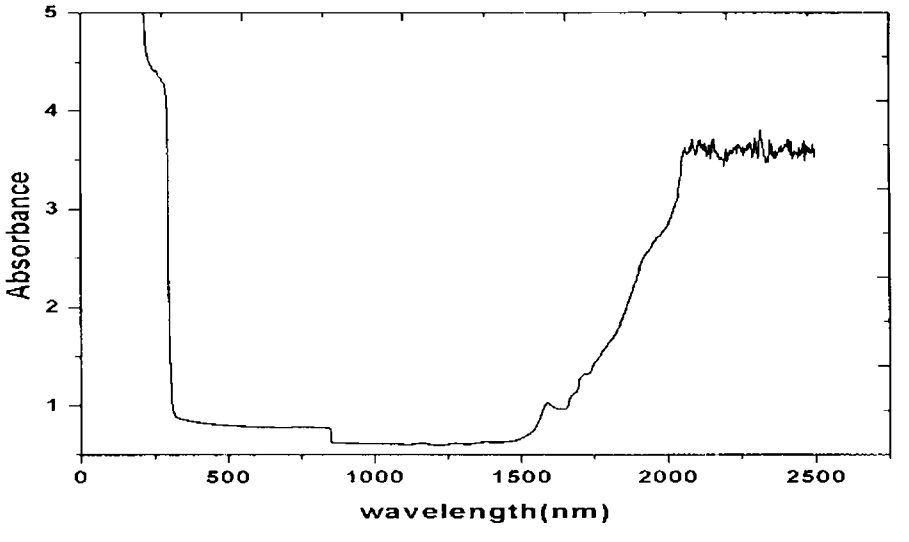

Fig.5.5. UV/Vis/NIR absorption spectrum of L-alaninium oxalate

It is well known that efficient NLO crystal has an optical transparency at lower cut-off wavelength between 200 and 400nm [12]. It is seen that LAO crystal has a wide transparency window without any absorption in the fundamental and

second harmonic wavelengths, ranging from 318 nm to 1524 nm suggesting its suitability for SHG of the 1064 nm radiation and other NLO applications. The low absorption in the visible and near infra red region and considerable absorption in the deep UV and far IR region enables its application as a suitable material for the construction of poultry roofs and walls and for coating eyeglasses as antireflection and thermal control coatings [13].

The relationship between absorption coefficient α and photon energy hυ [14-18] can be expressed as

$$\alpha h\upsilon = A (\alpha h\upsilon - Eg)^n \qquad (5.1)$$

where A is a constant nearly independent of photon energy and Eg is the optical energy gap. Here n represents an index that can take any of the values 1/2, 3/2, 2 or 3 depending on the type of transition responsible for the absorption. For allowed direct transitions n = 1/2 while for allowed indirect transitions n = 2. The range within which this equation is valid is very small and hence it becomes too difficult to determine exactly the value of the exponent n [19]. The simplest way to deduce the type of transition is to examine the value of n which relates hυ to αhυ with a straight line relationship. From figure 5.6 the value of optical band gap is calculated as equal to 4.09 eV.

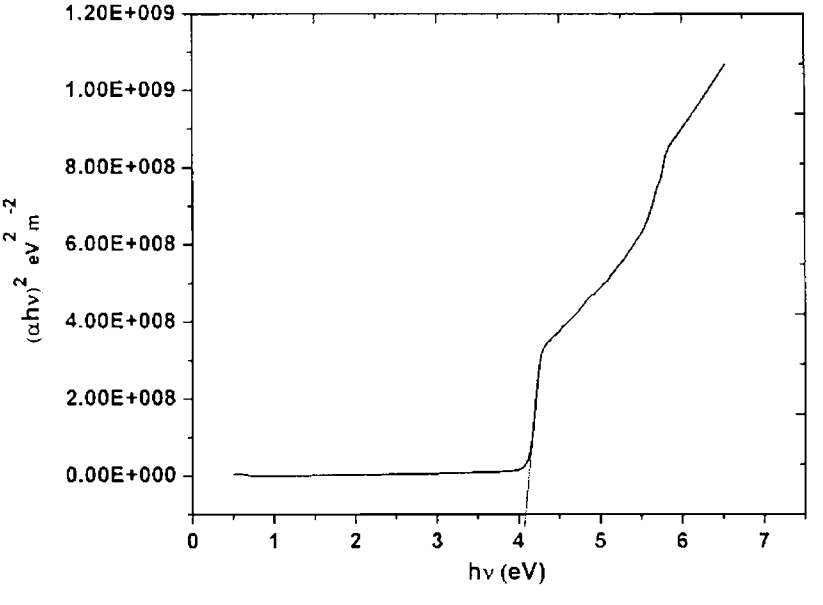

Fig. 5.6 Plot of $(\alpha h\upsilon)^2$ versus hν for the LAO crystal

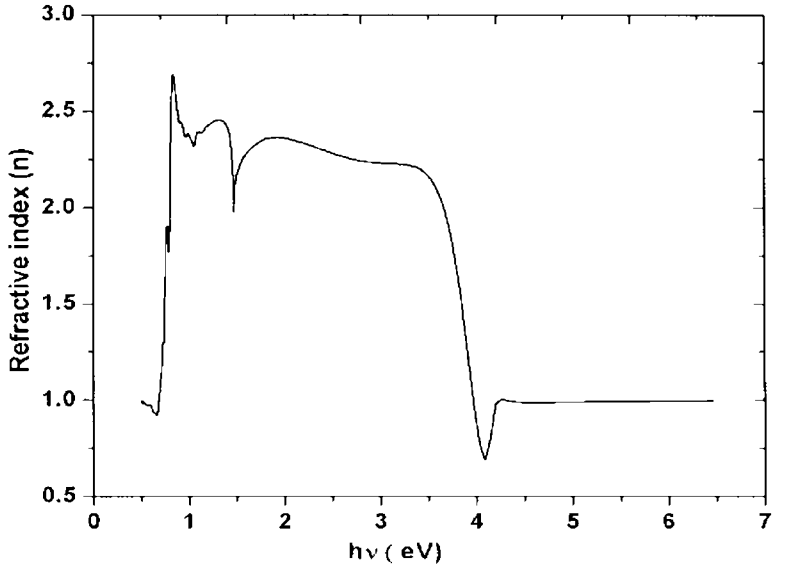

Fig. 5.7 Plot of variation of n with energy

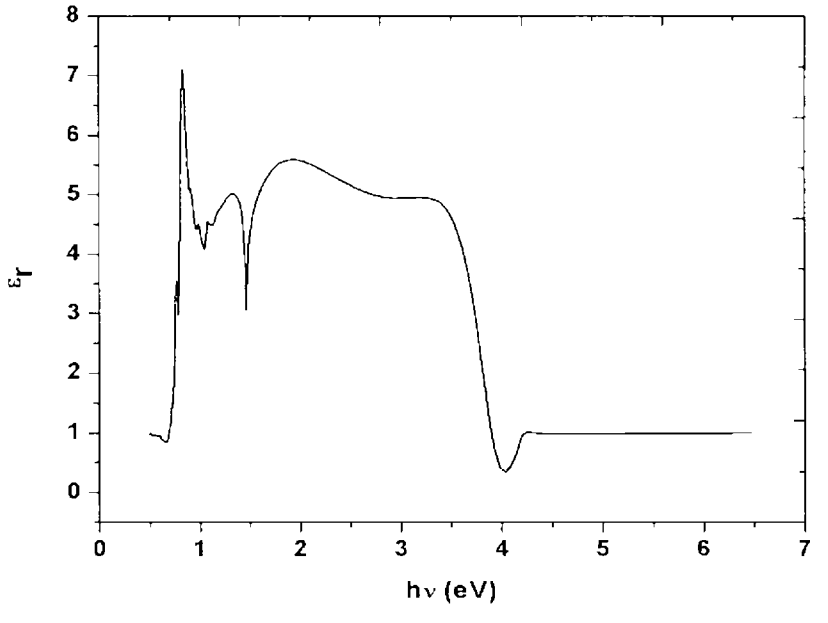

Fig. 5.8 Plot of variation of ε_r with energy

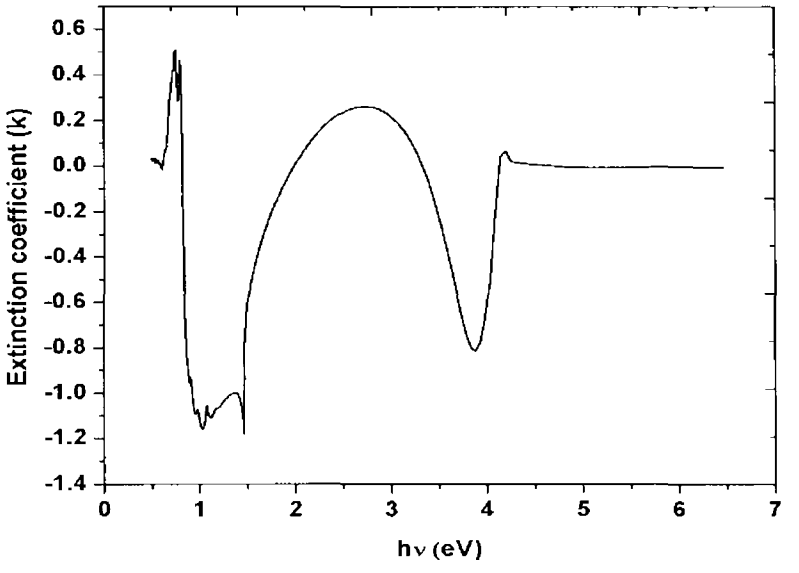

Fig. 5.9 plot of variation of k with energy

The optical constants (n, k) are determined from the transmission (T) and reflection (R) spectrum based on the following relations [20, 21].

$$T= (1-R)^2 \exp(-\alpha t) / 1-R^2 \exp(-\alpha t) \quad (5.2)$$

where t is the thickness and the absorption coefficient α is related to extinction coefficient k (absorption index) by

$$k= \alpha \lambda / 4\pi \quad (5.3)$$

For semiconductors and insulators (where $k^2 << n^2$) there exists a relationship between R and n (refractive index) given by [22, 23]

$$R = (n-1)^2/(n+1)^2 \quad (5.4)$$

The relationship between ε and k is given by [24] $\varepsilon = \varepsilon_r + i\varepsilon_i = (n + ik)^2$ (5.5)

$$\varepsilon_r = n^2-k^2 \quad (5.6)$$

$$\varepsilon_i= 2nk \quad (5.7)$$

The variation of both the extinction coefficient (k) [fig.5.9] and the imaginary part of the dielectric constant ε_i with energy preserves the same dependence of the absorption coefficient (α) while the variation of ε_r, the real part of the dielectric constant [fig.5.8], with energy is similar to that of the refractive index (n) variation [fig. 5.7].

5.3.5 Thermal Analysis

The good thermal stability of LAO crystals up to 196°C establishes that it has prospects in laser applications where crystals should withstand high temperature. In the TGA/DTA curve (Fig. 5.10) there is a large endothermic peak at196°C and a very small endothermic peak at around 98°C. The major peak is the melting point of the crystal as the major weight loss occurs after that point and the minor peak is assumed to be a weak solid to solid phase transition as there is no weight loss at this temperature and there is no water of crystallization in the crystal.

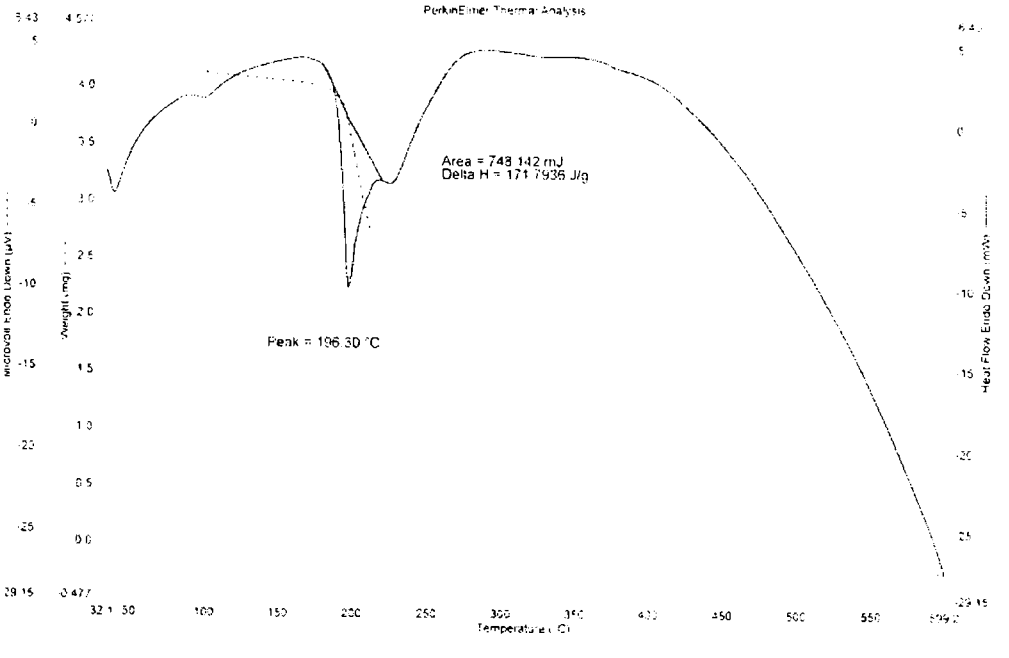

Fig. 5.10 TGA/DTA thermogram of L-alaninium oxalate

The differential scanning calorimetry (DSC) spectrum (Fig. 5.11) shows a minor endothermic peak at 98^0C and a major peak at 197^0C, supporting the observation found in TGA/DTA measurement. In organic crystals phase transitions between polymorphs are very common and the mechanisms remain unknown despite of extensive investigations. No such detailed phase transition studies are reported in the literature for LAO, even though results are available for other organic crystals [25, 26]. Hashizume *et al* [27] have observed the phase transition of L-ethyl-3-urea by means of detailed temperature resolved single crystal diffraction method. Crystal structures before and after the phase transition are isostructural where one-dimensional hydrogen bonding structure is formed and stacked to form a molecular layer. Their work shows a solid to solid phase transition at 90°C. Since these crystals are grown by slow evaporation method, they have taken care in omitting the occluded water, if any, during the growth by annealing the samples fairly at higher temperatures. In the present study LAO shows a phase transition (solid to solid) at 371 K (98°C), when the temperature is slowly increased from room temperature, which is of the same order as for L-ethyl-3-urea. The comparison with L-ethyl-3-urea is made here because both of them have layered structures. The layer structure of the present LAO, viewed from the *b* axis is shown in Figure 5.3. Even though the geometry of the layers is retained, the relative positions of the layers in LAO with their neighbors change gradually with temperature. The change is accelerated at the temperature representing the start of the endotherm in the TGA and DTA curves. The structural variation thus creates a void space in between the layers and as this grows, naturally the crystal will be unstable and so the carboxyl group of the molecules turns into a disordered structure with abrupt conformational changes to fill up the void space. This transition, being isostructural, may be visualized as the transition of two elementary processes—supramolecular and molecular.

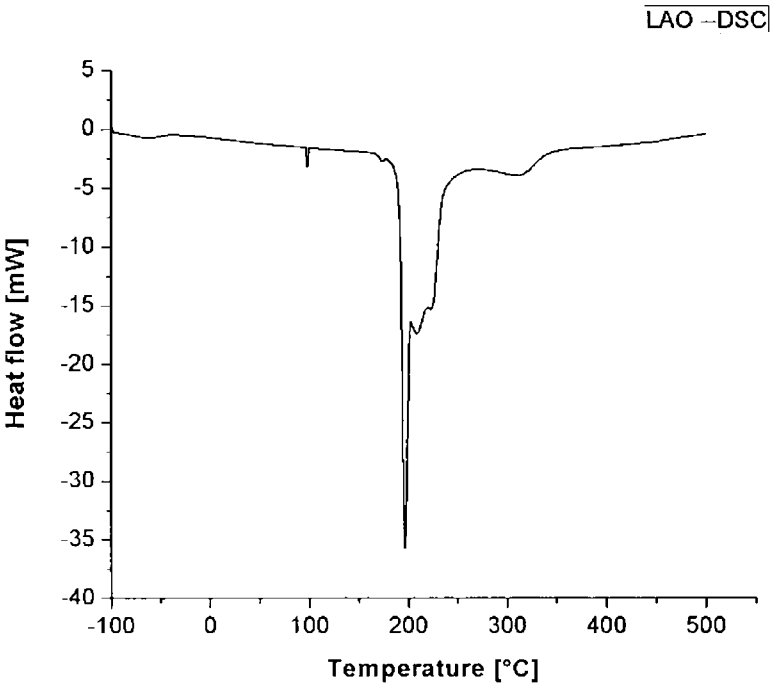

Fig. 5.11. Differential scanning calorimetry curve of L-alaninium oxalate

The specific heat at constant pressure Cp of the crystal is estimated from the DSC curve using the ratio method [28, 29]. In this method, base line corresponding to the temperature range of interest is first obtained. After this, two independent DSC runs are performed under identical conditions; one with weighed quantity (m') of α-Al_2O_3 and the other with a weighed quantity (m) of the sample. Then the specific heat Cp of the sample can be determined by using the relation

$$Cp/Cp' = m'y / my' \qquad (5.8)$$

where Cp' is the specific heat of α-Al_2O_3, y and y' are the ordinate deflections of the sample and reference standard respectively. Figure 5.12 gives the variation of specific heat of the sample with the temperature range of interest.

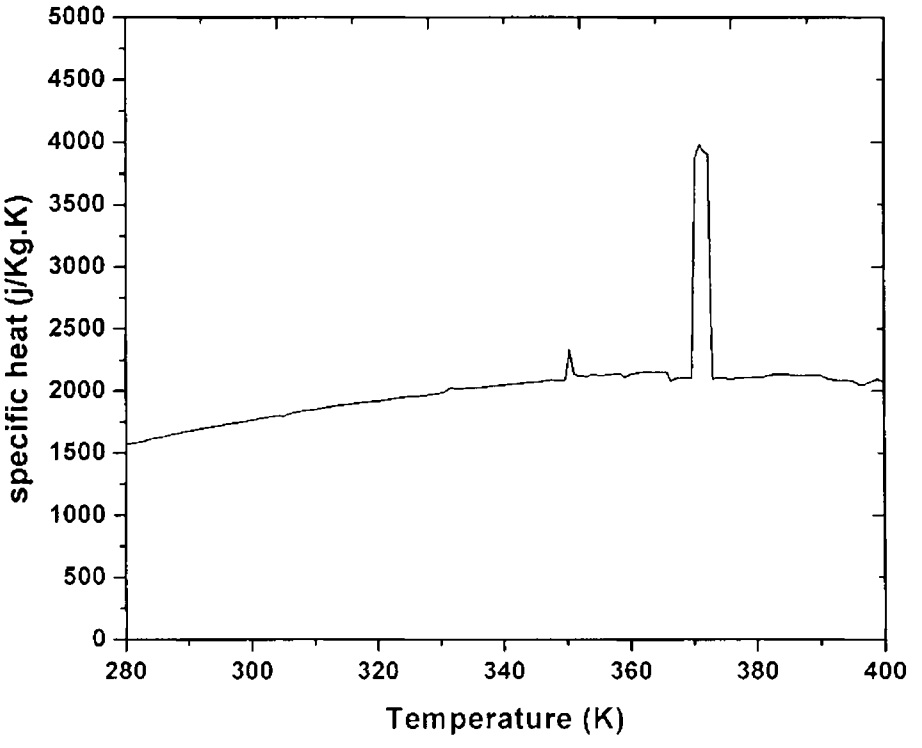

Fig.5.12. variation of Cp with temperature

5.3.6 The vibrational spectra of L-alaninium oxalate

In the present work, vibrational spectroscopic analysis of LAO crystal is performed based on the basis of vibrations of alaninium ion consisting of amino, methylene, and carboxylic acid groups and oxalate ion. The observed bands are assigned on the basis of characteristic vibrations.

Single crystals of L alaninium oxalate are grown by slow evaporation method. The FT IR spectrum (Fig.5.13) of the LAO crystal is recorded using AVTAR 370 system with a resolution of $4cm^{-1}$ in the range $400\text{-}4000cm^{-1}$. The FT Raman spectrum of the powdered sample (Fig.5.14) is recorded with BRUKER RFS100/S system with a resolution of 4 cm^{-1} using a standard InGaAs detector with a laser source of 150 mW. The vibrational wave numbers and their assignments are given in the table (5.2).

For saturated amines, it is established that the asymmetric NH_2 stretch will give rise to a band between 3380cm^{-1} and 3350 cm^{-1} while the symmetric stretch will appear between 3310 cm^{-1} and 3280 cm^{-1}[30]. But the protonation of NH_2 group can produce a shift in band position towards the lower wave number region. The shoulder band at 2902 cm^{-1}in the IR spectrum corresponds to NH_3^+symmetric stretch mode. The medium shoulder at 3200 cm^{-1} in the Raman spectrum shows NH_3^+ asymmetric stretching mode. The positions of these bands clearly indicate the presence of NH_3^+ group in the crystal. The NH_3^+ asymmetric and symmetric bending occur in the region 1625-1560 cm^{-1} and 1550-1500 cm^{-1} respectively [31]. The NH_3^+ rocking modes occur at frequencies around 1100 cm^{-1} for amino acids and exact band position depends on the position and strength of hydrogen bonds [32]. The IR bands at around 1106 cm^{-1} and 916cm^{-1} and corresponding Raman bands at 1107 cm^{-1} and 914 cm^{-1} are assigned to parallel and perpendicular NH_3^+ rocking modes respectively.

The weak band at 540 cm^{-1} in IR and Raman spectra is assigned to the NH_3^+ torsion mode. For amino acids, the asymmetric CH_2 stretching vibrations are generally observed in the region 3100 -3000 cm^{-1} while the symmetric stretch appears between 3000 and 2900 cm^{-1} [32,33]. In the present case, CH_2 symmetric stretching is observed as an intense broad band at 2900 cm^{-1} in the IR spectrum and the asymmetric stretching shows an intense band at 2950 cm^{-1} in the Raman spectrum. The C-H out of plane deformation is observed as weak band at 756 cm^{-1} in both IR and Raman spectrum. CH_2 wagging corresponds to 1325 cm^{-1}in IR and 1326 cm^{-1} in the Raman spectrum respectively. CH_2 rocking shows band at 1377 cm^{-1} in IR spectrum and 1367 cm^{-1} in Raman spectrum. The Raman band at 1407 cm^{-1} corresponds to CH_2 scissoring. The stretching vibration of the hydroxyl group of the oxalate appears as a broad shoulder in IR at 3243 cm^{-1}.Weak band at 613 cm^{-1} in the IR spectrum is assigned as OH bending. Carbonyl stretching vibrations are found in the region 1780-1700 cm^{-1}[34]. The sharp intense band in IR spectrum at 1717 cm^{-1} can be assigned to C= O stretching vibration, which is also observed in Raman at 1712 cm^{-1}. The vibrations of C= O bond might have been influenced by the hydrogen bonding network inside the crystal in shifting the band position towards the lower wave number. The asymmetric and symmetric C-O stretching frequencies are

observed at 1464 $cm^{-1}$and 1236cm^{-1} in the IR spectrum and the corresponding Raman bands are observed at 1457 cm^{-1} and 1202 cm^{-1}.The absorption arising from C-N and C-C stretching vibrations are generally observed at 1150-800cm^{-1}[34]. The C-C stretching is observed as an intense band at 821 cm^{-1}in the Raman spectrum and as a weak IR band at 821 cm^{-1} as is observed for other amino acids. [33,34]. The C-O-O bending is observed as intense bands in the IR spectrum in the expected region [34] at 707 cm^{-1} and in the Raman spectrum at 706cm^{-1}. The C-O out of plane deformation is observed at 493 cm^{-1} in the IR spectrum and at 495 cm^{-1} in the Raman spectrum. The C-O in plane deformation is observed at 648 cm^{-1}in both IR and Raman spectrum.

The presence of NH_3^+ ion in the crystal confirms the protonation of the amino acid group leading to the formation of l-alaninium oxalate molecule. In the vibrational spectra of LAO, there is excellent match between vibrational bands of the infrared and Raman spectra. This type of matching occurs only in materials, having a noncentrosymmetric crystal structure. Noncentrosymmetry is a decisive criterion determining the NLO activity particularly SHG.

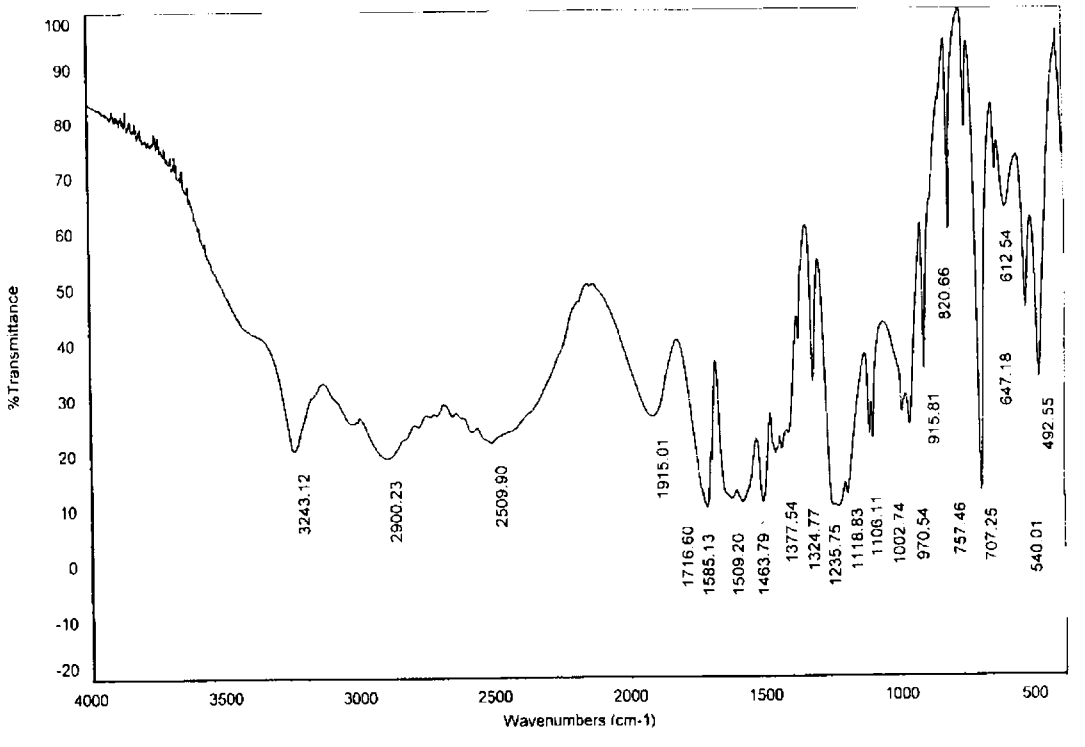

Fig. 5.13. Infra red spectrum of L –alaninium oxalate

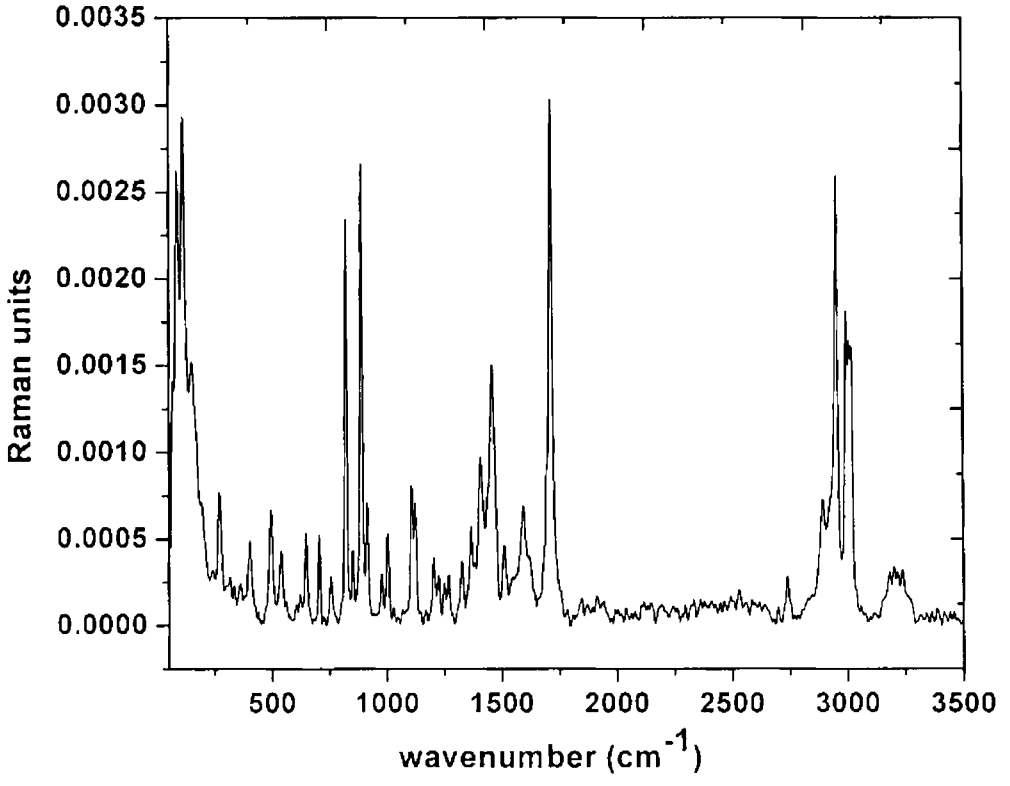

Fig.5.14. Raman Spectrum of LAO crystal

Table. 5.2 Vibrational assignments of LAO

γ_{IR}	γ_{Raman}	Assignment	γ_{IR}	γ_{Raman}	Assignment
	86.63 vs	δ lattice	1118.83 m		δ C-H
	112.18 vs	δ lattice	1235.75 vsbr	1202.29 m	Symmetric C-O stretch
	270.05 w	δ lattice	1324.77 m	1326.07 w	CH_2 wagging
	402.71w	δ lattice	1377.54 wsh	1365.97 w	CH_2 rocking
492.55 m	494.62 w	C-O out of plane deformation		1406.85 w	CH2 scissoring
540.01 w	539.84 w	NH_3^+torsion	1463.79 vs	1456.55 m	Asym C-O stretching
612.54 wbr		0-H bending	1509.2 vsbr	1509.95 wbr	NH_3^+Sym. bend
647.18 wsh	648 w	C-O in plane deformation	1585.13 sbr	1593.89 wbr	NH_3^+ asym.bending
707.25 vs	705.93 w	C=O bend	1716.6 vs	1712.14 v vs	C=O stretch
757.46 vw	756.98 w	C-H out of plane deformation	1915.01 mbr		C-C overtone
820.66 w	821.38 s	C-C stretch	2509.9 sbr		NH_3^+sym str out
	888.13 vs	CH_2 rocking		2738.19 v vw	CH_2 asym stretch
915.81 m	913.56 w	Perpendicular NH_3 rocking	2900.23 sbr	2949.52 s	CH_2 Sym Stretch
1002.74 ssh	1002.09 w	COO vibration		2992.44 msh	NH_3^+ sym.str in
				3199.51 wsh	NH_3^+ Asym. Str
1106.11 m	1106.96 m	parallel NH_3 rocking	3243.12 sbr		OH str of unchanged COOH group

5.3.7 Vickers' microhardness analysis

Hardness of a material is the measure of the resistance it offers to local deformation. General definition of indentation hardness which is related to the various forms of indenter is the ratio of applied load to the surface area of indentation [35]. In general, it comes from the intrinsic resistance of crystals and the resistance caused by imperfections in the crystals [36]. Good quality crystals with excellent optical performance and mechanical behviour are needed for device applications. In single crystals, second harmonic generation is always lower from the defective sectors compared to that from the more perfect sectors [37, 38]. Microhardness measurement on the (100) surface of the crystal is done for applied loads (P) from 5 g to 100g with a dwell time of 5 seconds using Leitz Miniload Hardness tester . The length of the two diagonals is measured by a calibrated micrometer attached to the eyepiece of the microscope after unloading and the average (d) is found out. For a particular load at least five well-defined impressions have considered and the Vicker's micro hardness profile of the crystal (Fig.5.15) calculated using the formula

$$Hv = 1.8544\ P/d^2 \quad Kg/mm^2 \qquad (5.9)$$

It is clear from the figure that microhardness increases with applied load. Increase in microhardness with increase of load in the low load region can be attributed to the heaping up of material at the edges of impression made by the indentor [35] due to the slipping of layers at the indentation centre since at this region it is plastic. Increase in load enables the defects to move and pin upon the boundaries. At higher loads, slipping of layers stops which in turn harden the crystal. This is shown in the region between 50 g and 100g. If we increase the load beyond 100 g crystal is found to be ruptured. The maximum hardness is found to be 38.9Kg/mm^2. We will first try to explain the observed ISE by traditional Meyer's law, which gives an expression regarding load and size of indentation [39] as

$$P = k_1 d^n \qquad (5.10)$$

where k_1 is the material constant and n is the Meyer index and the other symbols have their usual meanings. The plot of log P against log d before cracking after least

square fitting gives straight-line graph, which is in good agreement with Meyer's law (Fig.5.16). The value of n is found from the slope of the graph and it turns out to be 4.2 for (100) which is as expected for soft organic materials. Combining Equations (5.9) and (5.10), we have

$$Hv = 1.8544\, k_1 d^{n-2} \quad (5.11)$$

Or,

$$Hv = 1.8544\, k_1^{(1+2/n)} P^{(1-2/n)} \quad (5.12)$$

Or,

$$Hv = b\, P^{(n-2)/n} \quad (5.13)$$

where $b = 1.8544\, k_1^{(1+2/n)}$, a new constant. The above expression shows that Hv should increase with increase in P if $n > 2$ and decrease with the same if $n < 2$. This is in good agreement with the experimental data and thus confirms normal ISE. According to Onitsch [40] and Hanneman [41] n should lie between 1 and 1.6 for hard materials and above 1.6 for softer ones. Thus, LAO belongs to soft material category.

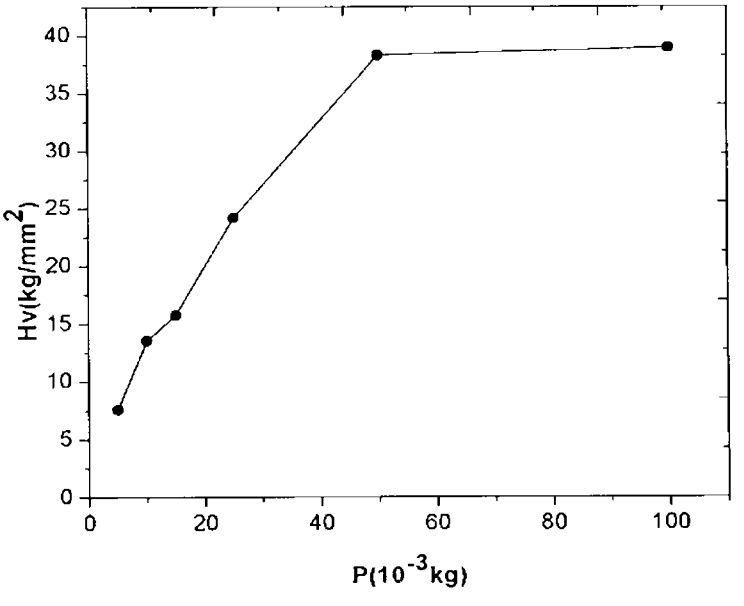

Fig 5.15 Plot of Vickers hardness number vs. load

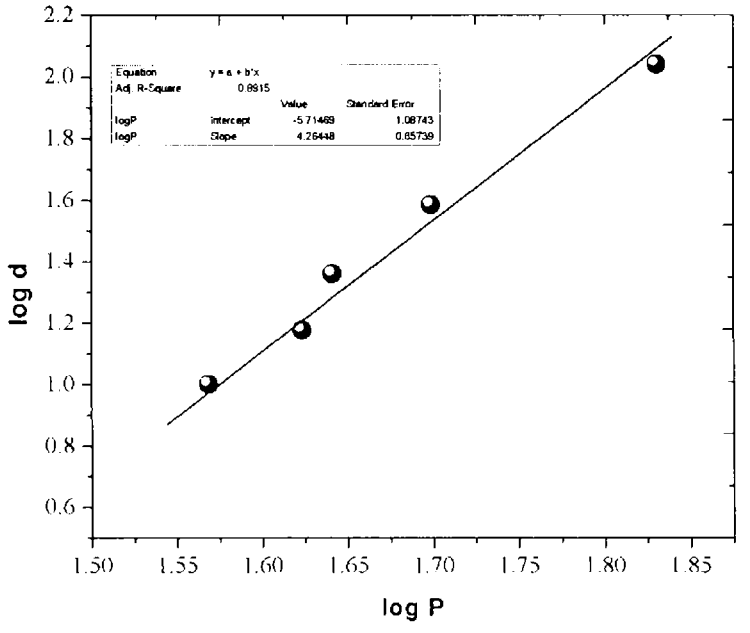

Fig 5.16 Plot of logp Vs log d

According to Hays and Kendall's theory of resistance pressure [42], there is a minimum level of indentation load (W), also known as resistance pressure, below which no plastic deformation occurs. Hays and Kendall have proposed a relationship between indentation test load and indentation size by modifying Kick's law [43] as

$$P = k_2 d^2 \qquad (5.14)$$

$$P - W = k_2 d^2 \qquad (5.15)$$

where k_2 is a new constant and $(P-W)$ is the effective indentation test load considered in the microhardness calculations. Combining expressions (5.14) and (5.15) we get:

$$W = k_1 d^n - k_2 d^2 \qquad (5.16)$$

Or,

$$d^n = W/k_1 + (k_2/k_1)\, d^2 \qquad (5.17)$$

The plot of d^n versus d^2 is a straight line (Fig. 5.17) having slope k_2/k_1 and intercept W/k_1. From these values, we have calculated the value of W and it turns out

to be 15.7gm which is the material resistance to the initiation of plastic flow. The high value of W shows that the mechanical property of the crystal is quite good. We have also calculated elastic stiffness constant (C_{11}) following Wooster's empirical relation [44] as

$$C_{11} = Hv^{7/4} \qquad (5.18)$$

The values of C_{11} for various loads are given in table 5.3. The stiffness constant C_{11} is quite high, revealing that the binding forces are quite strong. Figure 5.18 shows the indentation pattern formed on the crystal surface for a load of 50 gm. Slip lines are clearly visible in the microphotograph.

Table 5.3. Elastic stiffness constant of LAO crystals

Load (gm)	Hv (kg /mm^2)	C_{11} (x10^{14}Pa)
5	7.57	0.593
10	13.54	1.641
15	15.76	2.141
25	24.17	4.521
50	38.3	10.12
100	38.91	10.40

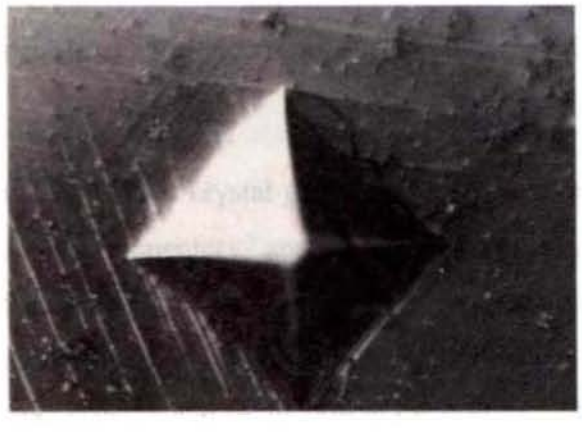

Fig.5.18 An indentation pattern (×100)

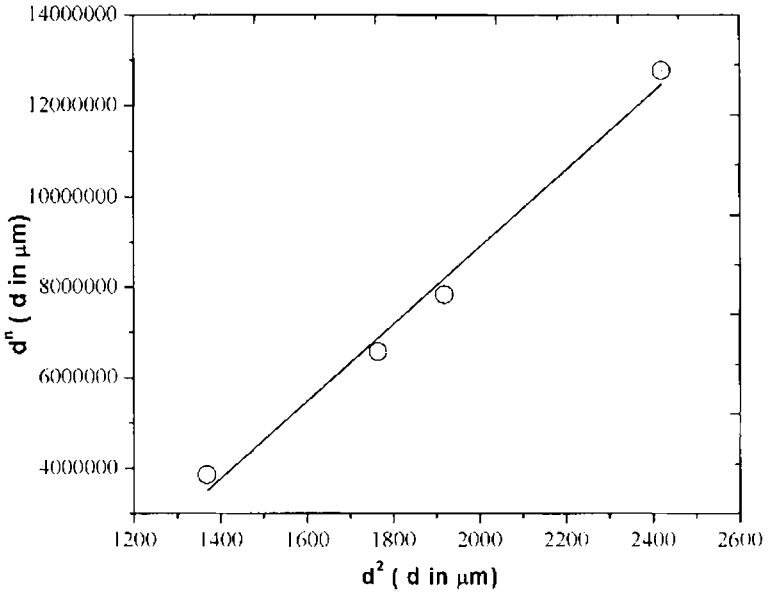

Fig 5.17 Plot of d^n vs. d^2.

5.3.8 Chemical etching studies

Dislocation study is dependent upon the time consuming and pain staking identification, by trial and error, of effective etchants which reveals a host of information about the microstructure of the single crystals. The microstructural aspects of crystals have deleterious effects on the performance of devices as they affect plasticity and crystal strength, electronic and ionic conductivity and diffusion properties [45].

There are several models of crystal growth and each crystal grows by one of these mechanisms. A complimentary approach of understanding the growth mechanism is to study the features on free and etched surfaces of the crystals. Patterns observed on surfaces like spirals, hillocks, slip pattern.....etc yield valuable information on the growth process and perfection in the crystal [46-48].

Good optical quality crystals of LAO grown by solvent evaporation technique are used for the present study. The surface features on the as grown crystal surfaces

and on the etched surfaces, etched with the dislocation etchants developed for the present study are examined using a Leica Q win Microsystems metallurgical microscope attached to a computer for easy viewing of surface patterns. N-propyl alcohol (60%) is used as the chemical polishing agent.

The chemical etching studies are carried out on the as grown single crystals of LAO to study the symmetry of the crystal face from the shape of etch pits, and the distribution of structural defects in the grown crystals . An observed layer structure of the crystal is shown in Fig. 5.19 (a). Fig.5.19 (b) shows the striation pattern observed on the surface, due to the thermal strain that may occur during growth. Secondary nucleation and overgrowth patterns on the growth surface are shown in Fig.5.19(c).

According to Buckley [49], overgrowth patterns are formed due to interruption in the continuity of deposition of material which in turn is due to change in growth conditions. When etched with water bunch pattern are formed as shown in Fig.5.19 (d). This is due to the fast dissolution of the surface the shape of which depends on the disorientation of the exposed crystallographic plane.

Development of bunches is determined by the directions of the operating etching vectors on crystal surface which are determined from an energy consideration involving the breaking of the lowest number of bonds. When the etch rate is high bunching will develop not only on the surface but also at the dissolution steps generated by dislocations [50].

Fig. 5.19(e) shows the terraced etch hillocks formed on the [101] face by etching with acetone and water taken in the ratio 1:2. When the surface dissolution is low, the surface is smooth, and the increased dissolution at dislocations can lead to terraced etch hillocks. Figure 5.19.(f) shows the lamellar structure. A solution of water in methanol in the volume ratio 1:5 is found to be produce rectangular etch pits (Fig.5.19 (g)) on the [100] surface when etched for 5-10 seconds. On successive etching no spurious development of pits are observed which suggests that etch pits are produced at the emergence of dislocation. The flat bottomed and shallow pits appear and disappear on successive layer etching indicating that they are due to

dislocations which extend only a few molecular layers. Micro topographical analysis suggests that the growth of these crystals is due to 2D nucleation and spreading of layers. Shallow and flat bottomed etch pits, which disappear on subsequent etching suggests that the defect is mainly due to edge dislocations. The absence of patterns like growth spirals, slip bands...etc also support this. Average dislocation density in the crystal is found to be order of $10^3/cm^2$, which implies a good crystalline perfection of the grown crystal. The low dislocation density found in the present study suggests that crystals grown by solvent evaporation method can be utilized for optical device applications.

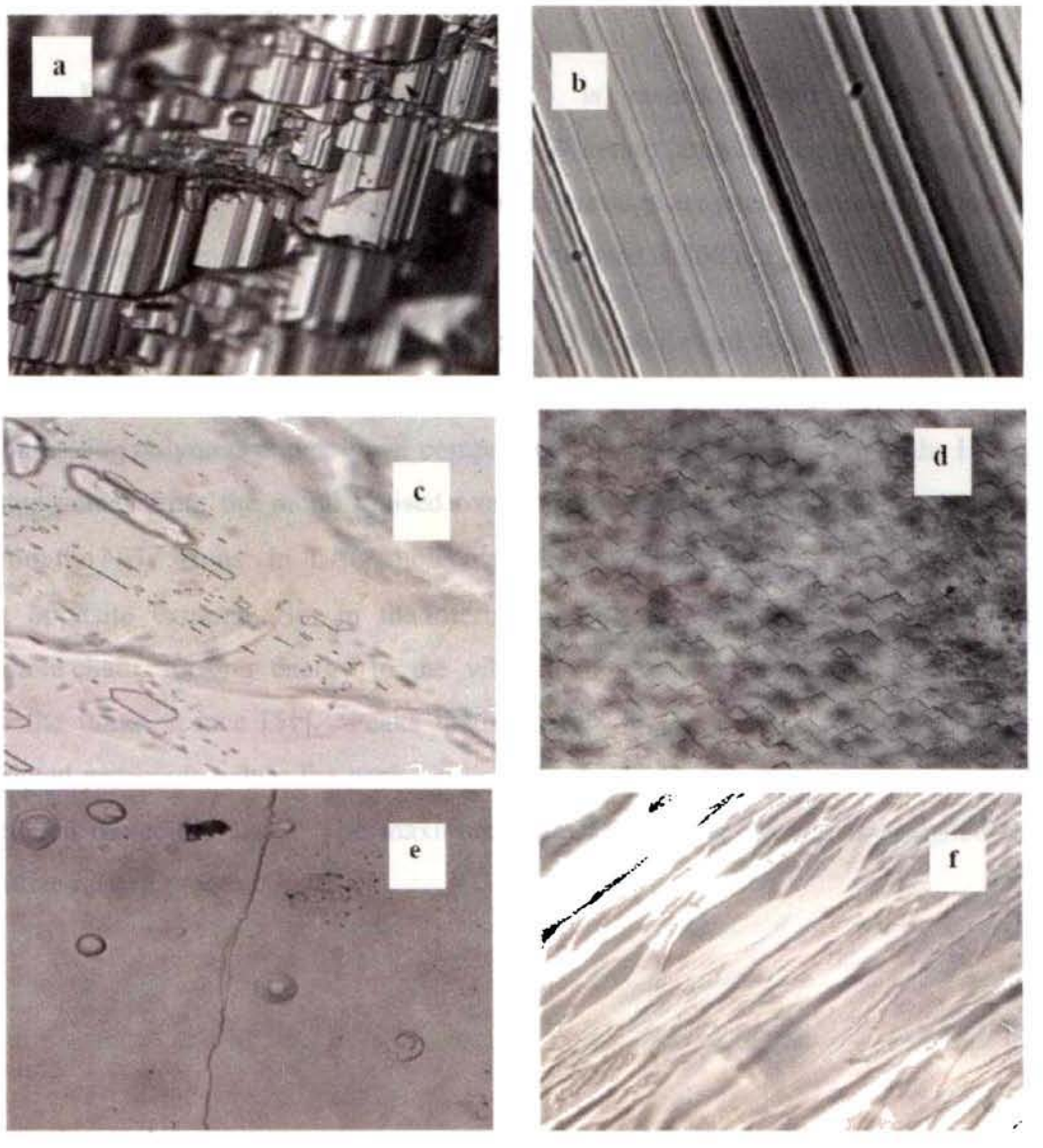

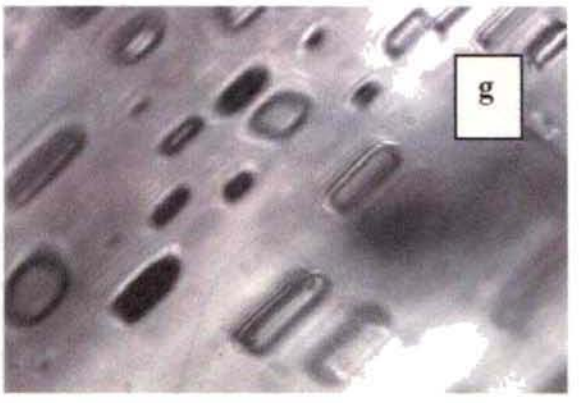

Fig .5.19 (a) Layer structure (b) striation pattern (c) overgrowth (d) bunch pattern (e) etch hillock (f) Lamellar structure (g) rectangular etch pits.(allx100)

5.3.9 Photoluminescence studies

Photo-luminescence spectrum (PL) is recorded with a Jobin Yvon Spectrofluorometer (Model FL3-22). A 450 W xenon lamp is used as the source and PMT (Model R928P) as the detector. Double gratings are used for the excitation and emission spectrometers. Excitation wavelength used is 300 nm.

PL spectrum of LAO crystal recorded is shown in figure 5.20. Spectrum shows a broad peak centered at 440 nm with intensity comparable to that of conducting polymers and polymer composites. The main contribution to the HOMO state comes from the mono ionised oxalate ions, while to the LUMO state comes from the NH_3^+ ions. In LAO molecular chains, these two molecular orbitals are at opposite extrema. So, in the interband transitions, the electron has to cross the whole chain, loosing energy to the vibrational modes of the crystal, contributing to the luminescence [51]. Peaks in the visible region can be assigned to lattice related processes, while the peaks in the UV region can be due to the relaxation of excited molecular states. The maximum intensity peak at 440nm is assigned to a lattice related process.

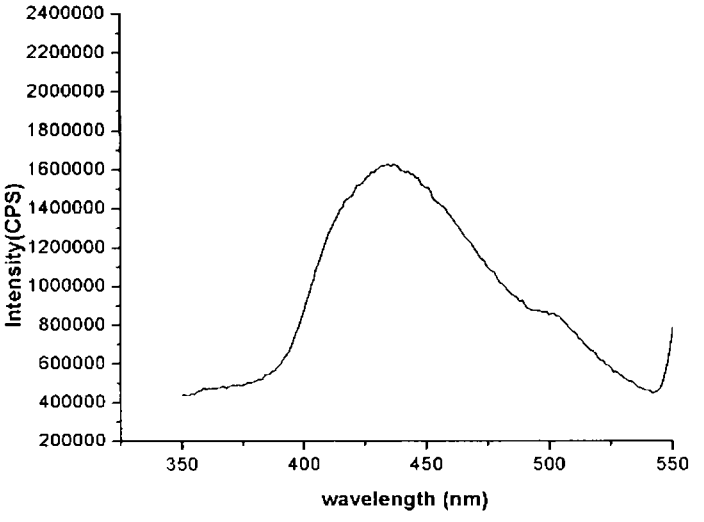

Fig.5.20 PL spectrum of LAO crystal

5.3.10 Dielectric studies by microwave cavity perturbation technique

The use of cavity for measuring properties of dielectric materials has been reported in 1968 by Stinehelfer and it has been improved by Itoh in 1974 [52]. Microwave study on the dielectric properties of NLO materials reveals some interesting observations. A detailed study on the complex permittivity, loss tangent and conductivity of the LAO crystal at different frequencies in the S band using the cavity perturbation technique [53] is presented in this section.

S-band wave-guide closed at both ends is used as the cavity resonator. The resonator is excited in the TE_{10p} mode. The resonant frequency 'f_0' and the corresponding quality factor 'Q_0' of each resonant peak of the cavity resonator, without sample placed at the maximum of the electric field, are noted. The sample is introduced into the cavity resonator through the non-radiating slot. The resonant frequencies of the sample loaded cavity are selected and the position of the sample is adjusted for maximum perturbation (that is, maximum shift of resonant frequency with minimum amplitude for the peak). The new resonant frequency f_s and quality factor Q_s are determined. The procedure is repeated for other resonant frequencies. The frequency dependence of effective conductivity, dielectric constant and dielectric loss and absorption coefficient are plotted in figure.5.21.

For LAO crystal the variation of dielectric constant is almost constant with frequency. Dielectric loss is very small which signifies the good crystalline perfection of the grown crystal. Very small dielectric loss is quite useful for device applications. As seen from the optical absorption studies, the crystal is quite transparent in the whole visible region and as expected the conductivity of the material is very small, of the order of 0.0035 S/m. Microwave absorption coefficient is also very small. So the material can be identified as a microwave transparent material in the frequency range 2-3GHz.

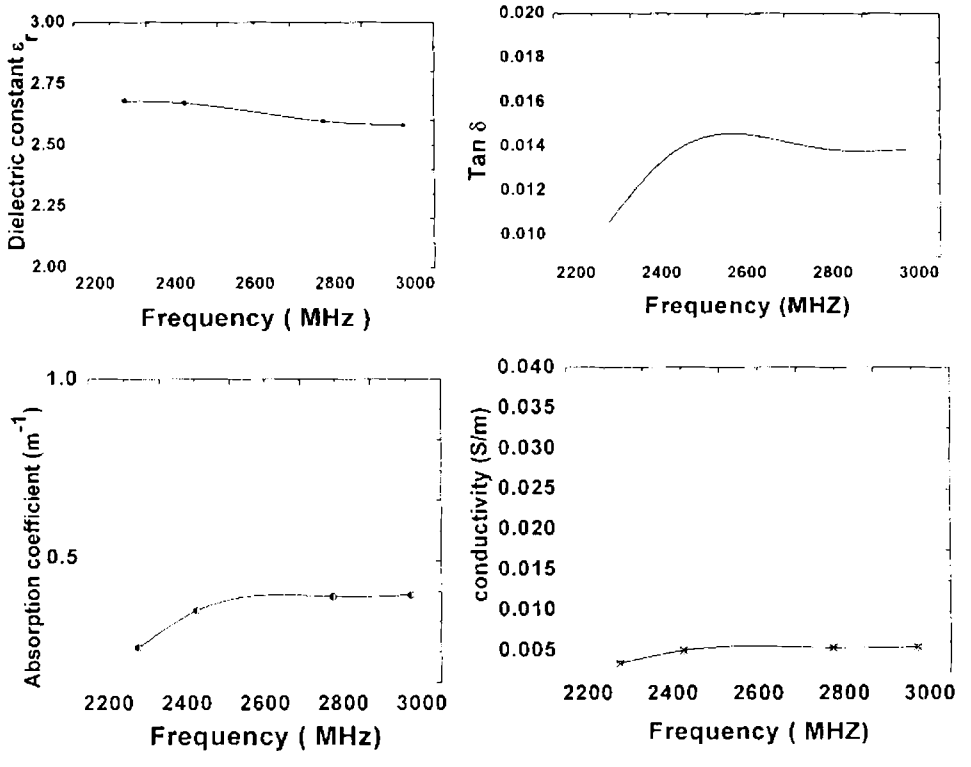

Fig . 5.21 Variation of dielectric parameters with frequency

5.3.11 SHG studies

The second harmonic generation behavior is tested by the Kurtz powder technique [54] using Q switched Nd: YAG laser as source. The sample is prepared by sandwiching the graded crystalline powder between two glass slides. The powder sample of L-alanininium oxalate is illuminated by the laser source (λ = 1064 nm, 7ns, 10Hz). A bright green emission is observed from the sample. The second harmonic signal (532 nm) generated in the sample is collected by the lens is detected by the monochromator and is filtered by IR filters to remove the fundamental and is measured. Powdered KDP sample of same particle size is used as the reference material, and the output power intensity of L-alaninium oxalate is compared with the output power of KDP, and also with its parent material L alanine.

The measured SHG values are listed in table 5.4. SHG efficiency will vary with the size of the powdered crystalline aggregates [55]. It is found that the defects and dislocations present in the crystal influences the NLO property especially second harmonic generation [56].

Table 5.4 SHG measurement data.

Input	KDP	L alanine	L alaninium oxalate
2.7 mJ	118mv	145mv	271mv
5.0 mJ	221mV	292mV	498mV

The very low value of dielectric loss found by microwave cavity perturbation technique implies the better crystallinity of the crystal grown, in the present study. In fact, the dislocation density measured by chemical etching studies is of the order of $10^3/cm^2$. Materials with good crystalline perfection will give better SHG output [57].

5.3.12 Laser damage threshold studies

Like other optical materials used in laser technology, NLO crystals are susceptible to optically induced catastrophic damage. Optical damage in non-metals (dielectrics) may severely affect the performance of high-power laser systems as well as the efficiency of optical systems based on nonlinear processes and has therefore

been subject to extensive research for years [58]. From this viewpoint we have carried out laser damage threshold measurements on the LAO crystal.

For pulse widths that stretch into several nanoseconds, thermal effects are unavoidable while for picosecond pulse widths thermal effects are negligible. This is because thermal effects take several nanoseconds to build up and could take several milliseconds to decay. Consequently the laser damage resistance of LAO in the nanosecond regime is expected to be different as compared to that observed in the picosecond regime. We have carried out a study of laser damage in LAO in the nanosecond regime and suggest a possible reason for the observed damage.

A Q-switched Nd: YAG laser in the TEM_{00} mode is used as the source of light for the damage study. This laser can be operated in two modes. In the single-shot mode the laser emits a single 7 ns pulse. In the multi-shot mode the laser produces a continuous train of 7 ns pulses at a repetition rate of 10 Hz.

Freshly cleaved samples with no sign of any surface defects are used for the present study. The sample is mounted on a sample holder. Single and multiple laser damage measurements are made on the (100) face of crystal. The sample is irradiated at different spots on the same crystal at different pulse energies. In our work, the damage almost always occurred by the formation of white spark accompanied by audible sound. The sample is then observed for damage under an optical microscope and a scanning electron microscope.

Figure5.22 (a) shows the morphology for the damage above the damage threshold for a single-shot 1064nm laser pulse at 29.64GW/cm^2. A typical cylindrical damage pattern accompanied by breakdown paths can be seen [59- 61]. The breakdown paths do not depend on the orientation of the crystal relative to the polarization of the electric field and lie within the reflection plane. As expected, the highest intensity is required to induce laser damage with a single shot. The laser damage threshold reduces to 20.60 GW/cm^2 for multi shot [62]. The sample shows distinct signs of laser ablation as can be seen from the damage pattern shown in Figure 5.22(b). Thermal effects need to be considered for pulse widths that are nanoseconds and longer and in the cases of picosecond and femtosecond lasers for

higher repetition rates where cumulative thermal effects become important [63, 64]. Since LAO has a room temperature specific heat of 1.766 J g−1 K−1 , it absorbs more heat energy when laser radiation is focused on it and one can expect a high threshold value for laser damage and that is what has been observed in our investigation. Another point to be noted here is that the spot size used in the present experiment is small as 44μm for 1064 nm radiation and hence the defect concentration in the focal volume is expected to be comparatively less, leading to a high threshold value.

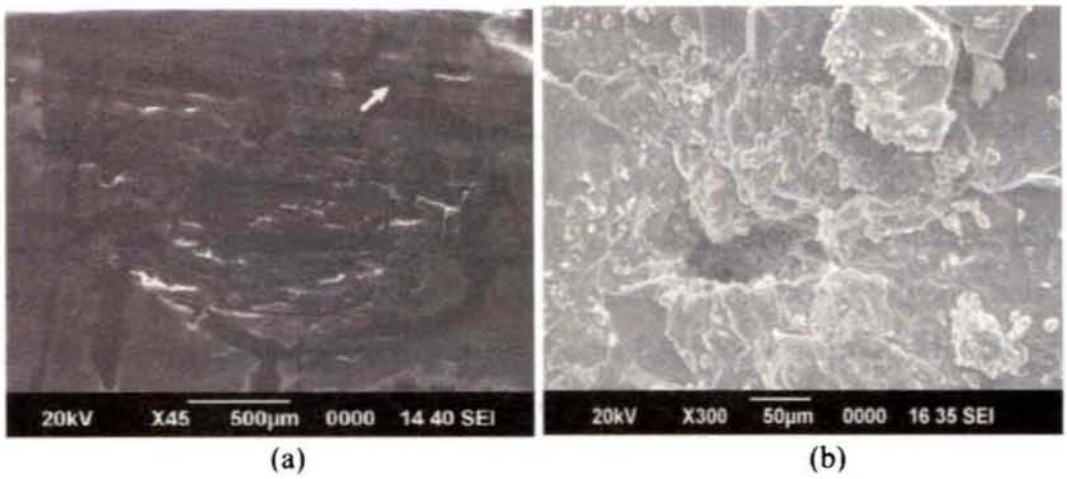

(a) (b)

Fig. 5.22 Laser damage pattern for (a) the single shot and (b) multiple shot

5.3.13 Z Scan measurement of the optical nonlinearity

Photonic sensors (including eye) have threshold intensity to electromagnetic radiation above which they can be damaged [65]. By using suitable materials as optical limiters, dynamical range of the sensor can be extended to function optimally at higher input intensities. For most protective applications rapid sensor response is desired with large saturation threshold, providing a greater safety margin [66]. Various nonlinear optical effects can be employed for designing an optical limiter.

Nonlinear optical (NLO) materials with large intensity dependent refractive index and absorption coefficients are useful for optical device applications. These parameters determine whether an intense laser beam will undergo self focusing or self defocusing as it propagates in the material medium [67]. Any NLO effect in the

organic molecules originates from a strong donor–acceptor intermolecular interaction.

Nonlinear optical characterization of the crystal is carried out using the well-known, single-beam, Z scan technique [71], which can accurately measure both the magnitude and sign of the nonlinear refractive index n_2. The measurements are carried out with the experimental setup shown in Fig. 1. The laser beam is provided by the output of a pulsed Nd: Yttrium Aluminum Garnet (YAG) laser, with a pulse width of 7 ns and a repetition rate of 10 Hz. The selected wavelength is 532 nm. The spatial distribution of the pulse has a nearly Gaussian profile. The crystal sample is placed on a translation stage controlled by a computer that moves the sample along the z-axis with respect to the focal point of a 50 mm convex lens. The transmittance of the samples is measured with and without an aperture in the far-field. The laser pulses adjusted by an attenuator are separated into two beams by using a splitter. The energy of the two beams are simultaneously measured using two energy detectors, Rjp-735 energy probes linked to energy ratio meter,Rj-7620. A personal computer is used to collect and process the data coming from energy meters.

The result of the open aperture Z scan measurement of the crystal is shown in Figure 5.23. The open aperture (OA) curve demonstrates a nonlinear absorption and the characteristic pattern of the curve shows that the nonlinear absorption is reverse saturable absorption (RSA). For 532nm resonant absorption, both excited state absorption and two-photon absorption (TPA) can be responsible for the observed NLO effects. The RSA coefficient β can be obtained from the fitting performed on the experimental data of the OA measurement with the equations (1) and (2)[72] where α and β are the linear and effective third order NLO absorption coefficients, respectively, τ is the time, I(z) is the irradiance and L is the optical path length. Since we are getting an excellent fit of the experimental data with the equations (5.19) and (5.20) corresponding to two photon absorption, it can be concluded that the two photon absorption is the mechanism responsible for the observed NLO effect.

$$T(Z)=\frac{1}{Q(z)\sqrt{\pi}}\int_{-\infty}^{+\infty}\ln\left[1+Q(z)\right]e^{-\tau^2}\,d\tau \qquad (5.19)$$

$$Q(Z)= \beta I(Z) \frac{1-e^{-\alpha L}}{\alpha} \quad (5.20)$$

where $\frac{1-e^{-\alpha L}}{\alpha}$ is the effective path length L_{eff}.

The value of the non linear absorption coefficient β is found to be equal to be 11.65 cm/GW.

The peak to valley configuration of the curve obtained under the closed aperture configuration in figure5.24 suggests that the refractive index change is negative, exhibiting a self defocusing effect. The nonlinear refraction index n_2 (m^2/W) is obtained through the following equation

$$\Delta\Phi_0 = k n_2 I_0 L_{eff} \quad (5.21)$$

In the above equation the phase shift $\Delta\Phi_0$ is equal to $2\pi/\lambda\ n_2\ I_0\ L_{eff}$.

The difference between the normalized transmittance at the peak and valley is related to $\Delta\Phi_0$ by the relation

$$\Delta T_{P-V} = 0.406\ (1-S)^{0.25}\ \Delta\Phi_0 \quad (5.22)$$

The value of n_2 is calculated to be equal to -3.984×10^{-13} m^2/W.

The molecular hyperpolarizability, γ, is obtained to be 10.424×10^{-24} esu with the equation below [73]

$$\gamma = 40\pi\ n_2/\ cn_0 \quad (5.23)$$

where n_0 is the linear refractive index which is estimated from the absorption spectrum of the crystal in the UV/Vis/NIR region.

The real and imaginary parts of the χ (3) of the sample can also be calculated by the following equations [73,74]

$$\text{Re}\ \chi^3\ (esu) = (cn_0^2/\ 120\pi^2)\ n_2, \quad (5.24)$$

$$\text{Im}\ \chi^3\ (esu) = (cn_0^2\varepsilon_0\lambda\ /2\pi)\ \beta \quad (5.25)$$

The value of the real part of nonlinear susceptibility Re χ^3 (esu) is - 2.586×10^{-11} and imaginary part Im χ^3 (esu) is 0.6376×10^{-11}.

Introducing the coupling factor ρ, the ratio of imaginary part to real part of third-order nonlinear susceptibility,

$$\rho = \text{Im}\,\chi^3 / \text{Re}\,\chi^3 \qquad (5.26)$$

The value of ρ in this case is found to be equal to 0.24. The observed value of coupling factor is seen to be less than 1/3, which indicates that the nonlinearity is electronic in origin [75].

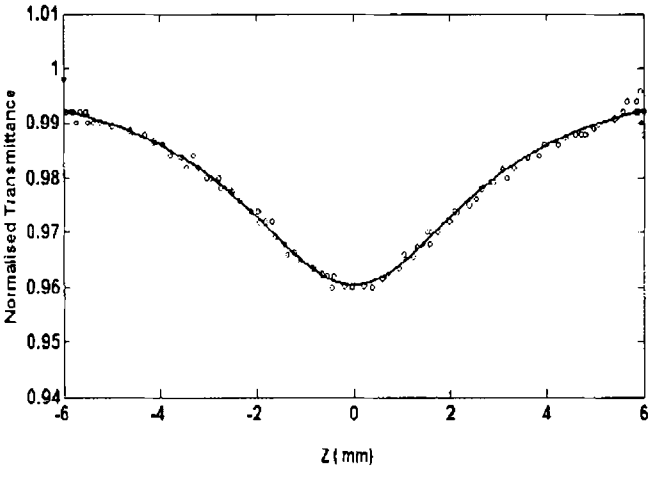

Fig.5.23 Open aperture Z scan curve of GLO crystal

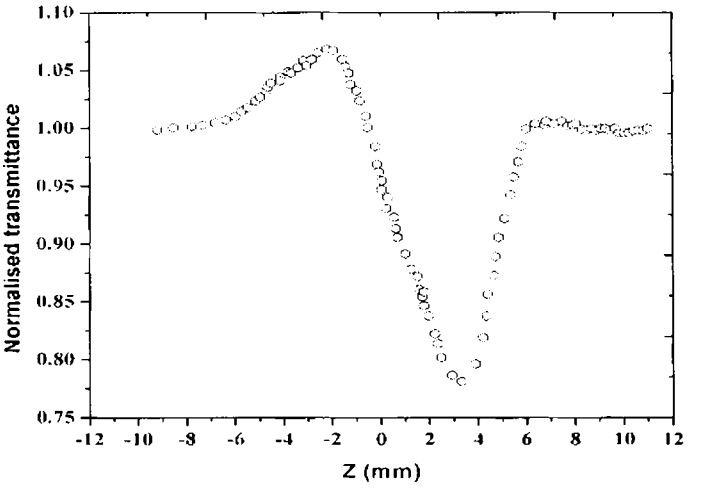

Fig. 5.24 closed aperture Z scan curve of LAO crystal

5.4 CONCLUSIONS

The bulk size single crystals of L-alanininium oxalate are successfully grown by the slow evaporation solution growth method at room temperature. To the best of our knowledge, growth of big LAO crystals of size 40x 15 x 8 mm^3 with good transparency is not reported elsewhere [8]. Exposure of the crystal surfaces to humid and dry atmospheres indicates that LAO is air stable and non hygroscopic. The grown crystals have been subjected to various characterization studies. Crystal structure has been confirmed by powder XRD. Elemental analysis (CHN) reveals that the crystal does not contain any water of crystallization in its structure and suggests the molecular formula to be $C_5H_9NO_6$. Thermal analysis by TGA/DTA and DSC studies establishes the good thermal stability of the crystal upto its melting temperature (197^0C), suggesting it to be a potential material for laser applications where crystal should withstand high temperatures. Since there is no decomposition observed up to 200°C, crystallization can be done by melt method too. High value of Cp enhances its prospects for applications in laser assisted devices.

FTIR and FT Raman studies confirm the various functional groups and their vibrational interactions. Minimum absorption is observed in the visible and NIR regions from the UV-Vis-NIR measurement. It is an important requirement for the materials showing NLO properties especially second harmonic generation, to have a wide transparency window. Linear optical constants of the crystal are determined from the UV/Vis/NIR data. Three potential etchants that delineate dislocations in the crystal are identified. Average dislocation density is small ($10^3/cm^2$). Microtopography and etching studies establish that the growth mechanism is 2D nucleation and subsequent spreading of layers.

The photo luminescence spectrum of the compound is explained. From the microhardness studies, maximum hardness is found to be 38.9Kg/mm^2. The high value of load independent resistance shows that the mechanical property of the crystal is quite good. The stiffness constant C_{11} is quite high, revealing that the binding forces are quite strong. Very low dielectric loss value (0.016) determined by microwave cavity perturbation technique shows the good crystalline perfection.

Second harmonic generation efficiency (SHG) of LAO crystal is 1.8 times that of L alanine and 2.3 times that of KDP. Laser damage threshold is considerably high and is higher than that of GLO. The reason for the increased SHG output and high value of laser damage threshold is the better crystalline perfection in the grown crystal with lesser defects, as revealed by dislocation studies. It is reveled from the Z scan studies that the crystal shows reverse saturable absorption and negative non linear refraction and hence can be effectively used for optical limiting applications.

5.5 REFERENCES

[1] M.D Aggarwal, J.Stephens, J.optoelectron.Adv.Mater 5, 3 (2003).

[2] Razzetti.C, Ardoino. M, Paorici.C, Cryst.Res. Technol. 37, 456(2002).

[3] McArdle. J, Sherwood. J. N, Damask. A. C, J. Cryst. Growth, 22, 193(1974).

[4] Hampton, E. M.; Shah, B. S.; Sherwood, J. N. J. Cryst. Growth, 22, 22(1974).

[5] S. Dhaushkodi, K.Vasantha Cryst. Res.Tech.39, 3 (2004)

[6] Bhat, H. L. Bull. Mater. Sci. 17. 1233(1994).

[7] Marder. S. R, Sohn J. E, Materials for Non-Linear Optics; American Chemical Society: Washington, DC, 1991.

[8] Arun.K.J, S.Jayalekshmi, Proceedings of the International conference on optoelectronic materials and thin films, CUSAT, Kochi, India, 2005.

[9] Arun.K.J, S.Jayalekshmi, J. Miner. Mater. Charact. Engg, USA, Vol. 8, No.8, 599(2009).

[10] M. Subha Nandhini, R. V.Krishnakumar, S.Natarajan, Acta Cryst. E57, 633(2001).

[11] G. S. Pawley, J. Appl. Cryst 14, 357(1981).

[12] Y. Le Fur, R. Masse, M. Z. Cherkaoui, and J. F. Nicoud, Z. Kristallogr. 210, 856 (1995).

[13] F. I. Ezema and C. E Okeke., Nig. Journ. Phys., 14(2), 48(2002).

[14] I. M. Tsidilkovsk, Band structure of semiconductors, Pergamon Press, Oxford, 1982.

[15] J. I. Pankove, Optical processes in semiconductors, Prentice-Hall, New York, 1971.

[16] A. Ashour, H.H. Afifi and S.A. Mahmoud, Thin Solid Films, 248, 253(1994).

[17] K. Yamaguchi, N. Nakayama, H. Matsumoto, Jpn. J. Appl. Phys., 16 1203(1977).

[18] O.P. Agnihotri and B.K. Gupta, Jpn. J. Appl. Phys., 18, 317(1979).

[19] Cohen. M, Frizsche.H, Ovshinskey.S, Phys. Rev. Lett., 22, 1065(1969).

[20] D. R. E. Campbell and R. D. Tomlin, J. Phys. D 5, 852 (1972).

[21] A. A. El-Kadry and N. Mahmoud, Thin Solid Films 269, 117 (1995).

[22] I. C. Ndukwe, Sol. Ener. Mater. Sol. Cells, 40, 123(1996).

[23] Janai, M., D. D. Alfred, D. C. Booth and B.O. Seraphin, Sol. Ener. Mater.1, 11(1979).

[24] J. I. Pankove, Optical processes in semiconductors, Prentice-Hall, New York, 1971.

[25] Preethi Menon C and Philip, J. Mater. Res. Bull. 36, 2407(2001).

[26] Pichon C, Appl. Phys. Lett. 35, 1435(1979).

[27] Hashizhume D et al. Acta Crystallogr. B59, 404(2003).

[28] M.J. O' Neill, Anal.chem.38, 1331(1966).

[29] K.Nandakumar, PhD thesis, Cochin University of science and technology, India, 1992.

[30] D.Rajan Babu, D.Jayaraman, J.Crystal Growth 245,121-125 (2002)

[31] D.Sajan, J.Binoy, V.S.Jayakumar, Spectrochimica Acta A, 60, 173(2004).

[31] I.Hubertjoe, G.Aruldhas, P.Ramasamy, Cryst.Res.Technol 29, 685(1994).

[32] G.Litvinov, XIII th Internat. Confer. on Raman Spectrosc.Wurzberg, Germany1992.

[33] L.Santra, A.L.Verma, J.Phys.Chem.solids 55, 405(1994).

[34] Arun.K.J, S.Jayalekshmi, AIP. Conf. Proc.1075 (2008).

[35] Meyer, Some aspects of the hardness of materials, PhD thesis, Dreft, (1951).

[36] P. N. Kotry, A. K. Razdan, B. M. Wnakyn, J. Mater. Sci. 24, 793(1989).

[37] J. N. Sherwood, Pure & Appl. Opt. 7, 229 (1998).

[38] I. V. Kityk, B. Marciniak, A. Mefleh, J. Phys. D: Appl.Phys. 34, 1 (2001).

[39] E. Meyer, Z. ver. Deut. Ing. 52, 645(1908).

[40] E.M. Onitsch, Mikroscopia 2, 131(1947).

[41] M. Hanneman, Metall. Manchu. 23, 135(1941)

[42] C. Hays, E.G. Kendall, Metallurgy 6, 275(1973).

[43] F. Kick, Das Gasetzder, Proportionalen Widerstande Und Science Anwendung, Felix, Leipzig, 1885

[44] W.A. Wooster, Rep. Progr. Phys. 16, 62(1953).

[45] W. G. Pfan, Solid state physics, Academic press, New York, 1957.

[46] M. S .Joshy, A. S. Vagh, Ind. J. Pure& App. Phys. 5, 318 (1967).

[47] J. Zyss, J. F. Nicoud, M. Coquillary, J.Chem.Phys. 81, 416(1984).

[48] B. G. Penn, H. C. Beatiz, D. O. Frazier, Prog. Cryst. Growth & Charact., 22, 19 (1991).

[49] H. E. Buckley, Crystal growth, John Wiley& sons, New York, 1951.

[50] K. Sangwal, Etching of crystals, North Holland Publishers, Oxford, 1987.

[51] E.W.S.Cateano, J.R.Pinheiro, M. Zimmer, AIP Conference Proceedings, 772, 1095 (2005).

[52] T. Itoh, IEEE Trans. On Microwave Theory and Techniques, May 1974.

[53] Mathew, K. T., "Perturbation Theory, Vol. 4, Wiley-Interscience, USA, 2005.

[54] S.K. Kurtz, T.T. Perry, J. Appl. Phys. 39, 3798(1968).

[55] Yetta Porter, Kang Min Ok, P.Shiv Halaasyamani, Chem.Mat.13, 1910 (2001).

[56] I.V.Kityk, B.Marciniak, A.N.Mefleh, J.Phys.D 34, 1 (2001) .

[57] G. Yang, W. T. Wang, L. Yan, H. B. Lu, and Z. G. Chen, Opt. Comm. 209. 445 (2002).

[58] H. O. Marcy, L. F. warren, M. S. Webb, G. C. Catella, Appl. Opt. 31, 5051 (1992).

[59] F. Seitz, Phys. Rev. 76 1376 (1949).

[60] J. W. Davisson, Phy. Rev 70 1376 (1946).

[61] R. J. Bolt, Optics Comm. 100, 399 (1993).

[62] H. Nakatani, W. R. Bosenberg, Appl. Phys. Lett., 53(26), 2587 (1988).

[63] F. Mauro, J. Opt. A: Pure Appl. Opt. 1, 662 (1999).

[64] S. S. Gupte and C. F. Desai, Cryst. Res. Tech, 34, 1329 (1999).

[65] D.H. Sliney, H.E. Bennett, D. Milan, NBS Special Publication 669, 355(1984).

[66] Lee W. Tutt, Thomas F. Boggess, Prog. Quant. Electron. 17, 299(1993).

[67] P.N. Prasad, D.J. Williams, Introduction to Nonlinear Optical Effects in Molecules and Polymers, Wiley, New York, 1991.

[68] M. Subhandinini, R. V. Krishnakumar, S. Natarajan, Acta Crystallogr.sec E, 57, 633 (2001).

[69] S. Dhanushkodi, K. Vasantha, Cryst.Res.Technol. 39, 259 (2004).

[70] K.J. Arun, S.Jayalekshmi, Optoelectron. Adv. Mater (RC) 2(12), 805 (2008).

[71] M. Sherk-Bahae, A. A. Said, E. W. Van Stryland, IEEE J. Quantum Electron,26,760(1990).

[72] M. Sherk-Bahae, A. A. Said and E. W. Van Stryland, Opt. Lett., 14, 955 (1989).

[73] G. Yang, W. T. Wang, L. Yan, H. B. Lu, and Z. G. Chen, Opt. Comm. 209, 445 (2002).

[74] S.F. Wang, W. T. Huang, T. Q. Zhang, and Y. F. Miura, Appl. Phys. Lett. 75, 1845 (1999).

[75] Seetharam.S, G. Umesh, K. Chandrasekharan, B.K. Sarojini, Opt. Mater. 30 1297(2008).

****ꕥ****

Chapter 6

INVESTIGATIONS ON THE GROWTH AND CHARACTERISATION OF POTASSIUM HYDROGEN PHTHALATE SINGLE CRYSTALS FOR NONLINEAR OPTICAL APPLICATIONS

Chapter 6

INVESTIGATIONS ON THE GROWTH AND CHARACTERISATION OF POTASSIUM HYDROGEN PHTHALATE SINGLE CRYSTALS FOR NONLINEAR OPTICAL APPLICATIONS

6.1 INTRODUCTION

Hydro phthalate crystals (XAP: C_6H_4 COOH COOX where X is a metal ion) are most useful for long wave X-ray spectroscopy. NaAP, NH_4AP, KAP, RbAP and TiAP have been investigated for their high resolution as analyzer crystals in spectrometers. The acid phthalate crystals are organic crystals with 2d spacing of the order of $26A^0$. The crystals cleave along the (010) planes and have a good record for long term stability [1].

Potassium acid phthalate (KAP) also known as potassium hydrogen phthalate belongs to the series of alkali acid phthalate used in the production of crystal analysers for long wave X-ray spectrometers [2]. It is also well known for its piezoelectric, pyroelectric, elastic and optical properties [3, 4]. KAP and other phthalate like cesium, rubidium and thallium acid phthalate are used in the preparation of buffer solutions. Recently KAP crystals have assumed an important role in the epitaxial growth of oriented poly [1, 6-bis (N- Carbozolyl)-2, 4-hexadiyne] (poly DCH), a conjugated polymer which shows a very large ($\chi^{(3)} = 10^{-7}$ esu) and fast (0.8 ps) nonlinear optical susceptibility[5, 6]. The importance of KAP crystals is related to its uniqueness as a substrate which allows the growth of oriented poly DCH. Usually the substances used for the deposition of organic thin films are chosen for their optical transparency in the spectral region of interest. In this case, KAP plays an active role in the growth process. The orientation of DCH molecules is driven by the molecular insertion of the carbozolyl side group between the KAP Phenyl rings. The molecular matching is stabilized through π interactions between

the phenyl groups of the monomer and those of KAP substrate. In a second step the sample is polymerized by heating. The oriented structure of the monomer is preserved in the polymerization process which does not affect the substrate. Hence photonic devices can be developed based on these highly oriented polymeric thin films grown using KAP as a substrate. Potassium acid phthalate (KAP) is an orthorhombic crystal, crystallizing in the space group $P_{ca}2_1$. It has unit cell dimension a=9.609 Å, b=13.857A^0, c=6.466A^0 and contains 4 KAP molecules. The habitual morphology of the crystal has 14 growth faces. It has a (010) face with a high morphological importance on which spiral patterns could be easily observed due to the relatively high monosteps. This material is a fine model material for studying the crystallization process especially the mechanism of spiral growth in crystals [7, 8].

Growth and structural characterization studies of this material have already been done but the NLO behaviour has not been dealt with in detail. In the present work, KAP crystals are grown by floating seed technique and by gel growth method. Grown crystals are characterized by various characterization techniques. The second and third order NLO behaviour of the material is explored and attempts made to establish a connection between structure and NLO behaviour.

6.2 CRYSTAL GROWTH TECHNIQUES

6.2.1 Growth of KAP crystals by floating seed technique

Seed crystals of potassium acid phthalate (KAP) are grown from its supersaturated solution taken in a Petri dish at room temperature. Good optical quality seed crystals free from defects and inclusions are used for the growth of crystals from its saturated solution using floating seed technique. One or two seed crystals are carefully placed in the saturated solution taken in a beaker at ambient temperature. The crystals thus placed float in the solution due to surface tension and gradually grow by the evaporation of solvent. One or two crystals are also formed in the bottom of solution on every trial. KAP crystals obtained by floating seed technique are shown in figure.6.1.

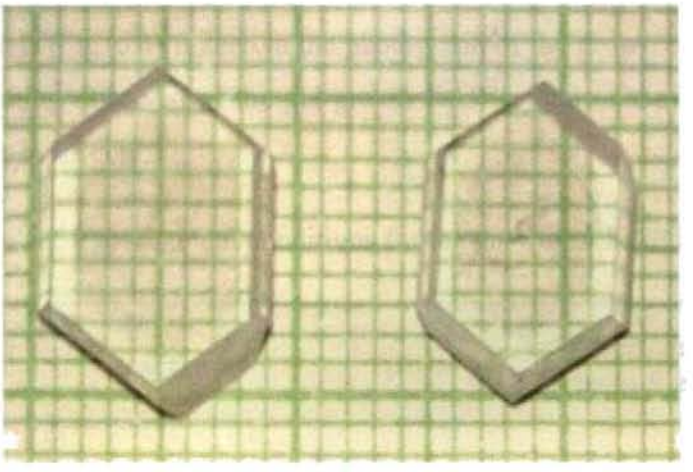

Fig.6.1 KAP crystals grown by floating seed technique

6.2.2 Growth of KAP crystals by Gel method

Single crystals of KAP are grown in silica gel by reduction of solubility method. Silica gel prepared from an aqueous solution of sodium metasilicate ($Na_2SiO_3.5H_2O$), is used as the crystal growth medium. Test tubes are used as crystal growth vessels. KAP is dissolved in an aqueous solution of sodium metasilicate of specific gravity 1.06 gm/ cm^3 and the pH of the gel solution is adjusted using 5 M oxalic acid. Acetone, ethyl alcohol and a mixture of these are placed over the set gel taken in the test tubes. The concentration of KAP dissolved in gel solution is varied and the volume ratio SMS: KAP in all the trial is maintained as 1.5:3.5. Different pH and concentration of the gel solution are tried, to obtain the best conditions for crystal growth. The best growth condition is determined based on the number of crystals obtained, their transparency, size and morphology. Transparent, nearly hexagonal massive aggregates of KAP are crystallized inside the gel medium (Fig.6.2).

Experiments are also carried out by placing aqueous solution of KAP as outer reactant over gel and mixing a mixture of ethyl alcohol and acetone with the gel (1:1v/v). Transparent tiny crystals of KAP are obtained, only at the gel-solution interface. The crystals are removed after a growth period of six weeks.

The crystal growth experiments are carried out at room temperature (≈30°C). The crystal growth conditions are presented in table 6.1. The characteristic habit of the gel grown crystals (Fig. 6.3) is seen in the photograph of the grown crystals. Growth layers and twinning observed in the gel grown KAP crystal is shown in figure 6.4 and figure 6.5 respectively.

Table 6.1 Experimental conditions for the growth of KAP in gel

Substance	Reactants	pH of gel	Transparency, Shape, Size (mm × mm × mm)
KAP	3M KAP in gel Ethyl alcohol and acetone over gel	5	Transparent, platelets, hexagonal, (5 × 4 × 3)
	4M KAP over gel Ethyl alcohol and acetone in gel	4.0	Transparent, aggregates (3 × 2× 1)

Fig.6.2 Growing KAP crystals in gel

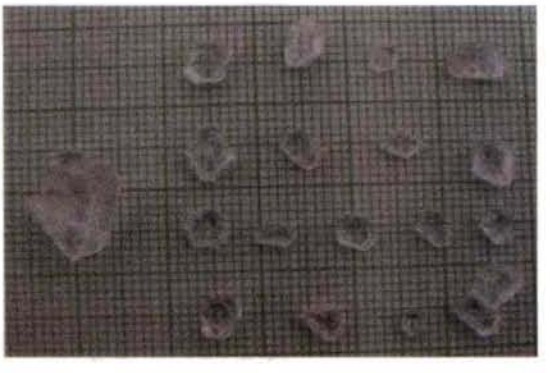

Fig.6.3 Characteristic habit of Gel grown KAP.

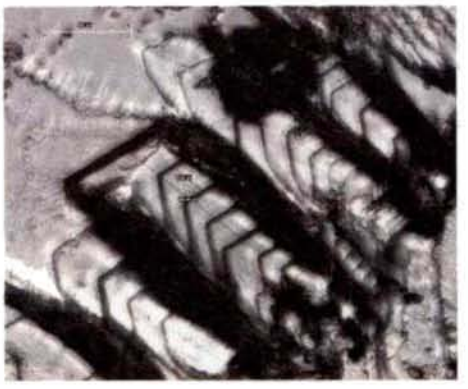

Fig.6.4 Growth layers on gel grown KAP (×100)

Fig.6.5 Twinning in gel grown KAP (×50)

6.3 CHARACTERISATION METHODS

6.3.1 X-ray powder diffraction studies

The powder X-ray diffractogram of the KAP crystal grown by floating seed technique and by gel method and recorded with Bruker D8 advance diffractometer operated at 40 KV and 50mA,using Cu target and graphite monochromator, are shown in Figs.6.6 and6.7 respectively. The intensity data is recorded by continuous scan from 5° to50° with a step size of 0.02°and scan speed of 4°/minute. The structure, refined by Pawley method [9] using the TOPAZ R version 3 program is given in table 6.2, and 6.3 for solution grown and gel grown KAP agrees well with the reported values [10].

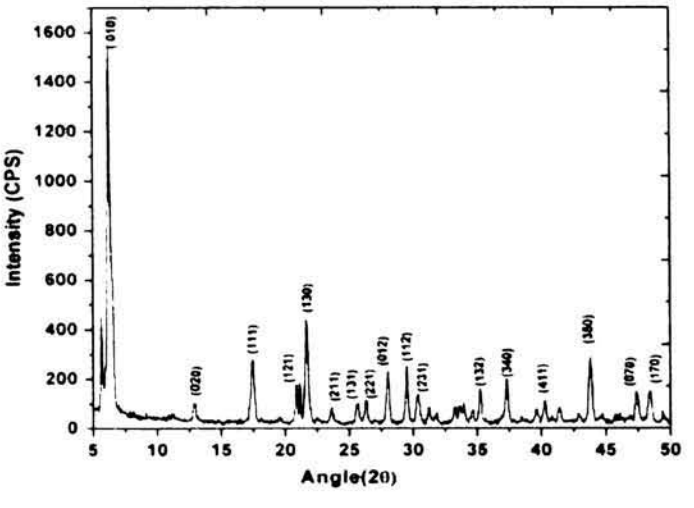

Fig.6.6 Powder XRD plot of solution grown KAP

Space group	**$Pca2_1$**
Cry. Size (nm)	232
Lattice parameters	
a (Å)	9.63
b (Å)	13.39
c (Å)	6.46
$\alpha = \beta = \gamma$	90
Volume(Å^3)	833.89

Table 6.2 unit cell parameters of the solution grown KAP

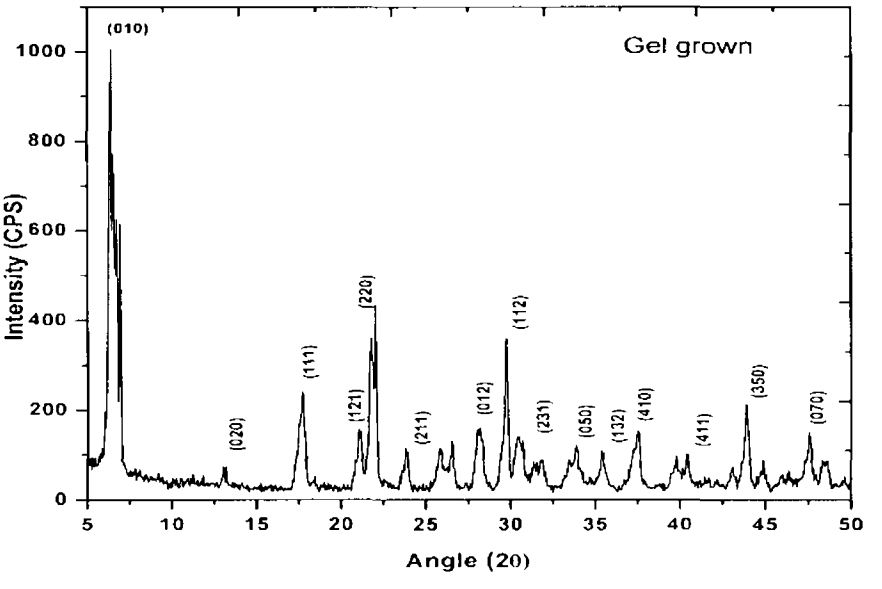

Fig 6.7 Powder XRD plot of Gel grown KAP

Space group	**$Pca2_1$**
Lattice parameters	
a (Å)	9.65
b (Å)	13.43
c (Å)	6.47
$\alpha = \beta = \gamma$	90
Volume(Å^3)	839.321

Table 6.3 unit cell parameters of Gel grown KAP

6.3.2 CHN analysis

The chemical composition of the grown KAP crystal determined by carbon, hydrogen, nitrogen (CHN) analysis using VarioEL III CHNS serial number11035060 is compared with the theoretical values of carbon, hydrogen present in the crystal and is shown in Table 4.4.

Table 4.4 CHN analysis data.

Element	Theoretical composition (%)	Measured composition (%)
Carbon	47.01	47.32
Hydrogen	2.45	2.36

6.3.3 EDX analysis

The chemical composition of a material can be determined by EDX. The EDX spectrum is a curve between binding energy and intensity of the emitted photoelectron. The peak heights or areas give a measure of the quantity of concerned elements in the specimen. The proportion of the different elements incorporated in the sample is obtained by comparing the EDX peaks of these elements. Figure 6.8 is the EDX spectrum of the potassium hydrogen phthalate crystal.

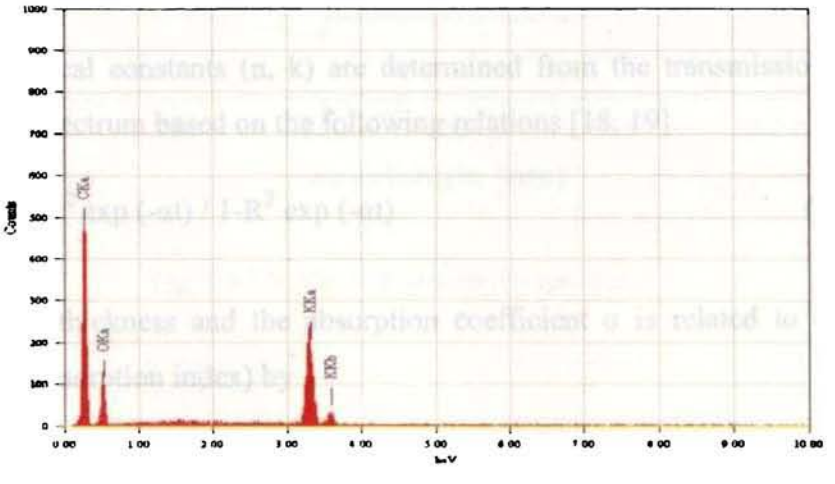

Fig.6.8 EDX spectrum of gel grown KAP crystals

6.3.4 UV/VIS/NIR spectrum and determination of linear optical constants

The optical absorption spectrum of potassium acid phthalate (KAP) single crystal (fig.6.9) is recorded in the wavelength region from 200 to 2000 nm. For optical device fabrications, a crystal should be highly transparent in the considerable region of wavelength [11]. The very low absorption and good transmission of the crystal in the entire visible region suggests its suitability for second harmonic generation applications [12]. The absorption coefficient near the fundamental absorption edge is dependent on the photon energy. In the high absorption region, the absorption coefficient takes on the following more general form as a function of photon energy [13, 14].

For optical transitions, $\alpha h\upsilon = A (\alpha h\upsilon - Eg)^n$, where υ is the frequency of the incident photon, h is Planck's constant, A and B are constants, Eg is the optical energy gap and n is the number which characterizes the optical processes, and n has the value 1/2 for the direct allowed transition, and 2 for the indirect allowed transition [15- 17]. When the straight portion of the graph of $(\alpha h\upsilon)^n$ against $h\upsilon$ is extrapolated to $\alpha = 0$ the intercept gives the transition band gap. The optical band gap of KAP is found to be 4.1 eV from the figure 6.10. The material has low absorption in the visible and NIR regions and high absorption in the deep UV region. Hence it can be utilised in the construction of poultry roofs and walls and for coating eyeglasses.

The optical constants (n, k) are determined from the transmission (T) and reflection (R) spectrum based on the following relations [18, 19].

$$T= (1-R)^2 \exp(-\alpha t) / 1-R^2 \exp(-\alpha t) \qquad (6.1)$$

where t is the thickness and the absorption coefficient α is related to extinction coefficient k (absorption index) by

$$K= \alpha \lambda / 4\pi \qquad (6.2)$$

For semiconductors and insulators (where $k^2 << n^2$) there exists a relationship between R and n (refractive index) given by [20, 21]

$$R = (n - 1)^2/(n + 1)^2 \quad (6.3)$$

The relationship between ε and k is given by [22] $\varepsilon = \varepsilon_r + i\varepsilon_i = (n + ik)^2$

$$\varepsilon_r = n^2 - k^2 \quad (6.4)$$

$$\varepsilon_i = 2nk \quad (6.5)$$

where ε_r, ε_i are the real part and imaginary part of dielectric constant respectively. The variation of n, k and the real part of dielectric constant with energy are shown in figures 6.11, 6.12 and figure 6.13 respectively.

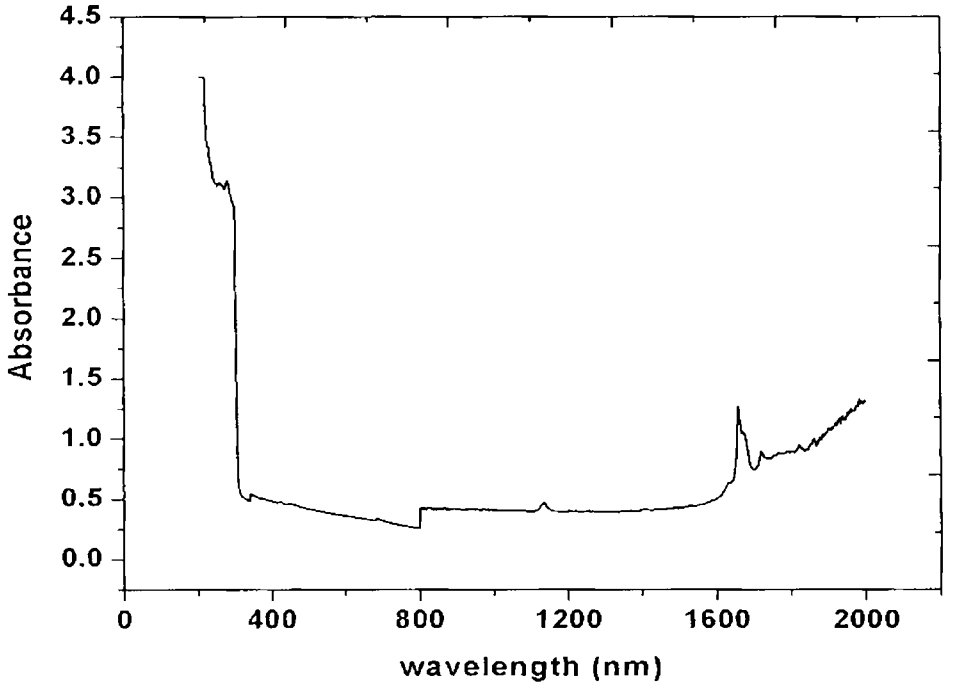

Fig. 6.9 UV/Vis/NIR absorption spectrum

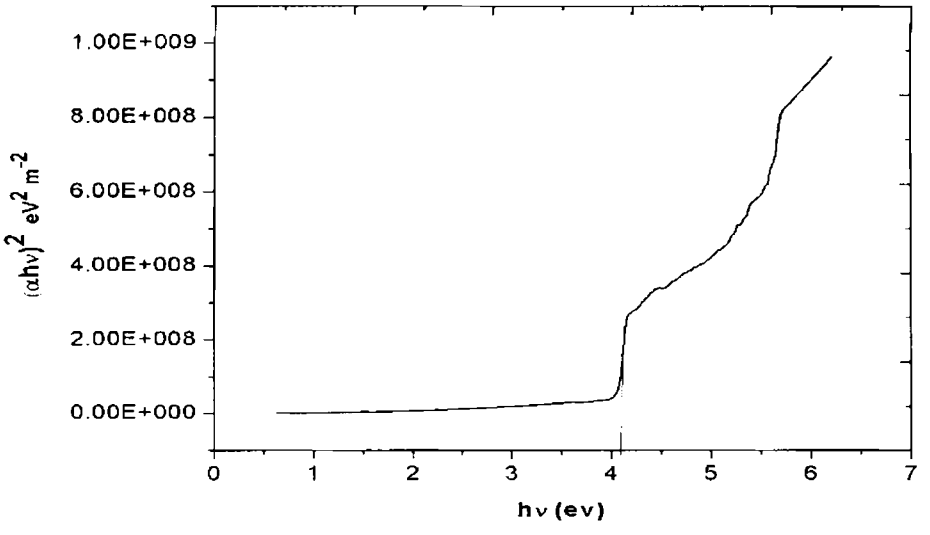

Fig. 6.10 Plot showing the optical band gap

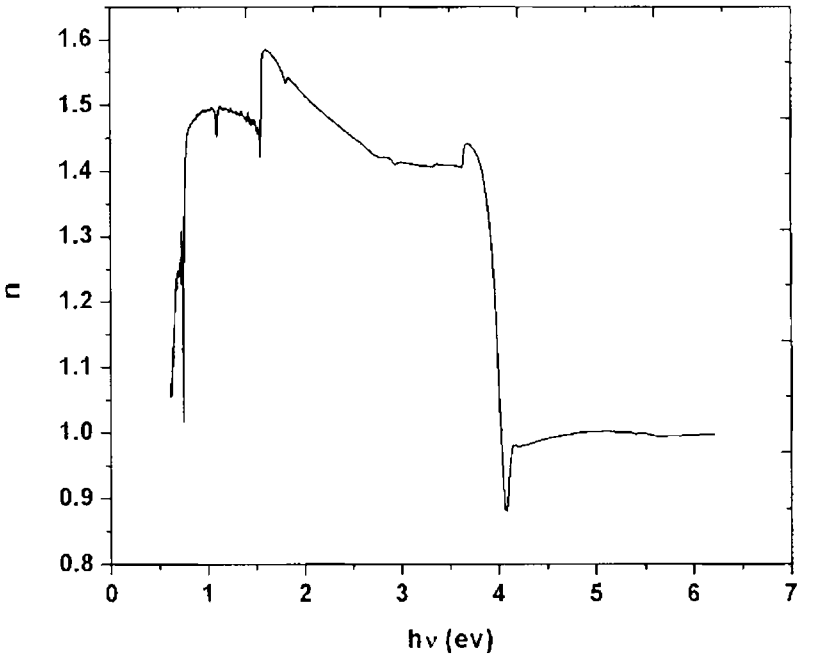

Fig 6.11 graph showing the variation of n with energy

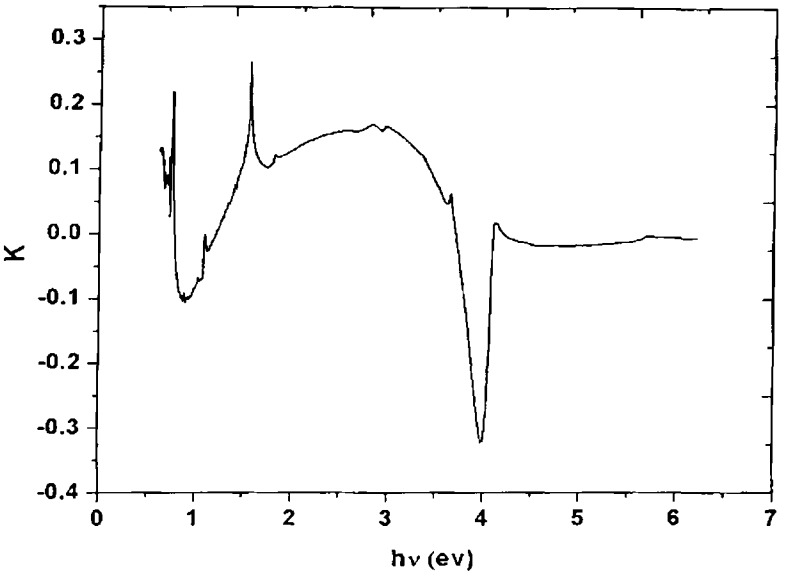

Fig 6.12 Plot of variation of K with energy

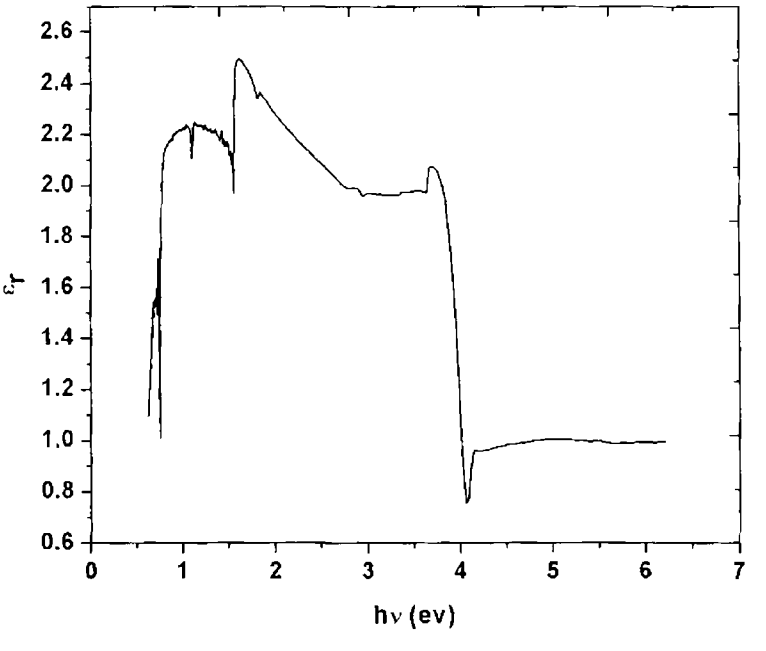

Fig. 6.13 variation of dielectric constant with energy

6.3.5 The vibrational spectral analysis of Potassium hydrogen phthalate crystal

The FT IR spectrum (Fig.6.15, 6.16) of the KAP crystal is recorded using AVTAR 370 system with a resolution of 4cm^{-1} in the range 400-4000cm^{-1}. The FT Raman spectrum of the powdered sample (Fig.6.17) is recorded with BRUKER RFS100/S system with a resolution of 4 cm^{-1} using a standard InGaAs detector with a laser source of 150 mW. The vibrational wave numbers and their assignments are given in the table 6.4.

The potassium acid phthalate molecular crystal is characterized by the presence of various bonds: covalent (inside anions [$C_6H_4COOH \cdot COO$]–), ionic (cation–anion), Vander-Waals (between chains of anions), and intermolecular hydrogen bonds O-H···O (H-bonds between anions in chains). In KAP crystal H-bonds are very short (~2.5 Å) and, hence, they may be attributed to strong H-bonds for which are possible the interactions of stretching vibrations (υ(O-H)) with sum combinations of bending in-plane (β (O-H)) and out-of-plane (γ(OH)) vibrations [23]. Structural model of KAP crystals and the unit cell [24] is shown in Fig. 6.14. In the parallel planes (010) the corrugated layers of the K^+ cations are situated. The anions consist of the phenylene and carboxyl groups and they are located by double layers between the cation layers. The groups -COO^- form H bonds with the carboxyl group –COOH of the nearest anion along the *c* axis [24]. H-bonds are marked by the dash line.

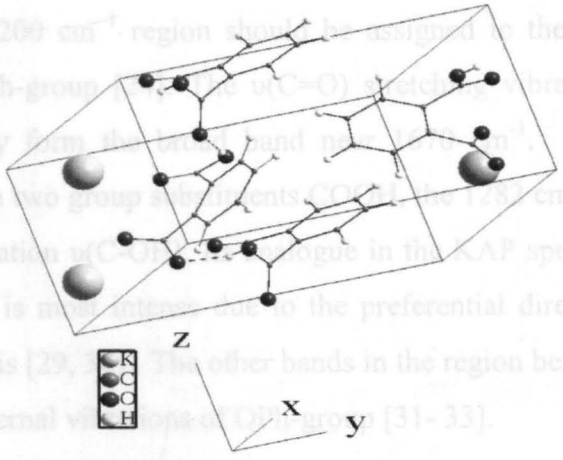

Fig. 6.14 structural model of the KAP unit cell

All atoms of the KAP formula unit are located in the general position. Therefore all $3N - 6$ internal vibrations, where N is the number of atoms in molecule ($N = 18$), should be active in the Raman spectra [10]. It is expedient to divide the vibrational representation of KAP into the vibrations of the orthophenylene (OPh) and carboxyl groups. The frequencies and forms of 30 internal vibrations of OPh-group are known [24, 25]: 15 stretching (C–H, C=C, C–C', skeletal), 6 bending in-plane (C–H, C–C'), and 9 bending out-of-plane (C–H, C–C', skeletal) vibrations, where C' is the carbon atom substituting the hydrogen atom in the benzene ring. In view of a weak (ionic) bond of the metal atoms with anions, it is difficult to expect an appearance of vibrations of the metal atoms in the Raman spectra. However, it is possible an influence of these atoms on the spectra of OPh and carboxyl groups. The frequencies below 220 cm^{-1} are likely corresponded to external vibrations of molecules. The characteristic frequencies for di-ortho substituted benzene [24] are also used to assign the Raman bands. It is known, that in case of the strong H-bands the stretching vibrations υ (O-H) are shifted in the region below 3000 cm^{-1}, as, for example, in the spectra of the KDP crystals [26]. In the Raman spectra of KAP it is seen a weak diffusive scattering in the 1800–3000 cm^{-1} region with the broad band near 2000 and 2450 cm^{-1}, and the less significant shoulder near 2700 cm^{-1}. Earlier [27] the 2590 cm^{-1} band was assigned to the sum combinations of the skeletal vibrations, and the broad bands to vibrations of H-bonds.

We have assigned the Raman bands at 1445 and 1087 cm^{-1} to β (O-H) and γ (O-H) in KAP that is in agreement with a suggestion in [27, 28]. The narrow Raman bands in the 2800–3200 cm^{-1} region should be assigned to the υ(C-H) stretching vibrations of the OPh-group [24]. The υ(C=O) stretching vibrations are specified unambiguously. They form the broad band near 1670 cm^{-1}. In the spectra of orthophtalic acid with two group substituents COOH, the 1282 cm^{-1} band is assigned to the stretching vibration υ(C-OH). Its analogue in the KAP spectra is also present in this region and it is most intense due to the preferential direction of the C-OH bond along the 'a' axis [29, 30]. The other bands in the region below 1600 cm^{-1} may be assigned to the internal vibrations of OPh-group [31- 33].

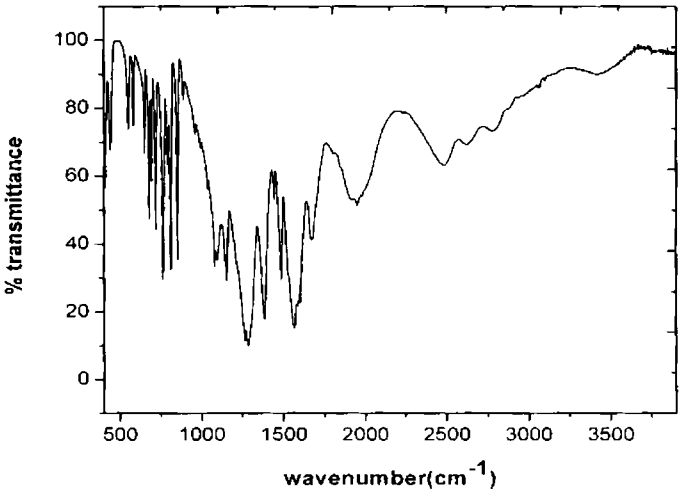

Fig. 6.15 FTIR spectrum of solution grown KAP

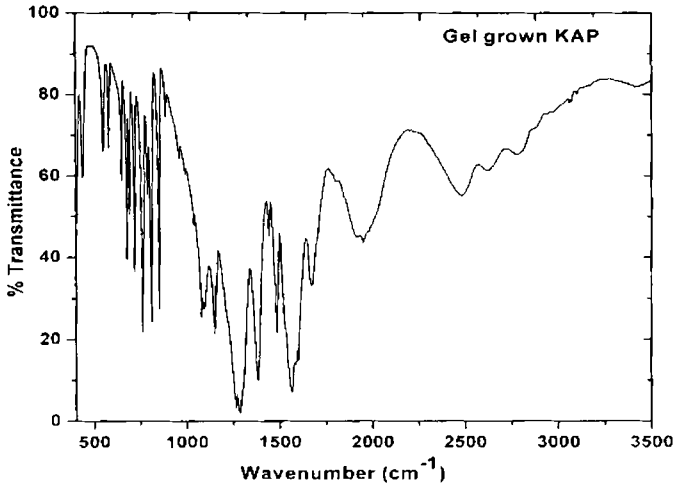

Fig. 6.16 FTIR spectrum of gel grown KAP

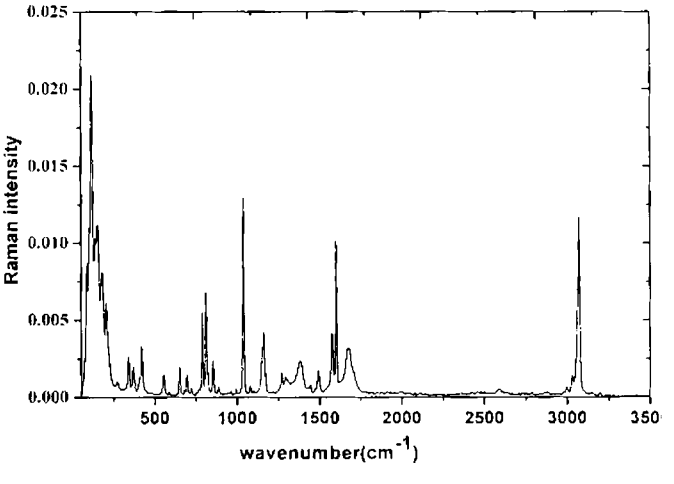

Fig.6.17 FT Raman spectrum of KAP crystal

Table 6.4 vibrational assignments

IR spectrum-KAP Solution grown (cm^{-1})	IR spectrum KAP Gel grown (cm^{-1})	Raman spectrum (cm^{-1})	Assignment of vibrations
		180, 204, 270	Lattice vibrations
440	339	340	C=C out of plane ring bending
552	553	554	C=C-C deformation
582	584		C=C-C out of plane ring deformation
650	651	651	C=O stretching
678			C-O wagging
694	694	695	=C-H out of plane deformation
720	721	722	C-C stretching
790	790	788	-C-H bending disubstituted benzene
811	812	812	C-H out of plane bending
852	853	855	=C-H out of plane bending
888	888	888	C-C-O stretching
		993	C-H stretching
		1039	C-H bending
1071	1072	1079	γ O-H
1151	1150		C-O stretching
		1162	C-O stretching out of plane
1266	1267	1270	C-H out of plane bending
1283	1283		C-COO stretching
		1292	C-OH bending
1384	1385	1385	-C=O Carboxylate ion =O Symmetric
1442	1442		β O-H
1488	1489	1492	C=C ring stretching
1566	1568	1575	C-C bending in plane
		1600	C-C bending out plane
1673	1674	1674	Symmetric C=O stretching
2483			O-H stretching
2996	2996	2996	C-H symmetric stretching of O-Ph group
		3030	C-H asymmetric stretching of O-Ph group
		3070	C=C stretching of O-Ph group

6.3.6 Thermal analysis

The thermal properties of the KAP crystal are studied using thermo gravimetric analysis (TGA)/differential thermal analysis (DTA) and differential scanning calorimetry (DSC). Powdered sample of 4.6 mg potassium hydrogen phthalate is analyzed in N_2 atmosphere by using Perkin Elmer Diamond TGA / DTA equipment. The analysis is carried out simultaneously in air at a heating rate of 10°C / min for a temperature range of 28°C to 810°C. The TGA/DTA curve is shown in Fig.6.18. Quite interesting and important point to be noticed is the very good thermal stability of the material up to 298°C. The absence of water of crystallization in the molecular structure is indicated by the absence of weight loss around 100°C. The endothermic peak in the DTA curve at 298°C represents the melting point of the sample. Another important observation is that there is no phase transition till the material melts and this aspect enhances the temperature range for the utility of the crystal for NLO applications. Further there is no decomposition up to the melting point. This ensures the suitability of the material for possible applications in lasers, where the crystals are required to withstand high temperatures. At higher temperatures, there is decomposition where the fragments like CO_2, CH_3 may be liberated.

The specific heat at constant pressure Cp of the crystal is estimated from the DSC curve using the ratio method [34, 35]. DSC run performed on the sample (Fig. 6.19) reveals that there is no phase transition up to its melting point and it agrees well with the TGA/DTA analysis. It is found that Cp increases linearly in the temperature region of interest (Fig 6.20). The specific heat value of KAP crystal at 333K is 860 J/kg K. Due to its relatively large Cp, KAP crystal need larger quantity of heat energy to get heated up, so that consequent damage due to localised heating can be avoided, which enhances its prospects for applications in laser assisted devices.

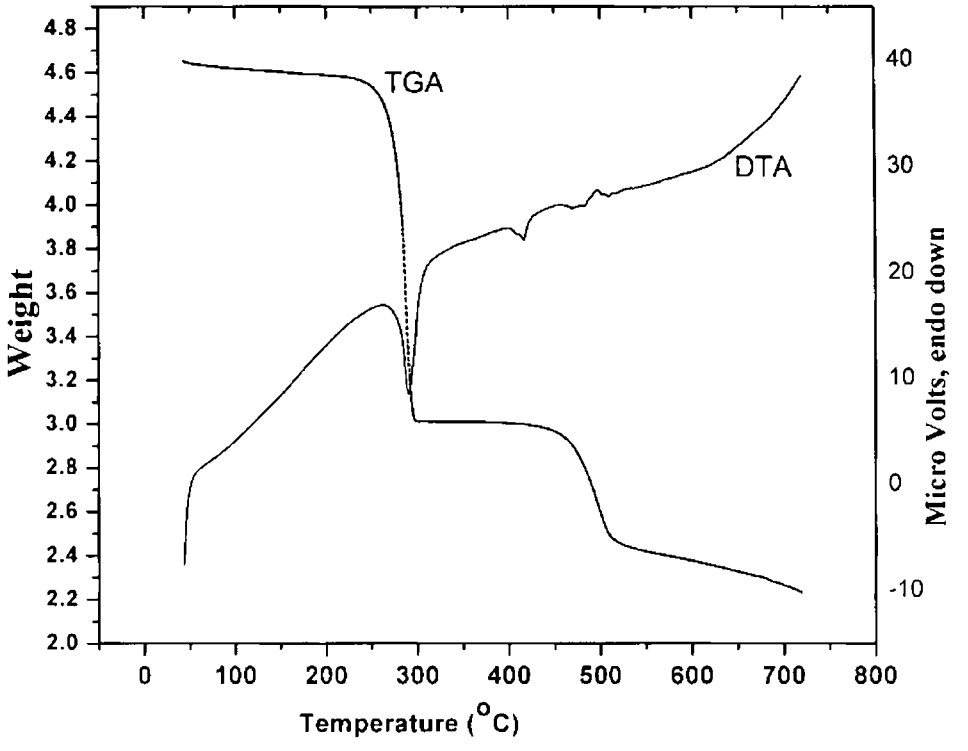

Fig.6.18 TGA/DTA curve of KAP crystal

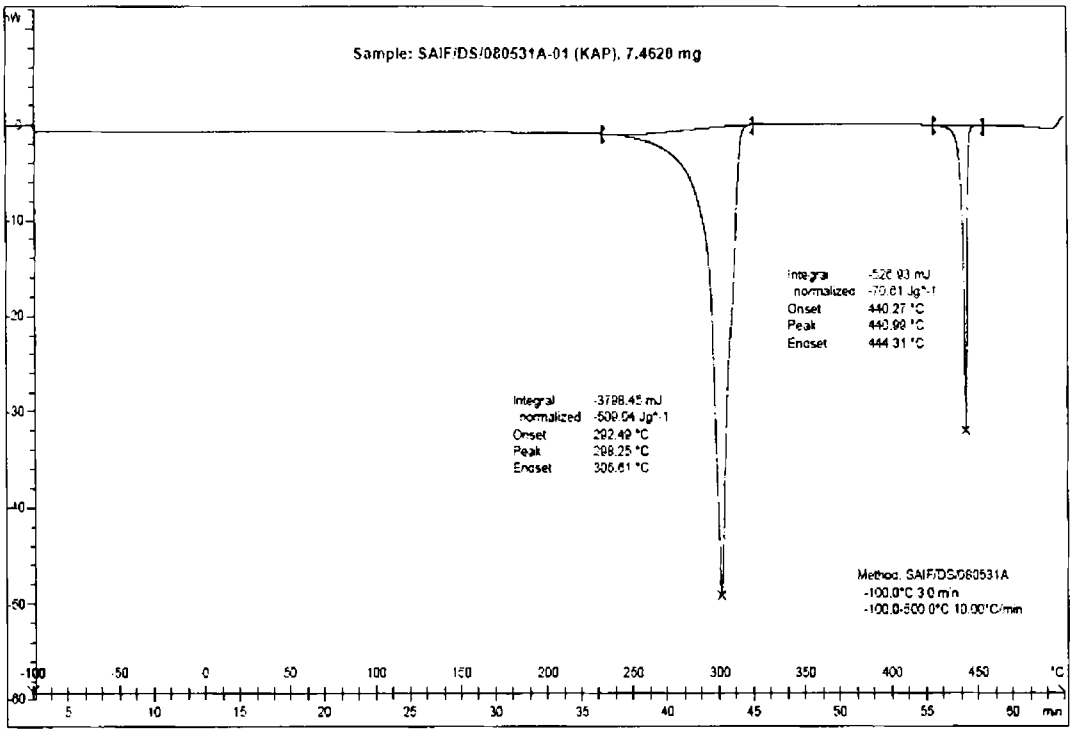

Fig.6.19 Differential scanning calorimetry curve of KAP crystal

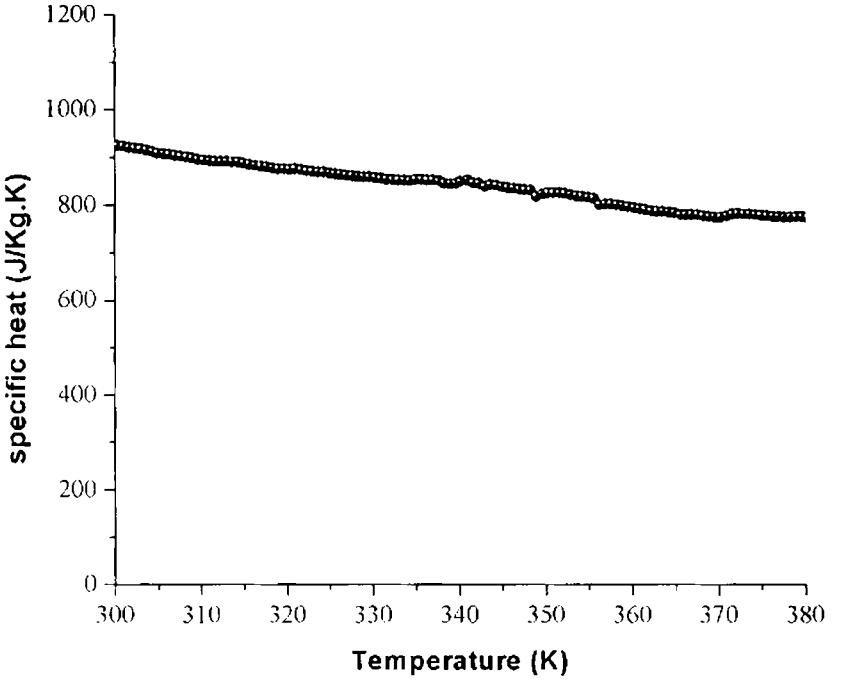

Fig. 6.20 Plot of variation of Cp with temperature

6.3.7 Vickers's microhardness analysis

Crystals with flat and smooth faces, microscopically free from signs of any damage are selected for indentation studies. Indentations are made on the cleaved (010) surface of a selected crystal using a Leitz Miniload microhardness tester. The crystal is mounted properly on the base of the microscope and the selected face is indented gently by the loads 10, 25 and 50 g for a dwell period of 10 s using Vickers diamond pyramid indenter attached to an incident ray research microscope. The indented impressions are approximately pyramidal in shape. The shape of the impression is structure dependent, face dependent and also material dependent. The lengths of the two diagonals of the indentations are measured by a calibrated micrometer attached to the eye piece of the microscope after unloading and the average (d) is found out. The Vickers hardness number is computed using the formula

$$Hv = 1.8544\ P/d^2 \qquad (6.6)$$

where Hv is the Vickers hardness number in kg/mm^2, P is the indenter load in kg and d is the diagonal length of the impression in mm. Since crack initiation and material chipping became significant beyond 50 g of the applied load, hardness test could not be carried out above this load. Elastic stiffness constant is calculated using Wooster's empirical formula [36]

$$C_{11} = H_v^{7/4} \tag{6.7}$$

Fig.6.21 shows the variation of Hv as a function of applied loads 10, 25 and 50 g on the (010) face of KAP crystal grown by floating seed technique. From the figure it is clear that Hv increases with increase in load. Meyer's law [37] relates load and size of indentation as

$$P = k_1 d^n \tag{6.8}$$

where 'k_1' is the material constant and 'n' is the Meyer's index.

$$\log P = \log k_1 + n \log d \tag{6.9}$$

The plot of log P against log d shown in Fig.6.22 is a straight line which is in good agreement with Meyer's law. The slope of the graph gives the value of work hardening coefficient, 'n'. Combining eqs. (1) and (3) we have

$$Hv = b\, p^{(n-2)/n} \tag{6.10}$$

where $b=1.8544k_1^{2/n}$ is a new constant. The above expression (5) shows that Hv should increase with increase in P for $n>2$ and decrease with the same for $n<2$.

This is in good agreement with our experimental data, since Hv increases with increase in load as shown in Fig. 6.2, the value of 'n' being greater than 2 (3.26). According to Onitsch [38] and Hanneman [39] 'n' should lie between 1 and 1.6 for hard materials and above 1.6 for softer ones. Hence KAP belongs to softer material category. According to Hays and Kendall's theory of resistance pressure [40], there is a minimum level of indentation load (W) also known as resistance

pressure below which no plastic deformation occurs. The relationship between indentation test load and indentation size is

$$P - W = k_2 d^2 \quad (6.11)$$

Where k_2 is a new constant and (P–W) is the effective indentation test load. Combining eqs. 6.10) and (6.11) we get

$$W = k_1 d^n - k_2 d^2 \quad (6.12)$$

Or

$$d^n = W/k_1 - (k_2/k_1)d^2 \quad (6.13)$$

The plot between d^n and d^2 is a straight line with slope k_2/k_1 and intercept W/k_1. From Fig.6.23, the value of 'W' is calculated as 10.6 gm. The elastic stiffness constant (C_{11}) for different loads calculated using Wooster's empirical formula $C_{11}=Hv^{7/4}$ are shown in Table 6.5 which gives an idea about the tightness of bonding between neighboring atoms. Figure 6.24 shows an indentation pattern for a load P=50 g.

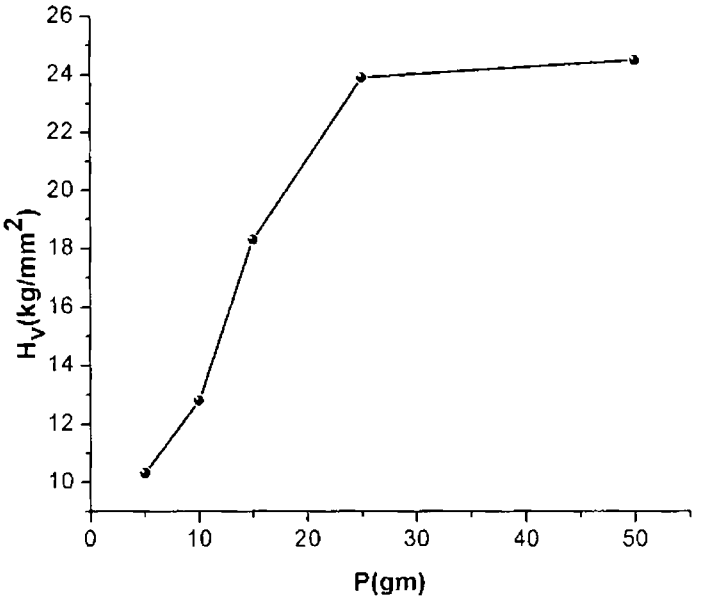

Fig6.21 Vickers' hardness profile of KAP (010 plane)

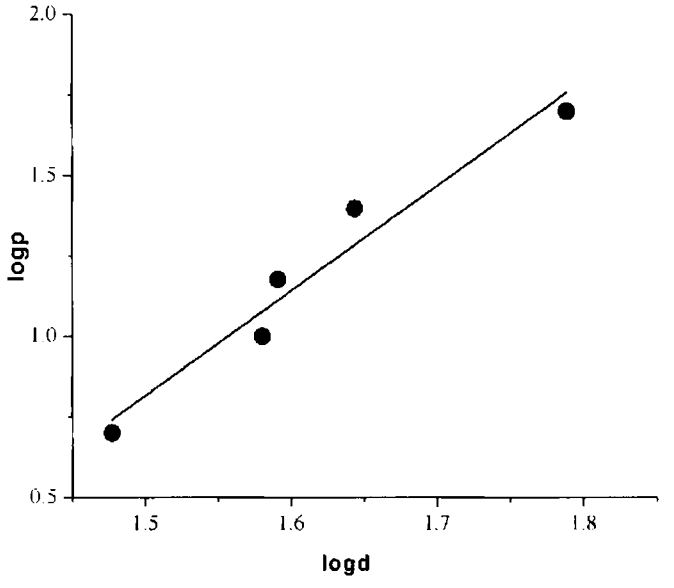

Fig. 6.22 Mayers plot of logp Vs log d

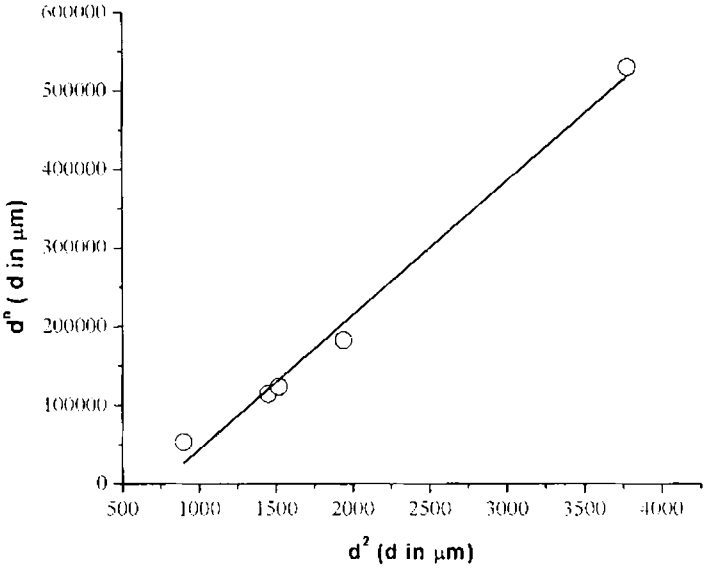

Fig 6.23 Plot of d^2 Vs d^n

Table 6.5 Variation of elastic stiffness constant with load

Load (gm)	Hv (kg /mm^2)	C_{11} (x10^{14}Pa)
5	10.3	1.0161
10	12.8	1.4868
15	18.3	2.7793
25	23.9	4.4344
50	24.5	4.6311

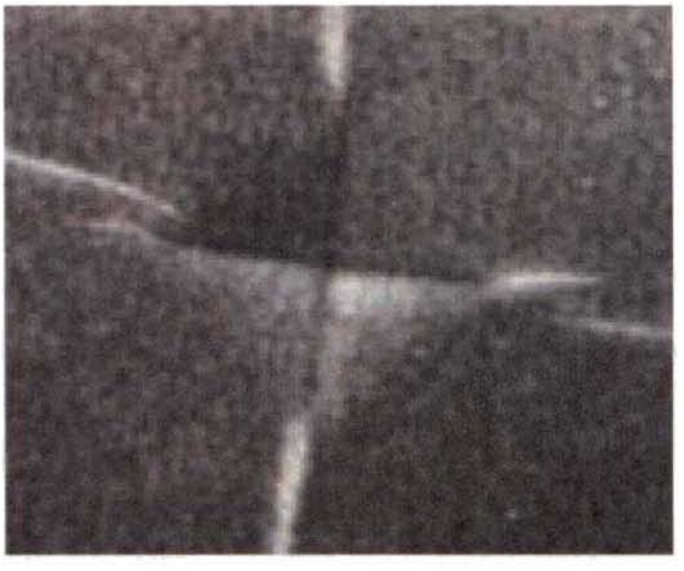

Fig 6.24 Indentation pattern (×100).

6.3.8 Microtopography and chemical etching studies

Potassium acid phthalate shows sharp cleavage along [010] plane. Figure 6.25(a) shows such a cleaved surface in which growth layers are clearly visible. Layers having the same direction and opposite sign are also seen in the figure. In the early stages of growth, when the super saturation is very is high, growth mainly takes place by either two-dimensional nucleation or by mutual attachment of crystallites, formed without the help of screw dislocations. When the crystals reach the critical size, the surface is strained by internal stresses or by pressure from other crystals, forming imperfection on the surface. Internal or external stresses help the

dislocations present to concentrate into a small area. Thus formed, growth layers preferentially start and spread two dimensionally. These growth layers often bunch together to form thick layers [41]. However, when the super saturation rate decreases the rate of spreading of the growth layers will decrease. As a matter of fact, when super saturation is very low, a thick layer will find it very difficult to advance.

Several etchants are tried to reveal the nature and extent of dislocations present in the crystal along [010] direction. Etchants described in the literature for organic crystals [41-45] or prepared by considering the various chemical reactions of the material are proved to be unsuitable to delineate the dislocation present in the crystal.

When etched with triply distilled water, fast dissolution layers are observed (fig.6.25 (b)) due to the large solubility of KAP in water. Fast dissolution is controlled by adding acetone to water in the volume ratio 1:4. The etch pits observed on the [010] cleavage plane of KAP crystal can be classified according to their shape as point bottomed pyramidal pits (figure 6.25 (c)); pyramidal pits with flat bottom, flat bottomed pyramidal pits with stepped sides (figure 6.25(d));flat bottomed rectangular pits with flat sides .

Flat sided pits are deeper compared to the terrace sided pits. According to Gatos [46], if the dissolution rate along the dislocation line, perpendicular to the surface and parallel to the surface vary considerably, terraced pits will result

Flat bottomed pits with flat sides in abundance as in the present case are observed by several researchers on other crystals [46- 48]. A reasonable explanation for the occurrence of these pits is the bending away of dislocations at the cleavage surface [49]. The systematic reduction in the number of small pits on successive etching suggests that these pits are due to shallow dislocations [50].

When etched with a solution of one part of methanol in eight parts of water and a drop of 1N potassium hydroxide resulted in almost hexagonal (shield type)

pits having curvature as shown in figure(6.25(e)). Dislocation line formed on etching is clearly seen in the photomicrograph (6.25(f)).

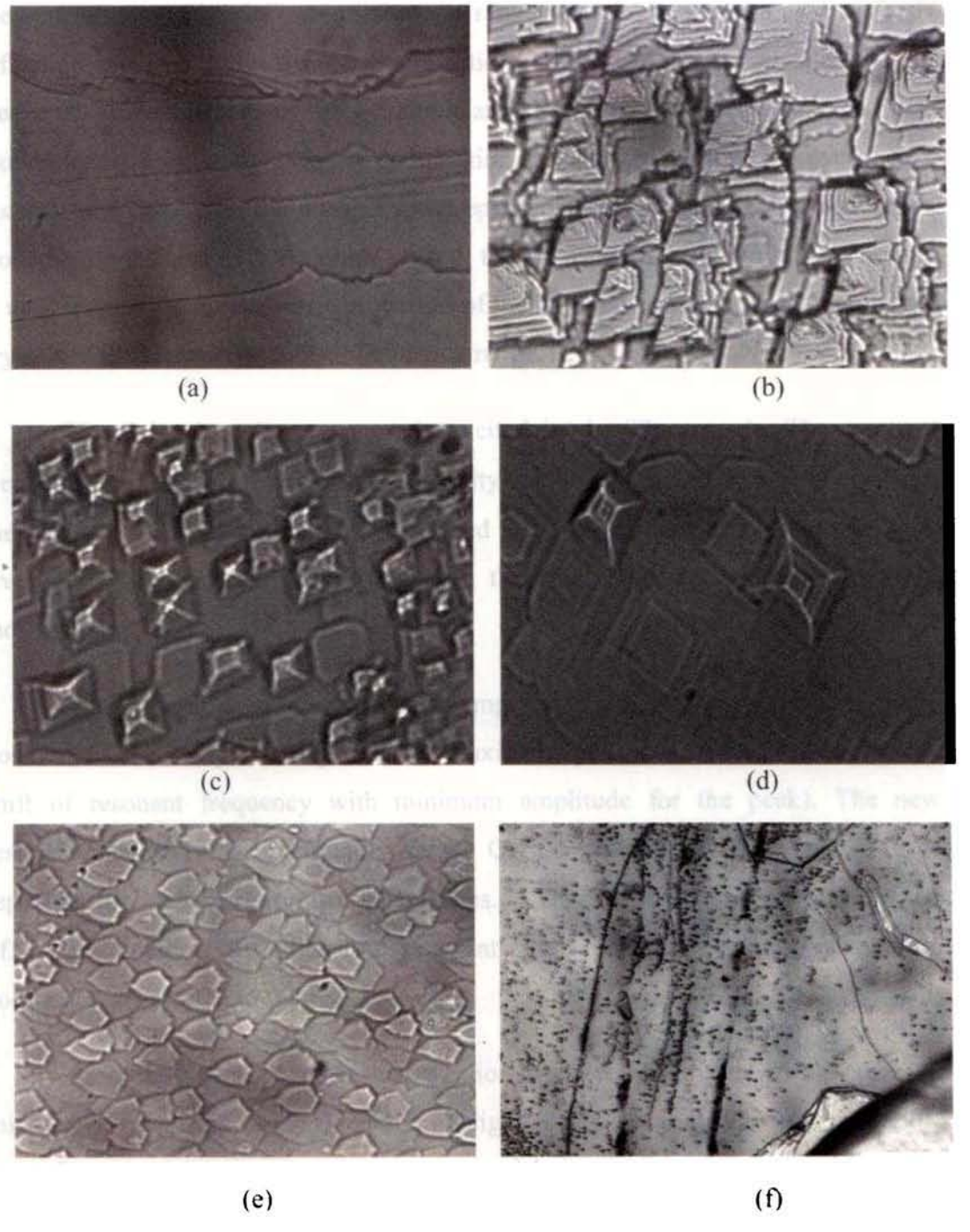

Fig. 6.25 (a) Growth layer (b) Fast dissolution layer (c) Point bottomed pyramidal pits (d) stepped pyramidal pits (e) hexagonal shield type pits (f) Pits on a dislocation line (all×100)

6.3.9 Microwave dielectric properties by cavity perturbation technique

Two main methods—nonresonant and resonant techniques—are available to measure the permittivity at microwave range. Nonresonant methods such as reflection methods and transmission/reflection methods [51, 52] can scan a wide frequency range, but require a large sample and strict preparation. Resonant methods like dielectric resonator and cavity perturbation methods [53, 54] are relatively more accurate and flexible to sample size and preparation, but run at discrete frequencies. Considering the shape of the single crystal, the resonant cavity perturbation method is used to measure the dielectric properties of the NLO potassium hydrogen phthalate crystals in the microwave S band frequency range.

The S band cavity resonator is excited in the TE_{10p} mode. The resonant frequency 'f_0' and the corresponding quality factor 'Q_0' of each resonant peak of the cavity resonator, without sample placed at the maximum of the electric field, are noted. The sample is introduced into the cavity resonator through the non-radiating slot.

The resonant frequencies of the sample loaded cavity are selected and the position of the sample is adjusted for maximum perturbation (that is, maximum shift of resonant frequency with minimum amplitude for the peak). The new resonant frequency f_s and quality factor Q_s are determined. The procedure is repeated for other resonant frequencies. The frequency dependence of effective conductivity, dielectric constant and dielectric loss and absorption coefficient are plotted in figure.6.26

From the figure it is clear that variation of dielectric constant with increase in microwave frequency in the S band is negligible. Dielectric loss is very negligible throughout the S band. The very low value of dielectric loss is an indication of the better crystallinity of the crystals formed. Samples with low dielectric loss are need for device applications. Conductivity is also very small indicating that sample is an insulator to microwaves in the frequency range 2-3 GHz. It is found that absorption coefficient increases slightly with frequency.

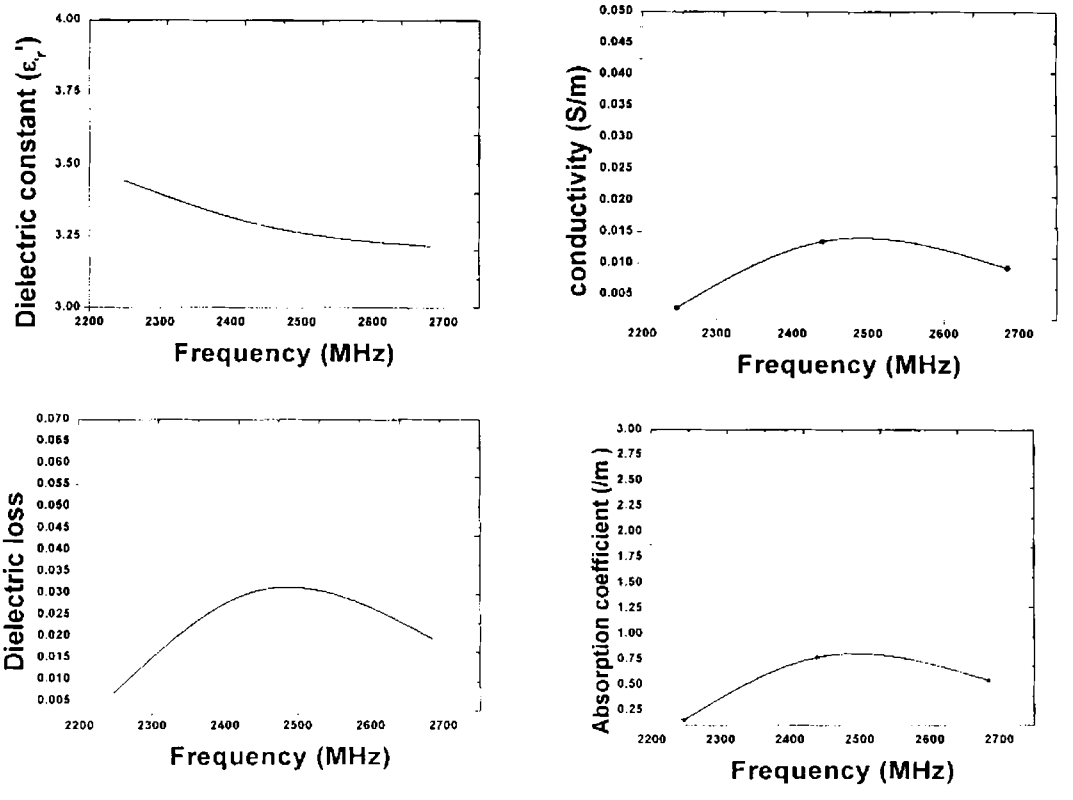

Fig 6.26 Variation of dielectric parameters with microwave frequency

6.3.10 Laser damage threshold studies

Laser damage studies on NLO crystals are extremely important as the surface damage of the crystal by high power lasers limits its performance in NLO applications [55, 56]. The knowledge of multiple shot damage threshold is essential as NLO crystals are generally used for long durations in repetitive mode as per the demands of various applications in research and industry.

A Q-switched Nd: YAG (yttrium aluminum garnet) Quanta Ray laser of pulse width 7 ns and 10 Hz repetition rate operating in TEM_{00} mode is used as the source. The energy per pulse of 1064 nm laser radiation is measured using an energy meter (Rj-7620, (Laser Probe Inc). All the experiments are performed on the freshly cleaved (010) plates. A plano-convex lens of focal length of 100 mm is used for focusing the laser beam onto the sample.

To determine the single shot damage threshold, the sample is irradiated at different spots on the same crystal at different pulse energies. This is done to avoid the cumulative effects resulting from multiple exposures. In the present investigation, the resulting damage pattern is characterized by observing it with an optical microscope and by scanning electron microscope. In our work, the damage almost always occurred by the formation of white spark accompanied by audible sound. According to Nakatani *et al.*, [57] the multiple shot damage threshold value is determined as the maximum power level at which the crystal remains undamaged even after exposing it to 1800 pulses. The single shot (*P*1) and multiple shot (*Pn)* damage threshold values for (010) cleaved plate of KAP is obtained to be 25 and 19.6 GW cm^{-2}, respectively for 1064 nm Nd: YAG laser radiation.

Potassium hydrogen phthalate crystal is observed to have reasonably high damage threshold value similar to the other solution grown nonlinear optical semi organic crystals such as zinc tris thiourea sulfate (ZTS), bis thiourea cadmium chloride (BTCC), L-arginine phosphate (LAP), deuterated LAP... etc [58,59]. It is generally noted that crystals having high specific heat exhibit higher resistance to the laser damage as the rise in temperature with the laser irradiation is one of the mechanisms causing the damage. The specific heat of LAP at room temperature is reported to be 0.55 J g^{-1} K^{-1} [60] and has a damage threshold value of 13 GW/cm^2 for 1064 nm laser radiation of 25 ns pulse width [61]. Since KAP has a room temperature specific heat of 0.860 J g^{-1} K^{-1} one can expect a high threshold value for laser damage and that is what we have observed in our investigation. In fact, the average dislocation density in this crystal is estimated to be 10^3 cm^{-2} by chemical etching. The very low value of dislocation density reveals the good crystalline perfection in the grown crystal. The low value of dielectric loss found by microwave absorption study also supports this. Crystals free from defects and imperfections with good crystalline perfection will give high damage threshold value.

Figure.6.27(a) shows the single shot damage pattern of 1064 nm laser radiation on (010) plate The scanning electron micrograph depicting the core of laser induced damage for multiple shot1064 nm laser radiation is shown in Fig.6.27(b). The different layers seen in the micrograph is the result of the rupturing of cleavage

Figure.6.27(a) shows the single shot damage pattern of 1064 nm laser radiation on (010) plate The scanning electron micrograph depicting the core of laser induced damage for multiple shot1064 nm laser radiation is shown in Fig.6.27(b). The different layers seen in the micrograph is the result of the rupturing of cleavage planes. This opening up of cleavage planes in the damage pattern may be responsible for the highly reflecting area surrounding the core of the damage. The multiple shot laser damage pattern is elliptical in nature. Fig. 6.27(c) shows the striation pattern observed on the surface, due to the thermal strain developed on irradiation with high laser input power at the time of damage.

Laser induced breakdown of materials is caused by various mechanisms, namely, electron avalanche, multiphoton absorption, photoionization by thermal absorption[56] photochemical dissociation[62] electrostrictive fracture, etc. Precisely which one dominates depends on various factors such as experimental geometry, specific properties of the material under investigation, pulse width, and wavelength of the laser radiation used [63]. The morphology of the damage pattern in many cases, give an insight into the nature and the possible origin of damage in the crystals [64]. When the damage is predominantly by thermal mechanism, the patterns observed do not show any symmetry and are characterized by melting and resolidification of the material which will be generally circular or elliptical in nature [65, 66]. The lower threshold values for multiple shot experiments can be attributed to the cumulative thermal effects which become dominant when there is insufficient time between shots to allow heat dissipation.

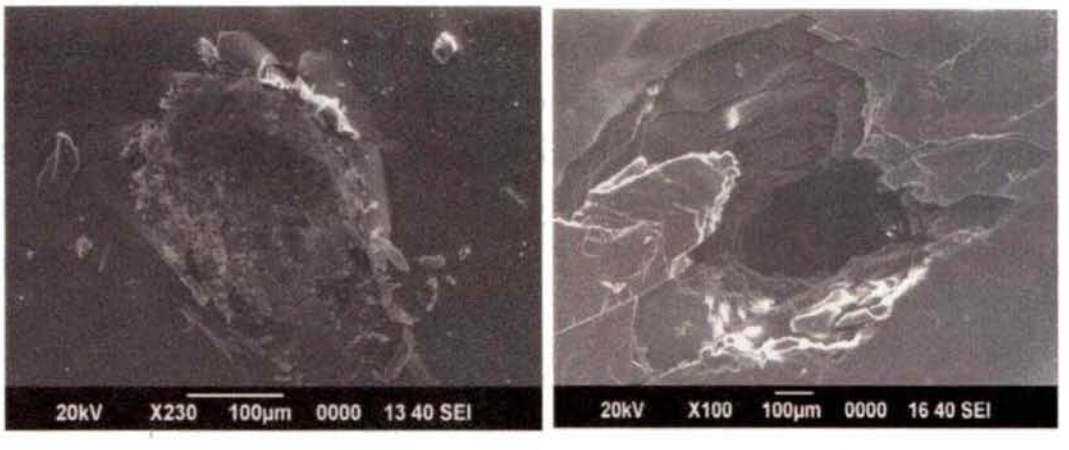

(a) (b)

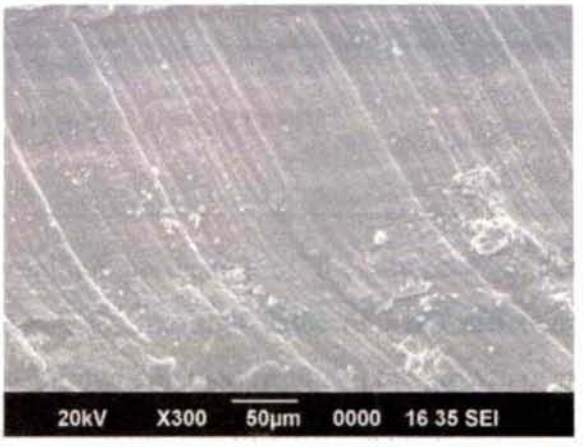

(c)

Fig. 6.27 Laser damage pattern for (a) single shot (b) multiple shot (c) thermal striation pattern

6.3.11 SHG studies

The SHG efficiency of KAP is measured by using the Kurtz & Perry method [67]. The sample is subjected to a Q-switched Nd: YAG laser with emission at 1064 nm having 7 ns pulse width and10 Hz repetition rate. The generated SHG signal at 532 nm is split from the fundamental frequency using IR separators and measured. The SHG efficiency is compared with KDP. From SHG test, the SHG efficiency of the solution grown KAP crystal is found to be nearly 1.5times greater than that of KDP and that of gel grown KAP is 2.1 times than that of KDP. The second-order optical properties of organic crystals are very sensitive to the number of crystal imperfections and defects [68, 69]. So varying this factor one can additionally enhance the susceptibility as this parameter may sometimes leads to the substantial deviations in the second order optical data. Table (6.6) gives a comparison of the second harmonic generation in the KAP crystal with KDP crystal for different laser inputs.

Table 6.6 SHG data of KAP.

Laser input	KDP	solution grown KAP	Gel grown KAP
2.7 mJ	118mV	177mV	247 mV
5.0 mJ	211mV	317 mV	443 mV

The good crystalline perfection of the samples in the present study is expected to be the reason for the high value of SHG efficiency. This study also supports the fact that gel growth method results in the growth of perfect crystals with good crystallinity even though the size of grown crystals is less compared with other crystal growth methods [70, 71]

6.3.12 Third order NLO properties by Z scan technique

The demand for optical power limiters to provide sensor and eye protections from laser radiation over a wide range of wavelengths is increasing because of the wide range of existing laser wavelengths. Materials with strong nonlinear optical properties are extensively investigated and generally well suited for the realization of passive optical limiters, i.e., where the switching process between two different transmission regimes is determined only by the intensity of the incoming light. An ideal optical limiting material must meet several requirements in terms of high nonlinear optical properties and damaging threshold together with low absorption losses. Therefore, the realization of an optical limiter with a single bulk material is still an open task.

The Z-scan method [72–74] provides a simple technique for measurement of nonlinear properties of optical materials [75–78] and therefore it is becoming ever more popular. The Gaussian pump beam is focused by a lens to obtain a sufficiently small beam waist and high intensity. The sample is placed in the beam waist region and it is scanned along the z-axis. At a sufficiently large distance from the sample, an aperture with an on-axis narrow opening and a detector that detects the energy changes behind the aperture are placed. When the sample is located far from the beam waist, where the beam intensity is low, the transmission through the aperture is

normalized to unity. As the sample is shifted closer to the waist, the induced nonlinear absorption and nonlinear refraction index exert stronger influence upon the beam and the normalized transmittance curve takes characteristic shape [72–78].

In our experiment we used Gaussian laser pulses of 532 nm, 7ns from the second harmonic output of a hybrid mode-locked Nd: YAG laser operating at 10 Hz repetition rate. The crystal is fixed on a microprocessor controlled translation stage, so that it can be accurately moved through the focal region of the laser beam. A fast photodiode monitors the input laser energy, and a large area photodiode collects the transmitted beam. For the closed aperture measurements, a suitable aperture is placed in front of the photo diode. Data acquisition is facilitated by the use of a personal computer.

Figure (6.28) clearly illustrates that the absorption increases as the incident light irradiance rises and that the light transmittance (T) is a function of the sample's Z-position (with respect to the focal point at Z ~ 0). The RSA coefficient β (m/W) can be obtained from a best fitting performed on the experimental data of the OA measurement with the equations (6.14) and (6.15)[78] where α and β are the linear and effective third order NLO absorption coefficients, respectively, τ is the time, I(z) is the irradiance and L is the optical path length.

$$T(Z)= \frac{1}{Q(z)\sqrt{\pi}} \int_{-\infty}^{+\infty} \ln[1 - Q(z)] e^{-\tau^2} d\tau \qquad (6.14)$$

$$Q(Z)= \beta I(Z) \frac{1-e^{-\alpha L}}{\alpha} \qquad (6.15)$$

The value of RSA coefficient β is found to be equal to be 9.089 cm/GW.

The peak to valley configuration of the closed aperture curve (Fig.6.29) is a clear indication of a negative refractive nonlinearity exhibited by the medium [73]. The nonlinear refraction coefficient n_2 (m^2/W) is obtained through the following equation

$$\Delta\Phi_0 = k n_2 I_0 L_{eff} \qquad (6.16)$$

The difference between the normalized transmittance at the peak and valley is related to $\Delta\Phi_0$ by the relation

$$\Delta T_{P\rightarrow V} = 0.406\,(1\text{-}S)^{0.25}\,\Delta\Phi_0 \qquad (6.17)$$

The value of n_2 is calculated to be equal to -53.651×10^{-14} m^2/W.

The molecular hyperpolarizability, γ, may be obtained to be 14.97×10^{-24} esu with the equation below [79]

$$\gamma = 40\pi\, n_2/\, cn_0 \qquad (6.18)$$

The real and imaginary parts of the χ^3 of the sample can also be calculated by the following equations [80, 81]

$$\text{Re}\,\chi^3\,(\text{esu}) = (cn_0^2/\,120\pi^2)\,n_2, \qquad (6.19)$$

$$\text{Im}\,\chi^3\,(\text{esu}) = (cn_0^2\varepsilon_0\lambda\,/2\pi)\,\beta \qquad (6.20)$$

The value of the real part of nonlinear susceptibility Re χ^3 (esu) and imaginary part Im χ^3 (esu) is found to be equal to -3.057×10^{-11} esu and 0.4391×10^{-11} esu respectively.

Introducing the coupling factor ρ, the ratio of imaginary part to real part of third-order nonlinear susceptibility,

$$\rho = \text{Im}\,\chi^3/\,\text{Re}\,\chi^3 \qquad (6.21)$$

The value of ρ in this case is found to be equal to 0 .143.

The observed value of coupling factor is seen to be less than 1/3, which indicates that the nonlinearity is electronic in origin [82]. The open aperture curve demonstrates a nonlinear absorption and the characteristic pattern of the curve shows that the nonlinear absorption is reverse saturation absorption (RSA) implying that the crystal can be effectively used for optical limiting applications. The peak to- valley

configuration of the closed aperture curve suggests that the refractive index change is negative, exhibiting a self defocusing effect. This may be an advantage for the application in the protection of optical sensors. The delocalized π electrons enhance the hyperpolarizability and the nonlinear susceptibility, which leads to large third-order NLO properties.

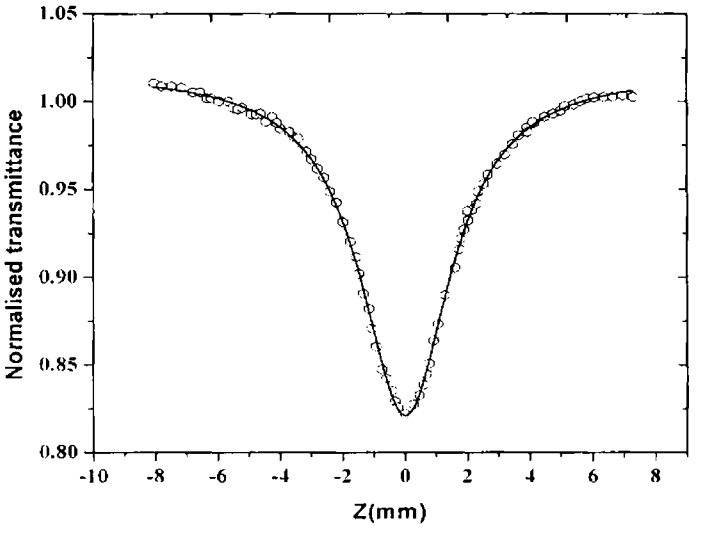

Fig. 6.28 Open aperture Z scan curve of KAP crystal

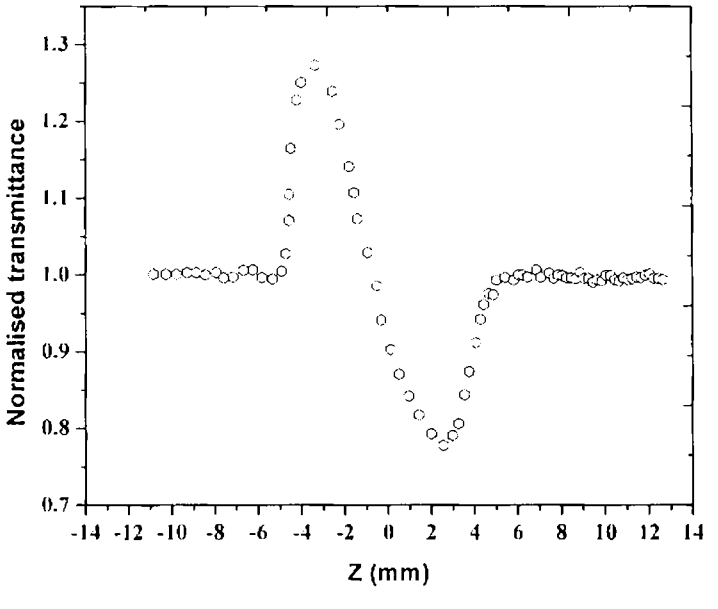

Fig 6.29 Closed aperture Z scan curve of KAP crystal

6.4 CONCLUSIONS

We have grown optical quality single crystals of KAP by floating seed technique and by gel growth method for the first time. Powder XRD data of gel grown and solution grown KAP agrees well with the reported values. CHN analysis and EDAX analysis are carried out to find the different elements incorporated in the sample. The crystal has wide transparency window extending from 313nm to 1800nm. The optical band gap of KAP is found to be 4.1 eV. Linear optical constants are found from the UV/VIS/NIR absorption spectrum. Various functional groups present in the crystal are confirmed by vibrational analysis. Noncentrosymmetric crystal structure is established from vibrational spectra. The relatively large value of Cp found from the thermal analysis reveals that KAP crystal needs larger quantity of heat energy to get heated up, so that consequent damage due to localised heating can be avoided, which enhances its prospects for applications in laser assisted devices. Average dislocation density found by chemical etching studies is of the order of 10^3 cm^{-2}, indicative of good crystalline perfection. It is established that two dimensional nucleation and spreading of layers is the relevant growth mechanism. Micro hardness analysis carried out in detail reveals the strong binding force existing between neighboring atoms. The crystal has a micro hardness value of 25kg/mm^2.

The good crystalline perfection of the samples in the present study is expected to be the reason for the high value of SHG efficiency. This study also supports the fact that gel growth method results in the growth of perfect crystals with good crystallinity even though the size of grown crystals is less compared with other crystal growth methods. KAP crystal is observed to have reasonably high damage threshold values similar to the other solution grown nonlinear optical semi organic crystals. The nonlinear absorption in the material is reverse saturable absorption (RSA) which implies that the crystal can be effectively used for optical limiting applications. The peak to- valley configuration of the closed aperture Z scan curve suggests that the refractive index change is negative, exhibiting a self defocusing effect.

6.5 REFERENCES

[1] Beck. L, Stemmler. P, Rev.Sci.Instr. 66, 1601(1995).

[2] Shujun. Z, Jihua .X, Zhilin. X, Nuclear Fusion and Plasma physics, Vol.13, 61(1993).

[3] Zho.Q.L, J.Appl.Cryst. 27, 283(1993).

[4] Miniewics.A, Barkiewics.S, Adv.Mat.Opt.Elect, 2, 157(1993).

[5] Comeretto.D, Rosy.L, J.Mat.Res, 12, 1262(1997).

[6] Krajewski.T, Bracksweski.T, Ferroelectrics, 25, 547 (1980).

[7] Van Enkevort.W.J.P, Jettin. L.A.M.J, J.Crystal. Growth, 60, 275(1982).

[8] Ester. G.R, Price.R, Halfpenny. P.J, J.Cryst.Growth, 182, 95(1998).

[9] G. S. Pawley, J. Appl. Cryst 14, 357(1981).

[10] R. Mohan Kumar, D. Rajan Babu, R. Jayavel, J. of Crystal Growth 245,297 (2002).

[11] A. Roshan and S. Cyriac Joseph, Mat. Lett. 49, 299 (2001).

[12] V. V. Maheswaran, S. Sherwood, and J. N. Bhat, J. Cryst. Growth 179, 605 (1997).

[13] I. M. Tsidilkovsk, Band structure of semiconductors, Pergamon Press, Oxford (1982).

[14] J. I. Pankove, Optical processes in semiconductors, Prentice-Hall, New York (1971).

[15] A. Ashour, H.H. Afifi and S.A. Mahmoud, Thin Solid Films, 248, 253(1994).

[16] K. Yamaguchi, N. Nakayama, S. Ikegami, Jpn. J. Appl. Phys., 16, 1203(1977)

[17] O.P. Agnihotri and B.K. Gupta, Jpn. J. Appl. Phys., 18, 317(1979).

[18] D. R. E. Campbell and R. D. Tomlin, J. Phys. D 5, 852 (1972).

[19] A. A. El-Kadry and N. Mahmoud, Thin Solid Films 269, 117 (1995).

[20] I. C. Ndukwe, Sol. Ener. Mater. Sol. Cells, 40, 123(1996).

[21] Janai, M., D. D. Alfred, D. C. Booth and B.O. Seraphin, Sol. Ener. Mater. 1,11(1979),.

[22] J. I. Pankove, Optical processes in semiconductors, Prentice-Hall, New York (1971).

[23] L. A. Dementieva, A. V. logansen, G. A.Kurkchi. Opt. spectroscopy, 29, 868 (1970).

[24] T. A. Eremina, N. G. Furmanova, L. F.Malakhova, Sov.Phys. Crystallogr. 38(4), 554 (1993).

[25] R. Mohan Kumar, D. Rajan Babu, R. Jayavel, J. of Crystal Growth 245, 297 (2002).

[26] G. Varsanyi, Assignments for vibrational spectra of 700 benzene derivatives, Academiai Kiado, Budapest. 1973. Vol.1. P.232.

[27] K.Uthayarani, R. Sankar, C. K.S.Nair, Cryst. Res.Technol. 43(7), 33(2008).

[28] B. N. Mavrin, E.Sterin, A. V. Michenko. Solid State Physics (Russ.) 15, 1682 (1973).

[29] B. Orel, D. Hadzi, and F. Cabassi, Spectrochim Acta 31A, 169 (1975).

[30] http://www.fi.infn.it/conferenze/galassie/Poster/zoppi_Tosca.ppt.

[31] The infrared spectra of complex molecules, L.J. Bellamy, Wiley & Sons, Newyork 1962.

[32] A. Smith, Acta Cryst. B 31, 2347 (1975).

[33] R. D. Fulton, R. R. Ryan, and J. H. Hall, Acta Cryst. C 46, 1621 (1990).

[34] M.J. O' Neill, Anal.chem.38, 1331(1966).

[35] K.Nandakumar, PhD thesis, Cochin University of science and technology, India (1992).

[36] W.A. Wooster, Rep. Prog. Phys. 16, 62(1953).

[37] E. Meyer, Z. ver, Dtsch. Ing. 52, 645(1908).

[38] E.M. Onitsch, Mikroscopia 2, 131(1947).

[39] M. Hanneman, Metall. Manchu. 23, 135(1941).

[40] C. Hays, E.G. Kendall, Mettallurgy 6, 275(1973).

[41] K. Sangwal, Etching of crystals, North Holland Physics Publication, Amsterdam, (1987)

[42] M.S.Joshi, M.A. Ittyachan Ind.J.Pure & Appl.Phys.7, 624 (1969).

[43] F.W.Young, J.Appl.Phys. 32, 192 (1961).

[44] S.Nendelson, J.Appl.Phys, 32, 1579(1961).

[45] J.W.Davisson, S.Levinson, J.Appl.Phys. 37, 488(1966).

[46] H.C.Gatos, Crystal growth &charecterisation, North Holland, P.313.

[47] W.J.P.Van Enckevort, W.H. Vander Linden, J.Cryst.Growth, 47, 196 (1979).

[48] K.Sato, M.Okada, Nature, 269, 399 (1977).

[49] J.J.Gilman, W.G.Jhonston, G.W. Sears, J.Appl.Phys, 29, 5, (1958).

[50] M.S.Joshi, P.N.Kotru, M.A.Ittyachen, American Minerologist, 63, 744 (1978).

[51] T. Itoh, IEEE Trans. On Microwave Theory and Techniques, May 1974.

[52] H.E. Bussey, Proc. IEEE, Vol. 55, No 6, pp. 1046(1967).

[53] K.T. Mathew, U. Raveendranath.K, Sensors Update (Ger.) 7,185(1999).

[54] K.T. Mathew, U. Raveendranath.K, K.G. Nair, Micro. Opt. Tech. Letts. 6,104 (1993).

[55] A. J. Glass and A. H. Guenther, Appl. Opt. 12, 637(1973).

[56] N. L. Boling, M. D. Crisp, and G. Dube, Appl. Opt. 12, 650(1973).

[57] H. Nakatani, W. R. Bosenberg, L. K. Cheng, C. L. Tang, Appl. Phys.Lett. 53, 2587(1988).

[58] V. Venkataramanan, C. K. Subramanian, and H. L. Bhat, J. Appl. Phys.77, 6049(1995).

[59] A. Yokotani, T. Sasaki, K. Yoshida, and S. Nakai, Appl. Phys. Lett. 55, 2692(1989).

[60] G. Dhanaraj, M. R. Srinivasan, S. V.Subramanyam, J. Appl. Phys. 72, 3464(1992).

[61] A. Yokotani, T. Sasaki, K. Yoshida, and S. Nakai, Appl. Phys. Lett. 55, 2692(1989).

[62] R. T. Bailey, F. R. Cruickshank, P. Kerkoc, J. N. Sherwood, Appl. Opt. 34, 1239(1995).

[63] B. C. Stuart, M. D. Feit, A. M. Rubenchik, M. D. Perry, Phys. Rev. Lett. 74, 2248(1995).

[64] M. Yoshimura, T. Kamimura, T. Sasiki, Jpn. J. Appl. Phys, 38, L129 (1999).

[65] P. Kerkoc, R. T. Bailey, F. R. Cruickshank, J. N. Sherwood, J. Mod. Opt. 43, 903(1996).

[66] S. S. Gupte, R. D. Pradhan, A. Marcano O., C. F. Desai, J. Appl. Phys. 91, 3125(2002).

[67] S.K. Kurtz, T.T. Perry, J. Appl. Phys. 39, 3798(1968).

[68] Yetta Porter, Kang Min Ok, P.Shiv Halaasyamani, Chem.Mat.13, 1910 (2001).

[69] I.V.Kityk, B.Marciniak, A.N.Mefleh, J.Phys.D 34, 1 (2001)

[70] E.M. Onitsch, Mikroscopia 2, 131(1947).

[71] P. Nisha Santha kumari, S. Kalainathan, N. Aruna Raj, Materials Letters 62,305(2008).

[72] M. Sheik-Bahae, A.A. Said, E.W. Van Stryland. Opt. Lett., 14, 955(1989).

[73] M. Sheik-Bahae, A.A. Said, T.H. Wei, D.J. Hagan, Proc. SPIE, 1438, 126(1989).

[74] M. Sheik-Bahae, D.J. Hagan, E.W.V. Stryland. IEEE J. Quantum Electron, 26, 7601990.

[75] R.L. Sutherland, Handbook of nonlinear optics, Marcel Dekker, New York, 1996.

[76] P.B. Chapple, J. Staromlynska, R.G. McDuff, J. Nonlin. Opt. Phys. Mat., 6, 251(1997).

[77] R.W. Waynant, M.N. Ediger, Electro-Optics Handbook, McGraw-Hill, New York, 2000.

[78] M. Sheik-Bahae, M.P. Hasselbeck, Handbook of Optics, McGraw-Hill, New York, 2001.

[79] G. Yang, W. T. Wang, L. Yan, H. B. Lu, and Z. G. Chen, Opt. Comm. 209, 445 (2002).

[80] S.F. Wang, W. T. Huang, T. Q. Zhang, and Y. F. Miura, Appl. Phys. Lett. 75, 1845 (1999).

[81] S. Hughes, B. Wherret, Phys. Rev. A 54, 3546 (1996).

[82] Seetharam.S, G. Umesh, K. Chandrasekharan, B.K. Sarojini, Opt. Mater. 30 1297(2008)

****ൠ****

Chapter 7

GENERAL CONCLUSION AND SCOPE FOR FUTURE WORK

General conclusion and scope for future work

Chapter 7

GENERAL CONCLUSION AND SCOPE FOR FUTURE WORK

Behind every new solid state device, there exists the contribution from a single crystal. This means that many new crystals have to be grown and characterized in order to assess their prospects in the design of newer and versatile devices to meet the needs of the present century. A decrease of crystal defects and inhomogenieties is demanded simultaneously with the development of large crystal dimensions. Nonlinear optical crystals play a dominant role in the field of photonics. Various kinds of organic nonlinear crystals have been developed in the past two decades because of the possibility of extremely high optical nonlinearity.

The single crystal growth along with the characterisation of three nonlinear optical crystals forms the basis of the present work. Two of them are completely organic, based on amino acids, glycine and L-alanine and the other is semi organic, potassium hydrogen phthalate. Glycinium oxalate single crystals are grown from the saturated solution at ambient temperature using the precursors glycine and oxalic acid. An aqueous solution of 1:1 molar ratio glycine and oxalic acid maintained at 60^0C yields a white crystalline powder which is then recrystallized several times to get ultrapure glycinium oxalate. It is then used for the preparation of seed crystals and for making saturated solution for the growth of large sized single crystals. Powder XRD study on the grown crystal agrees well with the reported single crystal XRD data. CHN analysis confirms the molecular formula as $C_4H_7NO_6$. The vibrational analysis carried out using the FTIR and FT Raman spectroscopy shows the presence of NH_3^+ ion, confirming the protonation of amino group leading to the formation of glycinium oxalate molecule. The non centrosymmetry in the grown crystals of glycinium oxalate is established on the basis of the excellent match between the various vibrational frequencies in the infrared and raman spectra.

Thermal studies carried out employing TGA/DTA and DSC techniques, establish that the crystal has thermal stability up to 179^0C (Melting point) and there is no phase transition till the material melts. The specific heat Cp, evaluated using the DSC data, is 898 J/kg K at 333k. This relatively high Cp value enhances its prospects of applications in laser assisted devices. Vickers' microhardness analysis carried out on the material suggests that the material belongs to soft material category. The value of load independent resistance to deformation is calculated as 19.2 g. The value of elastic stiffness coefficient C_{11} calculated is quite high, revealing the strong binding forces between ions. Microtopography and chemical etching studies are carried out to understand the growth mechanism and the nature and density of dislocations present in the crystal. Dislocation density for solution grown GLO, in the present study is about $10^4/cm^2$ which is quite small compared to many other solution grown inorganic semiconductors. It is established that the growth mechanism of GLO single crystals in the present work is 2D nucleation and subsequent spreading of layers.

From the optical absorption studies in the UV/Vis/NIR range, it is seen that the GLO crystal has a wide transparency window ranging from 324 nm to 2500nm and the absorption throughout this range is very small. This aspect highlights its prospects of applications as a material for higher harmonic generation in nonlinear optics. The optical band gap of the material is found to be 3.9 eV. The values of the linear optical constants, α, n and k are evaluated from these studies and these values are used to compute the non linear optical parameters from the Z scan studies.

The value of dielectric constant at the microwave frequency in the S band is calculated as 3.3 for GLO crystals and it remains almost constant with increase in frequency in the frequency range 2-3 GHz. The value of dielectric loss for this crystal is very small which is of the order of 0.006, and is an indication of the crystalline perfection of the grown crystal.

The photoluminescence spectrum obtained, on exciting with 260nm radiation shows an emission peak at 470 nm which is assigned to a lattice related de - excitation process from the LUMO to HOMO. This intense emission peak at 470 nm

observed in GLO crystal extends ample scope for further detailed investigations in this direction.

Kurtz & Perry Powder technique is employed to investigate the second harmonic generation (SHG) process in this crystal. The SHG efficiency of the crystal is found to be 0.92 times that of KDP.

The single shot (P_I) and multiple shot (P_{II}) laser damage threshold values for (010) cleaved face of GLO are found to be 15.5 and 11.5GW cm^{-2}, respectively for 1064 nm, pulsed Nd: YAG laser radiation. Open aperture Z scan studies carried out using 532nm radiation of the pulsed Nd: YAG laser of 7ns pulse width shows that there is reverse saturable absorption (RSA) in the material and two photon absorption is the mechanism responsible for RSA. The peak-valley structure of the curve obtained in the closed aperture Z scan studies is a clear indication of a negative nonlinear refraction exhibited by the crystal. The nonlinear refraction coefficient $n_2(m^2/W)$, hyperpolarizability (γ) and the real and imaginary parts of $\chi^{(3)}$ are evaluated. The ratio of the imaginary part of third order susceptibility to its real part is less than 1/3 which indicates that the observed non linearity in this crystal is electronic in origin.

In the present work, top seeded solution growth technique at ambient temperature is found to yield optical quality crystals of l- alaninium oxalate (LAO) of size 40 mm×15mm×8mm in three weeks time, which is reported for the first time. As before, the chemical composition of LAO is confirmed on the basis of CHN analysis and the crystal structure, by XRD analysis. The protonation of the amino acid group leading to the formation of LAO molecule is confirmed based on FTIR and Raman studies. Here also the excellent match between the various vibrational frequencies in the infrared and Raman data confirms that the grown LAO crystal is non centrosymmetric. The thermal studies on LAO crystal using TGA/DTA and DSC techniques show that the material is stable up to its melting point of 197^0C which is higher than that of GLO crystal. The value of Cp calculated from the DSC data is also greater than that of GLO. As before, from the micro hardness studies, the strong binding nature of ions in the crystal is established, which is an indication of its stability. Dislocation density evaluated for LAO crystal on the basis of etching study

is of the order of 10^3 /cm^2 which is an order of magnitude less than that of GLO. The growth mechanism in LAO crystal is identified as 2D nucleation and subsequent spreading of layers.

In this material, from the optical absorption studies, the transparency window is found to extend from 318 nm to 1524nm and the optical band gap estimated is around 4.01 eV. As before the linear optical constants n, k and α are determined.

PL spectrum shows a broad peak centered at 440 nm with intensity comparable to that of conducting polymers and polymer composites when excited with 300nm radiation, which is also assigned to a lattice related LUMO to HOMO de excitation process. The very low value of dielectric loss (0.016) obtained from the microwave absorption studies shows the good crystalline perfection of the grown LAO crystal.

SHG efficiency evaluated as explained before is 1.8 times that of L alanine and 2.3 times that of KDP. For the (100) plane, the single shot laser damage threshold P1 = 29.64 GW/cm^2 and multiple shot damage threshold Pn = 20.60 GW/cm^2 and these values are much higher compared to GLO. Reverse saturable absorption (RSA) due to two photon absorption is confirmed from the open aperture Z scan method. Negative nonlinear refraction present in the material is observed in closed aperture Z scan experiment. As before the various nonlinear optical parameters are evaluated for this material also.

In the growth of potassium hydrogen phthalate (KAP) single crystals, both floating seed technique and gel growth method are employed. In floating seed technique, the seed crystal placed on the saturated solution remains on the surface by surface tension and grows by evaporation of the solution. In three weeks time, hexagonal crystals without any inclusions and defects with size 12 mm×10mm×5 mm are obtained.

Solubility reduction method employing sodium meta silicate gel is also tried for the growth of KAP crystals. A PH value of 5 is maintained for the gel and 3 molar KAP solution is added to the gel. A mixture of ethyl alcohol and acetone is

poured over the gel and it is seen that in about one month, crystals of size 5 mm× 4mm × 3mm are grown.

CHN analysis and EDAX are used to confirm the formation of potassium hydrogen phthalate. Powder XRD data of the solution grown and gel grown KAP crystals matches very well with the reported values. Excellent thermal stability up to 298^0C (melting point) is observed In KAP crystal without any phase transition. The Cp value at 333K is 860 J/kg K, which is quite high. Vickers' microhardness analysis shows that KAP belongs to the soft material category and is a stable material owing to the strong binding forces between the ions.

Layer growth is seen to be the prominent growth mechanism in the crystals grown by floating seed technique and also by gel growth method. Dislocation density is small (10^3/cm^2) and comparable to GLO and LAO. The crystal has a wide transparency window from 313nm to 1800 nm. Optical band gap is found to be 4.1ev. The linear optical constants are also determined. The low dielectric loss found in the material by cavity perturbation technique underlines the crystalline perfection.

SHG efficiency is found to be 1.5 times that of KDP for solution grown crystals and 2.1 times that of KDP for gel grown crystals. Gel grown KAP crystal shows enhanced SHG output owing to the better crystalline perfection with lesser defects, which is a positive aspect of the gel growth technique.

The value of single shot laser damage threshold is 25 GW/cm^2 and that of multiple shot laser damage threshold is 19.6 GW/cm^2. The optical limiting and the non linear refraction in this crystal are established based on open aperture and closed aperture Z scan studies , similar to GLO and LAO crystals, and the various nonlinear optical parameters are evaluated.

A comparative analysis of the various important parameters of the three grown crystals, GLO, LAO and KAP is carried out for their possible applications in nonlinear optics.

Material	Glycinium oxalate	L-alaninium oxalate	Potassium hydrogen phthalate
Growth method & time	Solution growth, 3 weeks	Solution growth, 4 weeks	Solution(3) & gel growth,6weeks
Crystal structure	**Monoclinic, $P2_1$ / C**	**Orthorhombic, $P2_12_12_1$**	**Orthorhombic, $Pca2_1$**
Melting point	179°C	197°C	298°C
Sp.heat capacity , Cp at 330K	**898 J/Kg K**	**1766 J/Kg K**	**860 J/Kg K**
stability	Air stable	Air stable	Air stable
Maximum Microhardness	**58 Kg/mm^2**	**38.9Kg/mm^2**	**25 Kg/mm^2**
Work hardening coefficient	3.3	4.2	3.2
Transparency window	**324 nm- 2500nm**	**318 nm-1524 nm**	**313 nm-1800 nm**
Optical band gap	3.9ev	4.09ev	4.1ev
Dielectric constant	**3.37**	2.68	**3.4**
Dielectric loss	0.006	0.016	0.03
Dislocation density	10^4/cm^2	10^3 /cm^2	10^3 /cm^2
Growth mechanism	2Dnucleation &layer spreading	2Dnucleation &layer spreading	2D nucleation &layer spreading
Laser damage threshold, Pn	**11.5GW cm^{-2}**	20.60 GW/cm2	**19.6 GW/Cm2**
SHG efficiency	0.92 times KDP	2.3 times KDP	1.5 times KDP (solution grown)
Nonlinear absorption coefficient, β	7.429 cm/ GW	11.65 cm/GW	9.089 cm/GW
Hyperpolarisability, γ	**4.0424×10^{-24} esu**	**10.424×10^{-24} esu**	**14.97×10^{-24} esu**
NLR coefficient, n2	-1.689×10 $^{-13}$m^2/W	-3.984×10 $^{-13}$ m^2/W	-53.651×10 $^{-14}$ m^2/W

The results of the present investigations allow ample scope for further investigations in these single crystals as outlined below

- Studies on the prospects of GLO and LAO crystals as bio compatible capping agents for ZnS and ZnO nano particles for bio medical imaging and targeted drug delivery applications can be carried out.
- Other growth methods like melt growth can be employed to get still bigger crystals of GLO, LAO and KAP for possible industrial applications.
- Frequency doubling is a phase-sensitive process which usually requires phase matching to be efficient and hence the phase matching study for the crystals is to be done. The optimum crystal length and pump beam radius, taking into account factors such as beam divergence, spatial walk-off, group velocity mismatch, beam quality etc are to be studied in detail for device fabrication applications.
- Suitable dopants can be incorporated to modify the NLO behaviour of these crystals.
- Microwave absorption studies can be extended to the whole micro wave region.

****ꕥ****

List of Publications

In peer reviewed international journals

1. Growth and characterization of glycinium oxalate crystals for nonlinear optical applications, **Arun.K.J**, S.Jayalekshmi, Optoelectron.Adv.Mater (RC), Vol.2, No.11, p701-706, (2008).
2. Studies on the microstructure and micro hardness of L-Alaninium oxalate single crystals for optical devices, **Arun.K.J**, S.Jayalekshmi, Optoelectron.Adv.Mater (RC), Vol.2, No.12, p802-805, (2008).
3. Studies on the vibrational spectra of the nonlinear optical crystal L-Alaninium oxalate, **Arun.K.J**, S.Jayalekshmi, AIP Conf .Proc. 1075, 115-117, (2008)
4. Growth and charecterisation of nonlinear optical single crystals of L-Alaninium oxalate, **Arun.K.J**, S.Jayalekshmi Journal of Minerals and Materials Charecterisation & Engineering, U.S.A, Vol.8, No.8, P 635-646 (2009).
5. Growth of Potassium hydrogen phthalate in SMS gel and its characterisation, **Arun.K.J**, S.Jayalekshmi (communicated)

   Z scan measurements of the third order nonlinear optical properties of L alaninium oxalate crystal, **Arun.K.J**, et .al, (communicated).
7. Studies on the Vickers' microhardness and thermal properties of nonlinear optical glycinium oxalate single crystal, **Arun.K.J**, S.Jayalekshmi, (*communicated*).
8. Investigations on the two photon absorption and non linear refraction in Glycinium oxalate crystal, **Arun.K.J**, et .al (*communicated).*
9. Third order NLO properties of Potassium hydrogen phthalate crystal at 532nm, **Arun.K.J**, et .al, (*to be communicated).*

Conference Presentations

1. L-Alaninium Oxalate single crystals for NLO applications: A simple and novel synthesis route, **Arun. K.J**, S. Jayalekshmi, Proceedings of the International conference on Optoelectronic Materials and Thin films, October 24-27, 2005 Cochin University.

2. Growth and characterization of a new amino acid based mixed crystal for possible NLO applications, **Arun. K. J**, S. Jayalekshmi, M.A. Ittyachan, Proceedings of the National conference on advanced technologically important crystals, October 12- 14, 2006, University of Delhi

3. Micro topography and micro hardness of L alaninium oxalate crystal, **Arun.K.J**, S.Jayalekshmi, Proceedings of the national conference- New horizons in theoretical and experimental physics, CUSAT, 2007.

4. A novel nonlinear optical mixed crystal Bis thiourea Potassium acid phthalate, **Arun. K. J**, S. Jayalekshmi, Proceedings of the national conference on current trends in materials science, March 25-27, 2007, Christian college, Chengannur, Kerala

5. Studies on the Vibrational Spectra of the Nonlinear Optical Crystal L – Alaninium oxalate, **Arun.K.J**, S. Jayalekshmi, Proceedings of the International conference on perspectives in vibrational spectroscopy, February 2008, Kerala University.

6. Micro topography, Micro hardness and Vibrational Spectroscopic Studies on the Nonlinear Optical Crystal: Glycinium Oxalate, **Arun.K.J**, S.Jayalekshmi, Proceedings of the International conference on perspectives in vibrational spectroscopy, February 2008, Kerala University.

****